

ATTACHMENT 1

**SUBMITTAL OF IRRADIATED REACTOR VESSEL SURVEILLANCE CAPSULE
TEST RESULTS FOR CAPSULE T PER 10 CFR 50 APPENDIX H**

**WCAP-16641-NP, REVISION 0, "ANALYSIS OF CAPSULE T FROM DOMINION
ENERGY KEWAUNEE POWER STATION REACTOR VESSEL RADIATION
SURVEILLANCE PROGRAM," OCTOBER 2006**

KEWAUNEE POWER STATION

DOMINION ENERGY KEWAUNEE, INC.

Analysis of Capsule T from Dominion Energy Kewaunee Power Station Reactor Vessel Radiation Surveillance Program

WCAP-16641-NP, Revision 0

**Analysis of Capsule T from the Dominion Energy Kewaunee
Power Station Reactor Vessel Radiation Surveillance
Program**

B.N. Burgos *
J. Conermann
S.L. Anderson

October 2006

Approved: * *Electronically Approved*
 J.S. Carlson, Manager
 Primary Component Asset Management

** Electronically Approved Records Are Authenticated in the Electronic Document Management System*

Westinghouse Electric Company LLC
Energy Systems
P.O. Box 355
Pittsburgh, PA 15230-0355

©2006 Westinghouse Electric Company LLC
All Rights Reserved

This page intentionally blank

PREFACE

This report has been technically reviewed and verified by:

R.G. Lott : * *Electronically Approved*

* *Electronically Approved Records Are Authenticated in the Electronic Document Management System*

This page intentionally blank

FORWARD

The first application of the Master Curve approach for an irradiated reactor vessel weld metal was approved by the NRC for the Kewaunee Power Station (KPS) in 2001 (*Safety Evaluation by the Office of Nuclear Reactor Include the Use of a Master Curve-based Methodology for Reactor Pressure Vessel Integrity Assessment*, Docket No. 50-305, May 2001). Testing of the next surveillance capsule for KPS included the requirement to perform additional fracture toughness tests to help validate the previous Master Curve evaluation accepted by the NRC. Two reports have been prepared to describe the results and evaluation of the additional fracture toughness testing performed as part of the Capsule T evaluation.

Capsule Requirements

In accordance with the NRC SE, removal and testing of one additional capsule at a fluence equivalent to End-of-License-Renewal (EOLR) for the vessel weld of concern would be acceptable for monitoring radiation damage. The currently evaluated fluence for EOLR is documented in WCAP-16641-NP, the Capsule T analysis report, where the value was determined to be 5.37×10^{19} n/cm² (E>1.0 MeV).

Additionally, the removal and testing of the capsule with fluence equivalent to 60 yrs will complete the current KPS surveillance program requirements. In accordance with the SE requirement, Capsule T was removed at a calculated fluence of 5.62×10^{19} n/cm² (E>1.0 MeV), which closely approximates the EOLR vessel fluence.

Master Curve Fracture Toughness T_0 Determination

The methodology detailed in Appendix A of the NRC SE is the methodology accepted by the NRC. The licensee agreed to use this methodology for future Master Curve fracture toughness testing and to incorporate the results into the KPS licensing basis. All margin terms are defined in Appendix A. Specific to the testing requirements, the NRC stated the following:

1. Use of ASTM E 1921-97 is acceptable,
2. The use of multi-temperature maximum likelihood methodology is currently not endorsed (since it was not included in the ASTM Standard).

It was acknowledged that the state of knowledge regarding specific technical topics associated with the Master Curve approach may be improved in the future. Additional conservatisms may be reduced or removed provided technical justification is made. The NRC recognized that it may reconsider its' position based on action within ASME Standards organizations and revisions to ASTM E 1921.

In establishing a valid measurement of T_0 for weld wire heat 1P3571, several sources for the test specimens were deemed acceptable:

1. Charpy V-notch (CVN) weld specimens,
2. Reconstituted specimens from the weld portion of untested CVN heat-affected-zone (HAZ) specimens, and/or
3. Reconstituted weld specimens from broken halves of the original, broken weld CVN specimens.

All specimens for fracture toughness testing were to be single-edge bend, SE(B), geometry as defined in ASTM E 1921; these specimens when fatigue precracked and conforming to CVN size are generally referred to as precracked Charpy V-notch (PCVN) specimens. All of the information in paragraphs 11.1 through 11.2.3 of ASTM E1921-97 for Capsule T, Capsule S, the Maine Yankee Capsule A35, and any unirradiated specimens used for the current licensee submittal were required to be included in the final reports for Capsule T and the new Master Curve evaluation. Use of Code Case N-629 to define a suitable expression for calculating the RT_{T_0} parameter was considered acceptable.

The actual PCVN specimens utilized in determining the measurement of T_0 for Capsule T were a fabricated from a combination of the original irradiated CVN weld specimens (eight total) along with the reconstitution of four unbroken CVN HAZ specimen portions to provide a total of twelve specimens. Details concerning the testing of the PCVN specimens are documented in WCAP-16609-NP (Master Curve Report) and WCAP-16641-NP (Capsule T Analysis). In accordance with NRC guidance, the methodology in Appendix A of the SE was used and presented in WCAP-16609-NP. In addition to this methodology, a new methodology has been developed under International Atomic Energy Agency (IAEA) sponsorship which has been applied and documented in WCAP-16609-NP.

The actual test results are presented in WCAP-16641-NP and the analysis is described in WCAP-16609-NP.

Charpy V-Notch Testing and Analysis

In accordance with the NRC SE, a full CVN curve was not required to be developed for the surveillance weld, heat 1P3571. However, information regarding material properties were still required to be estimated to include the transition temperatures at 30 ft-lb, 50 ft-lb, and 35 mils along with the drop in upper shelf energy (USE). Accordingly, the methodology used in determining these values was documented in WCAP-16641-NP. Reconstitution of specimens needed to determine material properties was to be performed in accordance with ASTM E 1253, as described in WCAP-16641-NP. For the forging and correlation monitor materials, full CVN curves were required and testing/analysis performed in accordance with ASTM E 185-82. CVN impact testing of the HAZ material was not required.

A full CVN curve was not developed for the surveillance weld, however, the transition temperature values representing 30 ft-lbs, 50 ft-lbs and 35 mils were determined using the methodology presented in WCAP-16641-NP. The drop in the surveillance weld USE was also documented as a part of this analysis. The test results for the forging and correlation monitor materials also were documented in WCAP-16641-NP. As indicated earlier, four of the HAZ CVN specimens were reconstituted and used as weld metal PCVN specimens to help determine the Master Curve T_0 value for the surveillance weld.

TABLE OF CONTENTS

LIST OF TABLES	ix
LIST OF FIGURES	xi
EXECUTIVE SUMMARY	xiii
1 SUMMARY OF RESULTS	1-1
2 INTRODUCTION	2-1
3 BACKGROUND	3-1
4 DESCRIPTION OF PROGRAM.....	4-1
5 TESTING OF SPECIMENS FROM CAPSULE T	5-1
5.1 OVERVIEW	5-1
5.2 CHARPY V-NOTCH IMPACT TEST RESULTS (FORGING/SRM)	5-3
5.3 TENSILE TEST RESULTS (FORGING).....	5-5
5.4 MASTER CURVE TEST RESULTS (WELD).....	5-6
5.5 WEDGE OPENING LOADING SPECIMEN TESTS	5-7
6 RADIATION ANALYSIS AND NEUTRON DOSIMETRY	6-1
6.1 INTRODUCTION	6-1
6.2 DISCRETE ORDINATES ANALYSIS	6-2
6.3 NEUTRON DOSIMETRY	6-6
6.4 CALCULATIONAL UNCERTAINTIES.....	6-7
7 SURVEILLANCE CAPSULE WITHDRAWAL SCHEDULE	7-1
8 REFERENCES	8-1
APPENDIX A VALIDATION OF THE RADIATION TRANSPORT MODELS BASED ON NEUTRON DOSIMETRY MEASUREMENTS CREDIBILITY	
APPENDIX B LOAD-TIME RECORDS FOR CHARPY SPECIMEN TESTS	
APPENDIX C MASTER CURVE RESULTS FROM CAPSULE T AND PREVIOUS FRACTURE TOUGHNESS TESTS	
APPENDIX D CHARPY V-NOTCH PLOTS FOR EACH CAPSULE T MATERIAL	
APPENDIX E KPS SURVEILLANCE PROGRAM CREDIBILITY EVALUATION	

This page intentionally blank

LIST OF TABLES

Table 4-1	Chemical Composition (wt %) of the KPS Reactor Vessel Surveillance Materials.....	4-3
Table 4-2	Heat Treatment History of the KPS Reactor Vessel Beltline Region Surveillance Materials	4-4
Table 4-3	Chemical Composition of the A533 Grade B, Class 1 ASTM Correlation Monitor Material (HSST 02) in the KPS Vessel Surveillance Program.....	4-4
Table 4-4	Heat Treatment History of the A533 Grade B, Class 1 ASTM Correlation Monitor Material (HSST 02) in the KPS Vessel Surveillance Program.....	4-5
Table 5-1	Charpy V-Notch Data for the Kewaunee Power Station Intermediate Shell Forging 122X208VA1 Irradiated to a Fluence of 5.62×10^{19} n/cm ² (E > 1.0 MeV) (Tangential Orientation).....	5-8
Table 5-2	Charpy V-Notch Data for the Kewaunee Power Station Lower Shell Forging 123X167VA1 Irradiated to a Fluence of 5.62×10^{19} n/cm ² (E > 1.0 MeV) (Tangential Orientation).....	5-9
Table 5-3	Charpy V-notch Data for the Kewaunee Power Station Surveillance Representative Weld Metal Irradiated to a Fluence of 5.62×10^{19} n/cm ² (E> 1.0 MeV)	5-10
Table 5-4	Charpy V-notch Data for the Kewaunee Power Station Correlation Monitor Material Irradiated to a Fluence of 5.62×10^{19} n/cm ² (E> 1.0 MeV).....	5-10
Table 5-5	Instrumented Charpy Impact Test Results for the Kewaunee Power Station Intermediate Shell Forging 122X208VA1 Irradiated to a Fluence of 5.62×10^{19} n/cm ² (E> 1.0 MeV) (Tangential Orientation).....	5-11
Table 5-6	Instrumented Charpy Impact Test Results for the Kewaunee Power Station Lower Shell Forging 123X167VA1 Irradiated to a Fluence of 5.62×10^{19} n/cm ² (E> 1.0 MeV) (Tangential Orientation).....	5-12
Table 5-7	Instrumented Charpy Impact Test Results for the Kewaunee Power Station Weld Metal 1P3571 Irradiated to a Fluence of 5.62×10^{19} n/cm ² (E> 1.0 MeV).....	5-13
Table 5-8	Instrumented Charpy Impact Test Results for the Kewaunee Power Station Correlation Monitor Material Irradiated to a Fluence of 5.62×10^{19} n/cm ² (E> 1.0MeV)	5-13
Table 5-9	Effect of Irradiation to 5.62×10^{19} n/cm ² (E> 1.0 MeV) on the Capsule T Toughness Properties of the Kewaunee Power Station Reactor Vessel Surveillance Materials	5-14

LIST OF TABLES (Cont.)

Table 5-10	Comparison of the Kewaunee Power Station Surveillance Material 30 ft-lb Transition Temperature Shifts and Upper Shelf Energy Decreases with Regulatory Guide 1.99, Revision 2, Predictions	5-15
Table 5-11	Tensile Properties of the Kewaunee Capsule T Reactor Vessel Surveillance Materials Irradiated to 5.62×10^{19} n/cm ² (E > 1.0MeV)	5-17
Table 5-12	Previously Measured Tensile Properties for Kewaunee Weld Heat 1P3571.....	5-18
Table 5-13	Fracture Toughness Test Results from Capsule T	5-19
Table 6-1	Calculated Neutron Exposure Rates and Integrated Exposures at The Surveillance Capsule Center.....	6-9
Table 6-2	Calculated Azimuthal Variation of Maximum Exposure Rates and Integrated Exposures at the Reactor Vessel Clad/Base Metal Interface.....	6-13
Table 6-3	Relative Radial Distribution Of Neutron Fluence (E > 1.0 MeV) Within The Reactor Vessel Wall.....	6-17
Table 6-4	Relative Radial Distribution of Iron Atom Displacements (dpa) Within the Reactor Vessel Wall.....	6-17
Table 6-5	Calculated Fast Neutron Exposure of Surveillance Capsules Withdrawn from Kewaunee.....	6-18
Table 6-6	Calculated Surveillance Capsule Lead Factors	6-18
Table 6-7	Calculated Maximum Neutron Fluence (E > 1.0 MeV) for the Kewaunee Extended Beltline Materials	6-19
Table 6-8	Calculated Maximum Neutron and Gamma Ray Exposure of the Primary Biological Shield	6-19
Table 7-1	Recommended Surveillance Capsule Withdrawal Schedule.....	7-1

LIST OF FIGURES

Figure 4-1	Arrangement of Surveillance Capsules in the KPS Reactor Vessel	4-6
Figure 4-2	Capsule T Diagram Showing the Location of Specimens and Dosimeters.....	4-7
Figure 4-3	Dosimeter and Thermal Monitor Layout for KPS Capsule T	4-9
Figure 5-1	Charpy V-Notch Impact Energy vs. Temperature for KPS Reactor Vessel Intermediate Shell Forging 122X208VA1 (Tangential Orientation).....	5-20
Figure 5-2	Charpy V-Notch Lateral Expansion vs. Temperature for KPS Reactor Vessel Intermediate Shell Forging 122X208VA1 (Tangential Orientation).....	5-20
Figure 5-3	Charpy V-Notch Percent Shear vs. Temperature for KPS Reactor Vessel Intermediate Shell Forging 122X208VA1 (Tangential Orientation).....	5-21
Figure 5-4	Charpy V-Notch Impact Energy vs. Temperature for KPS Reactor Vessel Lower Shell Forging 123X167VA1 (Tangential Orientation).....	5-22
Figure 5-5	Charpy V-Notch Lateral Expansion vs. Temperature for KPS Reactor Vessel Lower Shell Forging 123X167VA1 (Tangential Orientation).....	5-22
Figure 5-6	Charpy V-Notch Percent Shear vs. Temperature for KPS Reactor Vessel Lower Shell Forging 123X167VA1 (Tangential Orientation).....	5-23
Figure 5-7	Charpy V-Notch Impact Energy vs. Temperature for KPS Reactor Correlation Monitor Material.....	5-24
Figure 5-8	Charpy V-Notch Lateral Expansion vs. Temperature for KPS Correlation Monitor Material.	5-24
Figure 5-9	Charpy V-Notch Percent Shear vs. Temperature for KPS Reactor Correlation Monitor Material	5-25
Figure 5-10	Charpy V-Notch Impact Energy vs. Temperature Best-Fit through the Transition Region for KPS Reactor Vessel Weld Metal	5-26
Figure 5-11	Charpy V-Notch Lateral Expansion vs. Temperature Best-Fit through the Transition Region for KPS Reactor Vessel Weld Metal.....	5-27
Figure 5-12	Charpy Impact Specimen Fracture Surfaces for Kewaunee Reactor Vessel Intermediate Shell Forging 122X208VA1 (Tangential Orientation).....	5-28

LIST OF FIGURES (Cont.)

Figure 5-13	Charpy Impact Specimen Fracture Surfaces for Kewaunee Reactor Vessel Lower Shell Forging 123X167VA1 (Tangential Orientation).....	5-29
Figure 5-14	Charpy Impact Specimen Fracture Surfaces for Kewaunee A553 Grade B Class 1 Correlation Monitor Material.....	5-30
Figure 5-15	Charpy Impact Specimen Fracture Surfaces for Kewaunee Reactor Vessel Reconstituted Weld Metal 5-29	5-30
Figure 5-16	Tensile Properties for Kewaunee, Capsule T Reactor Vessel Intermediate Shell Forging 122X208VA1 (Tangential Orientation).....	5-31
Figure 5-17	Tensile Properties for Kewaunee, Capsule T Reactor Vessel Lower Shell Forging 123X167VA1 (Tangential Orientation).....	5-32
Figure 5-18	Fractured Tensile Specimens from the Kewaunee, Capsule T Reactor Vessel Intermediate Shell Forging 122X208VA1 (Tangential Orientation).....	5-33
Figure 5-19	Fractured Tensile Specimens from the Kewaunee, Capsule T Reactor Vessel Lower Shell Forging 123X167VA1 (Tangential Orientation).....	5-34
Figure 5-20	Engineering Stress-Strain Curves for Kewaunee Reactor Vessel Intermediate Shell Forging 122X208VA1, Capsule T, Tensile Specimens P-13 and P-14	5-35
Figure 5-21	Engineering Stress-Strain Curves for Kewaunee Reactor Vessel Intermediate Shell Forging 122X208VA1, Capsule T, Tensile Specimens P-15 and P-16	5-36
Figure 5-22	Engineering Stress-Strain Curve for Kewaunee Reactor Vessel Intermediate Shell Forging 122X208VA1, Capsule T, Tensile Specimen P-17	5-37
Figure 5-23	Engineering Stress-Strain Curves for Kewaunee Reactor Vessel Lower Shell Forging 123X167VA1, Capsule T, Tensile Specimens S-10 and S-11	5-38
Figure 5-24	Engineering Stress-Strain Curves for Kewaunee Reactor Vessel Lower Shell Forging 123X167VA1, Capsule T, Tensile Specimens S-12 and S-13	5-39
Figure 6-1	Kewaunee r, θ Reactor Geometry at the Core Midplane	6-20
Figure 6-2	Kewaunee r,z Reactor Geometry	6-21

EXECUTIVE SUMMARY

The purpose of this report is to document the results of the testing of surveillance Capsule T from the Dominion Energy Kewaunee Power Station (KPS). Capsule T was removed at 24.6 EFPY and post irradiation mechanical tests of the Charpy V-notch and tensile specimens were performed. A fluence evaluation utilizing the recently released neutron transport and dosimetry cross-section libraries was derived from the ENDF/B-VI data-base. Capsule T received a fluence of 5.62×10^{19} n/cm² (E>1.0 MeV) after irradiation to 24.6 EFPY. The peak clad/base metal interface vessel fluence after 24.6 EFPY of plant operation was 2.60×10^{19} n/cm² (E>1.0 MeV).

This evaluation lead to the following conclusions: 1) Two out of the five measured 30 ft-lb shift in transition temperature values of the intermediate shell forging 122X208VA1 (tangential orientation) are greater than the Regulatory Guide 1.99, Revision 2 [Reference 1], predictions. 2) Two out of the five measured 30 ft-lb shift in transition temperature values of the lower shell forging 123X167VA1 (tangential orientation) are greater than the Regulatory Guide 1.99, Revision 2, predictions. 3) Two of the five measured 30 ft-lb shifts in transition temperature values of the weld metal are greater than the Regulatory Guide 1.99, Revision 2, predictions. 4) The measured percent decrease in upper shelf energy for all the surveillance materials contained in the KPS surveillance program are less than the Regulatory Guide 1.99, Revision 2 predictions with the exception of one weld metal data point. 5) All beltline materials exhibit a more than adequate upper shelf energy level for continued safe plant operation and are predicted to maintain an upper shelf energy greater than 50 ft-lb throughout the life of the vessel (33 EFPY) as required by 10CFR50, Appendix G [Reference 2]. 6) The KPS surveillance data from the intermediate and lower shell forgings 122X208VA1 and 123X167VA1 were found to be non-credible. The KPS surveillance data from the weld metal was found to be credible. The credibility evaluation can be found in Appendix E.

Lastly, a brief description of the Charpy V-notch and Master Curve testing can be found in Section 1.

Removal and testing of Capsule T completes the requested action items discussed in the NRC Safety Evaluation from May 2001 (*Safety Evaluation by the Office of Nuclear Reactor Include the Use of a Master Curve-based Methodology for Reactor Pressure Vessel Integrity Assessment*, Docket No. 50-305, May 2001) [Reference 22]. This report, along with WCAP-16609-NP [Reference 5], satisfies the agreement to use master curve technology and that the transmittal of the reports satisfies the utility requirements for surveillance capsule testing over the lifetime of the plant. One additional capsule remains in the vessel, but is outside the scope of the current licensing requirements.

This page intentionally blank

1 SUMMARY OF RESULTS

The analysis of the reactor vessel materials contained in surveillance Capsule T, the fifth capsule removed and tested from the KPS reactor pressure vessel, led to the following conclusions:

- Capsule T received an average fast neutron fluence ($E > 1.0$ MeV) of 5.62×10^{19} n/cm² after 24.6 effective full power years (EFPY) of plant operation.
- Irradiation of the reactor vessel intermediate shell forging 122X208VA1 Charpy specimens, oriented with the longitudinal axis of the specimen parallel to the major working direction (tangential orientation), resulted in an irradiated 30 ft-lb transition temperature of 65°F and an irradiated 50 ft-lb transition temperature of 110°F. This results in a 30 ft-lb transition temperature increase of 90°F and a 50 ft-lb transition temperature increase of 95°F for the longitudinal oriented specimens. See Table 5-9.
- Irradiation of the reactor vessel lower shell forging 123X167VA1 Charpy specimens, oriented with the longitudinal axis of the specimen perpendicular to the major working direction (tangential orientation), resulted in an irradiated 30 ft-lb transition temperature of 20°F and an irradiated 50 ft-lb transition temperature of 50°F. This results in a 30 ft-lb transition temperature increase of 70°F and a 50 ft-lb transition temperature increase of 75°F for the longitudinal oriented specimens. See Table 5-9.
- Irradiation of the correlation monitor material Charpy specimens resulted in an irradiated 30 ft-lb transition temperature of 220°F and an irradiated 50 ft-lb transition temperature of 245°F. This results in a 30 ft-lb transition temperature increase of 175°F and a 50 ft-lb transition temperature increase of 165°F. See Table 5-9.
- Irradiation of the reactor vessel representative weld Charpy specimens reconstituted from the HAZ material resulted in an irradiated 30 ft-lb transition temperature of 221°F and an irradiated 50 ft-lb transition temperature of 285°F. This results in a 30 ft-lb transition temperature increase of 271°F and a 50 ft-lb transition temperature increase of 295°F for the HAZ specimens. See Table 5-9.
- The average upper shelf energy of the intermediate shell forging 122X208VA1 (tangential orientation) resulted in an average energy decrease of 21 ft-lb after irradiation. This results in an irradiated average upper shelf energy of 139 ft-lb for the tangentially oriented specimens. See Table 5-9.
- The average upper shelf energy of the lower shell forging 123X167VA1 (tangential orientation) resulted in an average energy decrease of 13 ft-lb after irradiation. This results in an irradiated average upper shelf energy of 144 ft-lb for the tangentially oriented specimens. See Table 5-9.
- The average upper shelf energy of the correlation monitor material Charpy specimens resulted in an average energy decrease of 32 ft-lb after irradiation. This results in an irradiated average upper shelf energy of 91 ft-lb for the correlation monitor material specimens. See Table 5-9.

- The average upper shelf energy of the representative weld metal from reconstituted HAZ Charpy specimens resulted in an average energy decrease of 54 ft-lb after irradiation. An irradiated average upper shelf energy of 72 ft-lb for the representative weld metal from the reconstituted HAZ specimens was measured. See Table 5-9.
- A comparison, as presented in Table 5-10, of the KPS reactor vessel surveillance material test results with the Regulatory Guide 1.99, Revision 2 [Reference 1] predictions led to the following conclusions:
 - Two out of the five measured 30 ft-lb shifts in transition temperature values of the intermediate shell forging 122X208VA1 (tangential orientation) are greater than the Regulatory Guide 1.99, Revision 2, predictions.
 - Two out of the five measured 30 ft-lb shifts in transition temperature values of the lower shell forging 123X167VA1 (tangential orientation) are greater than the Regulatory Guide 1.99, Revision 2, predictions.
 - Three of the five measured 30 ft-lb shifts in transition temperature value of the weld metal are greater than the Regulatory Guide 1.99, Revision 2, predictions.
 - All of the correlation monitor material 30 ft-lb shifts in transition temperature were greater than the Regulatory Guide 1.99, Revision 2, predictions.
 - The measured percent decrease in upper shelf energy for all the surveillance materials contained in the KPS surveillance program are less than the Regulatory Guide 1.99, Revision 2 predictions with the exception of one weld measurement.
- All beltline materials exhibit a more than adequate upper shelf energy level for continued safe plant operation and are predicted to maintain an upper shelf energy greater than 50 ft-lb throughout the extended life of the vessel (33 EFPY) as required by 10CFR50, Appendix G [Reference 2].
- The calculated end-of-license (EOL) (33 EFPY) neutron fluence ($E > 1.0$ MeV) at the core mid-plane for the KPS reactor vessel using the Regulatory Guide 1.99, Revision 2 attenuation formula (i.e., Equation #3 in the guide) are as follows:

Calculated: Vessel inner radius* = 3.44×10^{19} n/cm²

Vessel 1/4 thickness = 2.329×10^{19} n/cm²

Vessel 3/4 thickness = 1.068×10^{19} n/cm²

*Clad/base metal interface. (From Table 6-2)

2 INTRODUCTION

This report presents the results of the examination of Capsule T, the fifth capsule removed from the reactor in the continuing surveillance program which monitors the effects of neutron irradiation on the Dominion Energy Kewaunee Power Station (KPS) reactor pressure vessel materials under actual operating conditions. Capsule T was withdrawn and tested as it relates to the NRC requirements of the Safety Evaluation dated May 21, 2001 [Reference 22]. The first application of the Master Curve approach for an irradiated reactor vessel weld metal was approved by the NRC for the Kewaunee Power Station (KPS) in 2001 (*Safety Evaluation by the Office of Nuclear Reactor Include the Use of a Master Curve-based Methodology for Reactor Pressure Vessel Integrity Assessment*, Docket No. 50-305, May 2001). The testing of Capsule T was performed as commitment to the NRC as a part of this Safety Evaluation and included the requirement to perform additional fracture toughness tests to help validate the previous Master Curve evaluation accepted by the NRC.

The surveillance program for the KPS reactor pressure vessel materials was designed and recommended by the Westinghouse Electric Corporation. A description of the surveillance program and the pre-irradiation mechanical properties of the reactor vessel materials are presented in WCAP-8107, Revision 0, "Wisconsin Public Service Corporation Kewaunee Nuclear Power Plant Reactor Vessel Radiation Surveillance Program." [Reference 3]. The surveillance program was planned to cover the 40-year design life of the reactor pressure vessel and was based on ASTM E 185-73, "Recommended Practice for Surveillance Tests on Structural Materials for Nuclear Reactors" [Reference 4]. Capsule T was removed from the reactor after 24.6 EFPY of exposure and shipped to the Westinghouse Science and Technology Department Hot Cell Facility, where the post-irradiation mechanical testing of the Charpy V-notch impact and tensile surveillance specimens was performed for the forging, correlation monitor, and weld material CVN specimens. The testing details, as discussed in the Forward to this report, satisfy the requirements of ASTM E 185-82, as amended by the Safety Evaluation from May 2001 [Reference 22].

In addition to summarizing the testing of and the post-irradiation data obtained from surveillance Capsule T removed from the KPS reactor vessel and discussing the analysis of the data, the report also presents the results of the master curve testing for circumferential weld 1P3571 that was documented in WCAP-16609-NP [Reference 5]. A full CVN curve was not developed for the surveillance weld, however, the transition temperature values representing 30 ft-lbs, 50 ft-lbs and 35 mils were determined along with the drop in Upper Shelf Energy (USE). Reconstitution of specimens needed to determine these material properties was performed in accordance with ASTM E 1253-99 [Reference 6].

This page intentionally blank

3 BACKGROUND

The ability of the large steel pressure vessel containing the reactor core and its primary coolant to resist fracture constitutes an important factor in ensuring safety in the nuclear industry. The beltline region of the reactor pressure vessel is the most critical region of the vessel because it is subjected to significant fast neutron bombardment. The overall effects of fast neutron irradiation on the mechanical properties of low alloy, ferritic pressure vessel steels such as SA533 Grade B-1 (base material of the KPS reactor pressure vessel beltline) are well documented in the literature. Generally, low alloy ferritic materials show an increase in hardness and tensile properties and a decrease in ductility and toughness during high-energy irradiation. The primary role of fracture mechanics testing of RPV steels is to provide estimates of the fracture toughness to be used in the analysis of reactor pressure vessel integrity. Therefore, analysis of the fracture behavior of the steel requires characterization of the toughness over a range of temperatures encompassing the ductile-to-brittle transition.

One such method for ensuring the integrity of reactor pressure vessels has been presented in "Fracture Toughness Criteria for Protection Against Failure," Appendix G to Section XI of the ASME Boiler and Pressure Vessel Code [Reference 7]. The method uses fracture mechanics concepts and is based on the reference nil-ductility transition temperature (RT_{NDT}).

RT_{NDT} is defined as the greater of either the drop weight nil-ductility transition temperature (NDTT per ASTM E-208 [Reference 8]) or the temperature 60°F less than the 50 ft-lb (and 35-mil lateral expansion) temperature as determined from Charpy specimens oriented perpendicular (transverse) to the major working direction of the plate. The RT_{NDT} of a given material is used to index that material to a reference stress intensity factor curve (K_{Ic} curve) which appears in Appendix G to the ASME Code [Reference 7]. The K_{Ic} curve is a lower bound of static fracture toughness results obtained from several heats of pressure vessel steel. When a given material is indexed to the K_{Ic} curve, allowable stress intensity factors can be obtained for this material as a function of temperature. Allowable operating limits can then be determined using these allowable stress intensity factors.

RT_{NDT} and, in turn, the operating limits of nuclear power plants can be adjusted to account for the effects of radiation on the reactor vessel material properties. The changes in mechanical properties of a given reactor pressure vessel steel, due to irradiation, can be monitored by a reactor vessel surveillance program, such as the KPS reactor vessel radiation surveillance program [Reference 3], in which a surveillance capsule is periodically removed from the operating nuclear reactor and the encapsulated specimens tested. The increase in the average Charpy V-notch 30 ft-lb temperature (ΔRT_{NDT}) due to irradiation is added to the initial RT_{NDT} , along with a margin (M) to cover uncertainties, to adjust the RT_{NDT} (ART) for radiation embrittlement. This ART (RT_{NDT} initial + M + ΔRT_{NDT}) is used to index the material to the K_{Ic} curve and, in turn, to set operating limits for the nuclear power plant that take into account the effects of irradiation on the reactor vessel materials.

In addition to the traditional RT_{NDT} approach used in characterizing the fracture toughness of ferritic steels, the development of the Master Curve testing procedure has provided a powerful new tool in determining the fracture toughness of a material.

The development of elastic-plastic fracture mechanics techniques introduced a new fracture toughness measure, the J-integral, which can be measured in small specimens. The J-integral has been used both as

a measure of ductile fracture toughness and to estimate equivalent linear-elastic toughness values in the lower transition region. The Master Curve provides a framework for using the linear-elastic toughness estimates derived from the J-integral to characterize the fracture toughness in the ductile-to-brittle transition regime.

Ferritic steels used in RPV construction exhibit a characteristic transition from brittle behavior at low temperatures to ductile behavior at higher temperatures. Under normal operating conditions, a nuclear RPV should always be in the high toughness ductile region. The stresses in the RPV must be carefully controlled during heatup and cooldown to avoid brittle fracture. It is therefore important to characterize the temperature at which the ductile-to-brittle transition occurs in a pressure vessel steel. A complete characterization of the transition requires testing at multiple temperatures. The temperature range over which this transition occurs depends on two factors: the properties of the material and the loading conditions. There are numerous tests designed to characterize the ductile-to-brittle transition in ferritic steels. Each test presents a unique combination of specimen geometry and loading and therefore a ductile-to-brittle behavior that is specific to the test method. This test-specific behavior is generally described in terms of a characteristic transition temperature. While it is common to speak of the ductile-to-brittle transition temperature of a material, there is not a unique definition of this value. In practice, any definition of transition temperature must refer to the test procedure (e.g., Charpy V-notch 30 ft-lb transition, drop weight nil-ductility temperature, and Master Curve T_0). In each test, the transition temperature describes the ductile-to-brittle transition in the material.

For RPV steels, the most commonly used tests are the nil-ductility drop weight test and the Charpy impact test. The characteristic temperature in the drop weight test is defined as the nil-ductility point at the low temperature end of the transition (NDT). For nuclear RPV steels, the Charpy V-notch transition is usually characterized by the temperature at a specific absorbed energy level (30 ft-lb or 50 ft-lb). However, Charpy V-notch tests may also be characterized in terms of the fracture appearance transition temperature (FATT) or the temperature at a specific level deformation (e.g., 35 mils lateral expansion).

Although it has long been recognized that fracture toughness, as defined in ASTM E 1820 [Reference 9], undergoes a ductile-to-brittle transition (which is what is really needed for accurate integrity assessment), a characteristic transition temperature for the fracture toughness has only recently been defined. The development of J-integral based techniques for measuring fracture toughness (J_C) in the transition region has allowed a much clearer definition of fracture toughness behavior in ferritic steels. Based on this experience, it has been observed that ferritic steels have a common temperature dependence of fracture toughness in the transition regime. It was this observation that led Wallin to the definition of a Master Curve [Reference 10] that allows the fracture toughness for any ferritic steel to be characterized solely in terms of a reference temperature, T_0 , corresponding to a fracture toughness of 100 MPa-m^{1/2} (91 ksi-in^{1/2}). ASTM E 1921 [Reference 11], which was originally adopted in 1997, provides a standard test method for the determination of T_0 . This reference temperature can be used to index the Master Curve or some bounding curve. This behavior is in sharp contrast to the Charpy V-notch behavior, where both the transition curve shape and characteristic temperature vary between materials and after irradiation.

The ductile-to-brittle transition behavior of a material may be characterized using any combination of the above mentioned tests. The availability of test specimens and the expense of performing the tests generally determine the particular test employed to characterize the material transition temperature. While there are multiple measures of the ductile-to-brittle transition, the underlying mechanisms of deformation and fracture are clearly inter-related. For this reason, the various measures of transition temperature tend to be correlated. These correlations allow a determination from one test technique to be used to estimate characteristic transition temperatures for the remaining tests. While it is difficult to demonstrate a correlation between NDT and the Charpy V-notch related transition temperature, recent test

results have indicated a reasonable correlation between Charpy V-notch transition temperatures and T_0 . This correlation is fundamental to all Charpy based procedures for estimating toughness values in current RPV integrity analysis.

This page intentionally blank

4 DESCRIPTION OF PROGRAM

Six surveillance capsules for monitoring the effects of neutron exposure on the KPS reactor pressure vessel core region (beltline) materials were inserted in the reactor vessel prior to initial plant start-up. The six capsules were positioned in the reactor vessel between the thermal shield and the vessel wall as shown in Figure 4-1. The vertical center of the capsules is opposite the vertical center of the core. The capsules contained specimens made from intermediate shell forging 122X208VA1, lower shell forging 123X167VA1 and weld metal fabricated with 3/16-inch Mil B-4 weld filler wire, heat number 1P3571 and Linde 1092 flux, lot number 3958. This is the identical weld sire heat and flux as that used in the actual fabrication of the KPS vessel intermediate to lower shell girth weld seam, which has been the limiting beltline material in the KPS reactor pressure vessel.

Capsule T, the fifth capsule removed as a part of the surveillance program, was removed after 24.6 effective full power years (EFPY) of plant operation. This capsule contained Charpy V-notch impact specimens, tensile specimens and Wedge Opening Loading (WOL) specimens from the two shell ring forgings of the reactor vessel and associated weld metal, and Charpy V-notch impact specimens of the Heat Affected Zone (HAZ) and the ASTM correlation monitor material. All test specimens were machined from the 1/4 thickness location of the forgings after performing a simulated post-weld, stress-relieving treatment on the test material. The test specimens represent material taken at least one forging thickness from the quenched ends of the forging. Specimens were machined from weld and HAZ metal from a stress-relieved weldment joining the intermediate shell forging 122X208VA1 and lower shell forging 123C167VA1. All HAZ specimens were obtained from the weld HAZ of the intermediate shell forging 122X208VA1.

All base metal Charpy V-notch impact and tensile specimens were machined with the longitudinal axis of the specimen parallel to the principal working direction of the forgings. The notch of the forging Charpy specimens was machined such that the direction of crack propagation in the specimen was transverse to the working direction. This orientation is termed "tangential." Charpy V-notch and tensile specimens from the weld metal were oriented such that the longitudinal axis of the specimen was normal to the welding direction. The notch of the weld Charpy specimens was machined such that the direction of crack propagation in the specimen was in the welding direction.

The chemical composition and heat treatment of the unirradiated surveillance materials are presented in Tables 4-1 through 4-4. The data in Tables 4-1 through 4-4 were obtained from the unirradiated surveillance program, WCAP-8107 Appendices A and B, and from the evaluation of the weld metal 1P3571 documented in WCAP-15074 [Reference 12].

Capsule T contained dosimeter wires of pure iron, copper, nickel, and aluminum-0.15 weight percent cobalt (cadmium-shielded and unshielded). In addition, cadmium shielded dosimeters of neptunium (NP^{237}) and uranium (U^{238}) were placed in the capsule to measure the integrated flux at specific neutron energy levels.

The capsule contained thermal monitors made from two low-melting-point eutectic alloys and sealed in Pyrex tubes. These thermal monitors were used to define the maximum temperature attained by the test specimens during irradiation. The composition of the two eutectic alloys and their melting points are as follows:

2.5% Ag, 97.5% Pb

Melting Point: 579°F (304°C)

1.75% Ag, 0.75% Sn, 97.5% Pb

Melting Point: 590°F (310°C)

The arrangement of the various testing specimens, dosimeters, and thermal monitors contained in Capsule T is shown in Figures 4-2 and 4-3.

Table 4-1 Chemical Composition (wt%) of the KPS Reactor Vessel Surveillance Materials			
Element	Intermediate Shell Forging 122X208VA1	Lower Shell Forging 123X167VA1	Weld Metal
C	0.21	0.20	0.12
Si	0.25	0.28	0.20
Mo	0.58	0.58	0.48
Cu	0.06	0.06	0.219 ^(a)
Ni	0.71	0.75	0.724 ^(a)
Mn	0.69	0.79	1.37
Cr	0.40	0.35	0.090
V	<0.02	<0.02	0.002
Co	0.011	0.012	<0.001
Sn	0.01	0.01	0.004
Ti	<0.001	<0.001	<0.001
Zr	0.001	0.001	<0.001
As	0.001	0.004	0.004
Sb	<0.001	0.001	0.001
S	0.011	0.009	0.011
P	0.01	0.01	0.016
Al	0.004	0.006	0.010
B	<0.003	<0.003	<0.003
N ₂	0.006	0.010	0.012
Zn	---	---	<0.001

Notes:

- a. Based upon average results as described in report WCAP-15074, Revision 1.

Material	Temperature (°F)	Time (hrs)	Coolant
Intermediate Shell Forging 122X208VA1	Austenitizing @ 1550	8	Water Quenched
	Tempered @ 1230	14	Air Cooled
	Stress Relieved @ 1150	21	Furnace Cooled
Lower Shell Forging 123X167VA1	Austenitizing @ 1550	8	Water Quenched
	Tempered @ 1230	14	Air Cooled
	Stress Relieved @ 1150	21	Furnace Cooled
Weldment	Stress Relieved @ 1150	19.25 hrs.	Furnace Cooled

Element	Chemical Analysis (wt%)
C	0.22
Mn	1.48
P	0.012
S	0.018
Si	0.25
Ni	0.68
Mo	0.52
Cu	0.14

Table 4-4 Heat Treatment of the A533 Grade B, Class 1 ASTM Correlation Monitor Material (HSST Plate 02) in the KPS Vessel Surveillance Program

Material	Temperature (°F)	Time (hrs)	Coolant
Correlation Monitor Material	1675 ± 25	4	Air Cooled
	1600 ± 25	4	Water Quenched
	Tempered @ 1225 ± 25	4	Furnace Cooled
	Stress Relieved @ 1150 ± 25	40	Furnace Cooled to 600°F

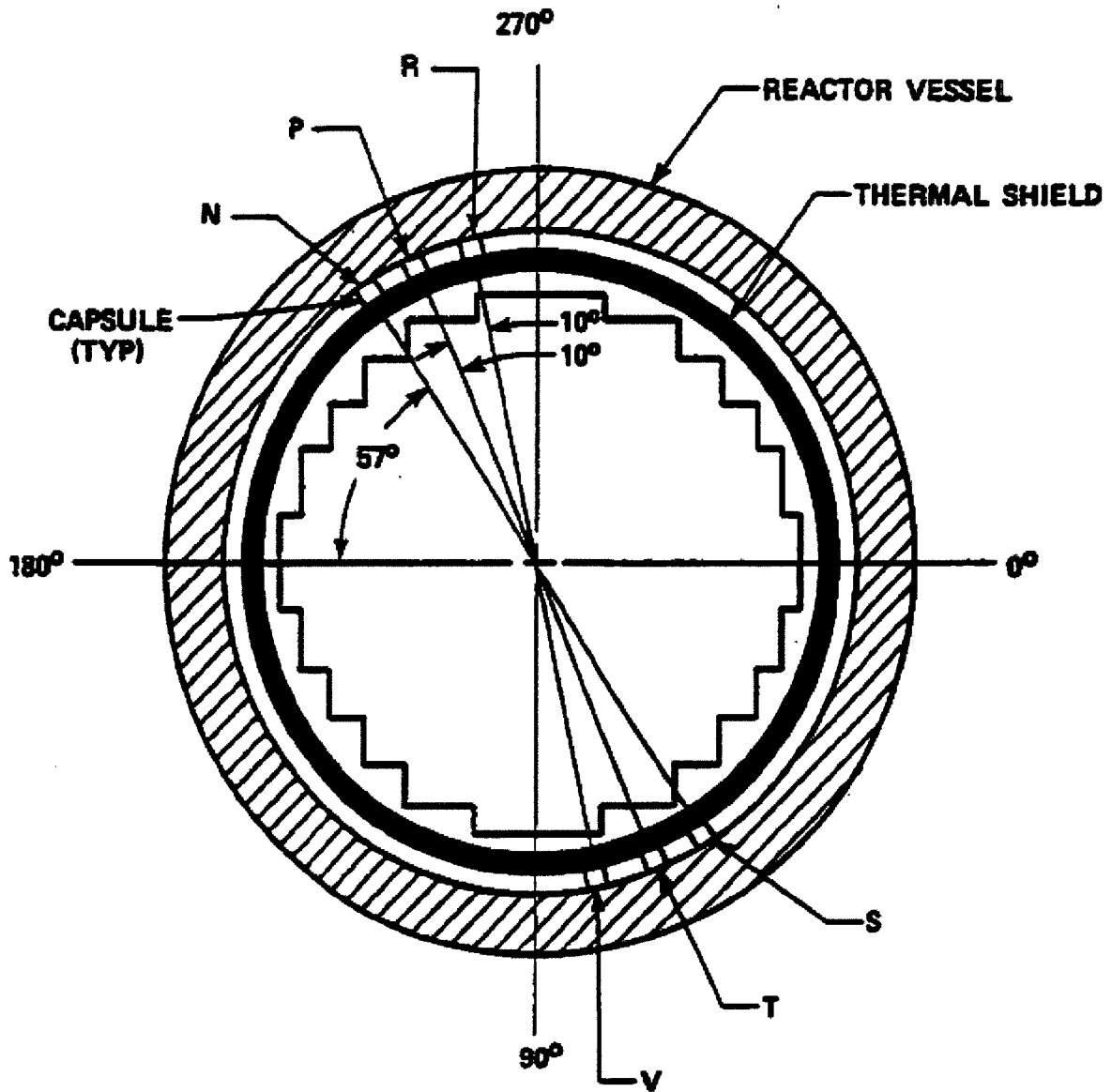


Figure 4-1 Arrangement of Surveillance Capsules in the KPS Reactor Vessel

- LEGEND:**
- P** – INTERMEDIATE SHELL FORGING 122X208VA1 (TANGENTIAL)
 - S** – LOWER SHELL FORGING 123X167VA1 (TANGENTIAL)
 - W** – WELD METAL (HEAT # 1P3571)
 - H** – HEAT AFFECTED ZONE METAL
 - R** – CORRELATION MONITOR MATERIAL

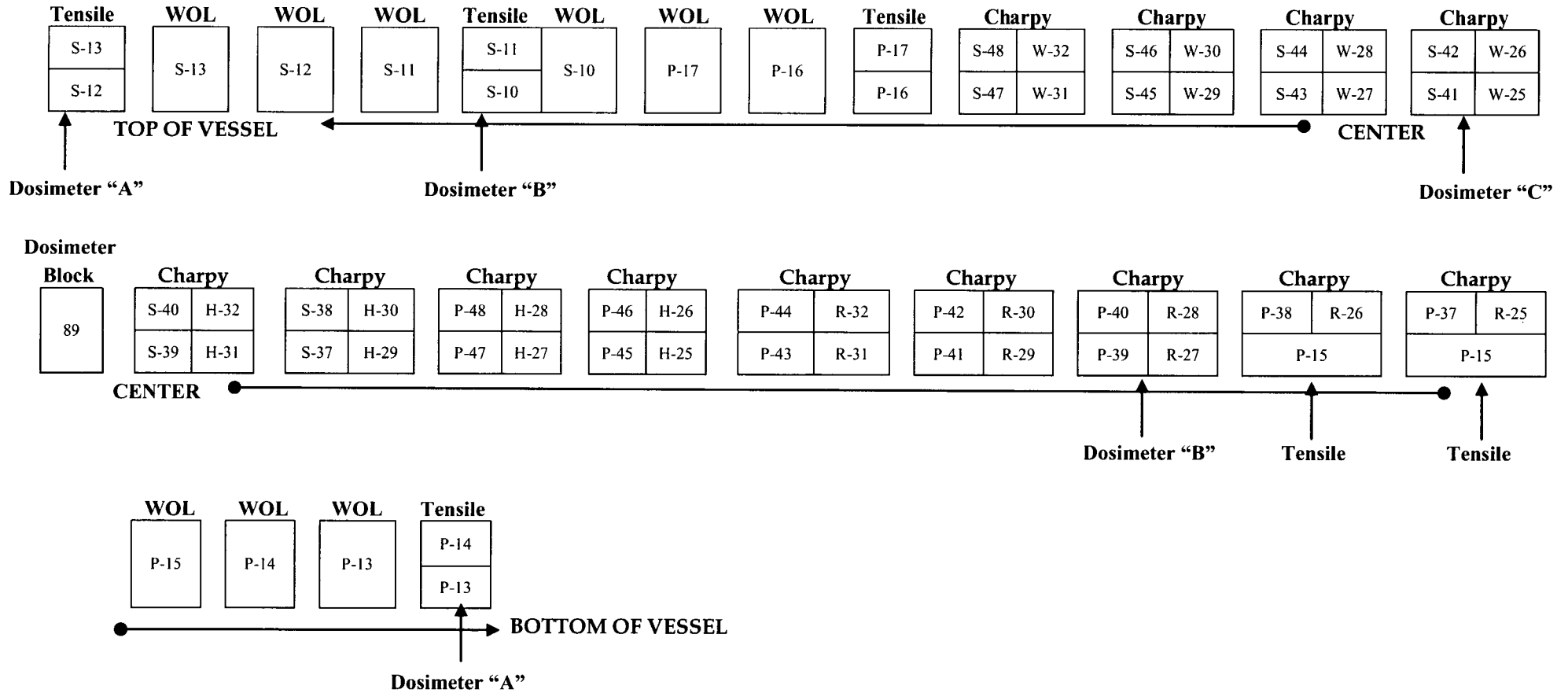
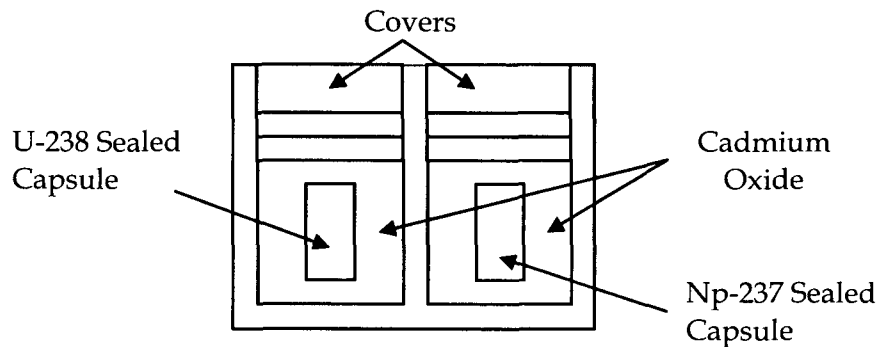


Figure 4-2 Capsule T Diagram Showing the Location of Specimens and Dosimeters

This page intentionally blank

Dosimeter Block "89"



Dosimeter and Thermal Monitors

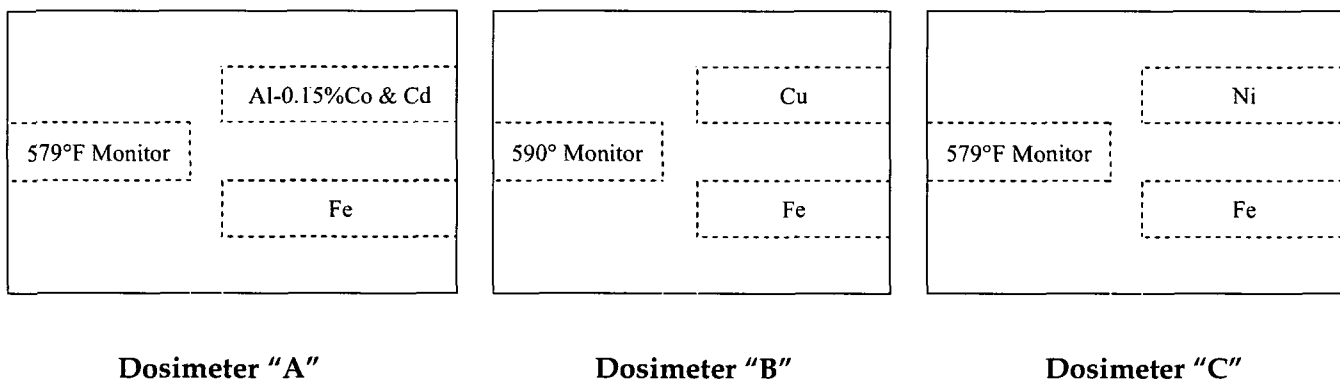


Figure 4-3 Dosimeter and Thermal Monitor Layout for KPS Capsule T

This page intentionally blank

5 TESTING OF SPECIMENS FROM CAPSULE T

5.1 OVERVIEW

The post-irradiation mechanical testing of the Charpy V-notch impact specimens and tensile specimens was performed in the Remote Metallographic Facility (RMF) at the Westinghouse Science and Technology Department. Testing on Charpy and tensile specimens was performed in accordance with 10CFR50, Appendices G and H [Reference 2], ASTM Specification E185-82 [Reference 13], and Westinghouse Procedure RMF 8402, Revision 2 [Reference 14] as detailed by Westinghouse RMF Procedures 8102, Revision 3 [Reference 15], and 8103, Revision 2 [Reference 16].

Upon receipt of the capsule at the hot cell laboratory, the specimens and spacer blocks were carefully removed, inspected for identification number, and checked against the master list in WCAP-8107 [Reference 3]. No discrepancies were found.

Examination of the two low-melting point 579°F (304°C) and 590°F (310°C) eutectic alloys indicated no melting of either type of thermal monitor. Based on this examination, the maximum temperature to which the test specimens were exposed was less than 579°F (304°C).

The Charpy impact tests were performed per ASTM Specification E23-02a [Reference 17] and RMF Procedure 8103 [Reference 16] on a Tinius-Olsen Model 74, 358J machine. The tup (striker) of the Charpy impact test machine is instrumented with an Instron Impulse instrumentation system, feeding information into an IBM compatible computer. With this system, load-time and energy-time signals can be recorded in addition to the standard measurement of Charpy energy (E_D). From the load-time curve (Appendix B), the load of general yielding (P_{GY}), the time to general yielding (T_{GY}), the maximum load (P_M), and the time to maximum load (t_M) can be determined. Under some test conditions, a sharp drop in load indicative of fast fracture was observed. The load at which fast fracture was initiated is identified as the fast fracture load (P_F), and the load at which fast fracture terminated is identified as the arrest load (P_A).

The energy at maximum load (E_M) was determined by comparing the energy-time record and the load-time record. The energy at maximum load is approximately equivalent to the energy required to initiate a crack in the specimen. Therefore, the propagation energy for the crack (E_p) is the difference between the total energy to fracture (E_D) and the energy at maximum load (E_M).

The yield stress (σ_Y) was calculated from the three-point bend formula having the following expression:

$$\sigma_Y = (P_{GY} * L) / [B * (W - a)^2 * C] \quad (1)$$

where: L = distance between the specimen supports in the impact machine
 B = the width of the specimen measured parallel to the notch
 W = height of the specimen, measured perpendicularly to the notch
 a = notch depth

The constant C is dependent on the notch flank angle (ϕ), notch root radius (ρ) and the type of loading (i.e., pure bending or three-point bending). In three-point bending, for a Charpy specimen in which $\phi = 45^\circ$ and $\rho = 0.010$ inch, Equation 1 is valid with $C = 1.21$. Therefore, (for $L = 4W$),

$$\sigma_y = (P_{GY} * L) / [B * (W - a)^2 * 1.21] = (3.305 * P_{GY} * W) / [B * (W - a)^2] \quad (2)$$

For the Charpy specimen, $B = 0.394$ inch, $W = 0.394$ inch and $a = 0.079$ inch. Equation 2 then reduces to:

$$\sigma_y = 33.3 * P_{GY} \quad (3)$$

where σ_y is in units of psi and P_{GY} is in units of lbs. The flow stress was calculated from the average of the yield and maximum loads, also using the three-point bend formula.

The symbol A in columns 5, 6, and 7 of Tables 5-5 through 5-8 is the cross-section area under the notch of the Charpy specimens:

$$A = B * (W - a) = 0.1241 \text{ sq.in.} \quad (4)$$

Percent shear was determined from post-fracture photographs using the ratio-of-areas methods in compliance with ASTM Specification E23-02a and A370-97a [Reference 18]. The lateral expansion was measured using a dial gage rig similar to that shown in the same specification.

Tensile tests were performed on a 20,000-pound Instron, split-console test machine (Model 1115) per ASTM Specification E8-04 [Reference 19] and E21-03 [Reference 20], and Procedure RMF 8102. All pull rods, grips, and pins were made of Inconel 718. The upper pull rod was connected through a universal joint to improve axiality of loading. The tests were conducted at a constant crosshead speed of 0.05 inches per minute throughout the test.

Extension measurements were made with a linear variable displacement transducer extensometer. The extensometer knife-edges were spring-loaded to the specimen and operated through specimen failure. The extensometer gage length was 1.00 inch. The extensometer is rated as Class B-2 per ASTM E83-93 [Reference 21].

Elevated test temperatures were obtained with a three-zone electric resistance split-tube furnace with a 9-inch hot zone. All tests were conducted in air. Because of the difficulty in remotely attaching a thermocouple directly to the specimen, the following procedure was used to monitor specimen temperatures. Chromel-Alumel thermocouples were positioned at the center and at each end of the gage section of a dummy specimen and in each tensile machine gripper. In the test configuration, with a slight load on the specimen, a plot of specimen temperature versus upper and lower tensile machine gripper and controller temperatures was developed over the range from room temperature to 550°F. During the actual testing, the grip temperatures were used to obtain desired specimen temperatures. Experiments have indicated that this method is accurate to $\pm 2^\circ\text{F}$.

The yield load, ultimate load, fracture load, total elongation, and uniform elongation were determined directly from the load-extension curve. The yield strength, ultimate strength, and fracture strength were

calculated using the original cross-sectional area. The final diameter and final gage length were determined from post-fracture photographs. The fracture area used to calculate the fracture stress (true stress at fracture) and percent reduction in area was computed using the final diameter measurement.

The fracture toughness of the surveillance specimens is measured in terms of the J-integral. ASTM E 1820 provides a general procedure for conducting J-integral tests. The Master Curve used in ASTM E 1921 describes the temperature dependence of the cleavage initiation toughness. A cleavage event is readily identifiable as a rapid, unstable crack advance. Cleavage initiation implies that this fracture instability must occur prior to the onset of significant stable tearing crack extension. For a known starting crack length, the elastic and plastic contributions to the J-integral can be determined by measuring the specimen load and the amount of plastic work applied to the specimen. The testing procedure requires unloading compliance measurements to demonstrate that stable tearing has not initiated prior to the cleavage failure. If cleavage initiation occurs and the measurement meets the various validity requirements of the testing standard, the value of the J-integral at the point of instability is defined as J_C . The equivalent linear elastic plane-strain fracture toughness at cleavage instability is K_{Jc} . The Master Curve describes the temperature dependence of K_{Jc} .

The determination of the fracture toughness transition temperature, T_0 , requires multiple measurements of K_{Jc} . In the original testing program, fracture toughness measurements were conducted on irradiated weld specimens from KPS Capsule S and Maine Yankee Capsule A-35. Unirradiated archival material from the KPS surveillance weld was also tested. Fracture toughness values for the unirradiated Maine Yankee were provided by the utility. Additional fracture toughness tests were conducted as part of the surveillance testing program for KPS Capsule T.

The first application of the Master Curve approach for an irradiated reactor vessel weld metal (Heat # 1P3571) was approved by the NRC for the Kewaunee Power Station (KPS) in 2001 [Reference 22]. In accordance with the NRC SE, the transition temperature values representing 30 ft-lbs, 50 ft-lbs, 35 mils, and the USE needed to be determined without having to meet the requirement of developing a full Charpy V-notch curve. The original 8 weld specimens that were contained in Capsule T were used for Master Curve testing. It was decided that the HAZ specimens would be reconstituted in accordance with ASTM E 1253 with five specimens being made available for additional Master Curve testing and 3 specimens available for Charpy testing. The reconstituted specimens were taken from the weld portion of the HAZ specimens and were deemed representative of the weld material. The methodology used to determine the transition temperature properties and the drop in USE for the reconstituted HAZ specimens is discussed in Appendix D.

5.2 CHARPY V-NOTCH IMPACT TEST RESULTS

The results of the Charpy V-notch impact tests performed on the various materials contained in Capsule T, which received a fluence of 5.62×10^{19} n/cm² ($E > 1.0$ MeV) in 24.6 EFPY of operation, are presented in Tables 5-1 through 5-10 and are plotted in Figures 5-1 through 5-11.

The transition temperature increases and upper shelf energy decreases for the Capsule T materials are summarized in Table 5-9 and led to the following results:

Irradiation of the reactor vessel intermediate shell forging 122X208VA1 Charpy specimens, oriented with the longitudinal axis of the specimen parallel to the major working direction (tangential orientation), resulted in an irradiated 30 ft-lb transition temperature of 65°F and an irradiated 50 ft-lb transition temperature of 110°F. This results in a 30 ft-lb transition temperature increase of 90°F and a 50 ft-lb transition temperature increase of 95°F for the longitudinal oriented specimens. See Table 5-9.

Irradiation of the reactor vessel lower shell forging 123X167VA1 Charpy specimens, oriented with the longitudinal axis of the specimen perpendicular to the major working direction (tangential orientation), resulted in an irradiated 30 ft-lb transition temperature of 20°F and an irradiated 50 ft-lb transition temperature of 50°F. This results in a 30 ft-lb transition temperature increase of 70°F and a 50 ft-lb transition temperature increase of 75°F for the longitudinal oriented specimens. See Table 5-9.

Irradiation of the correlation monitor material Charpy specimens resulted in an irradiated 30 ft-lb transition temperature of 220°F and an irradiated 50 ft-lb transition temperature of 245°F. This results in a 30 ft-lb transition temperature increase of 175°F and a 50 ft-lb transition temperature increase of 165°F. See Table 5-9.

Irradiation of the reactor vessel representative weld Charpy specimens reconstituted from the HAZ material resulted in an irradiated 30 ft-lb transition temperature of 221°F and an irradiated 50 ft-lb transition temperature of 285°F. This results in a 30 ft-lb transition temperature increase of 271°F and a 50 ft-lb transition temperature increase of 295°F for the HAZ specimens. See Table 5-9.

The average upper shelf energy of the intermediate shell forging 122X208VA1 (tangential orientation) resulted in an average energy decrease of 21 ft-lb after irradiation. This results in an irradiated average upper shelf energy of 139 ft-lb for the tangentially oriented specimens. See Table 5-9.

The average upper shelf energy of the lower shell forging 123X167VA1 (tangential orientation) resulted in an average energy decrease of 13 ft-lb after irradiation. This results in an irradiated average upper shelf energy of 144 ft-lb for the tangentially oriented specimens. See Table 5-9.

The average upper shelf energy of the correlation monitor material Charpy specimens resulted in an average energy decrease of 32 ft-lb after irradiation. This results in an irradiated average upper shelf energy of 91 ft-lb for the correlation monitor material specimens. See Table 5-9.

The average upper shelf energy of the representative weld metal from reconstituted HAZ Charpy specimens resulted in an average energy decrease of 54 ft-lb after irradiation. An irradiated average upper shelf energy of 72 ft-lb for the representative weld metal from the reconstituted HAZ specimens was measured. See Table 5-9.

A comparison, as presented in Table 5-10, of the KPS reactor vessel surveillance material test results with the Regulatory Guide 1.99, Revision 2 predictions led to the following conclusions:

- Two out of the five measured 30 ft-lb shifts in transition temperature values of the intermediate shell forging 122X208VA1 (tangential orientation) are greater than the Regulatory Guide 1.99, Revision 2, predictions.
- Two out of the five measured 30 ft-lb shifts in transition temperature values of the lower shell forging 123X167VA1 (tangential orientation) are greater than the Regulatory Guide 1.99, Revision 2, predictions.
- Three of the five measured 30 ft-lb shifts in transition temperature value of the weld metal are greater than the Regulatory Guide 1.99, Revision 2, predictions.
- All of the correlation monitor material 30 ft-lb shifts in transition temperature were greater than the Regulatory Guide 1.99, Revision 2, prediction.
- The measured percent decrease in upper shelf energy for all the surveillance materials contained in the KPS surveillance program are less than the Regulatory Guide 1.99, Revision 2 predictions with the exception of one weld measurement.

All beltline materials exhibit a more than adequate upper shelf energy level for continued safe plant operation and are predicted to maintain an upper shelf energy greater than 50 ft-lb throughout the extended life of the vessel (33 EFPY) as required by 10CFR50, Appendix G.

The fracture appearance of each irradiated Charpy specimen from the various surveillance Capsule T materials is shown in Figures 5-12 through 5-15 and shows an increasingly ductile or tougher appearance with increasing test temperature.

The load-time records for individual instrumented Charpy specimen tests are shown in Appendix B. Appendix D presents the curve fits for the Charpy specimens from Capsule T along with a detailed explanation on how the best-fit line was drawn for the weld data where only three PCVN specimens were available.

5.3 TENSILE TEST RESULTS

The results of the tensile tests performed on the various materials contained in Capsule T irradiated to 5.62×10^{19} n/cm² ($E > 1.0$ MeV) are presented in Table 5-11 and are compared with unirradiated results as shown in Figures 5-16 and 5-17. Note that no tensile weld specimens were contained in Capsule T. A summary of previous tensile test results for weld heat 1P3571 is contained in Table 5-12.

The results of the tensile tests performed on the intermediate shell forging 122X208VA1 (tangential orientation) indicated that irradiation to 5.62×10^{19} n/cm² ($E > 1.0$ MeV) caused approximately a 12 to 13 ksi increase in the 0.2 percent offset yield strength and approximately a 10 to 12 ksi increase in the ultimate tensile strength when compared to unirradiated data (see Figure 5-16).

The results of the tensile tests performed on the lower shell forging 123X167VA1 (tangential orientation) indicated that irradiation to 5.62×10^{19} n/cm² (E > 1.0 MeV) caused approximately a 13 to 15 ksi increase in the 0.2 percent offset yield strength and approximately a 13 to 14 ksi increase in the ultimate tensile strength when compared to unirradiated data (see Figure 5-17).

The fractured tensile specimens for the shell forgings 122X208VA1 and 123X167VA1 are shown in Figures 5-18 and 5-19. The engineering stress-strain curves for the tensile tests are shown in Figures 5-20 through 5-24.

5.4 MASTER CURVE TEST RESULTS

The determination of the fracture toughness transition temperature, T_0 , requires multiple measurements of K_{Jc} . In the original testing program, fracture toughness measurements were conducted on irradiated weld specimens from KPS Capsule S and Maine Yankee Capsule A-35. Unirradiated archival material from the KPS surveillance weld was also tested. Fracture toughness values for the unirradiated Maine Yankee were provided by the utility. Additional fracture toughness tests were conducted as part of the surveillance testing program for KPS Capsule T.

The initial testing was carried out using the eight weld Charpy specimens from Capsule T. The Charpy V-notches in the surveillance specimens were modified to produce sharp crack starters for the pre-cracks. The specimens were side-grooved after pre-cracking to provide uniform crack fronts for testing. Note that specimens from the previous capsules and for the unirradiated condition were not side-grooved; use of side-grooved specimens is now recommended in ASTM E 1921, but side-grooving is not a requirement.

The minimum number of specimens required to determine T_0 is set by ASTM E1921. However the standard also indicates that additional tests may be required to minimize the effect of material variability. All eight of the weld Charpy V-notch specimens were converted to PCVN specimens and tested at 136°F. The initial results verified previous observations of significant variability in data from weld 1P3571. For materials with significant variability, the testing of a minimum of twelve specimens is recommended by ASTM E1921 to minimize the effects of the scatter. In accordance with the recommendations of the standard, an additional four PCVN specimens were reconstituted using the weld portion of unbroken HAZ specimens. These additional weld specimens were also tested at 136°F as indicated in Table 5-13. The ASTM Standard requires that all measurements be included in the T_0 determination. The values for the measured K_{Jc} are listed as well as the 1T size adjusted values, $K_{Jc(1T)}$.

A summary of all of the Master Curve testing data for 1P3571 along with photographs of the fracture surfaces are presented in Appendix C. Cleavage fracture points are indicated by the sharp drops in the load-displacement curves. The elastic contribution to the fracture toughness is determined by the load at failure, the plastic contribution is determined by the area under the load-displacement curve (plastic work) up to failure. Details of the fracture toughness analysis are discussed in WCAP-16609-NP, "Master Curve Assessment of the Kewaunee Power Station Weld Metal."

The cleavage initiation point in any individual specimen is determined by the distribution of potential cleavage initiation sites. The corresponding distribution of cleavage initiation toughness values can be described by a characteristic Weibull distribution. The scatter in the measured toughness values for weld 1P3571 is broader than the normal width of Weibull distributions in the Master Curve. This scatter can be attributed to inhomogeneous microstructure. This inhomogeneity is evident in the fracture surface photographs in Appendix C, which show broad bands across the specimen. The width of these bands, which is comparable to the thickness of the specimens, is believed to be related to individual weld passes. Variations in the density of cleavage initiation sites across the weld passes and between consecutive weld passes would explain the observed level of scatter.

5.5 WEDGE OPENING LOADING (WOL) SPECIMEN TESTS

Per the surveillance capsule testing contract, the WOL specimens were not tested and are being stored at the Westinghouse Science and Technology Center Hot Cell facility.

Table 5-1 Charpy V-notch Data for the Kewaunee Power Station Intermediate Shell Forging 122X208VA1 Irradiated to a Fluence of 5.62×10^{19} n/cm² (E > 1.0 MeV) (Tangential Orientation)

Sample Number	Temperature		Impact Energy		Lateral Expansion		Shear %
	°F	°C	ft-lbs	Joules	mils	mm	
P47	-50	-46	6	8	7	0.18	0
P46	50	10	22	30	17	0.43	10
P45	75	24	31	42	23	0.58	15
P43	100	38	65	88	50	1.27	40
P40	125	52	43	58	35	0.89	30
P37	150	66	81	110	57	1.45	60
P44	175	79	77	104	55	1.40	55
P41	200	93	109	148	74	1.88	85
P48	250	121	119	161	85	2.16	90
P38	325	163	140	190	82	2.08	100
P39	350	177	141	191	85	2.16	100
P42	400	204	137	186	84	2.13	100

**Table 5-2 Charpy V-notch Data for the Kewaunee Power Station Lower Shell Forging
123X167VA1 Irradiated to a Fluence of 5.62×10^{19} n/cm² (E > 1.0 MeV) (Tangential
Orientation)**

Sample Number	Temperature		Impact Energy		Lateral Expansion		Shear
	°F	°C	ft-lbs	Joules	mils	mm	%
S45	-50	-46	9	12	8	0.20	0
S47	0	-18	7	9	5	0.13	2
S40	25	-4	15	20	11	0.28	5
S38	50	10	67	91	52	1.32	20
S37	75	24	62	84	44	1.12	20
S48	100	38	124	168	77	1.96	90
S43	125	52	88	119	61	1.55	55
S44	150	66	97	132	67	1.70	65
S46	175	79	139	188	89	2.26	100
S41	250	121	142	193	86	2.18	100
S39	300	149	147	199	85	2.16	100
S42	350	177	146	198	83	2.11	100

Table 5-3 Charpy V-notch Data for the Kewaunee Power Station Surveillance Representative Weld Metal Irradiated to a Fluence of 5.62×10^{19} n/cm² (E > 1.0 MeV)

Sample Number	Temperature		Impact Energy		Lateral Expansion		Shear %
	°F	°C	ft-lbs	Joules	mils	mm	
H26	190	88	13	18	13	0.33	25
H27	215	102	36	49	28	0.71	45
H32	400	204	72	98	59	1.50	100

Table 5-4 Charpy V-notch Data for the Kewaunee Power Station Correlation Monitor Material Irradiated to a Fluence of 5.62×10^{19} n/cm² (E > 1.0 MeV)

Sample Number	Temperature		Impact Energy		Lateral Expansion		Shear %
	°F	°C	Ft-lbs	Joules	mils	mm	
R31	100	38	4	5	7	0.18	5
R30	200	93	15	20	11	0.28	15
R28	225	107	43	58	29	0.74	40
R26	250	121	46	62	32	0.81	50
R27	275	135	68	92	53	1.35	70
R29	300	149	93	126	66	1.68	85
R32	400	204	93	126	73	1.85	95
R25	450	232	87	118	69	1.75	100

**Table 5-5 Instrumented Charpy Impact Test Results for the Kewaunee Power Station Capsule T Intermediate Shell Forging
122X208VA1 Irradiated to a Fluence of 5.62×10^{19} n/cm² (E>1.0 MeV)**

Sample No.	Test Temp. (°F)	Charpy Energy E _D (ft-lb)	Normalized Energies (ft-lb/in ²)			Yield Load P _{GY} (lb)	Time to Yield t _{GY} (msec)	Max. Load P _M (lb)	Time to Max. t _M (msec)	Fast Fract. Load P _F (lb)	Arrest Load P _A (lb)	Yield Stress σ _Y (ksi)	Flow Stress (ksi)
			Charpy E _D /A	Max. E _M /A	Prop. E _p /A								
P47	-50	6	48	25	24	2816	0.13	2905	0.14	2905	0	94	95
P46	50	22	177	131	46	3246	0.14	4126	0.34	4121	0	108	123
P45	75	31	250	184	65	3496	0.14	4452	0.42	4437	0	116	132
P43	100	65	524	318	206	3370	0.15	4463	0.68	4229	0	112	130
P40	125	43	346	233	114	3225	0.15	4367	0.54	4352	0	107	126
P37	150	81	653	313	340	3231	0.15	4397	0.68	3980	580	108	127
P44	175	77	620	320	300	3234	0.19	4279	0.73	4021	671	108	125
P41	200	109	878	299	579	3191	0.15	4308	0.67	2935	1432	106	125
P48	250	119	959	298	661	2925	0.14	4176	0.68	2274	1466	97	118
P38	325	140	1128	305	823	3054	0.14	4314	0.68	N/A	N/A	102	123
P39	350	141	1136	299	837	3052	0.15	4138	0.69	N/A	N/A	102	120
P42	400	137	1104	292	812	2941	0.16	4111	0.69	N/A	N/A	98	117

Table 5-6 Instrumented Charpy Impact Test Results for Kewaunee Power Station Capsule T Lower Shell Forging 123X167VA1 Irradiated to a Fluence of 5.62×10^{19} n/cm² (E>1.0 MeV)

Sample No.	Test Temp. (°F)	Charpy Energy E _D (ft-lb)	Normalized Energies (ft-lb/in ²)			Yield Load P _{GY} (lb)	Time to Yield t _{GY} (msec)	Max. Load P _M (lb)	Time to Max. t _M (msec)	Fast Fract. Load P _F (lb)	Arrest Load P _A (lb)	Yield Stress σ _Y (ksi)	Flow Stress (ksi)
			Charpy E _D /A	Max. E _M /A	Prop. E _p /A								
S45	-50	9	73	41	31	3743	0.14	4075	0.17	4075	0	125	130
S47	0	7	56	34	23	3520	0.15	3533	0.16	3533	0	117	117
S40	25	15	121	69	51	3629	0.14	4411	0.22	4404	0	121	134
S38	50	67	540	331	208	3534	0.15	4620	0.68	4208	0	118	136
S37	75	62	500	331	169	3516	0.15	4636	0.68	4427	0	117	136
S48	100	124	999	346	653	3658	0.16	4801	0.69	3029	1533	122	141
S43	125	88	709	316	393	3338	0.15	4499	0.67	3862	469	111	130
S44	150	97	782	316	466	3230	0.15	4416	0.69	3281	707	108	127
S46	175	139	1120	311	809	3290	0.15	4438	0.68	N/A	N/A	110	129
S41	250	142	1144	302	843	3006	0.15	4306	0.68	N/A	N/A	100	122
S39	300	147	1184	312	872	3101	0.14	4367	0.68	N/A	N/A	103	124
S42	350	146	1176	297	879	3012	0.14	4254	0.67	N/A	N/A	100	121

Sample No.	Test Temp. (°F)	Charpy Energy E _D (ft-lb)	Normalized Energies (ft-lb/in ²)			Yield Load P _{GY} (lb)	Time to Yield t _{GY} (msec)	Max. Load P _M (lb)	Time to Max. t _M (msec)	Fast Fract. Load P _F (lb)	Arrest Load P _A (lb)	Yield Stress σ _Y (ksi)	Flow Stress (ksi)
			Charpy E _D /A	Max. E _M /A	Prop. E _P /A								
H26	190	13	105	42	63	3586	0.16	3780	0.17	3780	556	119	123
H27	215	36	290	149	141	3321	0.14	4861	0.35	4680	1157	111	136
H32	400	72	580	216	364	3263	0.14	4563	0.48	N/A	N/A	109	130

Sample No.	Test Temp. (°F)	Charpy Energy E _D (ft-lb)	Normalized Energies (ft-lb/in ²)			Yield Load P _{GY} (lb)	Time to Yield t _{GY} (msec)	Max. Load P _M (lb)	Time to Max. t _M (msec)	Fast Fract. Load P _F (lb)	Arrest Load P _A (lb)	Yield Stress σ _Y (ksi)	Flow Stress (ksi)
			Charpy E _D /A	Max. E _M /A	Prop. E _P /A								
R31	100	4	32	17	15	2109	0.12	2132	0.13	2132	0	70	71
R30	200	15	121	63	58	3204	0.14	4027	0.21	4027	0	107	120
R28	225	43	346	224	123	3538	0.15	4719	0.49	4708	1361	118	137
R26	250	46	371	235	135	3555	0.15	4811	0.50	4801	1282	118	139
R27	275	68	548	239	309	3355	0.15	4541	0.53	4455	2143	112	131
R29	300	93	749	240	509	3398	0.18	4599	0.54	2369	1571	113	133
R32	400	93	749	234	515	3380	0.19	4496	0.54	3466	3015	113	131
R25	450	87	701	222	479	3287	0.16	4438	0.51	N/A	N/A	109	129

Material	Average 30 (ft-lb) ^(a) Transition Temperature (°F)			Average 35 mil Lateral ^(b) Expansion Temperature (°F)			Average 50 ft-lb ^(a) Transition Temperature (°F)			Average Energy Absorption ^(a) at Full Shear (ft-lb)		
	Unirradiated	Irradiated	ΔT	Unirradiated	Irradiated	ΔT	Unirradiated	Irradiated	ΔT	Unirradiated	Irradiated	ΔE
Intermediate Shell Forging 122X208VA1 (Tangential)	-25	65	90	-15	100	115	15	110	95	160	139	21
Lower Shell Forging 123X167VA1 (Tangential)	-50	20	70	-45	50	95	-25	50	75	157	144	13
Reconstituted Representative Weld Metal (Heat # 1P3571)	-50	221	271	-35	249	284	-10	285	295	126	72	54
Correlation Monitor Material	45	220	175	60	245	185	80	245	165	123	91	32

- a. "Average" is defined as the value read from the curve fit through the data points of the Charpy tests (see Figures 5-1, 5-4, 5-7 and 5-10).
- b. "Average" is defined as the value read from the curve fit through the data points of the Charpy tests (see Figures 5-2, 5-5, 5-8 and 5-11).

Table 5-10 Comparison of the Kewaunee Power Station Surveillance Material 30 ft-lb Transition Temperature Shifts and Upper Shelf Energy Decreases with Regulatory Guide 1.99, Revision 2, Predictions

Material	Capsule	Fluence ($\times 10^{19}$ n/cm ² , E > 1.0 MeV)	30 ft-lb Transition Temperature Shift		Upper Shelf Energy Decrease	
			Predicted (°F) ^(a)	Measured (°F) ^(b)	Predicted (%) ^(a)	Measured (%) ^(c)
Intermediate Shell Forging 122X208VA1	V	0.586	31.45	0	17	0
	R	1.76	42.74	15	22	0
	P	2.61	46.51	25	24	2
	S	3.67	49.47	60	26	8
	T	5.62	52.73	90	29	13
Lower Shell Forging 123X167VA1	V	0.586	31.45	0	17	0
	R	1.76	42.74	20	22	3
	P	2.61	46.51	20	24	0
	S	3.67	49.47	50	26	3
	T	5.62	52.73	70	29	8
Surveillance Program Weld Metal	V	0.586	159.12	175	33	35
	R	1.76	216.22	235	42	38
	P	2.61	235.31	230	44	40
	S	3.67	250.29	250	49	49
	T	5.62	266.76	271	54	43
Correlation Monitor Material	V	0.586	86.7	95	21	11
	R	1.76	117.81	140	27	23
	P	2.61	128.21	155	29	18
	S	3.67	136.37	158	31	20
	T	5.62	145.35	175	35	26
Heat Affected Zone Material	V	0.586	---	80	---	19
	R	1.76	---	150	---	22
	P	2.61	---	220	---	24
	S	3.67	---	200	---	23
	T	5.62	---	(d)	---	(d)

Notes:

- (a) Based on Regulatory Guide 1.99, Revision 2, methodology using the mean weight percent values of copper and nickel of the surveillance material.
- (b) Calculated using measured Charpy data (See Appendix D).
- (c) Values are based on the definition of USE given in ASTM E185-82 with the exception of the representative weld specimen reconstituted from HAZ material, where the USE was defined by a single point.
- (d) Not required to be measured at a part of the NRC SE [Reference 22].

This page intentionally blank

Table 5-11 Tensile Properties of the Kewaunee Capsule T Reactor Vessel Surveillance Materials Irradiated to 5.62×10^{19} n/cm² (E > 1.0 MeV) ^(a)										
Material	Sample Number	Test Temperature (°F)	0.2% Yield Strength (ksi)	Ultimate Strength (ksi)	Fracture Load (kip)	Fracture Stress (ksi)	Fracture Strength (ksi)	Uniform Elongation (%)	Total Elongation (%)	Reduction in Area (%)
Intermediate Shell Forging 122X208VA1	P-13	75	80.1	100.2	3.05	201.0	62.1	10.1	23.7	69
	P-14	125	77.7	97.3	2.95	194.4	60.1	9.5	23.3	69
	P-15	200	74.4	93.2	2.83	206.4	57.6	8.9	22.4	72
	P-16	300	70.8	90.7	2.85	196.2	58.1	9.0	21.9	70
	P-17	550	68.8	92.1	3.05	189.9	62.1	9.0	21.2	67
Lower Shell Forging 123X167VA1	S-10	75	82.5	102.4	3.08	211.7	62.6	10.1	24.2	70
	S-11	125	80.5	100.3	3.10	198.5	63.2	8.9	21.8	68
	S-12	200	76.9	96.2	3.00	215.9	61.1	9.3	22.0	72
	S-13	550	71.5	95.1	3.25	161.6	66.2	8.7	20.0	59

Notes:

(a) No weld data is reported since Capsule T did not contain weld tensile specimens.

Source	Sample Number	Test Temp (F)	0.2% Yield Strength (ksi)	Ultimate Strength (ksi)	Fracture Load (kip)	Fracture Stress (ksi)	Fracture Strength (ksi)	Uniform Elingation (%)	Total Elongation (%)	Reduction in Area (%)
MY Capsule A25	3JK	300	107.0	118.2	4.5	193.7	91.7	10.8	19.5	53
	3J5	560	98.8	110.5	4.3	151.7	87.6	10.0	18.0	42
MY Capsule W253	3JM	74	107.0	115.1	4.0	152.2	81.5	12.7	24.8	46
	3J7	300	93.7	105.9	3.9	171.8	79.5	12.0	21.6	54
	3L4	560	87.6	105.9	4.2	174.6	85.6	10.5	17.9	51
MY Capsule A35	3JT	Room	102.2	116.9	---	---	---	---	24.2	52.1
	3J3	566	93.3	110.8	---	---	---	---	21.8	42.8
	3KJ(a)	650	---	104.1	---	---	---	---	18.2	44.0
MY Capsule W263	3JE	86	100.8	114.4	---	200.5	82.3	15.1	26.0	58.9
	3J1	550	88.7	105.4	---	162.6	87.6	10.1	17.9	46.1
	3JB	560	84.0	103.3	---	164.0	84.5	13.03	20.6	48.5
Kewaunee Unirradiated Surveillance Weld	1	Room	69.0	84.9	---	---	---	15.7	27.5	72.2
	2	Room	68.6	84.4	---	---	---	15.4	26.5	72.3
	3	300	66.6	78.4	---	---	---	10.2	21.9	69.9
	4	300	62.7	76.8	---	---	---	12.9	23.3	68.8
	5	600	59.6	80.7	---	---	---	13.8	22.7	65.0
	6	600	60.1	81.0	---	---	---	13.2	22.4	66.4
Kewaunee Capsule R	W3	250	97.8	109.9	3.80	188.6	77.5	12.0	22.5	59
	W4	550	87.6	103.8	3.98	175.5	80.9	12.0	19.2	54
Kewaunee Capsule V	W2	200	94.7	105.9	---	74.3	188.5	10.4	22.0	61.6
	W1	550	83.5	102.0	---	81.5	206.5	10.4	20.5	52.7
Kewaunee Capsule S	W5	200	101.3	112.0	4.00	192.9	81.5	10.5	21.8	58
	W6	550	91.7	105.9	4.00	176.2	81.5	9.8	19.7	54

Notes:

(a) Accidental pre-straining of specimen prior to testing resulted in unreliable yield strength measurement and questionable test results.

Specimen Code	Specimen Type	Test Temperature (°F)	K_{Jc} (ksi-in^{1/2})	K_{Jc(1T)} (ksi-in^{1/2})
W25	PCVN	136	54.6	47.0
W26	PCVN	136	65.0	55.3
W27	PCVN	136	90.1	75.1
W28	PCVN	136	149.7	122.4
W29	PCVN	136	79.6	66.8
W30	PCVN	136	78.9	66.3
W31	PCVN	136	46.0	40.2
W32	PCVN	136	59.6	51.0
H25	Recon. PCVN	136	119.0	98.0
H29	Recon. PCVN	136	75.6	63.6
H30	Recon. PCVN	136	53.1	45.0
H31	Recon. PCVN	136	53.2	46.0

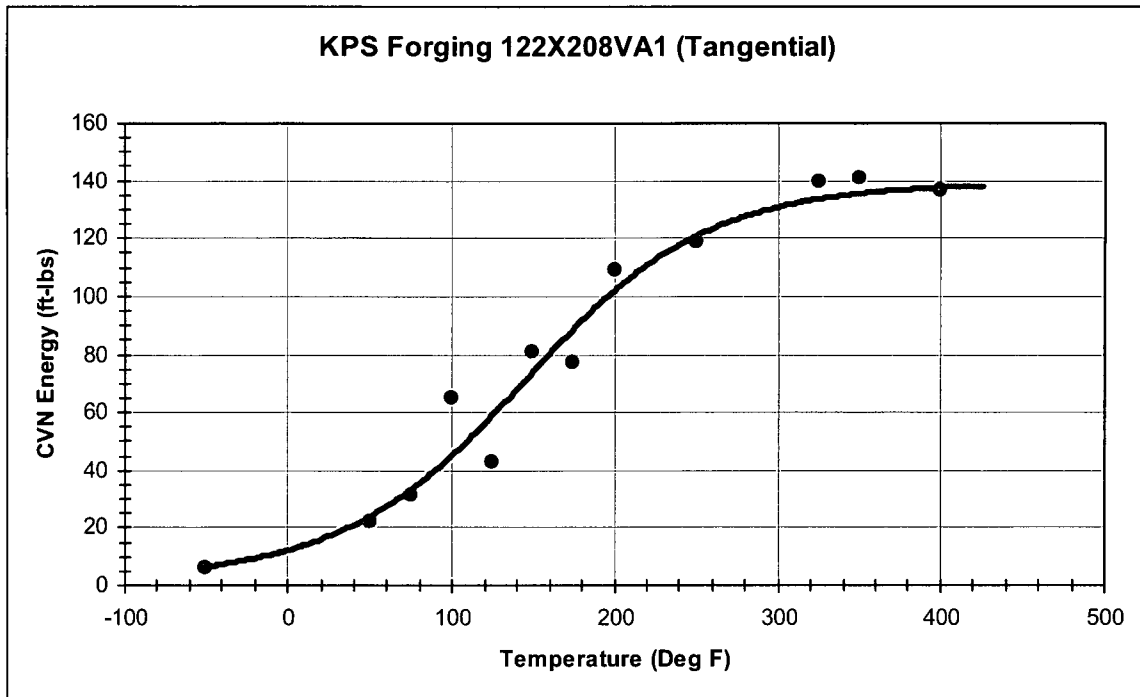


Figure 5-1 Charpy V-Notch Impact Energy vs. Temperature for KPS Reactor Vessel Intermediate Shell Forging 122X208VA1 (Tangential Orientation)

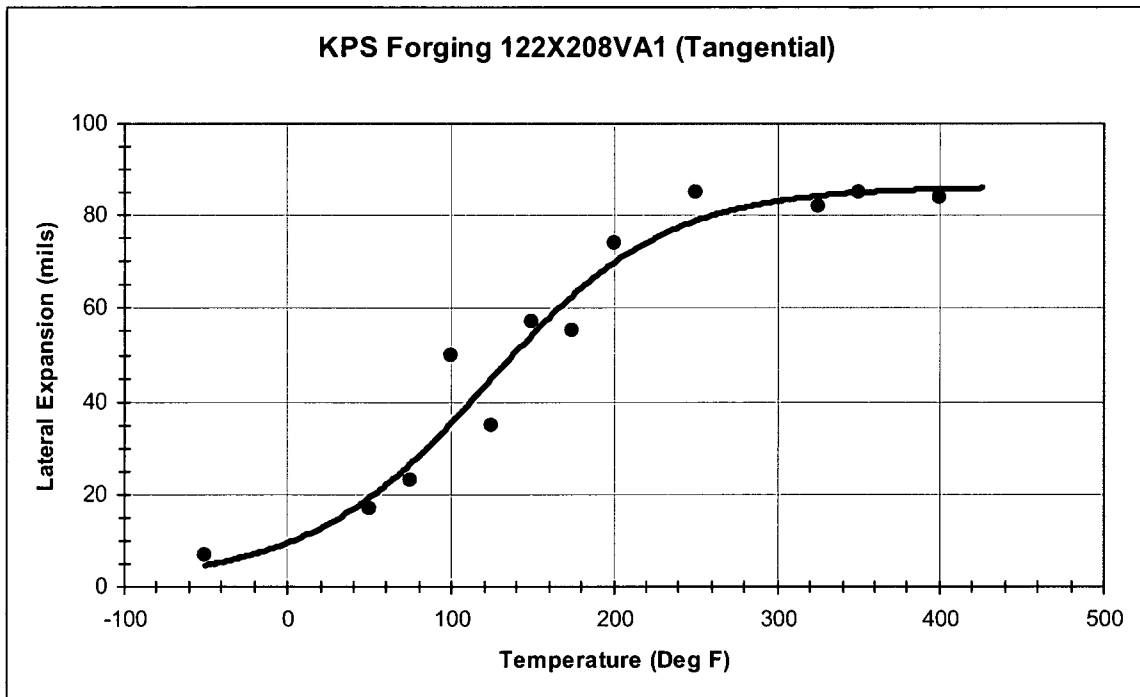


Figure 5-2 Charpy V-Notch Lateral Expansion vs. Temperature for KPS Reactor Vessel Intermediate Shell Forging 122X208VA1 (Tangential Orientation)

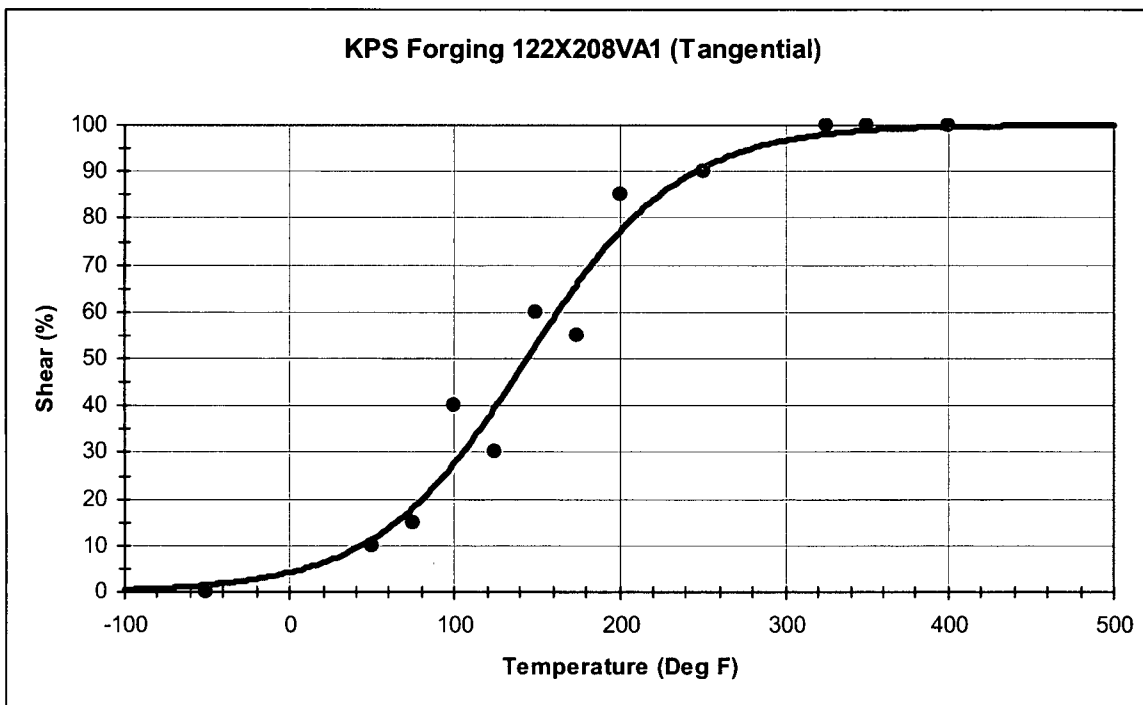


Figure 5-3 Charpy V-Notch Percent Shear vs. Temperature for KPS Reactor Vessel Intermediate Shell Forging 122X208VA1 (Tangential Orientation)

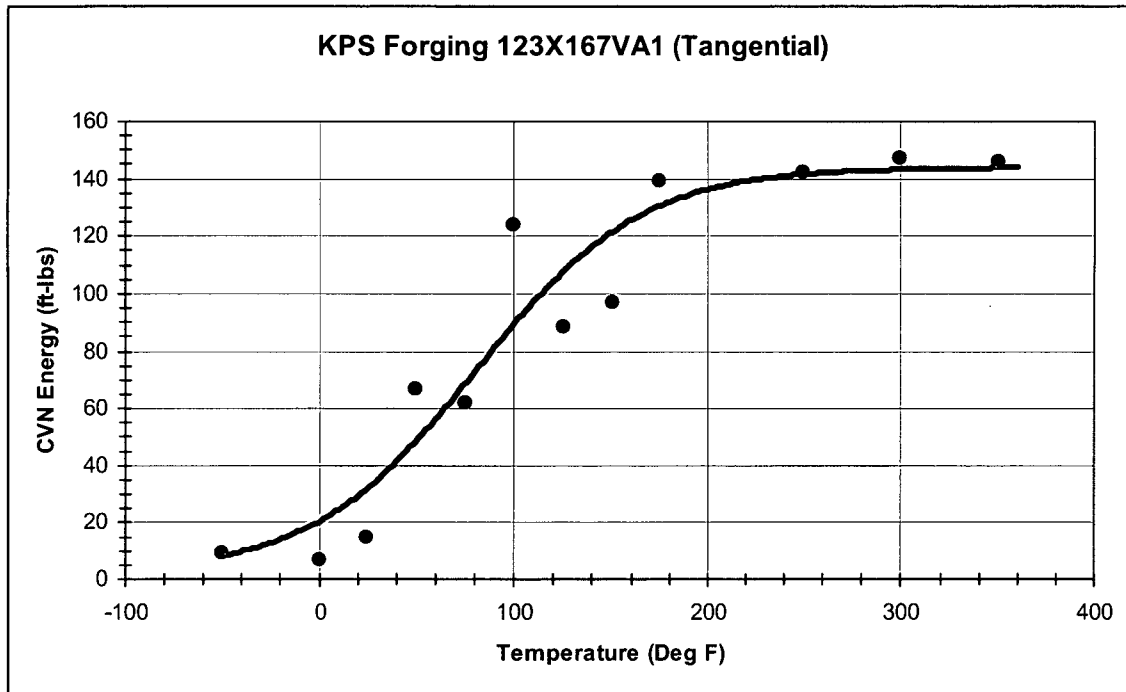


Figure 5-4 Charpy V-Notch Impact Energy vs. Temperature for KPS Reactor Vessel Lower Shell Forging 123X167VA1 (Tangential Orientation)

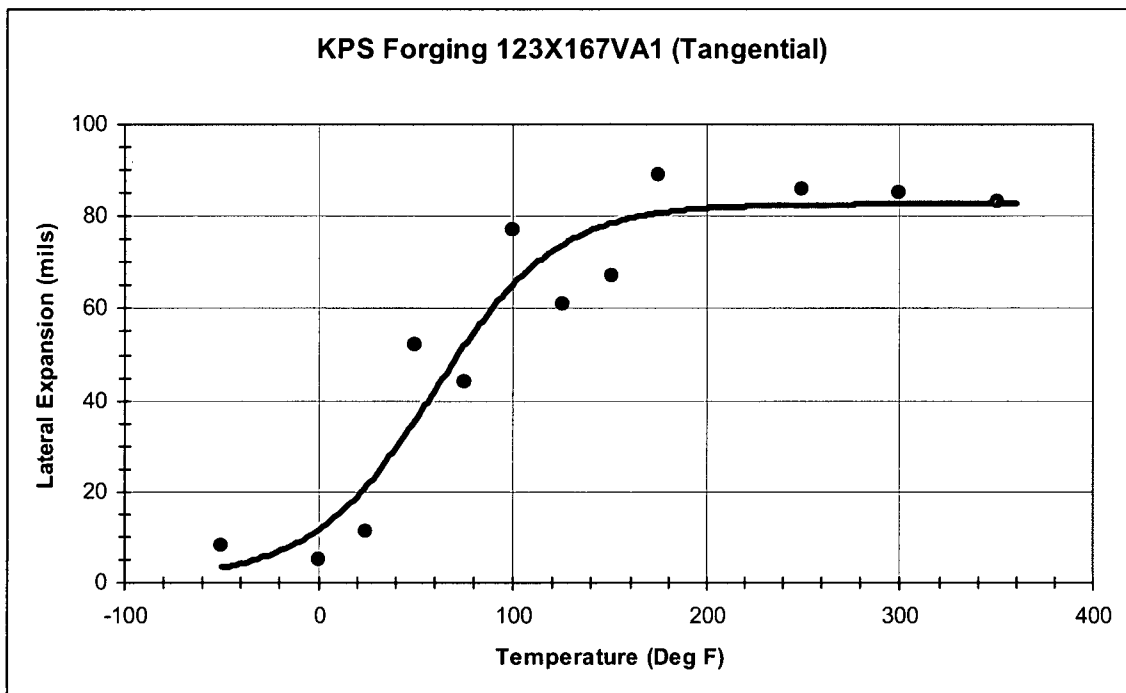


Figure 5-5 Charpy V-Notch Lateral Expansion vs. Temperature for KPS Reactor Vessel Lower Shell Forging 123X167VA1 (Tangential Orientation)

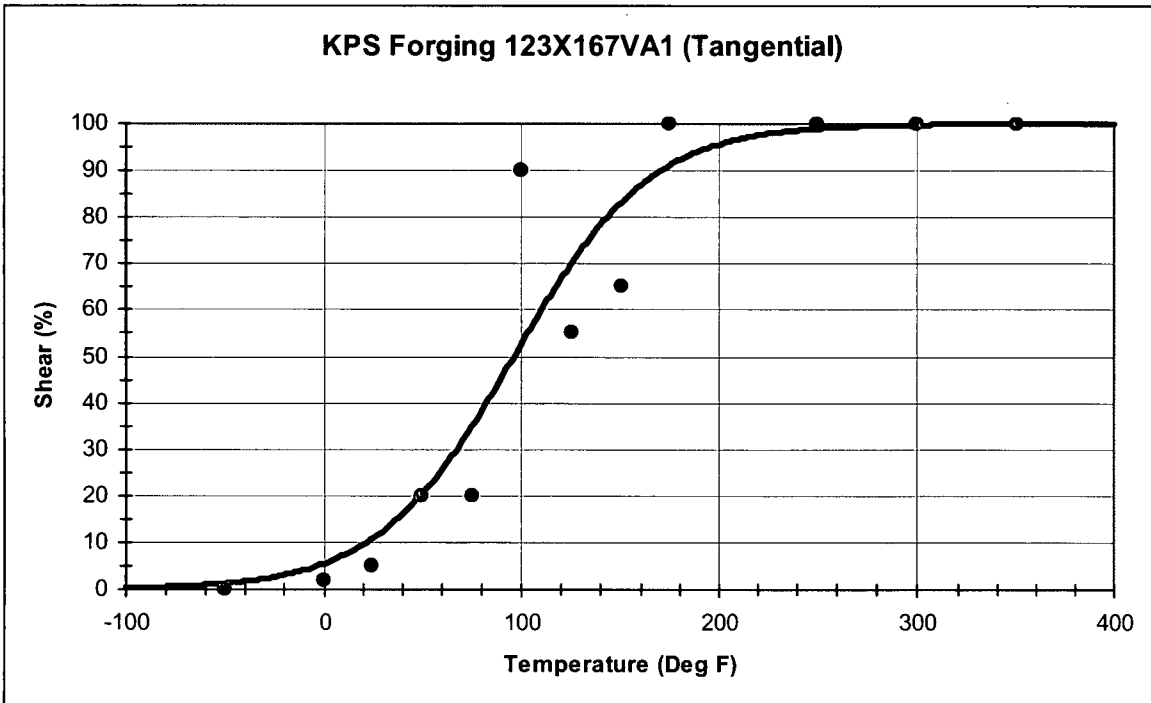


Figure 5-6 Charpy V-Notch Percent Shear vs. Temperature for KPS Reactor Vessel Lower Shell Forging 123X167VA1 (Tangential Orientation)

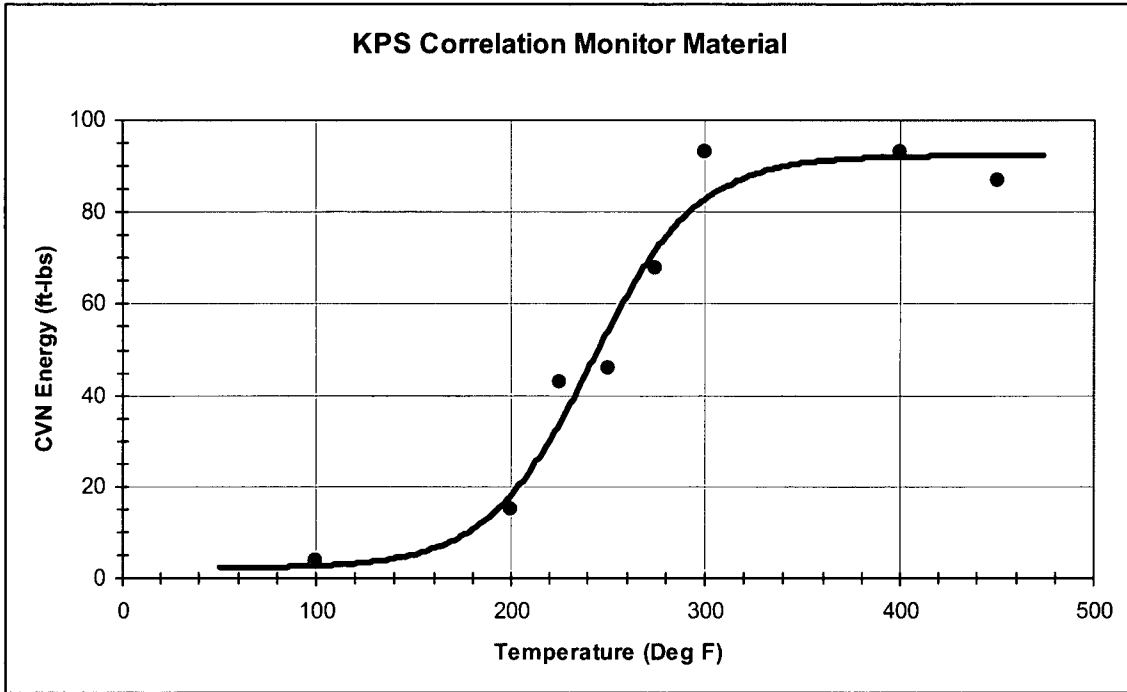


Figure 5-7 Charpy V-Notch Impact Energy vs. Temperature for KPS Reactor Vessel Correlation Monitor Material

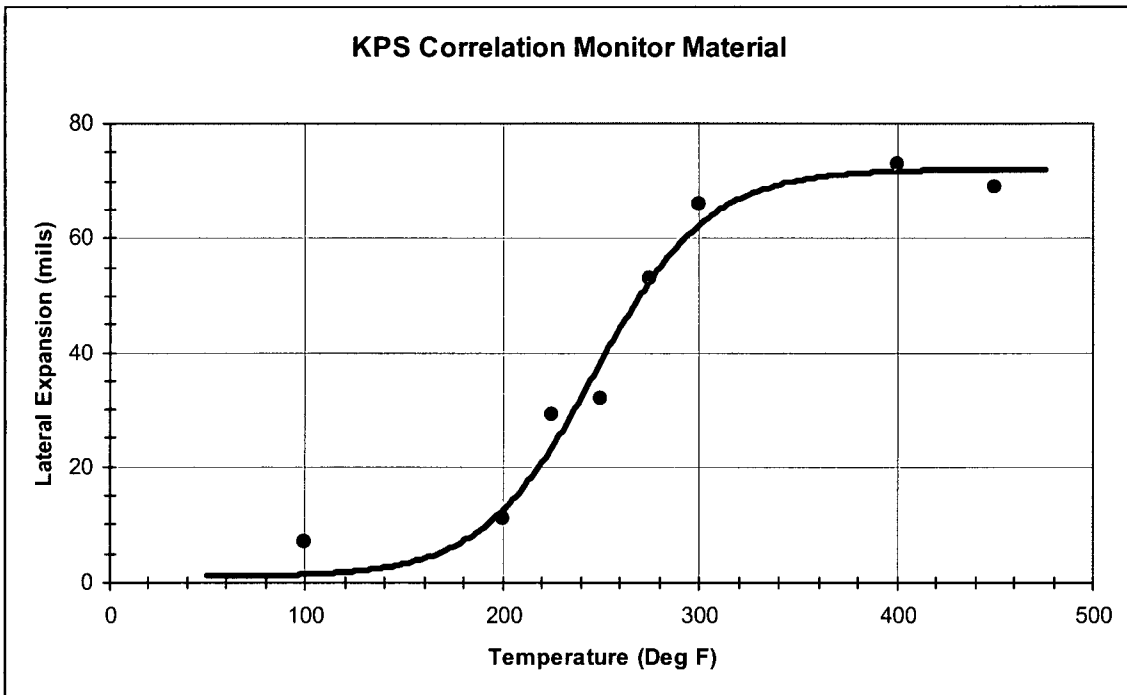


Figure 5-8 Charpy V-Notch Lateral Expansion vs. Temperature for KPS Reactor Vessel Correlation Monitor Material

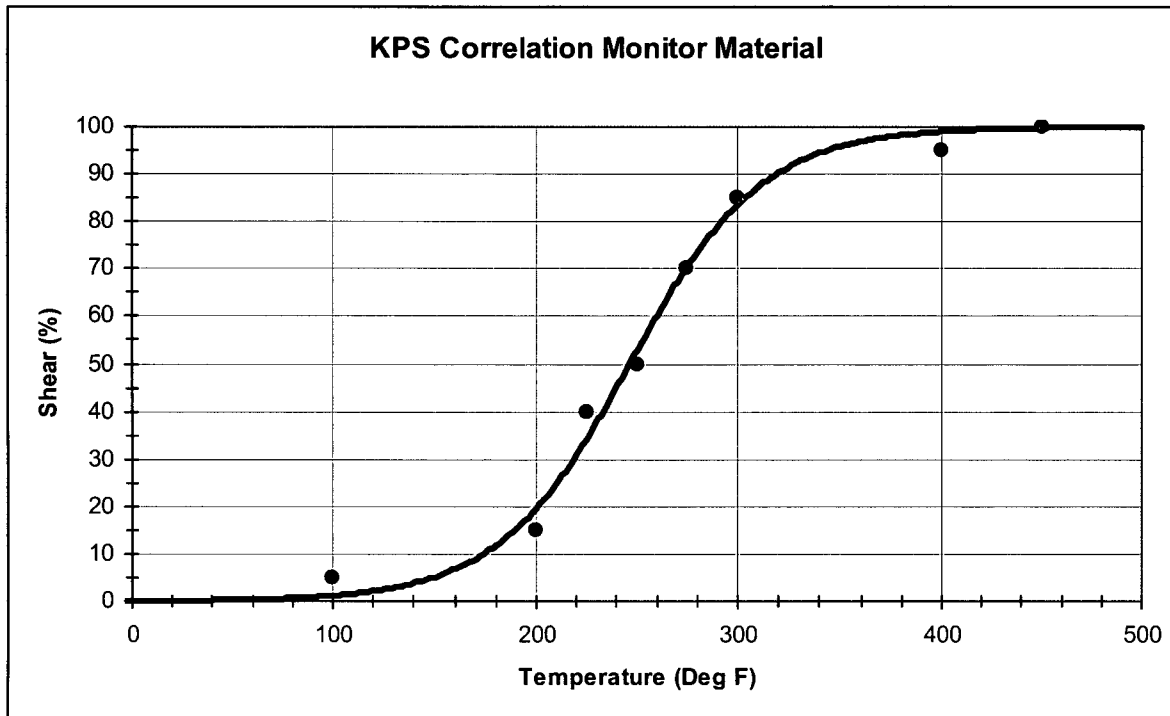


Figure 5-9 Charpy V-Notch Percent Shear vs. Temperature for KPS Reactor Vessel Correlation Monitor Material

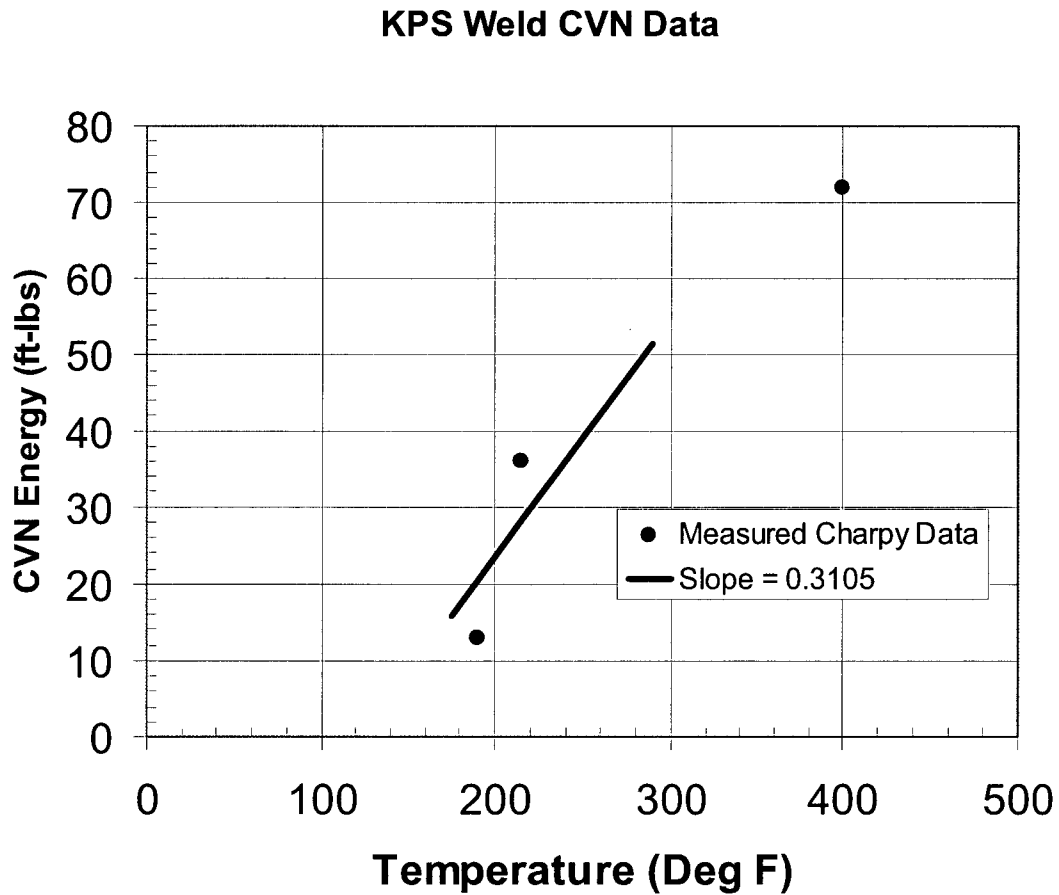


Figure 5-10 Charpy V-Notch Impact Energy vs. Temperature Best-Fit through the Transition Region for KPS Reactor Vessel Weld Metal

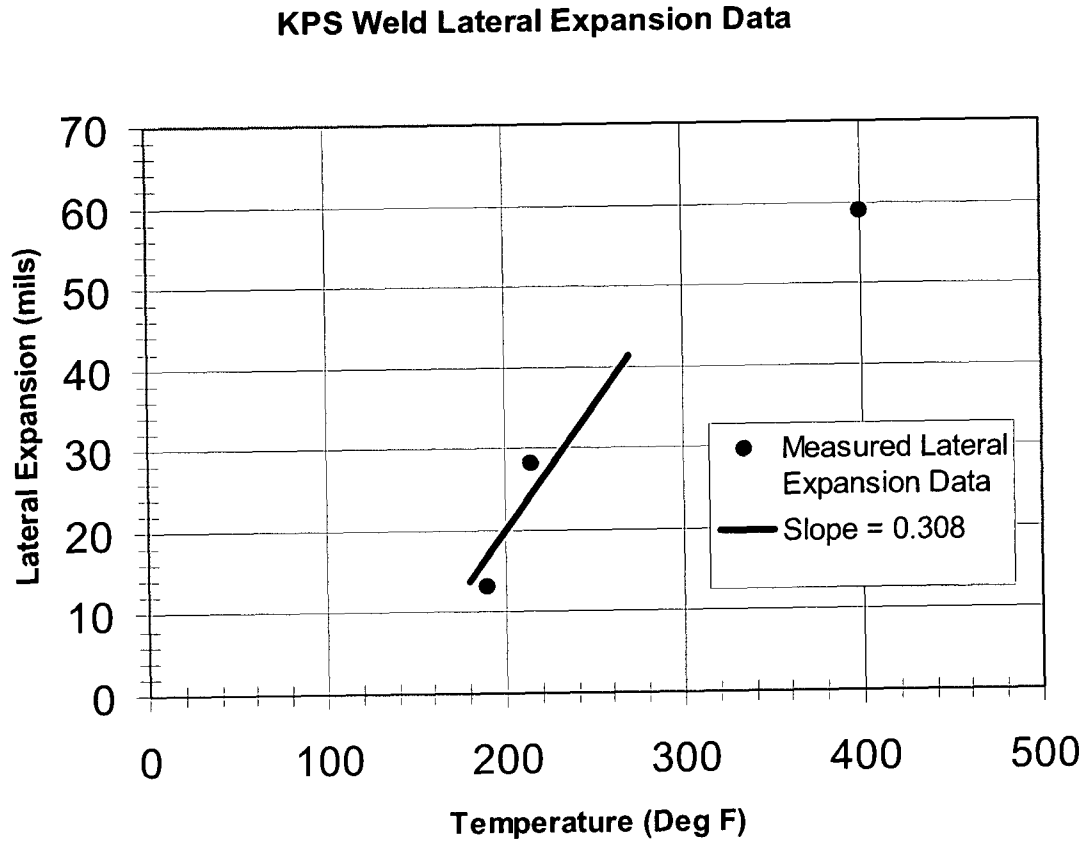


Figure 5-11 Charpy V-Notch Lateral Expansion vs. Temperature Best-Fit through the Transition Region for KPS Reactor Vessel Weld Metal

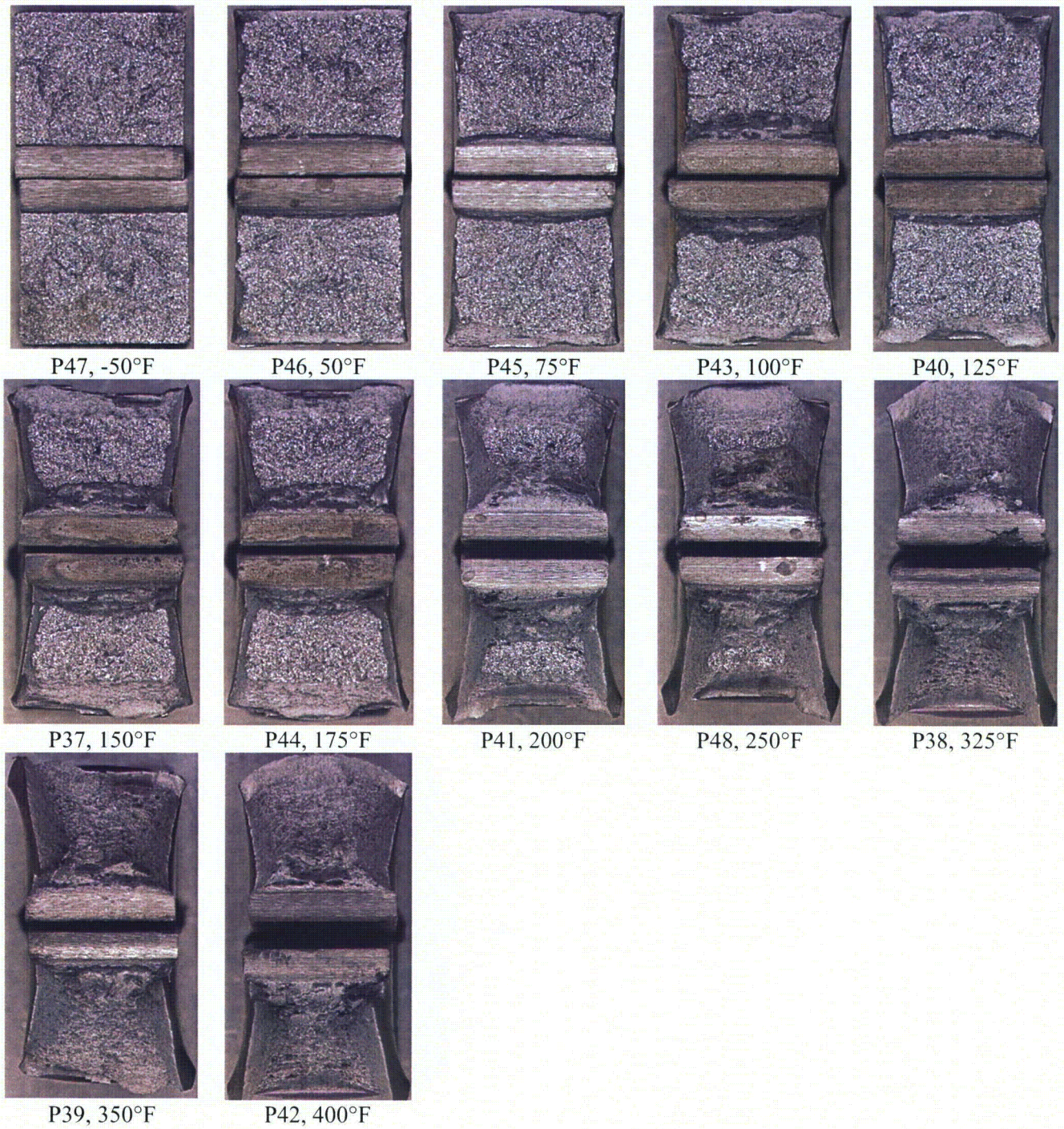


Figure 5-12 Charpy Impact Specimen Fracture Surfaces of the Kewaunee Reactor Vessel Intermediate Shell Forging 122X208VA1 (Tangential Orientation).

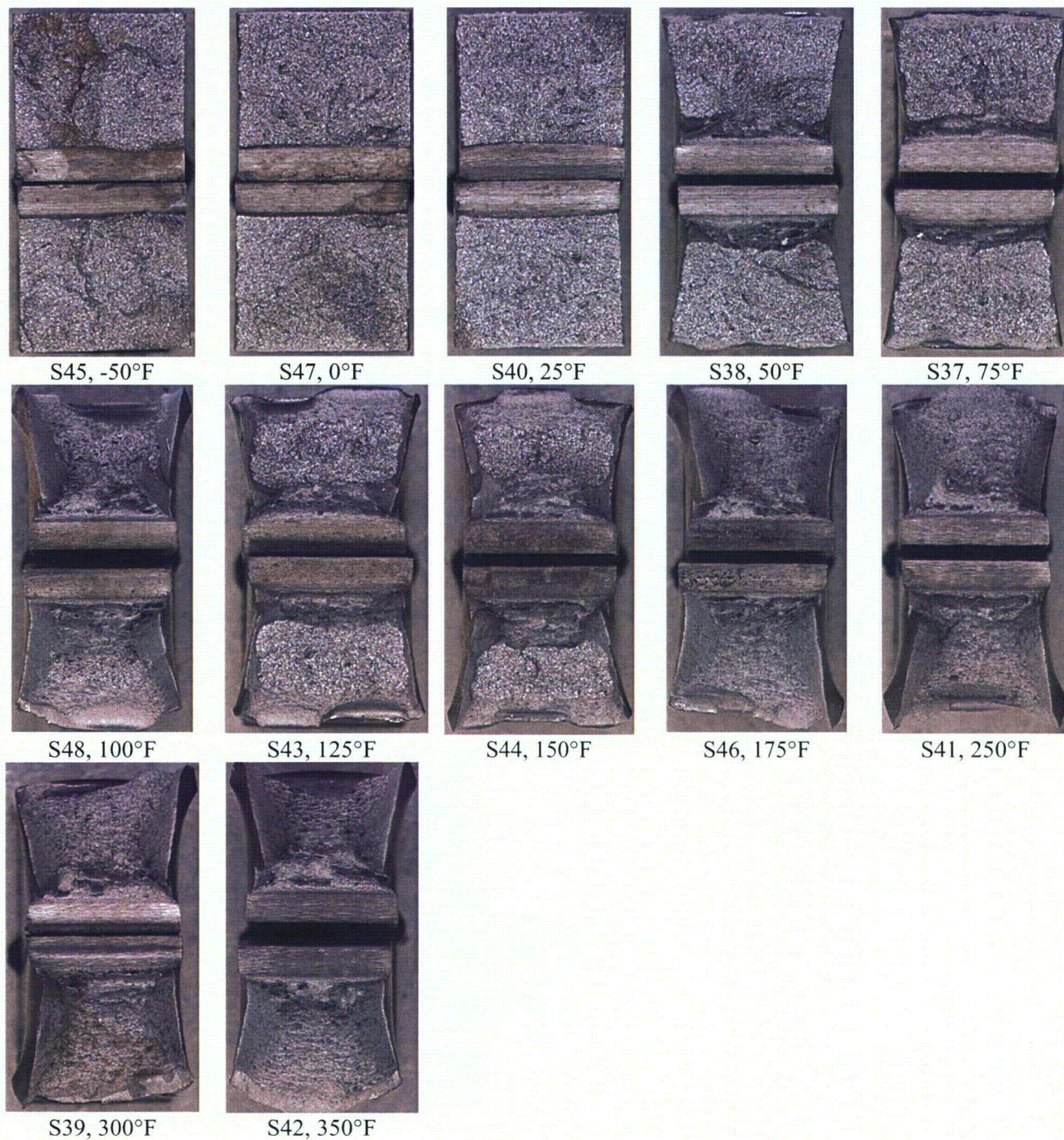


Figure 5-13 Charpy Impact Specimen Fracture Surfaces of the Kewaunee Reactor Vessel Lower Shell Forging 123X167VA1 (Tangential Orientation).

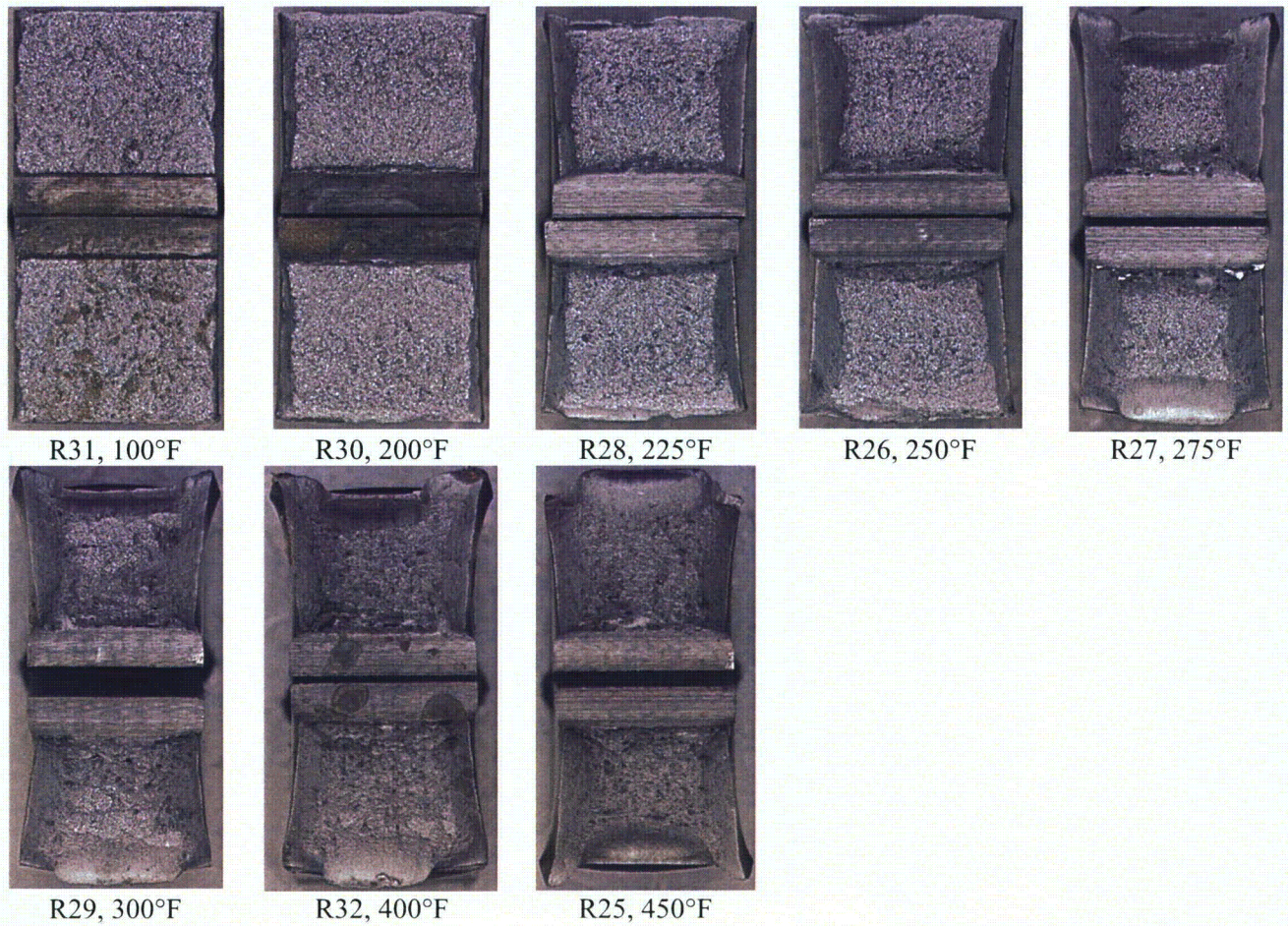


Figure 5-14 Charpy Impact Specimen Fracture Surfaces of the Kewaunee A533 Grade B Class 1 Correlation Monitor Material.

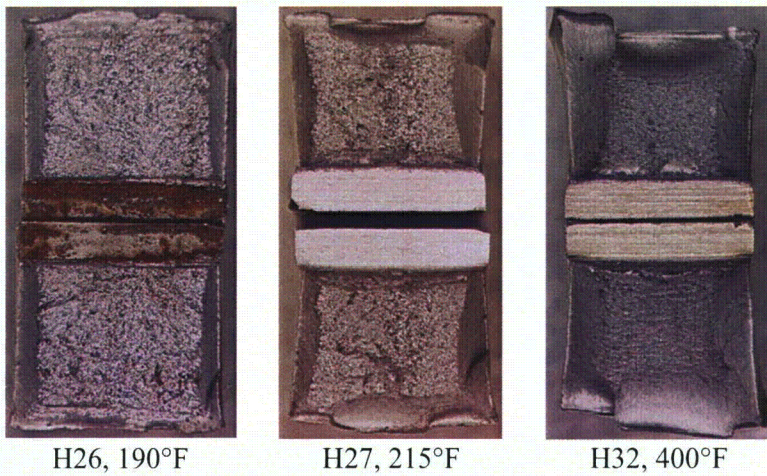


Figure 5-15 Charpy Impact Specimen Fracture Surfaces of the Kewaunee Reactor Vessel Reconstituted Weld Metal.

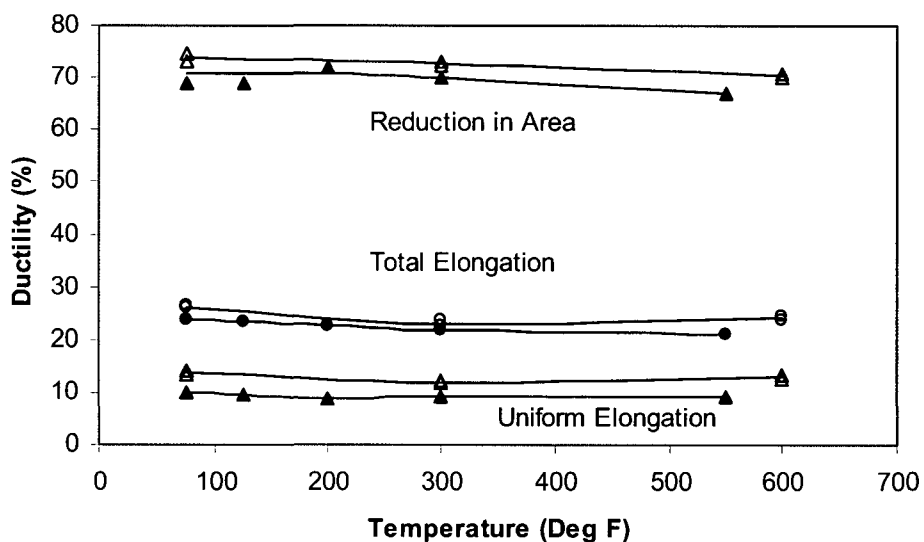
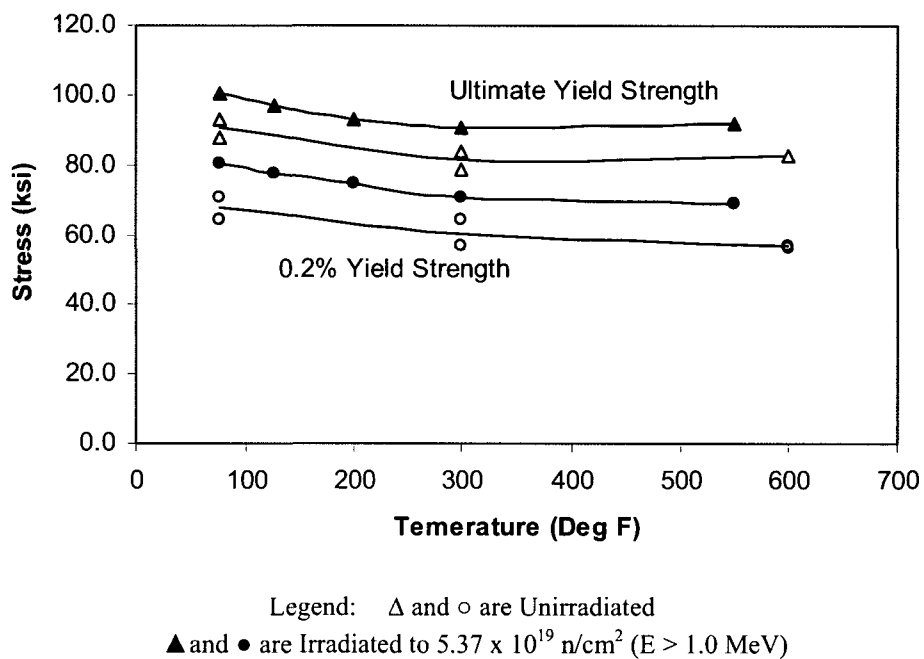
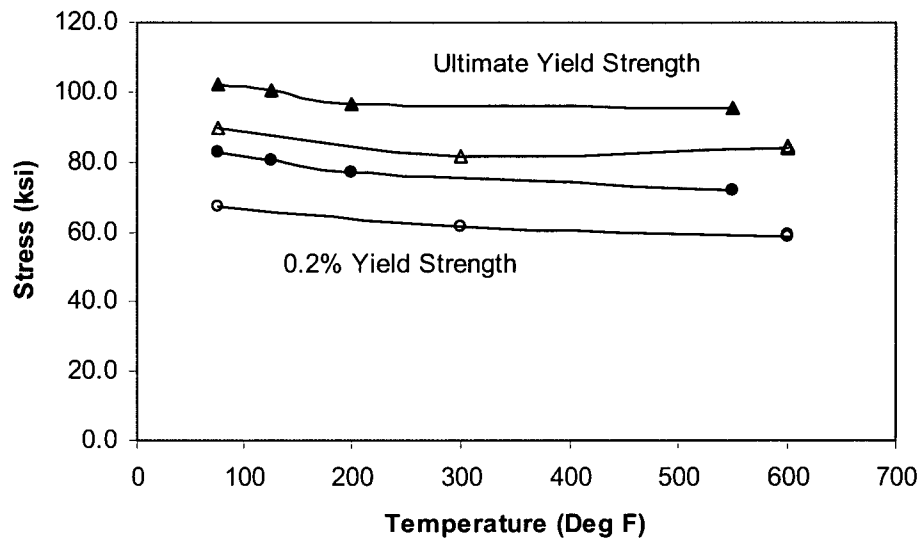


Figure 5-16 Tensile Properties for Kewaunee, Capsule T Reactor Vessel Intermediate Shell Forging 122X208VA1 (Tangential Orientation).



Legend: Δ and \circ are Unirradiated
 \blacktriangle and \bullet are Irradiated to 5.37×10^{19} n/cm² (E > 1.0 MeV)

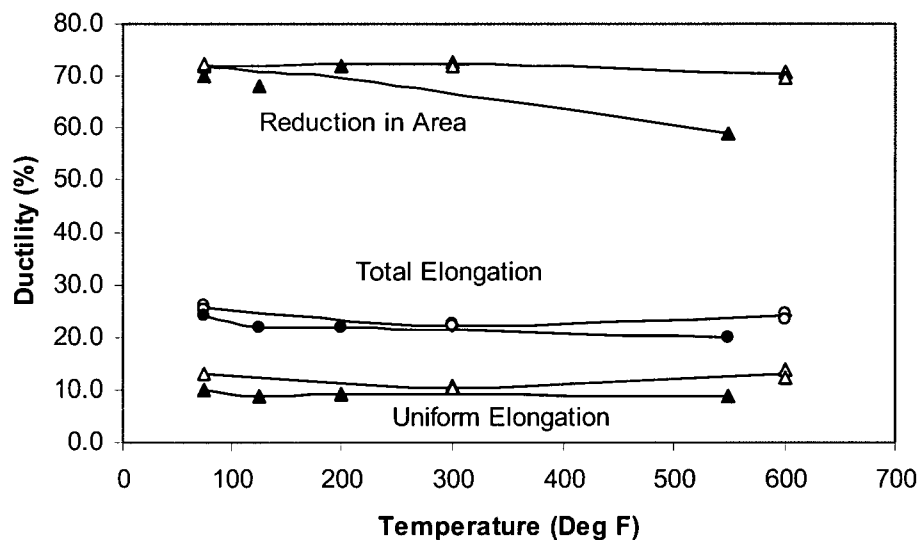


Figure 5-17 Tensile Properties for Kewaunee, Capsule T Reactor Vessel Lower Shell Forging 123X167VA1 (Tangential Orientation).

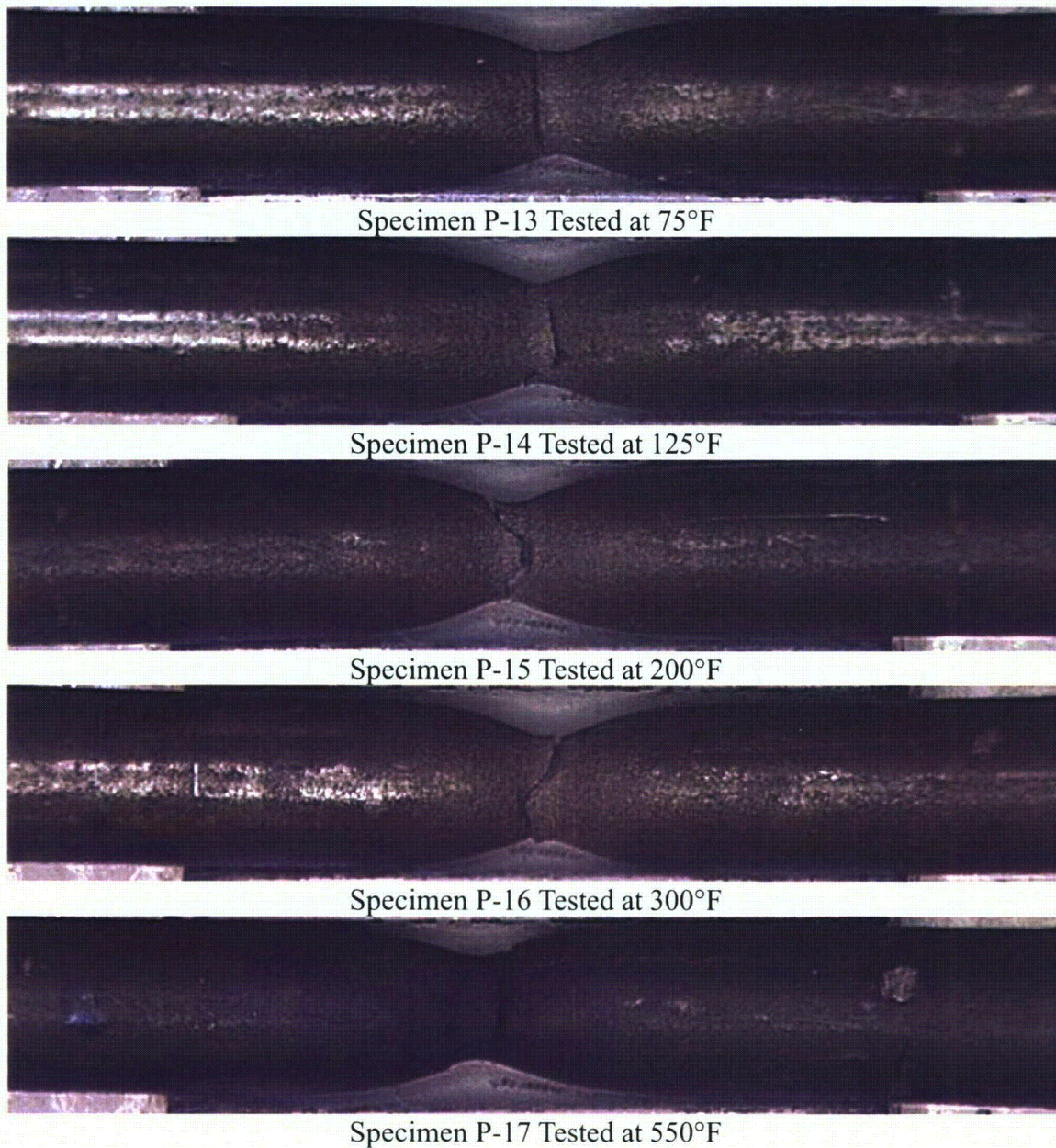
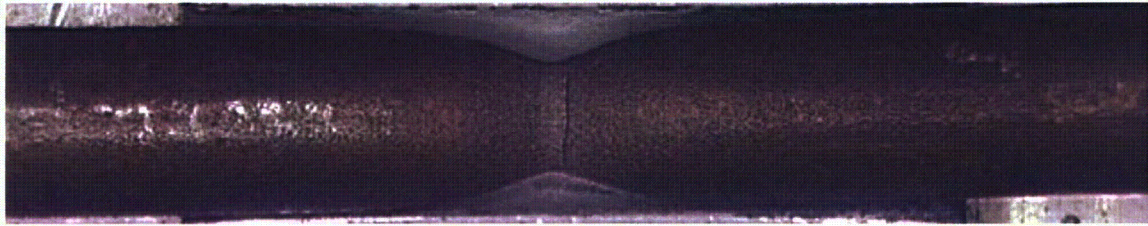


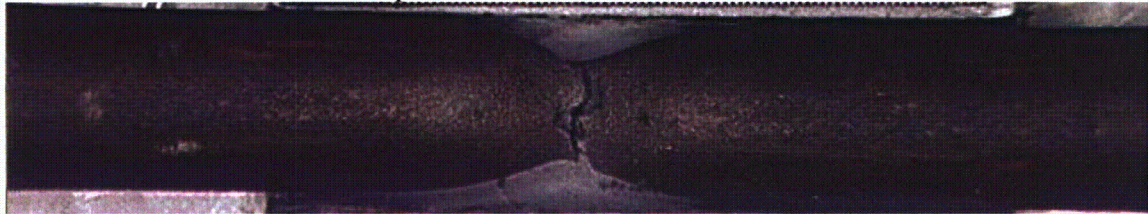
Figure 5-18 Fractured Tensile Specimens from the Kewaunee, Capsule T Reactor Vessel Intermediate Shell Forging 122X208VA1 (Tangential Orientation).



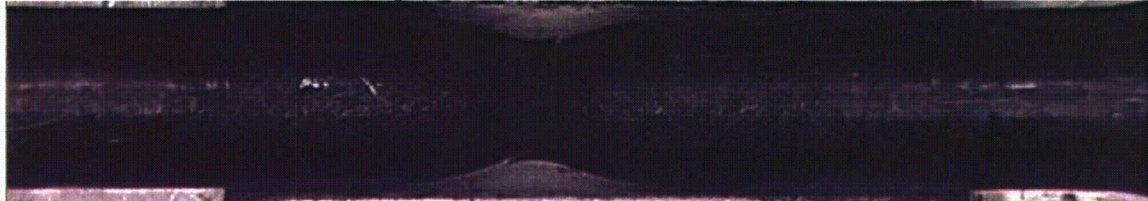
Specimen S-10 Tested at 75°F



Specimen S-11 Tested at 125°F



Specimen S-12 Tested at 200°F



Specimen S-13 Tested at 550°F

Figure 5-19 Fractured Tensile Specimens from the Kewaunee, Capsule T Reactor Vessel Lower Shell Forging 123X167VA1 (Tangential Orientation).

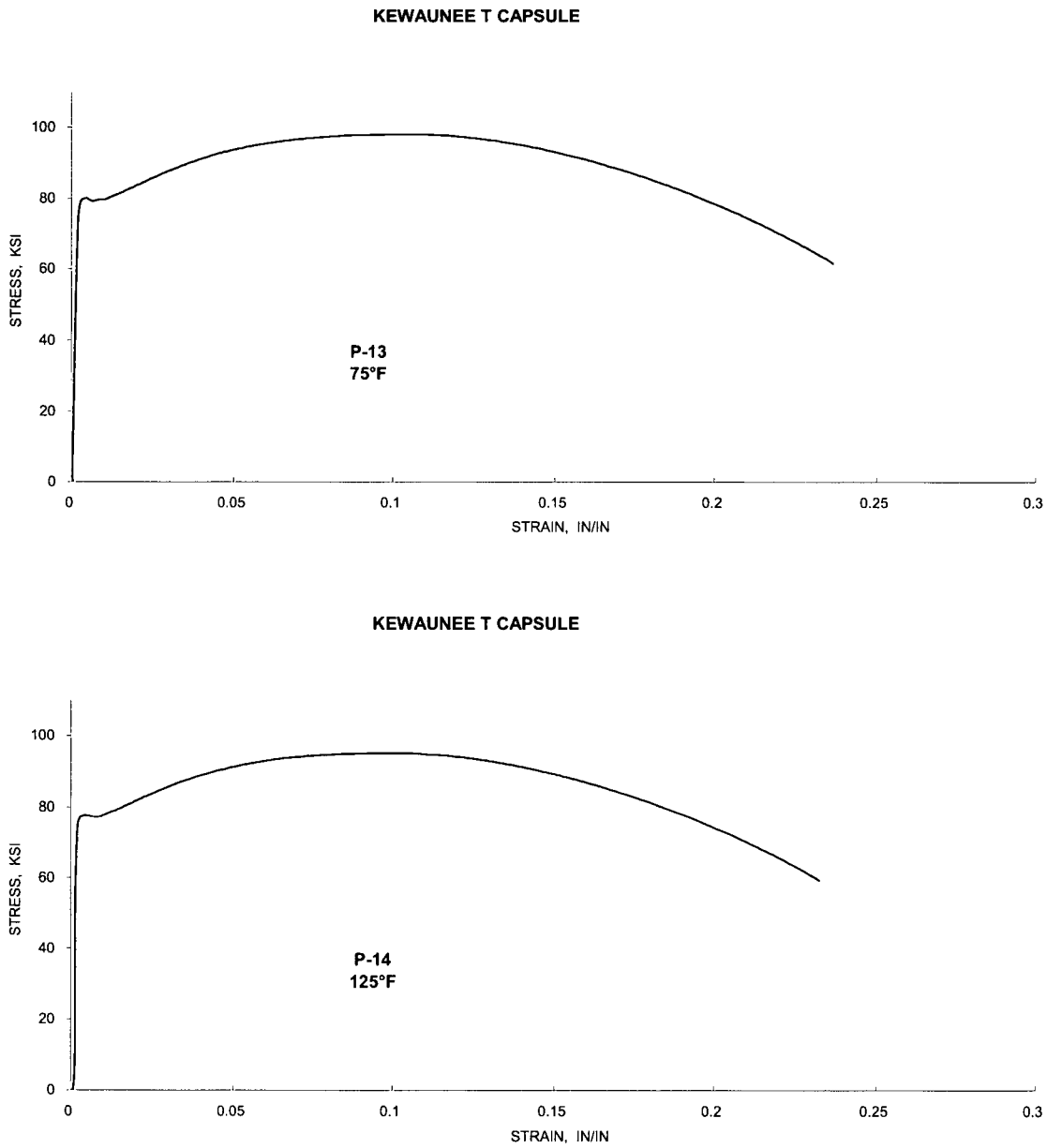


Figure 5-20 Engineering Stress-Strain Curves for Kewaunee Reactor Vessel Intermediate Shell Forging 122X208VA1, Capsule T, Tensile Specimens P-13 and P-14.

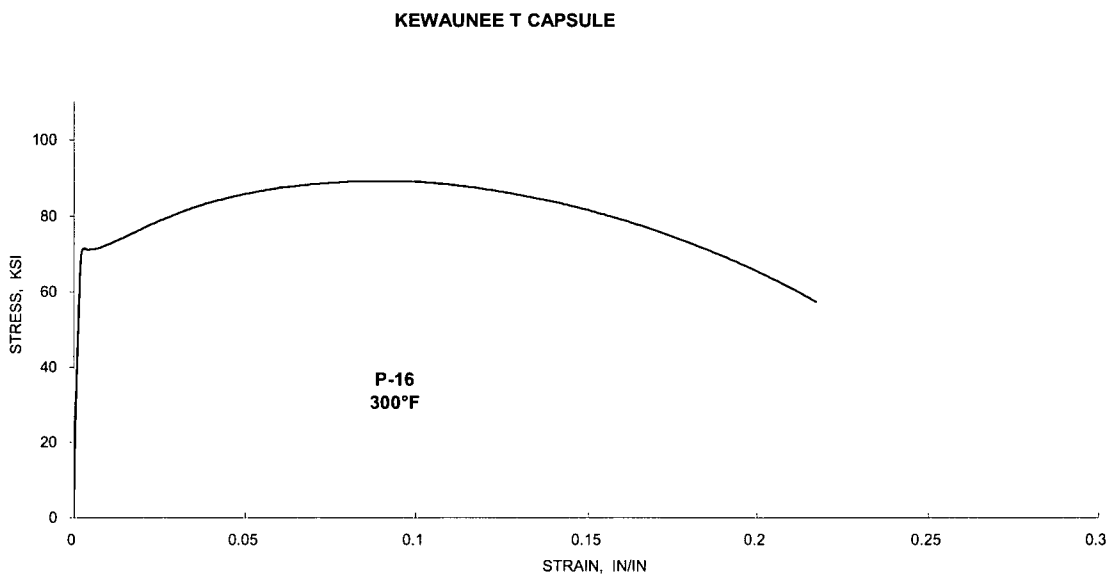
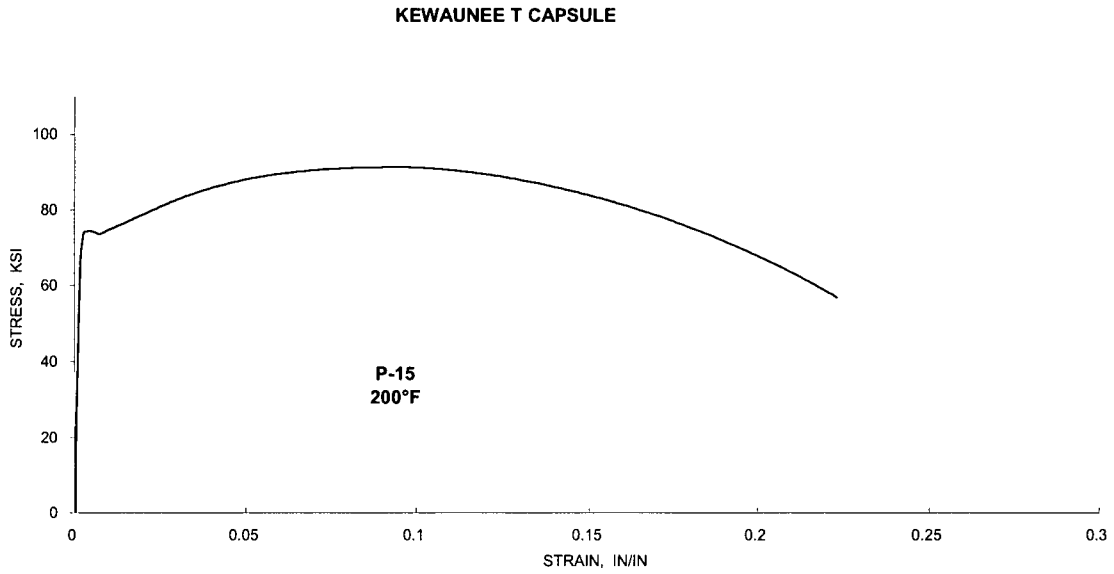


Figure 5-21 Engineering Stress-Strain Curves for Kewaunee Reactor Vessel Intermediate Shell Forging 122X208VA1, Capsule T, Tensile Specimens P-15 and P-16.

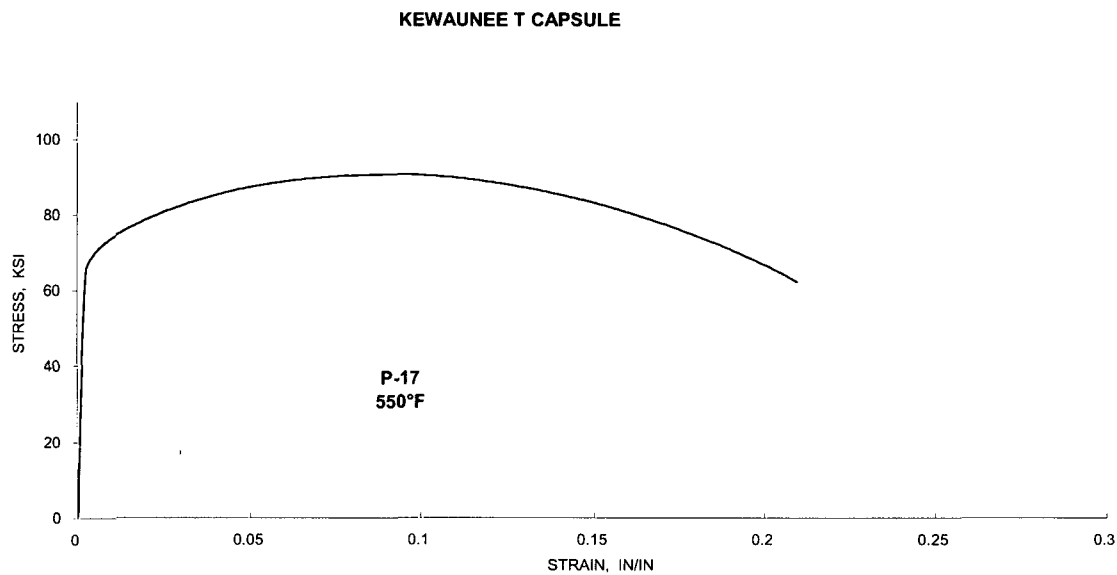


Figure 5-22 Engineering Stress-Strain Curve for Kewaunee Reactor Vessel Intermediate Shell Forging 122X208VA1, Capsule T, Tensile Specimen P-17.

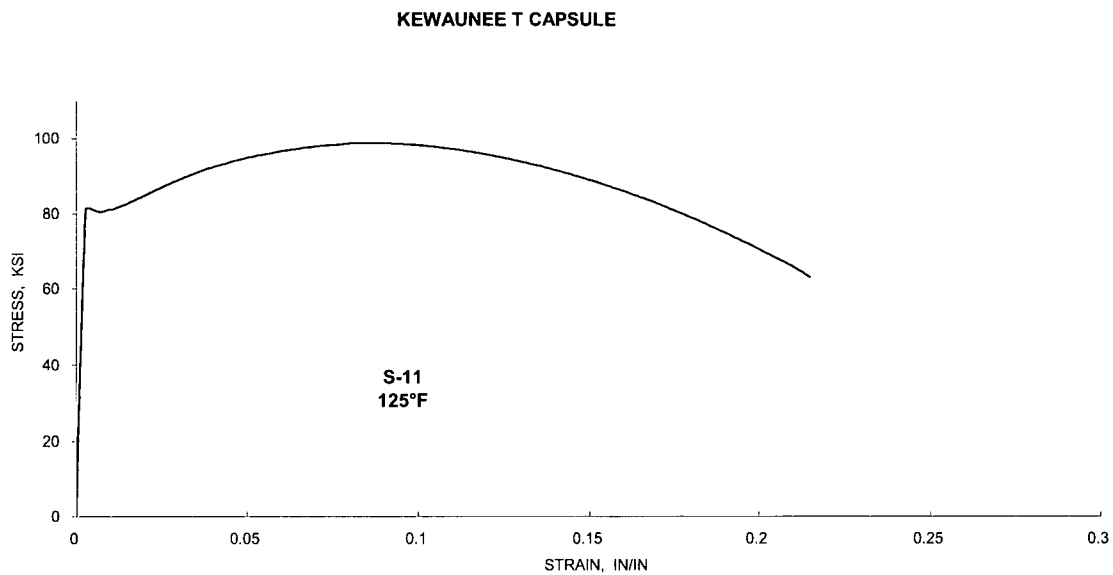
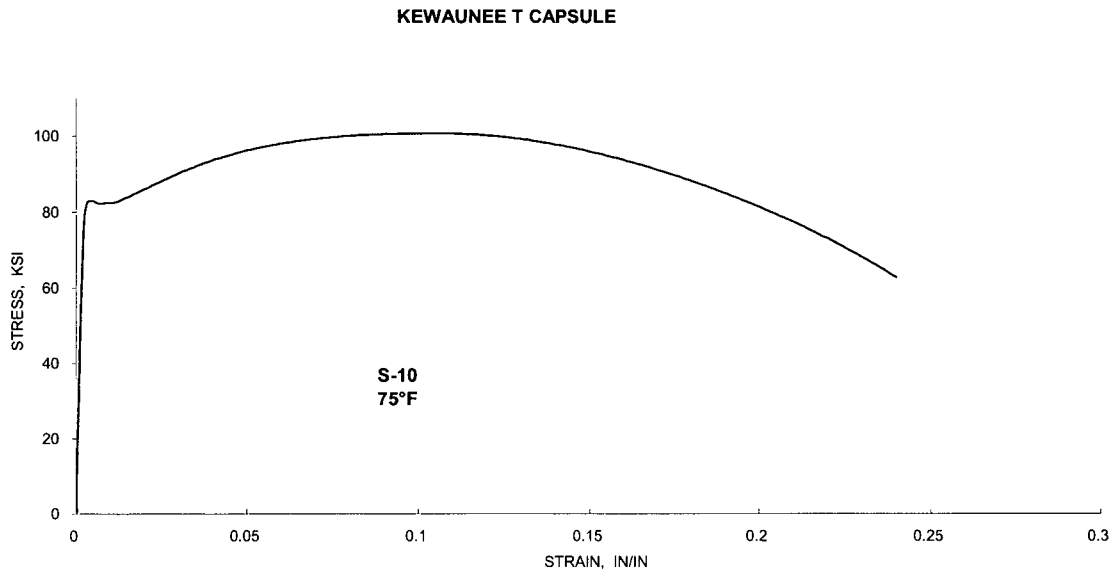


Figure 5-23 Engineering Stress-Strain Curves for Kewaunee Reactor Vessel Lower Shell Forging 123X167VA1, Capsule T, Tensile Specimens S-10 and S-11.

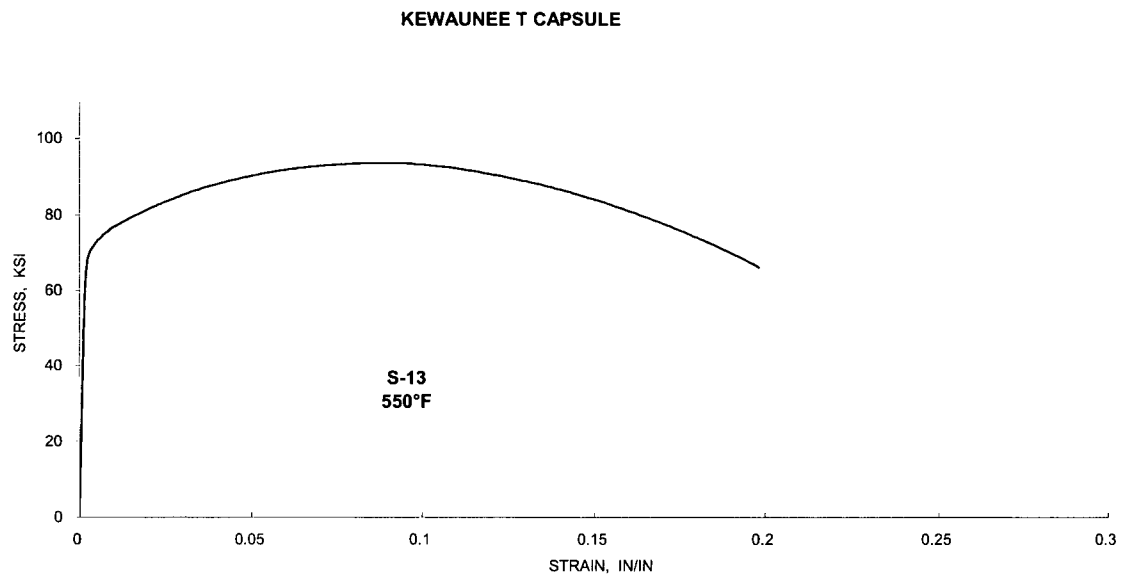
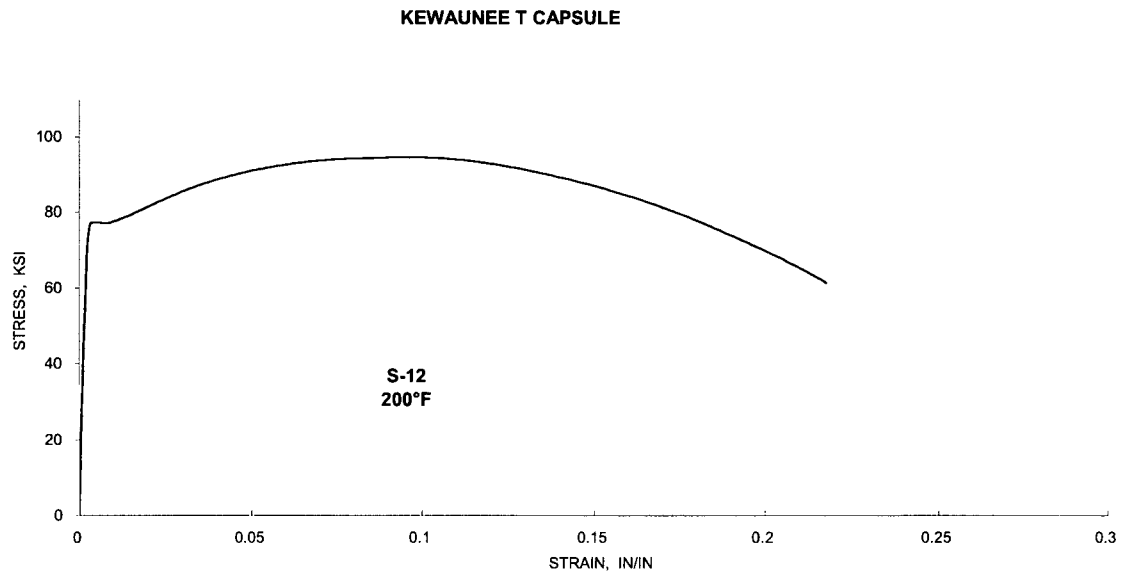


Figure 5-24 Engineering Stress-Strain Curves for Kewaunee Reactor Vessel Lower Shell Forging 123X167VA1, Capsule T, Tensile Specimens S-12 and S-13.

This page intentionally blank

6 RADIATION ANALYSIS AND NEUTRON DOSIMETRY

6.1 INTRODUCTION

This section describes a discrete ordinates S_n transport analysis performed for the Kewaunee reactor to determine the neutron radiation environment within the reactor pressure vessel and surveillance capsules. In this analysis, fast neutron exposure parameters in terms of fast neutron fluence ($E > 1.0$ MeV) and iron atom displacements (dpa) were established on a plant and fuel cycle specific basis. An evaluation of the most recent dosimetry sensor set from Capsule T, withdrawn at the end of the twenty sixth plant operating cycle, is provided. In addition, to provide an up-to-date data base applicable to the Kewaunee reactor, the sensor sets from the previously withdrawn capsules (V, R, P and S) were re-analyzed using the current dosimetry evaluation methodology. The dosimetry evaluations for all capsules withdrawn to date are presented in Appendix A of this report. Comparisons of the results from the dosimetry evaluations with the analytical predictions served to validate the plant specific neutron transport calculations. These validated calculations subsequently formed the basis for providing projections of the neutron exposure of the reactor pressure vessel for operating periods extending to 60 calendar years.

The use of fast neutron fluence ($E > 1.0$ MeV) to correlate measured material property changes to the neutron exposure of the material has traditionally been accepted for the development of damage trend curves as well as for the implementation of trend curve data to assess the condition of the vessel. However, it has also been suggested that an exposure model that accounts for differences in neutron energy spectra between surveillance capsule locations and positions within the vessel wall could lead to an improvement in the uncertainties associated with damage trend curves and improved accuracy in the evaluation of damage gradients through the reactor vessel wall.

Because of this potential shift away from a threshold fluence toward an energy dependent damage function for data correlation, ASTM Standard Practice E853, "Analysis and Interpretation of Light-Water Reactor Surveillance Results," [Reference 23] recommends reporting displacements per iron atom (dpa) along with fluence ($E > 1.0$ MeV) to provide a database for future reference. The energy dependent dpa function to be used for this evaluation is specified in ASTM Standard Practice E693, "Characterizing Neutron Exposures in Iron and Low Alloy Steels in Terms of Displacements per Atom." [Reference 24] The application of the dpa parameter to the assessment of embrittlement gradients through the thickness of the reactor vessel wall has already been promulgated in Revision 2 to Regulatory Guide 1.99, "Radiation Embrittlement of Reactor Vessel Materials."

All of the calculations and dosimetry evaluations described in this section and in Appendix A were based on the latest available nuclear cross-section data derived from ENDF/B-VI and made use of the latest available calculational tools. Furthermore, the neutron transport and dosimetry evaluation methodologies follow the guidance of Regulatory Guide 1.190, "Calculational and Dosimetry Methods for Determining Pressure Vessel Neutron Fluence." Reference [25] The NRC approved neutron transport and dosimetry evaluation methodologies used for the Kewaunee application are described in WCAP-14040-NP-A, "Methodology Used to Develop Cold Overpressure Mitigating System Setpoints and RCS Heatup and Cooldown Limit Curves," May 2004 [Reference 26] and WCAP-16083-NP-A, "Benchmark Testing of the FERRET Code for Least Squares Evaluation of Light Water Reactor Dosimetry, May 2006," [Reference 27] respectively.

6.2 DISCRETE ORDINATES ANALYSIS

A plan view of the Kewaunee reactor geometry at the core midplane is shown in Figure 4-1. Six irradiation capsules attached to the thermal shield are included in the reactor design to constitute the reactor vessel surveillance program. The capsules are located at azimuthal angles of 57°, 67°, 77°, 237°, 247°, and 257° as shown in Figure 4-1. These full core positions correspond to the following octant symmetric locations represented in Figure 6-1: 13° from the core cardinal axes (for the 77° and 257° capsule holder locations), 23° from the core cardinal axes (for the 67° and 247° capsule holder locations), and 33° from the core cardinal axes (for the 57° and 237° capsule holder locations). The stainless steel specimen containers are approximately 1-inch square and 64 inches in height. The containers are positioned axially such that the test specimens are centered on the core midplane, thus spanning the central 5.33 feet of the 12-foot high reactor core.

From a neutronic standpoint, the surveillance capsules and associated support structures are significant. The presence of these materials has a marked effect on both the spatial distribution of neutron flux and the neutron energy spectrum in the water annulus between the neutron pads and the reactor vessel. In order to determine the neutron environment at the test specimen locations, the capsules themselves must be included in the analytical model.

In performing the fast neutron exposure evaluations for the Kewaunee reactor vessel and surveillance capsules, a series of fuel cycle specific forward transport calculations was carried out using the following three-dimensional flux synthesis technique:

$$\phi(r, \theta, z) = \phi(r, \theta) * \frac{\phi(r, z)}{\phi(r)}$$

where $\phi(r, \theta, z)$ is the synthesized three-dimensional neutron flux distribution, $\phi(r, \theta)$ is the transport solution in r, θ geometry, $\phi(r, z)$ is the two-dimensional solution for a cylindrical reactor model using the actual axial core power distribution, and $\phi(r)$ is the one-dimensional solution for a cylindrical reactor model using the same source per unit height as that used in the r, θ two-dimensional calculation. This synthesis procedure was carried out for each operating cycle at Kewaunee.

For the Kewaunee transport calculations, the eighth core r, θ model depicted in Figure 6-1 was utilized since the reactor is octant symmetric. The r, θ model included the core, the reactor internals, the thermal shield, including explicit representations of surveillance capsules, the pressure vessel cladding and vessel wall, the insulation external to the pressure vessel, and the primary biological shield wall. This model formed the basis for the calculated results and enabled comparisons to the surveillance capsule dosimetry evaluations. In developing the analytical model, nominal design dimensions were employed for the various structural components. Likewise, water temperatures, and hence, coolant densities in the reactor core and downcomer regions of the reactor were taken to be representative of full power operating conditions. The coolant densities were treated on a fuel cycle specific basis. The reactor core itself was treated as a homogeneous mixture of fuel, cladding, water, and miscellaneous core structures such as fuel assembly grids, guide tubes, et cetera. The geometric mesh description of the r, θ reactor model consisted

of 148 radial by 105 azimuthal intervals. Mesh sizes were chosen to assure that proper convergence of the inner iterations was achieved on a pointwise basis. The pointwise inner iteration flux convergence criterion utilized in the r,θ calculations was set at a value of 0.001.

The r,z model used for the Kewaunee calculations is shown in Figure 6-2 and extends radially from the centerline of the reactor core out to a location interior to the primary biological shield and over an axial span from an elevation below the lower core plate to above the upper core plate. As in the case of the r,θ model, nominal design dimensions and full power coolant densities were employed in the calculations. In this case, the homogenous core region was treated as an equivalent cylinder with a volume equal to that of the active core zone. The stainless steel former plates located between the core baffle and core barrel regions were also explicitly included in the model. The r,z geometric mesh description consisted of 127 radial by 155 axial intervals. As in the case of the r,θ model, mesh sizes were chosen to assure that proper convergence of the inner iterations was achieved on a pointwise basis. The pointwise inner iteration flux convergence criterion utilized in the r,z calculations was also set at a value of 0.001.

The one-dimensional radial model used in the synthesis procedure consisted of the same 127 radial mesh intervals included in the r,z model. Thus, radial synthesis factors could be determined on a meshwise basis throughout the entire geometry.

The power distributions used in the plant specific transport analysis were based on the individual core designs for each of the first twenty seven fuel cycles at Kewaunee. Specifically, the data utilized included cycle dependent fuel assembly initial enrichments, burnups, and axial power distributions. This information was used to develop spatial and energy dependent core source distributions averaged over each fuel cycle. Therefore, the results from the neutron transport calculations provided data in terms of fuel cycle averaged neutron flux, which when multiplied by the appropriate fuel cycle length, generated the incremental fast neutron exposure for each fuel cycle. In constructing these core source distributions, the energy distribution of the source was computed using an appropriate fission split for uranium and plutonium isotopes based on the initial enrichment and burnup history of each fuel assemblies. From these assembly dependent fission splits, composite values of energy release per fission, neutron yield per fission, and fission spectrum were determined.

All of the transport calculations supporting this analysis were carried out using the DORT discrete ordinates code Version 3.1 [Reference 28] and the BUGLE-96 cross-section library [Reference 29]. The BUGLE-96 library provides a 67 group coupled neutron-gamma ray cross-section data set produced specifically for light water reactor (LWR) applications. In these analyses, anisotropic scattering was treated with a P_5 legendre expansion and angular discretization was modeled with an S_{16} order of angular quadrature. Energy and space dependent core power distributions, as well as system operating temperatures, were treated on a fuel cycle specific basis.

Selected results from the neutron transport analyses are provided in Tables 6-1 through 6-8. In Table 6-1, the calculated exposure rates and integrated exposures, expressed in terms of both neutron fluence ($E > 1.0$ MeV) and dpa, are given at the radial and azimuthal center of the octant symmetric surveillance capsule positions, i.e., for the 13° , 23° , and 33° locations. These results, representative of the axial midplane of the active core, establish the calculated exposure of the surveillance capsules withdrawn to date as well as projected into the future. Similar information is provided in Table 6-2 for the reactor

vessel inner radius at four azimuthal locations. The vessel data given in Table 6-2 were taken at the clad/base metal interface, and thus, represent maximum calculated exposure levels on the vessel.

From the data provided in Table 6-2 it is noted that the peak clad/base metal interface vessel fluence ($E > 1.0$ MeV) at the end of the twenty sixth fuel cycle (i.e., after 24.6 effective full power years (EFPY) of plant operation) was 2.60×10^{19} n/cm².

Both calculated fluence ($E > 1.0$ MeV) and dpa data are provided in Table 6-1 and Table 6-2. These data tabulations include fuel cycle specific calculated neutron exposures at the end of the twenty sixth fuel cycle (the last completed at Kewaunee) as well as future projections to the end of Cycle 27 (the current operating cycle) and for several intervals extending to 60 calendar years of operation. The calculations account for a core power uprate from 1650 MWt to 1772 MWt that occurred during Cycle 26. The projections were based on the assumption that the core power distributions and associated plant operating characteristics from the Cycle 27 uprated core design were representative of future plant operation. The future projections are also based on the current reactor power level of 1772 MWt.

Radial gradient information applicable to fast ($E > 1.0$ MeV) neutron fluence and dpa are given in Tables 6-3 and 6-4, respectively. The data, based on the cumulative integrated exposures from Cycles 1 through 26, are presented on a relative basis for each exposure parameter at several azimuthal locations. Exposure distributions through the vessel wall may be obtained by multiplying the calculated exposure at the vessel inner radius by the gradient data listed in Tables 6-3 and 6-4.

The calculated fast neutron exposures for the five surveillance capsules withdrawn from the Kewaunee reactor are provided in Table 6-5. These assigned neutron exposure levels are based on the plant and fuel cycle specific neutron transport calculations discussed in this section.

From the data provided in Table 6-5 it is noted that Capsule T received a fluence ($E > 1.0$ MeV) of 5.62×10^{19} n/cm² after exposure through the end of the twenty sixth fuel cycle (i.e., after 24.6 EFPY of plant operation).

In addition to the Kewaunee surveillance capsule evaluations, the Master Curve Assessment of the Kewaunee pressure vessel weld metal [Reference 5] was supported by fracture toughness data derived from an accelerated capsule (A-35) withdrawn from the Maine Yankee reactor. In order to provide a consistent data base for use in this evaluation, the neutron exposure of the Maine Yankee accelerated capsule was re-calculated using current technology and ENDF/B-VI cross-sections. This re-calculation of the Maine Yankee accelerated capsule utilized the same methodology described earlier in this section. The results of the re-calculation of Maine Yankee Capsule A-35 indicated that the surveillance specimens had been irradiated for a period of 4.5 EFPY and had received a fluence ($E > 1.0$ MeV) of 6.11×10^{19} n/cm².

Updated lead factors for the Kewaunee surveillance capsules are provided in Table 6-6. The capsule lead factor is defined as the ratio of the calculated fluence ($E > 1.0$ MeV) at the geometric center of the surveillance capsule to the corresponding maximum calculated fluence at the pressure vessel clad/base metal interface. In Table 6-6, the lead factors for capsules that have been withdrawn from the reactor (V, R, P, S, and T) were based on the calculated fluence values for the irradiation period corresponding to the time of withdrawal for the individual capsules. For the capsule remaining in the reactor (N), the lead

factor corresponds to the calculated fluence values at the end of Cycle 26, the last completed fuel cycle at Kewaunee.

In Table 6-7, fast neutron fluence ($E > 1.0$ MeV) projections are provided for all materials comprising the extended beltline region of the Kewaunee reactor pressure vessel. Fluence data are provided for the end of Cycle 26 (24.6 EFPY), for 40 calendar years of operation (33.0 EFPY), and for 60 calendar years of operation (52.1 EFPY). The information included in Table 7 shows that the maximum vessel exposures listed in Table 2 of this section occur on the intermediate shell base material with all other vessel materials experiencing a lower neutron exposure. The data in Table 6-7 also shows that through 40 years of operation the primary loop nozzles and associated welds remain below a fluence of $1.0E+17$ n/cm², but the lower regions of the RCS inlet nozzle and both the inlet nozzle and outlet nozzle welds are projected to reach the $1.0E+17$ n/cm² threshold during the 40 – 60 year operating period.

In Table 6-8 projections of maximum fast neutron fluence ($E > 1.0$ MeV) and gamma ray dose experienced by the primary biological shield are listed. The data are provided as a function of axial position relative to the active core midplane and extending from the bottom to the top of the active fuel. The data traverses were taken along the 0° azimuth. The exposure data are tabulated for the end of Cycle 26 (24.6 EFPY), for 40 calendar years of operation (33.0 EFPY), and for 60 calendar years of operation (52.1 EFPY).

Neutron exposure projections beyond the end of Cycle 27 were based on an operating scenario that consisted of a series of 18 month operating cycles followed by a 25 day refueling outage. The reactor was considered to be operating at full power for the entire 18 month cycle. This full power period coupled with the 25 day refueling outage resulted in a net capacity factor of 95.6% with a total operating time of 33.0 EFPY at EOL and 52.1 EFPY at EOLE. Both of these operating times are including in the exposure projections tabulated in this section.

The neutron exposure projections were also based on continued use of low leakage fuel management. The specific radial power distribution used for the projections was as follows:

Relative Radial Power Distribution Used for Neutron Exposure Projections

	7	8	9	10	11	12	13
G	0.887	1.113	1.265	1.203	1.186	1.235	0.420
H	1.121	1.223	1.208	1.280	1.239	1.145	0.342
I	1.269	1.208	1.284	1.193	1.231	0.563	
J	1.208	1.282	1.188	1.215	1.118	0.348	
K	1.192	1.246	1.238	1.134	0.487		
L	1.242	1.155	0.568	0.353			
M	0.421	0.345					

These values represent the average relative radial power over the fuel cycle and can be estimated from the following equation:

$$P_{Avg} = \frac{EOCBurnup - BOCBurnup}{CycleAverageBurnup}$$

where:

P_{Avg} = Cycle Average Relative Power for an individual fuel assembly.

BOC Burnup = Beginning of Cycle Burnup for the individual fuel assembly.

EOC Burnup = End of Cycle Burnup for the individual fuel assembly.

Cycle Average Burnup = The Cycle Average Burnup for the Entire Core.

Actual future fuel cycle designs can be compared to the power distribution map shown above in order to evaluate actual performance compared to projections. To maintain the validity of the projections, the peripheral power distributions averaged over multiple cycles should be maintained at or below those shown above.

6.3 NEUTRON DOSIMETRY

The validity of the calculated neutron exposures previously reported in Section 6.2 is demonstrated by a direct comparison against the measured sensor reaction rates and via a least squares evaluation performed for each of the capsule dosimetry sets. However, since the neutron dosimetry measurement data merely serves to validate the calculated results, only the direct comparison of measured-to-calculated results for the most recent surveillance capsule removed from service is provided in this section of the report. For completeness, the assessment of all measured dosimetry removed to date, based on both direct and least squares evaluation comparisons, is documented in Appendix A.

The direct comparison of measured versus calculated fast neutron threshold reaction rates for the sensors from Capsule T, that was withdrawn from Kewaunee at the end of the twenty sixth fuel cycle, is summarized below.

Reaction	Reaction Rates (rps/atom)		M/C Ratio
	Measured	Calculated	
$^{63}\text{Cu}(n,\alpha)^{60}\text{Co}$	4.76E-17	4.92E-17	0.97
$^{54}\text{Fe}(n,p)^{54}\text{Mn}$	5.20E-15	5.25E-15	0.99
$^{58}\text{Ni}(n,p)^{58}\text{Co}$	7.22E-15	7.20E-15	1.00
$^{238}\text{U}(n,p)^{137}\text{Cs}$ (Cd)	2.35E-14	2.52E-14	0.93
$^{237}\text{Np}(n,f)^{137}\text{Cs}$ (Cd)	2.11E-13	1.97E-13	1.07
Average:			0.99
% Standard Deviation:			5.2

The measured-to-calculated (M/C) reaction rate ratios for the Capsule T threshold reactions range from 0.93 to 1.07, and the average M/C ratio is $0.99 \pm 5.2\%$ (1σ). This direct comparison falls well within the $\pm 20\%$ criterion specified in Regulatory Guide 1.190; furthermore, it is consistent with the full set of comparisons given in Appendix A for all measured dosimetry removed to date from the Kewaunee reactor. These comparisons validate the current analytical results described in Section 6.2; therefore, the calculations are deemed applicable for Kewaunee.

6.4 CALCULATIONAL UNCERTAINTIES

The uncertainty associated with the calculated neutron exposure of the Kewaunee surveillance capsule and reactor pressure vessel is based on the recommended approach provided in Regulatory Guide 1.190. In particular, the qualification of the methodology was carried out in the following four stages:

- 1 - Comparison of calculations with benchmark measurements from the Pool Critical Assembly (PCA) simulator at the Oak Ridge National Laboratory (ORNL).
- 2 - Comparisons of calculations with surveillance capsule and reactor cavity measurements from the H. B. Robinson power reactor benchmark experiment.
- 3 - An analytical sensitivity study addressing the uncertainty components resulting from important input parameters applicable to the plant specific transport calculations used in the neutron exposure assessments.
- 4 - Comparisons of the plant specific calculations with all available dosimetry results from the Kewaunee surveillance program.

The first phase of the methods qualification (PCA comparisons) addressed the adequacy of basic transport calculation and dosimetry evaluation techniques and associated cross-sections. This phase, however, did not test the accuracy of commercial core neutron source calculations nor did it address uncertainties in operational or geometric variables that impact power reactor calculations. The second phase of the qualification (H. B. Robinson comparisons) addressed uncertainties in these additional areas that are primarily methods related and would tend to apply generically to all fast neutron exposure evaluations. The third phase of the qualification (analytical sensitivity study) identified the potential uncertainties introduced into the overall evaluation due to calculational methods approximations as well as to a lack of knowledge relative to various plant specific input parameters. The overall calculational uncertainty applicable to the Kewaunee analysis was established from results of these three phases of the methods qualification.

The fourth phase of the uncertainty assessment (comparisons with Kewaunee measurements) was used solely to demonstrate the validity of the transport calculations and to confirm the uncertainty estimates associated with the analytical results. The comparison was used only as a check and was not used in any way to modify the calculated surveillance capsule and pressure vessel neutron exposures previously described in Section 6.2. As such, the validation of the Kewaunee analytical model based on the measured plant dosimetry is completely described in Appendix A.

The following summarizes the uncertainties developed from the first three phases of the methodology qualification. Additional information pertinent to these evaluations is provided in Reference 26.

	Capsule	Vessel IR
PCA Comparisons	3%	3%
H. B. Robinson Comparisons	3%	3%
Analytical Sensitivity Studies	10%	11%
Additional Uncertainty for Factors not Explicitly Evaluated	5%	5%
Net Calculational Uncertainty	12%	13%

The net calculational uncertainty was determined by combining the individual components in quadrature. Therefore, the resultant uncertainty was treated as random and no systematic bias was applied to the analytical results.

The plant specific measurement comparisons described in Appendix A support these uncertainty assessments for Kewaunee. The least squares data comparisons for the five surveillance capsules withdrawn to date from the Kewaunee reactor indicate an average Adjusted to Calculated (A/C) ratio of 0.99 with a standard deviation of 4.1% and 1.00 with a standard deviation of 4.3% for fluence ($E > 1.0$ MeV) and iron atom displacements (dpa), respectively. This data comparison is not only self consistent for the Kewaunee reactor, but is in excellent agreement with the overall Westinghouse surveillance capsule dosimetry database which currently includes data evaluations for 125 sets of reactor dosimetry. The overall database comparisons indicate an average Adjusted to Calculated (A/C) ratio of 0.99 with a standard deviation of 7.1% and 1.00 with a standard deviation of 6.6% for fluence ($E > 1.0$ MeV) and iron atom displacements (dpa), respectively. These comparisons are similar to the Kewaunee specific results.

Table 6-1
 Calculated Neutron Exposure Rates And Integrated Exposures
 At The Surveillance Capsule Center

Cycle	Cycle Length [EFPS]	Cumulative Irradiation Time [EFPS]	Cumulative Irradiation Time [EFPY]	Neutron Flux (E > 1.0 MeV) [n/cm ² -s]		
				13°	23°	33°
1	4.06E+07	4.06E+07	1.3	1.44E+11	8.10E+10	7.64E+10
2	2.14E+07	6.20E+07	2.0	1.43E+11	8.64E+10	8.43E+10
3	3.24E+07	9.44E+07	3.0	9.14E+10	7.63E+10	7.90E+10
4	2.97E+07	1.24E+08	3.9	1.10E+11	7.19E+10	6.88E+10
5	2.18E+07	1.46E+08	4.6	1.11E+11	7.25E+10	7.02E+10
6	2.44E+07	1.70E+08	5.4	1.08E+11	7.70E+10	7.81E+10
7	2.56E+07	1.96E+08	6.2	1.02E+11	6.91E+10	6.93E+10
8	2.49E+07	2.21E+08	7.0	1.05E+11	7.38E+10	7.32E+10
9	2.57E+07	2.47E+08	7.8	1.10E+11	7.33E+10	7.01E+10
10	2.33E+07	2.70E+08	8.6	1.02E+11	7.11E+10	6.88E+10
11	2.71E+07	2.97E+08	9.4	9.99E+10	6.93E+10	6.58E+10
12	2.61E+07	3.23E+08	10.2	1.09E+11	6.87E+10	6.24E+10
13	2.81E+07	3.51E+08	11.1	1.08E+11	7.48E+10	7.22E+10
14	2.57E+07	3.77E+08	11.9	1.03E+11	7.26E+10	6.99E+10
15	2.68E+07	4.04E+08	12.8	1.05E+11	7.30E+10	6.93E+10
16	2.75E+07	4.31E+08	13.7	8.33E+10	7.02E+10	7.06E+10
17	2.53E+07	4.56E+08	14.5	8.73E+10	7.05E+10	6.91E+10
18	2.67E+07	4.83E+08	15.3	8.47E+10	7.11E+10	7.38E+10
19	2.81E+07	5.11E+08	16.2	9.28E+10	7.15E+10	6.97E+10
20	2.57E+07	5.37E+08	17.0	9.24E+10	7.33E+10	7.47E+10
21	3.88E+07	5.76E+08	18.2	9.21E+10	7.09E+10	7.32E+10
22	3.96E+07	6.15E+08	19.5	1.01E+11	7.21E+10	6.82E+10
23	4.08E+07	6.56E+08	20.8	9.68E+10	7.33E+10	7.29E+10
24	3.84E+07	6.95E+08	22.0	1.03E+11	6.87E+10	6.64E+10
25	3.96E+07	7.34E+08	23.3	1.07E+11	7.12E+10	6.83E+10
26	4.27E+07	7.77E+08	24.6	1.01E+11	6.36E+10	6.07E+10
27	4.31E+07	8.20E+08	26.0	9.86E+10	6.15E+10	5.94E+10
Future	6.37E+07	8.84E+08	28.0	9.86E+10	6.15E+10	5.94E+10
Future	1.58E+08	1.04E+09	33.0	9.86E+10	6.15E+10	5.94E+10
Future	9.47E+07	1.14E+09	36.0	9.86E+10	6.15E+10	5.94E+10
Future	1.26E+08	1.26E+09	40.0	9.86E+10	6.15E+10	5.94E+10
Future	1.26E+08	1.39E+09	44.0	9.86E+10	6.15E+10	5.94E+10
Future	1.26E+08	1.51E+09	48.0	9.86E+10	6.15E+10	5.94E+10
Future	1.29E+08	1.64E+09	52.1	9.86E+10	6.15E+10	5.94E+10

Note: 1) Neutron exposure values reported for the surveillance capsules are centered at the core midplane.

Table 6-1 cont'd
 Calculated Neutron Exposure Rates And Integrated Exposures
 At The Surveillance Capsule Center

Cycle	Cycle Length [EFPS]	Cumulative Irradiation Time [EFPS]	Cumulative Irradiation Time [EFPY]	Neutron Fluence (E > 1.0 MeV) [n/cm ²]		
				13°	23°	33°
1	4.06E+07	4.06E+07	1.3	5.86E+18	3.29E+18	3.10E+18
2	2.14E+07	6.20E+07	2.0	8.91E+18	5.14E+18	4.91E+18
3	3.24E+07	9.44E+07	3.0	1.19E+19	7.61E+18	7.47E+18
4	2.97E+07	1.24E+08	3.9	1.51E+19	9.74E+18	9.51E+18
5	2.18E+07	1.46E+08	4.6	1.76E+19	1.13E+19	1.10E+19
6	2.44E+07	1.70E+08	5.4	2.02E+19	1.32E+19	1.29E+19
7	2.56E+07	1.96E+08	6.2	2.28E+19	1.50E+19	1.47E+19
8	2.49E+07	2.21E+08	7.0	2.54E+19	1.68E+19	1.65E+19
9	2.57E+07	2.47E+08	7.8	2.82E+19	1.87E+19	1.83E+19
10	2.33E+07	2.70E+08	8.6	3.06E+19	2.04E+19	1.99E+19
11	2.71E+07	2.97E+08	9.4	3.33E+19	2.22E+19	2.17E+19
12	2.61E+07	3.23E+08	10.2	3.62E+19	2.40E+19	2.34E+19
13	2.81E+07	3.51E+08	11.1	3.92E+19	2.61E+19	2.54E+19
14	2.57E+07	3.77E+08	11.9	4.18E+19	2.80E+19	2.72E+19
15	2.68E+07	4.04E+08	12.8	4.46E+19	2.99E+19	2.90E+19
16	2.75E+07	4.31E+08	13.7	4.69E+19	3.19E+19	3.10E+19
17	2.53E+07	4.56E+08	14.5	4.91E+19	3.37E+19	3.27E+19
18	2.67E+07	4.83E+08	15.3	5.14E+19	3.56E+19	3.47E+19
19	2.81E+07	5.11E+08	16.2	5.40E+19	3.76E+19	3.67E+19
20	2.57E+07	5.37E+08	17.0	5.64E+19	3.95E+19	3.86E+19
21	3.88E+07	5.76E+08	18.2	6.00E+19	4.22E+19	4.14E+19
22	3.96E+07	6.15E+08	19.5	6.40E+19	4.51E+19	4.41E+19
23	4.08E+07	6.56E+08	20.8	6.79E+19	4.80E+19	4.71E+19
24	3.84E+07	6.95E+08	22.0	7.19E+19	5.07E+19	4.96E+19
25	3.96E+07	7.34E+08	23.3	7.61E+19	5.35E+19	5.23E+19
26	4.27E+07	7.77E+08	24.6	8.04E+19	5.62E+19	5.49E+19
27	4.31E+07	8.20E+08	26.0	8.47E+19	5.89E+19	5.75E+19
Future	6.37E+07	8.84E+08	28.0	9.10E+19	6.28E+19	6.13E+19
Future	1.58E+08	1.04E+09	33.0	1.07E+20	7.25E+19	7.07E+19
Future	9.47E+07	1.14E+09	36.0	1.16E+20	7.83E+19	7.63E+19
Future	1.26E+08	1.26E+09	40.0	1.28E+20	8.61E+19	8.38E+19
Future	1.26E+08	1.39E+09	44.0	1.41E+20	9.38E+19	9.13E+19
Future	1.26E+08	1.51E+09	48.0	1.53E+20	1.02E+20	9.88E+19
Future	1.29E+08	1.64E+09	52.1	1.66E+20	1.10E+20	1.06E+20

Note: 1) Neutron exposure values reported for the surveillance capsules are centered at the core midplane.

Table 6-1 cont'd
 Calculated Neutron Exposure Rates And Integrated Exposures
 At The Surveillance Capsule Center

Cycle	Cycle Length [EFPS]	Cumulative Irradiation Time [EFPS]	Cumulative Irradiation Time [EFPY]	Iron Atom Displacement Rate [dpa/s]		
				13°	23°	33°
1	4.06E+07	4.06E+07	1.3	2.63E-10	1.41E-10	1.34E-10
2	2.14E+07	6.20E+07	2.0	2.59E-10	1.50E-10	1.48E-10
3	3.24E+07	9.44E+07	3.0	1.65E-10	1.32E-10	1.38E-10
4	2.97E+07	1.24E+08	3.9	1.99E-10	1.25E-10	1.20E-10
5	2.18E+07	1.46E+08	4.6	2.01E-10	1.26E-10	1.23E-10
6	2.44E+07	1.70E+08	5.4	1.96E-10	1.33E-10	1.37E-10
7	2.56E+07	1.96E+08	6.2	1.84E-10	1.20E-10	1.21E-10
8	2.49E+07	2.21E+08	7.0	1.90E-10	1.28E-10	1.28E-10
9	2.57E+07	2.47E+08	7.8	1.98E-10	1.27E-10	1.23E-10
10	2.33E+07	2.70E+08	8.6	1.85E-10	1.23E-10	1.21E-10
11	2.71E+07	2.97E+08	9.4	1.81E-10	1.20E-10	1.15E-10
12	2.61E+07	3.23E+08	10.2	1.96E-10	1.19E-10	1.09E-10
13	2.81E+07	3.51E+08	11.1	1.95E-10	1.30E-10	1.27E-10
14	2.57E+07	3.77E+08	11.9	1.86E-10	1.26E-10	1.22E-10
15	2.68E+07	4.04E+08	12.8	1.90E-10	1.26E-10	1.21E-10
16	2.75E+07	4.31E+08	13.7	1.50E-10	1.21E-10	1.24E-10
17	2.53E+07	4.56E+08	14.5	1.57E-10	1.22E-10	1.21E-10
18	2.67E+07	4.83E+08	15.3	1.52E-10	1.23E-10	1.29E-10
19	2.81E+07	5.11E+08	16.2	1.67E-10	1.24E-10	1.22E-10
20	2.57E+07	5.37E+08	17.0	1.67E-10	1.27E-10	1.31E-10
21	3.88E+07	5.76E+08	18.2	1.66E-10	1.23E-10	1.28E-10
22	3.96E+07	6.15E+08	19.5	1.82E-10	1.25E-10	1.20E-10
23	4.08E+07	6.56E+08	20.8	1.75E-10	1.27E-10	1.28E-10
24	3.84E+07	6.95E+08	22.0	1.87E-10	1.19E-10	1.16E-10
25	3.96E+07	7.34E+08	23.3	1.94E-10	1.23E-10	1.20E-10
26	4.27E+07	7.77E+08	24.6	1.82E-10	1.10E-10	1.06E-10
27	4.31E+07	8.20E+08	26.0	1.78E-10	1.06E-10	1.04E-10
Future	6.37E+07	8.84E+08	28.0	1.78E-10	1.06E-10	1.04E-10
Future	1.58E+08	1.04E+09	33.0	1.78E-10	1.06E-10	1.04E-10
Future	9.47E+07	1.14E+09	36.0	1.78E-10	1.06E-10	1.04E-10
Future	1.26E+08	1.26E+09	40.0	1.78E-10	1.06E-10	1.04E-10
Future	1.26E+08	1.39E+09	44.0	1.78E-10	1.06E-10	1.04E-10
Future	1.26E+08	1.51E+09	48.0	1.78E-10	1.06E-10	1.04E-10
Future	1.29E+08	1.64E+09	52.1	1.78E-10	1.06E-10	1.04E-10

Note: 1) Neutron exposure values reported for the surveillance capsules are centered at the core midplane.

Table 6-1 cont'd
 Calculated Neutron Exposure Rates And Integrated Exposures
 At The Surveillance Capsule Center

Cycle	Cycle Length [EFPS]	Cumulative Irradiation Time [EFPS]	Cumulative Irradiation Time [EFPY]	Iron Atom Displacements [dpa]		
				13°	23°	33°
1	4.06E+07	4.06E+07	1.3	1.07E-02	5.72E-03	5.44E-03
2	2.14E+07	6.20E+07	2.0	1.62E-02	8.94E-03	8.61E-03
3	3.24E+07	9.44E+07	3.0	2.15E-02	1.32E-02	1.31E-02
4	2.97E+07	1.24E+08	3.9	2.74E-02	1.69E-02	1.67E-02
5	2.18E+07	1.46E+08	4.6	3.18E-02	1.97E-02	1.93E-02
6	2.44E+07	1.70E+08	5.4	3.66E-02	2.29E-02	2.27E-02
7	2.56E+07	1.96E+08	6.2	4.13E-02	2.60E-02	2.58E-02
8	2.49E+07	2.21E+08	7.0	4.60E-02	2.92E-02	2.90E-02
9	2.57E+07	2.47E+08	7.8	5.11E-02	3.24E-02	3.21E-02
10	2.33E+07	2.70E+08	8.6	5.54E-02	3.53E-02	3.49E-02
11	2.71E+07	2.97E+08	9.4	6.03E-02	3.85E-02	3.81E-02
12	2.61E+07	3.23E+08	10.2	6.55E-02	4.16E-02	4.09E-02
13	2.81E+07	3.51E+08	11.1	7.09E-02	4.53E-02	4.45E-02
14	2.57E+07	3.77E+08	11.9	7.57E-02	4.85E-02	4.76E-02
15	2.68E+07	4.04E+08	12.8	8.08E-02	5.19E-02	5.09E-02
16	2.75E+07	4.31E+08	13.7	8.49E-02	5.52E-02	5.43E-02
17	2.53E+07	4.56E+08	14.5	8.89E-02	5.83E-02	5.73E-02
18	2.67E+07	4.83E+08	15.3	9.30E-02	6.16E-02	6.08E-02
19	2.81E+07	5.11E+08	16.2	9.77E-02	6.51E-02	6.42E-02
20	2.57E+07	5.37E+08	17.0	1.02E-01	6.83E-02	6.76E-02
21	3.88E+07	5.76E+08	18.2	1.08E-01	7.31E-02	7.25E-02
22	3.96E+07	6.15E+08	19.5	1.16E-01	7.80E-02	7.73E-02
23	4.08E+07	6.56E+08	20.8	1.23E-01	8.32E-02	8.25E-02
24	3.84E+07	6.95E+08	22.0	1.30E-01	8.77E-02	8.69E-02
25	3.96E+07	7.34E+08	23.3	1.38E-01	9.26E-02	9.17E-02
26	4.27E+07	7.77E+08	24.6	1.45E-01	9.73E-02	9.62E-02
27	4.31E+07	8.20E+08	26.0	1.53E-01	1.02E-01	1.01E-01
Future	6.37E+07	8.84E+08	28.0	1.64E-01	1.09E-01	1.07E-01
Future	1.58E+08	1.04E+09	33.0	1.93E-01	1.26E-01	1.24E-01
Future	9.47E+07	1.14E+09	36.0	2.09E-01	1.36E-01	1.34E-01
Future	1.26E+08	1.26E+09	40.0	2.32E-01	1.49E-01	1.47E-01
Future	1.26E+08	1.39E+09	44.0	2.54E-01	1.62E-01	1.60E-01
Future	1.26E+08	1.51E+09	48.0	2.77E-01	1.76E-01	1.73E-01
Future	1.29E+08	1.64E+09	52.1	3.00E-01	1.90E-01	1.86E-01

Note: 1) Neutron exposure values reported for the surveillance capsules are centered at the core midplane.

Table 6-2
 Calculated Azimuthal Variation Of Maximum Exposure Rates
 And Integrated Exposures At The Reactor Vessel
 Clad/Base Metal Interface

Cycle	Cycle Length [EFPS]	Cumulative Irradiation Time [EFPS]	Cumulative Irradiation Time [EFPY]	Neutron Flux (E > 1.0 MeV) [n/cm ² -s]			
				0°	15°	30°	45°
1	4.06E+07	4.06E+07	1.3	4.76E+10	2.84E+10	1.88E+10	1.61E+10
2	2.14E+07	6.20E+07	2.0	4.61E+10	2.84E+10	2.06E+10	1.77E+10
3	3.24E+07	9.44E+07	3.0	3.13E+10	2.00E+10	1.93E+10	1.66E+10
4	2.97E+07	1.24E+08	3.9	3.56E+10	2.25E+10	1.71E+10	1.45E+10
5	2.18E+07	1.46E+08	4.6	3.72E+10	2.28E+10	1.73E+10	1.51E+10
6	2.44E+07	1.70E+08	5.4	3.66E+10	2.26E+10	1.90E+10	1.68E+10
7	2.56E+07	1.96E+08	6.2	3.45E+10	2.11E+10	1.70E+10	1.50E+10
8	2.49E+07	2.21E+08	7.0	3.51E+10	2.19E+10	1.79E+10	1.56E+10
9	2.57E+07	2.47E+08	7.8	3.77E+10	2.26E+10	1.74E+10	1.42E+10
10	2.33E+07	2.70E+08	8.6	3.40E+10	2.13E+10	1.70E+10	1.41E+10
11	2.71E+07	2.97E+08	9.4	3.32E+10	2.08E+10	1.64E+10	1.39E+10
12	2.61E+07	3.23E+08	10.2	3.72E+10	2.23E+10	1.57E+10	1.31E+10
13	2.81E+07	3.51E+08	11.1	3.56E+10	2.24E+10	1.79E+10	1.47E+10
14	2.57E+07	3.77E+08	11.9	3.46E+10	2.16E+10	1.74E+10	1.42E+10
15	2.68E+07	4.04E+08	12.8	3.51E+10	2.19E+10	1.73E+10	1.39E+10
16	2.75E+07	4.31E+08	13.7	2.40E+10	1.82E+10	1.74E+10	1.43E+10
17	2.53E+07	4.56E+08	14.5	2.53E+10	1.89E+10	1.72E+10	1.41E+10
18	2.67E+07	4.83E+08	15.3	2.47E+10	1.84E+10	1.80E+10	1.54E+10
19	2.81E+07	5.11E+08	16.2	2.67E+10	1.99E+10	1.73E+10	1.43E+10
20	2.57E+07	5.37E+08	17.0	2.72E+10	1.98E+10	1.82E+10	1.60E+10
21	3.88E+07	5.76E+08	18.2	2.84E+10	1.96E+10	1.79E+10	1.56E+10
22	3.96E+07	6.15E+08	19.5	3.21E+10	2.12E+10	1.69E+10	1.36E+10
23	4.08E+07	6.56E+08	20.8	3.01E+10	2.06E+10	1.81E+10	1.53E+10
24	3.84E+07	6.95E+08	22.0	3.36E+10	2.14E+10	1.64E+10	1.42E+10
25	3.96E+07	7.34E+08	23.3	3.46E+10	2.22E+10	1.69E+10	1.41E+10
26	4.27E+07	7.77E+08	24.6	3.23E+10	2.06E+10	1.52E+10	1.36E+10
27	4.31E+07	8.20E+08	26.0	3.20E+10	2.03E+10	1.46E+10	1.39E+10
Future	6.37E+07	8.84E+08	28.0	3.20E+10	2.03E+10	1.48E+10	1.38E+10
Future	1.58E+08	1.04E+09	33.0	3.20E+10	2.03E+10	1.48E+10	1.38E+10
Future	9.47E+07	1.14E+09	36.0	3.20E+10	2.03E+10	1.48E+10	1.38E+10
Future	1.26E+08	1.26E+09	40.0	3.20E+10	2.03E+10	1.48E+10	1.38E+10
Future	1.26E+08	1.39E+09	44.0	3.20E+10	2.03E+10	1.48E+10	1.38E+10
Future	1.26E+08	1.51E+09	48.0	3.20E+10	2.03E+10	1.48E+10	1.38E+10
Future	1.29E+08	1.64E+09	52.1	3.20E+10	2.03E+10	1.48E+10	1.38E+10

Table 6-2 cont'd
 Calculated Azimuthal Variation Of Maximum Exposure Rates
 And Integrated Exposures At The Reactor Vessel
 Clad/Base Metal Interface

Cycle	Cycle Length [EFPS]	Cumulative Irradiation Time [EFPS]	Cumulative Irradiation Time [EFPY]	Neutron Fluence (E > 1.0 MeV) [n/cm ²]			
				0°	15°	30°	45°
1	4.06E+07	4.06E+07	1.3	1.93E+18	1.15E+18	7.64E+17	6.55E+17
2	2.14E+07	6.20E+07	2.0	2.92E+18	1.76E+18	1.20E+18	1.03E+18
3	3.24E+07	9.44E+07	3.0	3.93E+18	2.41E+18	1.83E+18	1.57E+18
4	2.97E+07	1.24E+08	3.9	4.99E+18	3.08E+18	2.34E+18	2.00E+18
5	2.18E+07	1.46E+08	4.6	5.80E+18	3.57E+18	2.71E+18	2.33E+18
6	2.44E+07	1.70E+08	5.4	6.69E+18	4.12E+18	3.18E+18	2.74E+18
7	2.56E+07	1.96E+08	6.2	7.57E+18	4.66E+18	3.61E+18	3.13E+18
8	2.49E+07	2.21E+08	7.0	8.45E+18	5.21E+18	4.06E+18	3.52E+18
9	2.57E+07	2.47E+08	7.8	9.42E+18	5.79E+18	4.51E+18	3.88E+18
10	2.33E+07	2.70E+08	8.6	1.02E+19	6.29E+18	4.90E+18	4.21E+18
11	2.71E+07	2.97E+08	9.4	1.11E+19	6.85E+18	5.35E+18	4.59E+18
12	2.61E+07	3.23E+08	10.2	1.21E+19	7.43E+18	5.76E+18	4.93E+18
13	2.81E+07	3.51E+08	11.1	1.31E+19	8.06E+18	6.26E+18	5.34E+18
14	2.57E+07	3.77E+08	11.9	1.40E+19	8.61E+18	6.71E+18	5.71E+18
15	2.68E+07	4.04E+08	12.8	1.49E+19	9.20E+18	7.17E+18	6.08E+18
16	2.75E+07	4.31E+08	13.7	1.56E+19	9.70E+18	7.65E+18	6.47E+18
17	2.53E+07	4.56E+08	14.5	1.62E+19	1.02E+19	8.08E+18	6.83E+18
18	2.67E+07	4.83E+08	15.3	1.69E+19	1.07E+19	8.56E+18	7.24E+18
19	2.81E+07	5.11E+08	16.2	1.76E+19	1.12E+19	9.05E+18	7.64E+18
20	2.57E+07	5.37E+08	17.0	1.83E+19	1.17E+19	9.52E+18	8.05E+18
21	3.88E+07	5.76E+08	18.2	1.94E+19	1.25E+19	1.02E+19	8.65E+18
22	3.96E+07	6.15E+08	19.5	2.07E+19	1.33E+19	1.09E+19	9.19E+18
23	4.08E+07	6.56E+08	20.8	2.19E+19	1.42E+19	1.16E+19	9.82E+18
24	3.84E+07	6.95E+08	22.0	2.32E+19	1.50E+19	1.23E+19	1.04E+19
25	3.96E+07	7.34E+08	23.3	2.46E+19	1.59E+19	1.29E+19	1.09E+19
26	4.27E+07	7.77E+08	24.6	2.60E+19	1.68E+19	1.36E+19	1.15E+19
27	4.31E+07	8.20E+08	26.0	2.73E+19	1.76E+19	1.42E+19	1.21E+19
Future	6.37E+07	8.84E+08	28.0	2.94E+19	1.89E+19	1.51E+19	1.30E+19
Future	1.58E+08	1.04E+09	33.0	3.44E+19	2.21E+19	1.75E+19	1.52E+19
Future	9.47E+07	1.14E+09	36.0	3.75E+19	2.41E+19	1.89E+19	1.65E+19
Future	1.26E+08	1.26E+09	40.0	4.15E+19	2.66E+19	2.07E+19	1.82E+19
Future	1.26E+08	1.39E+09	44.0	4.56E+19	2.92E+19	2.26E+19	2.00E+19
Future	1.26E+08	1.51E+09	48.0	4.96E+19	3.18E+19	2.45E+19	2.17E+19
Future	1.29E+08	1.64E+09	52.1	5.37E+19	3.44E+19	2.64E+19	2.35E+19

Table 6-2 cont'd
 Calculated Azimuthal Variation Of Fast Neutron Exposure Rates
 And Iron Atom Displacement Rates At The Reactor Vessel
 Clad/Base Metal Interface

Cycle	Cycle Length [EFPS]	Cumulative Irradiation Time [EFPS]	Cumulative Irradiation Time [EFPY]	Iron Atom Displacement Rate [dpa/s]			
				0°	15°	30°	45°
1	4.06E+07	4.06E+07	1.3	7.75E-11	4.79E-11	3.09E-11	2.62E-11
2	2.14E+07	6.20E+07	2.0	7.51E-11	4.79E-11	3.38E-11	2.87E-11
3	3.24E+07	9.44E+07	3.0	5.09E-11	3.35E-11	3.15E-11	2.69E-11
4	2.97E+07	1.24E+08	3.9	5.80E-11	3.78E-11	2.80E-11	2.35E-11
5	2.18E+07	1.46E+08	4.6	6.05E-11	3.83E-11	2.83E-11	2.45E-11
6	2.44E+07	1.70E+08	5.4	5.92E-11	3.80E-11	3.12E-11	2.73E-11
7	2.56E+07	1.96E+08	6.2	5.63E-11	3.54E-11	2.78E-11	2.43E-11
8	2.49E+07	2.21E+08	7.0	5.74E-11	3.68E-11	2.94E-11	2.53E-11
9	2.57E+07	2.47E+08	7.8	6.11E-11	3.80E-11	2.86E-11	2.31E-11
10	2.33E+07	2.70E+08	8.6	5.58E-11	3.57E-11	2.79E-11	2.28E-11
11	2.71E+07	2.97E+08	9.4	5.39E-11	3.51E-11	2.69E-11	2.25E-11
12	2.61E+07	3.23E+08	10.2	6.05E-11	3.75E-11	2.58E-11	2.12E-11
13	2.81E+07	3.51E+08	11.1	5.80E-11	3.77E-11	2.94E-11	2.38E-11
14	2.57E+07	3.77E+08	11.9	5.60E-11	3.62E-11	2.84E-11	2.30E-11
15	2.68E+07	4.04E+08	12.8	5.71E-11	3.66E-11	2.84E-11	2.25E-11
16	2.75E+07	4.31E+08	13.7	3.93E-11	3.05E-11	2.84E-11	2.30E-11
17	2.53E+07	4.56E+08	14.5	4.11E-11	3.16E-11	2.81E-11	2.29E-11
18	2.67E+07	4.83E+08	15.3	4.01E-11	3.07E-11	2.96E-11	2.51E-11
19	2.81E+07	5.11E+08	16.2	4.38E-11	3.35E-11	2.81E-11	2.31E-11
20	2.57E+07	5.37E+08	17.0	4.44E-11	3.31E-11	3.00E-11	2.57E-11
21	3.88E+07	5.76E+08	18.2	4.61E-11	3.30E-11	2.91E-11	2.53E-11
22	3.96E+07	6.15E+08	19.5	5.23E-11	3.56E-11	2.80E-11	2.20E-11
23	4.08E+07	6.56E+08	20.8	4.90E-11	3.43E-11	2.94E-11	2.50E-11
24	3.84E+07	6.95E+08	22.0	5.47E-11	3.59E-11	2.68E-11	2.29E-11
25	3.96E+07	7.34E+08	23.3	5.63E-11	3.71E-11	2.80E-11	2.27E-11
26	4.27E+07	7.77E+08	24.6	5.27E-11	3.49E-11	2.48E-11	2.22E-11
27	4.31E+07	8.20E+08	26.0	5.22E-11	3.43E-11	2.41E-11	2.23E-11
Future	6.37E+07	8.84E+08	28.0	5.21E-11	3.41E-11	2.42E-11	2.24E-11
Future	1.58E+08	1.04E+09	33.0	5.21E-11	3.41E-11	2.42E-11	2.24E-11
Future	9.47E+07	1.14E+09	36.0	5.21E-11	3.41E-11	2.42E-11	2.24E-11
Future	1.26E+08	1.26E+09	40.0	5.21E-11	3.41E-11	2.42E-11	2.24E-11
Future	1.26E+08	1.39E+09	44.0	5.21E-11	3.41E-11	2.42E-11	2.24E-11
Future	1.26E+08	1.51E+09	48.0	5.21E-11	3.41E-11	2.42E-11	2.24E-11
Future	1.29E+08	1.64E+09	52.1	5.21E-11	3.41E-11	2.42E-11	2.24E-11

Table 6-2 cont'd
 Calculated Azimuthal Variation Of Maximum Exposure Rates
 And Integrated Exposures At The Reactor Vessel
 Clad/Base Metal Interface

Cycle	Cycle Length [EFPS]	Cumulative Irradiation Time [EFPS]	Cumulative Irradiation Time [EFPY]	Iron Atom Displacements [dpa]			
				0°	15°	30°	45°
1	4.06E+07	4.06E+07	1.3	3.15E-03	1.95E-03	1.26E-03	1.06E-03
2	2.14E+07	6.20E+07	2.0	4.76E-03	2.97E-03	1.98E-03	1.68E-03
3	3.24E+07	9.44E+07	3.0	6.40E-03	4.05E-03	3.00E-03	2.55E-03
4	2.97E+07	1.24E+08	3.9	8.13E-03	5.18E-03	3.83E-03	3.25E-03
5	2.18E+07	1.46E+08	4.6	9.45E-03	6.01E-03	4.45E-03	3.78E-03
6	2.44E+07	1.70E+08	5.4	1.09E-02	6.94E-03	5.21E-03	4.45E-03
7	2.56E+07	1.96E+08	6.2	1.23E-02	7.85E-03	5.92E-03	5.07E-03
8	2.49E+07	2.21E+08	7.0	1.38E-02	8.76E-03	6.66E-03	5.70E-03
9	2.57E+07	2.47E+08	7.8	1.53E-02	9.74E-03	7.39E-03	6.29E-03
10	2.33E+07	2.70E+08	8.6	1.66E-02	1.06E-02	8.04E-03	6.82E-03
11	2.71E+07	2.97E+08	9.4	1.81E-02	1.15E-02	8.77E-03	7.43E-03
12	2.61E+07	3.23E+08	10.2	1.97E-02	1.25E-02	9.44E-03	7.99E-03
13	2.81E+07	3.51E+08	11.1	2.13E-02	1.36E-02	1.03E-02	8.65E-03
14	2.57E+07	3.77E+08	11.9	2.27E-02	1.45E-02	1.10E-02	9.25E-03
15	2.68E+07	4.04E+08	12.8	2.43E-02	1.55E-02	1.18E-02	9.85E-03
16	2.75E+07	4.31E+08	13.7	2.54E-02	1.63E-02	1.25E-02	1.05E-02
17	2.53E+07	4.56E+08	14.5	2.64E-02	1.71E-02	1.33E-02	1.11E-02
18	2.67E+07	4.83E+08	15.3	2.75E-02	1.79E-02	1.40E-02	1.17E-02
19	2.81E+07	5.11E+08	16.2	2.87E-02	1.89E-02	1.48E-02	1.24E-02
20	2.57E+07	5.37E+08	17.0	2.98E-02	1.97E-02	1.56E-02	1.30E-02
21	3.88E+07	5.76E+08	18.2	3.16E-02	2.10E-02	1.67E-02	1.40E-02
22	3.96E+07	6.15E+08	19.5	3.37E-02	2.24E-02	1.78E-02	1.49E-02
23	4.08E+07	6.56E+08	20.8	3.57E-02	2.38E-02	1.90E-02	1.59E-02
24	3.84E+07	6.95E+08	22.0	3.78E-02	2.52E-02	2.01E-02	1.68E-02
25	3.96E+07	7.34E+08	23.3	4.00E-02	2.67E-02	2.12E-02	1.77E-02
26	4.27E+07	7.77E+08	24.6	4.23E-02	2.82E-02	2.22E-02	1.86E-02
27	4.31E+07	8.20E+08	26.0	4.45E-02	2.96E-02	2.33E-02	1.96E-02
Future	6.37E+07	8.84E+08	28.0	4.78E-02	3.18E-02	2.48E-02	2.10E-02
Future	1.58E+08	1.04E+09	33.0	5.61E-02	3.72E-02	2.87E-02	2.46E-02
Future	9.47E+07	1.14E+09	36.0	6.10E-02	4.04E-02	3.09E-02	2.67E-02
Future	1.26E+08	1.26E+09	40.0	6.76E-02	4.47E-02	3.40E-02	2.95E-02
Future	1.26E+08	1.39E+09	44.0	7.41E-02	4.90E-02	3.71E-02	3.23E-02
Future	1.26E+08	1.51E+09	48.0	8.07E-02	5.33E-02	4.01E-02	3.51E-02
Future	1.29E+08	1.64E+09	52.1	8.74E-02	5.77E-02	4.32E-02	3.80E-02

Table 6-3
Relative Radial Distribution Of Neutron Fluence ($E > 1.0$ MeV)
Within The Reactor Vessel Wall

Radius (cm)	Azimuthal Angle			
	0°	15°	30°	45°
168.04	1.000	1.000	1.000	1.000
172.25	0.638	0.645	0.634	0.646
176.46	0.364	0.375	0.364	0.374
180.66	0.200	0.211	0.203	0.209
184.87	0.103	0.116	0.112	0.114
Base Metal Inner Radius = 168.04 Base Metal 1/4T = 172.25 Base Metal 1/2T = 176.46 Base Metal 3/4T = 180.66 Base Metal Outer Radius = 184.87				

Note: Relative radial distribution data are based on the cumulative integrated exposures from Cycles 1 through 26.

Table 6-4
Relative Radial Distribution Of Iron Atom Displacements (dpa)
Within The Reactor Vessel Wall

Radius (cm)	Azimuthal Angle			
	0°	15°	30°	45°
168.04	1.000	1.000	1.000	1.000
172.25	0.707	0.724	0.710	0.718
176.46	0.472	0.497	0.481	0.487
180.66	0.304	0.334	0.321	0.322
184.87	0.180	0.214	0.207	0.206
Base Metal Inner Radius = 168.04 Base Metal 1/4T = 172.25 Base Metal 1/2T = 176.46 Base Metal 3/4T = 180.66 Base Metal Outer Radius = 184.87				

Note: Relative radial distribution data are based on the cumulative integrated exposures from Cycles 1 through 26.

Table 6-5
Calculated Fast Neutron Exposure of Surveillance Capsules
Withdrawn from Kewaunee

Capsule	Irradiation Time [EFPY]	Fluence (E > 1.0 MeV) [n/cm ²]	Iron Displacements [dpa]
V	1.3	5.86E+18	1.07E-02
R	4.6	1.76E+19	3.18E-02
P	11.1	2.61E+19	4.53E-02
S	16.2	3.67E+19	6.42E-02
T	24.6	5.62E+19	9.73E-02

Table 6-6
Calculated Surveillance Capsule Lead Factors

Capsule ID And Location	Status	Lead Factor ^(a)
V (13°)	Withdrawn EOC 1	3.03
R (13°)	Withdrawn EOC 5	3.03
P (23°)	Withdrawn EOC 13	2.00
S (33°)	Withdrawn EOC 19	2.08
T (23°)	Withdrawn EOC 26	2.17
N (33°)	In Reactor	2.12

Note: (a) Lead factor for capsule remaining in the reactor is based on cycle specific exposure calculations through the last completed fuel cycle, i.e., Cycle 26.

Table 6-7
Calculated Maximum Neutron Fluence ($E > 1.0$ MeV) for the Kewaunee Extended Beltline Materials

	Neutron Fluence ($E > 1.0$ MeV) [n/cm^2]		
	24.6 EFPY	33.0 EFPY	52.1 EFPY
Lower Shell to Lower Closure Head Weld	< 1.00E+17	< 1.00E+17	< 1.00E+17
Lower Shell	2.57E+19	3.38E+19	5.22E+19
Lower Shell to Intermediate Shell Weld	2.47E+19	3.27E+19	5.07E+19
Intermediate Shell	2.60E+19	3.44E+19	5.37E+19
Intermediate Shell to Upper Shell Weld	2.58E+18	3.42E+18	5.33E+18
Upper Shell	2.58E+18	3.42E+18	5.33E+18
RCS Inlet Nozzle to Upper Shell Weld	< 1.00E+17	< 1.00E+17	1.34E+17
RCS Inlet Nozzle	< 1.00E+17	< 1.00E+17	1.20E+17
RCS Outlet Nozzle to Upper Shell Weld	< 1.00E+17	< 1.00E+17	1.10E+17
RCS Outlet Nozzle	< 1.00E+17	< 1.00E+17	< 1.00E+17
Safety Injection Nozzle	< 1.00E+17	< 1.00E+17	< 1.00E+17
Vessel Support Bracket	< 1.00E+17	< 1.00E+17	< 1.00E+17
Core Support Guide Lugs	< 1.00E+17	< 1.00E+17	< 1.00E+17

Table 6-8
Calculated Maximum Neutron and Gamma Ray Exposure of the Primary Biological Shield

Distance from Core Midplane [ft]	Neutron ($E > 1.0$ MeV) Fluence [n/cm^2]			Gamma Ray Dose [rad]		
	24.6 EFPY	33.0 EFPY	52.1 EFPY	24.6 EFPY	33.0 EFPY	52.1 EFPY
-6.0	6.14E+17	7.86E+17	1.18E+18	2.58E+09	3.30E+09	4.93E+09
-5.5	9.57E+17	1.23E+18	1.86E+18	4.07E+09	5.23E+09	7.85E+09
-4.5	1.46E+18	1.90E+18	2.90E+18	6.29E+09	8.14E+09	1.24E+10
-3.5	1.69E+18	2.21E+18	3.40E+18	7.53E+09	9.81E+09	1.50E+10
-2.5	1.82E+18	2.39E+18	3.69E+18	8.17E+09	1.07E+10	1.64E+10
-1.5	1.85E+18	2.44E+18	3.79E+18	8.46E+09	1.11E+10	1.71E+10
-0.5	1.87E+18	2.48E+18	3.85E+18	8.59E+09	1.13E+10	1.75E+10
0.0	1.88E+18	2.49E+18	3.88E+18	8.61E+09	1.13E+10	1.75E+10
0.5	1.87E+18	2.49E+18	3.87E+18	8.59E+09	1.13E+10	1.75E+10
1.5	1.83E+18	2.43E+18	3.79E+18	8.42E+09	1.11E+10	1.72E+10
2.5	1.79E+18	2.37E+18	3.69E+18	8.11E+09	1.07E+10	1.65E+10
3.5	1.66E+18	2.19E+18	3.41E+18	7.44E+09	9.79E+09	1.51E+10
4.5	1.41E+18	1.85E+18	2.87E+18	6.25E+09	8.20E+09	1.26E+10
5.5	9.28E+17	1.21E+18	1.86E+18	4.34E+09	5.67E+09	8.67E+09
6.0	6.58E+17	8.57E+17	1.31E+18	3.26E+09	4.24E+09	6.46E+09

Figure 6-1
Kewaunee r,θ Reactor Geometry at the Core Midplane

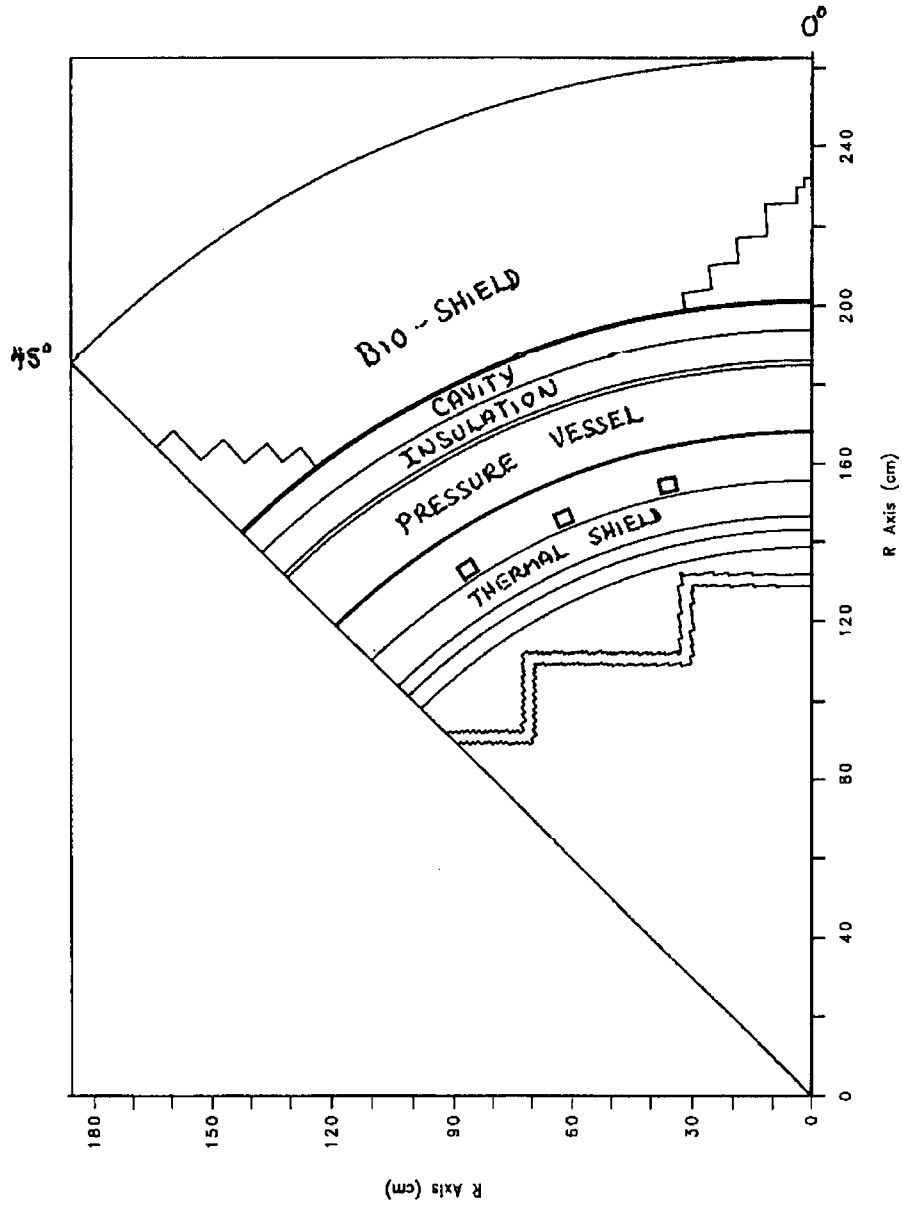
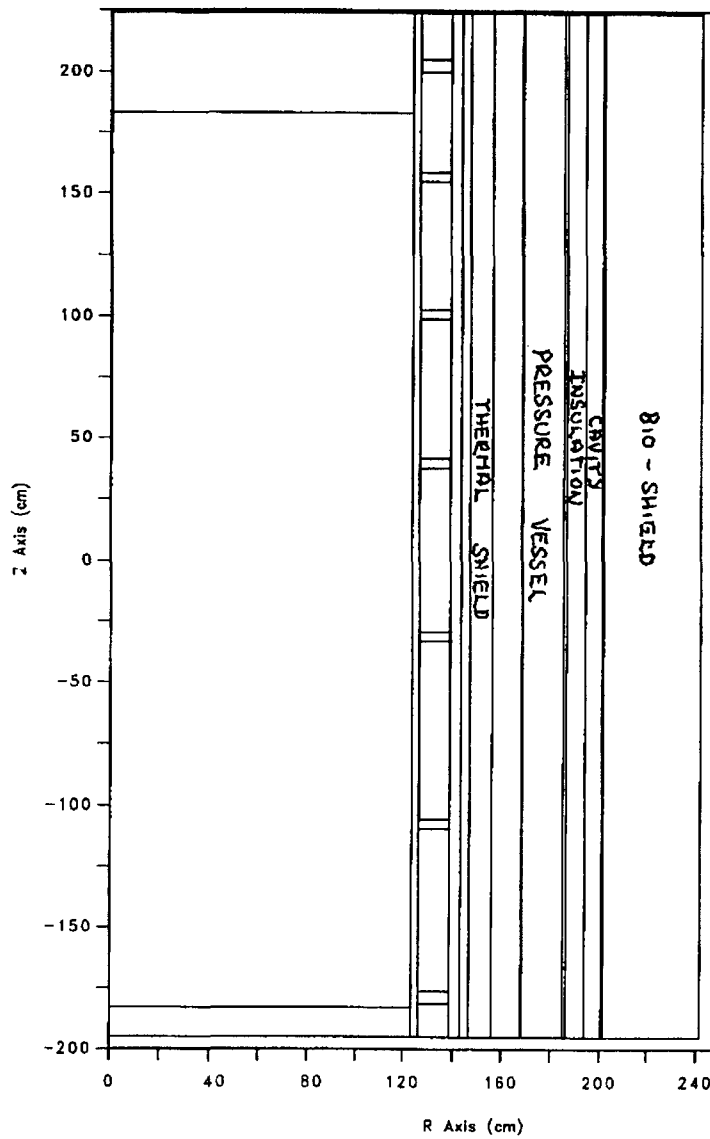


Figure 6-2
Kewaunee r,z Reactor Geometry



This page intentionally blank

7 SURVEILLANCE CAPSULE REMOVAL SCHEDULE

The following surveillance capsule removal schedule meets the requirements of ASTM E185-82 [Reference 13] and is recommended for future capsules to be removed from the KPS reactor vessel.

Capsule	Capsule Location	Lead Factor ^(a)	Withdrawal EFPY ^(b)	Fluence (n/cm²) ^(c)
V	13°	3.03	1.3	5.86E+18
R	13°	3.03	4.6	1.76E+19
P	23°	2.00	11.1	2.61E+19
S	33°	2.08	16.2	3.67E+19
T	23°	2.17	24.6	5.62E+19
N	33°	2.12	(d)	(d)

Notes:

- (a) Updated in Capsule T dosimetry analysis.
- (b) Effective Full Power Years (EFPY) from plant startup.
- (c) Actual plant evaluation calculated fluence.
- (d) This capsule will reach a fluence of approximately 7.4×10^{19} (72 EFPY Peak Fluence) which occurs at 29.44 EFPY. It is recommended that this standby capsule be withdrawn between 29 and 30 EFPY and placed in storage. Since it is the last capsule to be removed, other means of monitoring vessel fluence should be implemented prior to its removal (e.g., ex-vessel dosimetry).

This page intentionally blank

8 REFERENCES

1. Regulatory Guide 1.99, Revision 2, *Radiation Embrittlement of Reactor Vessel Materials*, U.S. Nuclear Regulatory Commission, May, 1988.
2. Code of Federal Regulations, 10CFR50, Appendix G, *Fracture Toughness Requirements*, and Appendix H, *Reactor Vessel Material Surveillance Program Requirements*, U.S. Nuclear Regulatory Commission, Washington, D.C.
3. WCAP-8107, *Wisconsin Public Service Corporation Kewaunee Nuclear Power Plant Reactor Vessel Radiation Surveillance Program*, S.E. Yanichko, et al, April 1973.
4. ASTM E185-73, Annual Book of ASTM Standards, *Standard Practice for Conducting Surveillance Tests for Light-Water Cooled Nuclear Power Reactor Vessels*.
5. WCAP-16609-NP, *Master Curve Assessment of the Dominion Energy Kewaunee Power Station Reactor Pressure Vessel Weld Metal*, R.G. Lott, et al, dated August 2006.
6. ASTM E1253-99, Annual Book of ASTM Standards, *Standard Guide for Reconstitution of Irradiated Charpy-Sized Specimen*.
7. Section XI of the ASME Boiler and Pressure Vessel Code, Appendix G, *Fracture Toughness Criteria for Protection Against Failure*.
8. ASTM E208, Annual Book of Standards, *Standard Test Method for Conducting Drop-Weight Test to Determine Nil-Ductility Transition Temperature of Ferritic Steels*.
9. ASTM E1820, Annual Book of Standards, *Standard Test Method for Measurement of Fracture Toughness*.
10. K. Wallin, *The Scatter in K_{Ic} Results*, Engineering Fracture Mechanics, Vol. 19, pp. 1085-1093, 1984.
11. ASTM E1921, Annual Book of Standards, *Standard Test Method for Determination of Reference Temperature, T_o , for Ferritic Steels in the Transition Region*.
12. WCAP-15074, Revision 1, *Evaluation of the 1P3571 Weld Metal from the Surveillance Programs for Kewaunee and Maine Yankee*, W.L. Server, et al, dated August 2006.
13. ASTM E185-82, Annual Book of ASTM Standards, Section 12, Volume 12.02, *Standard Practice for Conducting Surveillance Tests for Light-Water Cooled Nuclear Power Reactor Vessels*.
14. Procedure RMF 8402, *Surveillance Capsule Testing Program*, Revision 2.
15. Procedure RMF 8102, *Tensile Testing*, Revision 3.

16. Procedure RMF 8103, *Charpy Impact Testing*, Revision 2.
17. ASTM E23-02a, Annual Book of ASTM Standards, *Standard Test Method for Notched Bar Impact Testing of Metallic Materials*.
18. ASTM A370-97a, Annual Book of ASTM Standards, *Standard Test Methods and Definitions for Mechanical Testing of Steel Products*.
19. ASTM E8-04, Annual Book of ASTM Standards, *Standard Test Methods for Tension Testing of Metallic Materials*, ASTM.
20. ASTM E21-03 (1998), Annual Book of ASTM Standards, *Standard Test Methods for Elevated Temperature Tension Tests of Metallic Materials*, ASTM.
21. ASTM E83-93, Annual Book of ASTM Standards, *Standard Practice for Verification and Classification of Extensometers*.
22. Safety Evaluation by the Office of Nuclear Reactor, *Kewaunee Nuclear Power Plant, Exemption from the Requirements of 10 CFR Part 50, Appendix G, Appendix H, and Section 50.61*, Docket No. 50-305, May 2001.
23. ASTM E853, Annual Book of ASTM Standards, *Standard Practice for Analysis and Interpretation of Light-Water Reactor Vessel Surveillance Results, E 706*.
24. ASTM E693, Annual Book of ASTM Standards, *Standard Practice for Characterizing Neutron Exposures in Iron and Low Alloy Steels in Terms of Displacements per Atom, E 706*.
25. Regulatory Guide RG-1.190, *Calculational and Dosimetry Methods for Determining Pressure Vessel Neutron Fluence*, U. S. Nuclear Regulatory Commission, Office of Nuclear Regulatory Research, March 2001.
26. WCAP-14040-NP-A, Revision 4, *Methodology Used to Develop Cold Overpressure Mitigating System Setpoints and RCS Heatup and Cooldown Limit Curves*, May 2004.
27. WCAP-16083-NP-A, Revision 0, *Benchmark Testing of the FERRET Code for Least Squares Evaluation of Light Water Reactor Dosimetry*, May 2006.
28. RSICC Computer Code Collection CCC-650, *DOORS 3.2, One, Two- and Three-Dimensional Discrete Ordinates Neutron/Photon Transport Code System*, April 1998.
29. RSIC Data Library Collection DLC-185, *BUGLE-96, Coupled 47 Neutron, 20 Gamma-Ray Group Cross Section Library Derived from ENDF/B-VI for LWR Shielding and Pressure Vessel Dosimetry Applications*, March 1996

APPENDIX A

**VALIDATION OF THE RADIATION TRANSPORT
MODELS BASED ON NEUTRON DOSIMETRY
MEASUREMENTS**

This page intentionally blank

A.1 Neutron Dosimetry

Comparisons of measured dosimetry results to both the calculated and least squares adjusted values for all surveillance capsules withdrawn from service to date at Kewaunee are described herein. The sensor sets from these capsules have been analyzed in accordance with the requirements of Regulatory Guide 1.190, "Calculational and Dosimetry Methods for Determining Pressure Vessel Neutron Fluence"[Reference A-1] using the NRC approved methodology described in WCAP-16083-NP-A, Revision 0, "Benchmark Testing of the FERRET Code for Least Squares Evaluation of Light Water Reactor Dosimetry."[Reference A-2] One of the main purposes for presenting this material is to demonstrate that the overall measurements agree with the calculated and least squares adjusted values to within $\pm 20\%$ as specified by Regulatory Guide 1.190, thus serving to validate the calculated neutron exposures previously reported in Section 6.2 of this report.

A.1.1 Sensor Reaction Rate Determinations

In this section, the results of the evaluations of the five neutron sensor sets analyzed to date as part of the Kewaunee Reactor Vessel Materials Surveillance Program are presented. The capsule designation, location within the reactor, and time of withdrawal of each of these dosimetry sets were as follows:

<u>Capsule ID</u>	<u>Azimuthal Location</u>	<u>Withdrawal Time</u>	<u>Irradiation Time [EFPY]</u>
V	13°	End of Cycle 1	1.3
R	13°	End of Cycle 5	4.6
P	23°	End of Cycle 13	11.1
S	33°	End of Cycle 19	16.2
T	23°	End of Cycle 26	24.6

The azimuthal locations included in the above tabulation represent the first octant equivalent azimuthal angle of the geometric center of the respective surveillance capsules.

The passive neutron sensors included in the evaluations of Surveillance Capsules V, R, P, S, and T are summarized as follows:

<u>Sensor Material</u>	<u>Reaction</u>	<u>Capsule V</u>	<u>Capsule R</u>	<u>Capsule P</u>	<u>Capsule S</u>	<u>Capsule T</u>
	<u>Of Interest</u>					
Copper	$^{63}\text{Cu}(n,\alpha)^{60}\text{Co}$	X	X	X	X	X
Iron	$^{54}\text{Fe}(n,p)^{54}\text{Mn}$	X	X	X	X	X
Nickel	$^{58}\text{Ni}(n,p)^{58}\text{Co}$	X	X	X	X	X
Uranium-238 ^(a)	$^{238}\text{U}(n,f)^{137}\text{Cs}$	X	X	X	X	X
Neptunium-237 ^(a)	$^{237}\text{Np}(n,f)^{137}\text{Cs}$	X		X	X	X
Cobalt-Aluminum ^(b)	$^{59}\text{Co}(n,\gamma)^{60}\text{Co}$	X	X	X	X	X

(a) The Uranium and Neptunium sensors were cadmium covered.

(b) The cobalt-aluminum sensors included both bare and cadmium-covered wire.

Pertinent physical and nuclear characteristics of the passive neutron sensors are listed in Table A-1.

Since the construction of the surveillance capsules used in the Kewaunee reactor design places individual sensors at several radial locations within the materials test specimen array [Reference A-3], gradient corrections based on the plant specific neutron transport calculations were applied to the measured sensor reaction rates to index all of the measured data to the geometric center of the surveillance capsule. The applicable gradient corrections used to index the measured results to the capsule center (Radius = 158.35 cm) are summarized in the following tabulation.

Sensor Type	Sensor Radius [cm]	Gradient Correction factor		
		13° Location (V and R)	23° Location (P and T)	33° Location (S)
Copper	158.11	0.957	0.954	0.954
Nickel	158.11	0.955	0.953	0.951
Cd Covered Cobalt-Aluminum	158.11	0.952	0.955	0.952
Uranium-238	158.35	1.000	1.000	1.000
Neptunium-237	158.35	1.000	1.000	1.000
Iron	159.11	1.158	1.140	1.141
Bare Cobalt-Aluminum	159.11	0.984	0.988	0.985

The use of passive monitors such as those listed above does not yield a direct measure of the energy dependent neutron flux at the point of interest. Rather, the activation or fission process is a measure of the integrated effect that the time and energy dependent neutron flux has on the target material over the course of the irradiation period. An accurate assessment of the average neutron flux level incident on the various monitors may be derived from the activation measurements only if the irradiation parameters are well known. In particular, the following variables are of interest:

- the measured specific activity of each monitor,
- the physical characteristics of each monitor,

- the operating history of the reactor,
- the energy response of each monitor, and
- the neutron energy spectrum at the monitor location.

Results from the radiometric counting of the neutron sensors from Capsules V, R, P, S, and T are summarized in Table A-4. In all cases, the radiometric counting followed established ASTM procedures. Following sample preparation and weighing, the specific activity of each sensor was determined by means of a high-resolution gamma spectrometer. For the copper, iron, nickel, and cobalt-aluminum sensors, these analyses were performed by direct counting of each of the individual samples. In the case of the uranium and neptunium fission sensors, the analyses were carried out by direct counting preceded by dissolution and chemical separation of cesium from the sensor material.

The irradiation history of the reactor over the irradiation periods experienced by Capsules V, R, P, S, and T was based on the monthly power generation of the Kewaunee reactor from initial criticality through the end of the respective dosimetry evaluation periods. For the sensor sets utilized in the surveillance capsules, the half-lives of the product isotopes are long enough that a monthly histogram describing reactor operation has proven to be an adequate representation for use in radioactive decay corrections for the reactions of interest in the exposure evaluations. The irradiation history applicable to Capsules V, R, P, S, and T is given in Table A-2.

Having the measured specific activities, the physical characteristics of the sensors, and the operating history of the reactor, reaction rates referenced to full-power operation were determined from the following equation:

$$R = \frac{A}{N_0 F Y \sum \frac{P_j}{P_{ref}} C_j [1 - e^{-\lambda t_j}] [e^{-\lambda t_d}]}$$

where:

- R = Reaction rate averaged over the irradiation period and referenced to operation at a core power level of P_{ref} (rps/nucleus).
- A = Measured specific activity (dps/gm).
- N_0 = Number of target element atoms per gram of sensor.
- F = Atom fraction of the target isotope in the target element.
- Y = Number of product atoms produced per reaction.
- P_j = Average core power level during irradiation period j (MW).
- P_{ref} = Maximum or reference power level of the reactor (MW).
- C_j = Calculated ratio of $\phi(E > 1.0 \text{ MeV})$ during irradiation period j to the time weighted average $\phi(E > 1.0 \text{ MeV})$ over the entire irradiation period.
- λ = Decay constant of the product isotope (1/sec).

t_j = Length of irradiation period j (sec).

t_d = Decay time following irradiation period j (sec).

and the summation is carried out over the total number of monthly intervals comprising the irradiation period.

In the equation describing the reaction rate calculation, the ratio $[P_j]/[P_{ref}]$ accounts for month-by-month variation of reactor core power level within any given fuel cycle as well as over multiple fuel cycles. The ratio C_j , which was calculated for each fuel cycle using the transport methodology discussed in Section 6.2, accounts for the change in sensor reaction rates caused by variations in flux level induced by changes in core spatial power distributions from fuel cycle to fuel cycle. For a single-cycle irradiation, C_j is normally taken to be 1.0. However, for multiple-cycle irradiations, particularly those employing low leakage fuel management, the additional C_j term should be employed. The impact of changing flux levels for constant power operation can be quite significant for sensor sets that have been irradiated for many cycles in a reactor that has transitioned from non-low leakage to low leakage fuel management or for sensor sets contained in surveillance capsules that have been moved from one capsule location to another. The fuel cycle specific neutron flux values along with the computed values for C_j are listed in Table A-3. These flux values represent the cycle dependent results at the radial and azimuthal center of the respective capsules at the axial elevation of the active fuel midplane.

Prior to using the measured reaction rates in the least-squares evaluations of the dosimetry sensor sets, additional corrections were made to the ^{238}U measurements to account for the presence of ^{235}U impurities in the sensors as well as to adjust for the build-in of plutonium isotopes over the course of the irradiation. Corrections were also made to the ^{238}U and ^{237}Np sensor reaction rates to account for gamma ray induced fission reactions that occurred over the course of the capsule irradiations. The correction factors applied to the Kewaunee fission sensor reaction rates are summarized as follows:

Correction	Capsule V	Capsule R	Capsule P	Capsule S	Capsule T
^{235}U Impurity/Pu Build-in	0.861	0.817	0.789	0.754	0.690
$^{238}\text{U}(\gamma, f)$	0.950	0.950	0.955	0.953	0.955
Net ^{238}U Correction	0.819	0.776	0.753	0.718	0.659
$^{237}\text{Np}(\gamma, f)$	0.983	0.983	0.984	0.983	0.984

These factors were applied in a multiplicative fashion to the decay corrected uranium and neptunium fission sensor reaction rates.

Results of the sensor reaction rate determinations for Capsules V, R, P, S, and T are also provided in Table A-4. Along with the measured specific activities, decay corrected saturated specific activities and computed reaction rates for each sensor indexed to the radial center of the capsule are listed. The fission sensor reaction rates are listed both with and without the applied corrections for ^{238}U impurities, plutonium build-in, and gamma ray induced fission effects.

A.1.2 Least Squares Evaluation of Sensor Sets

Least squares adjustment methods provide the capability of combining the measurement data with the corresponding neutron transport calculations resulting in a best estimate adjusted neutron energy spectrum with associated uncertainties. Best estimates adjusted values for key exposure parameters such as $\phi(E > 1.0 \text{ MeV})$ or dpa/s along with their uncertainties are then easily obtained from the adjusted spectrum. In general, the least squares methods, as applied to surveillance capsule dosimetry evaluations, act to reconcile the measured sensor reaction rate data, dosimetry reaction cross-sections, and the calculated neutron energy spectrum within their respective uncertainties. For example,

$$R_i \pm \delta_{R_i} = \sum_g (\sigma_{ig} \pm \delta_{\sigma_{ig}})(\phi_g \pm \delta_{\phi_g})$$

relates a set of measured reaction rates, R_i , to a single neutron spectrum, ϕ_g , through the multigroup dosimeter reaction cross-section, σ_{ig} , each with an uncertainty δ . The primary objective of the least squares evaluation is to produce unbiased estimates of the neutron exposure parameters at the location of the measurement.

For the least squares evaluation of the Kewaunee surveillance capsule dosimetry, the FERRET code^[A-2] was employed to combine the results of the plant specific neutron transport calculations and sensor set reaction rate measurements to determine adjusted values of exposure parameters ($\phi(E > 1.0 \text{ MeV})$ and dpa) along with associated uncertainties for the five in-vessel capsules analyzed to date.

The application of the least squares methodology requires the following input:

- 1 - The calculated neutron energy spectrum and associated uncertainties at the measurement location.
- 2 - The measured reaction rates and associated uncertainty for each sensor contained in the multiple foil set.
- 3 - The energy dependent dosimetry reaction cross-sections and associated uncertainties for each sensor contained in the multiple foil sensor set.

For the Kewaunee application, the calculated neutron spectra were obtained from the results of plant specific neutron transport calculations described in Section 6.2 of this report. The sensor reaction rates were derived from the measured specific activities using the procedures described in Section A.1.1. The dosimetry reaction cross-sections and uncertainties were obtained from the SNLRML dosimetry cross-section library [Reference A-4]. The SNLRML library is an evaluated dosimetry reaction cross-section compilation recommended for use in LWR evaluations by ASTM Standard E1018, "Application of ASTM Evaluated Cross-Section Data File, Matrix E 706 (IIB)".

The uncertainties associated with the measured reaction rates, dosimetry cross-sections, and calculated neutron spectrum were input to the least squares procedure in the form of variances and covariances. The

assignment of the input uncertainties followed the guidance provided in ASTM Standard E 944, "Application of Neutron Spectrum Adjustment Methods in Reactor Surveillance."

The following provides a summary of the uncertainties associated with the least squares evaluation of the Kewaunee surveillance capsule sensor sets.

Reaction Rate Uncertainties

The overall uncertainty associated with the measured reaction rates includes components due to the basic measurement process, irradiation history corrections, and corrections for competing reactions. A high level of accuracy in the reaction rate determinations is assured by utilizing laboratory procedures that conform to the ASTM National Consensus Standards for reaction rate determinations for each sensor type.

After combining all of these uncertainty components, the sensor reaction rates derived from the counting and data evaluation procedures were assigned the following net uncertainties for input to the least squares evaluation:

Reaction	Uncertainty
$^{63}\text{Cu}(n,\alpha)^{60}\text{Co}$	5%
$^{54}\text{Fe}(n,p)^{54}\text{Mn}$	5%
$^{58}\text{Ni}(n,p)^{58}\text{Co}$	5%
$^{238}\text{U}(n,f)^{137}\text{Cs}$	10%
$^{237}\text{Np}(n,f)^{137}\text{Cs}$	10%
$^{59}\text{Co}(n,\gamma)^{60}\text{Co}$	5%

These uncertainties are given at the 1σ level.

Dosimetry Cross-Section Uncertainties

The reaction rate cross-sections used in the least squares evaluations were taken from the SNLRML library. This data library provides reaction cross-sections and associated uncertainties, including covariances, for 66 dosimetry sensors in common use. Both cross-sections and uncertainties are provided in a fine multigroup structure for use in least squares adjustment applications. These cross-sections were compiled from the most recent cross-section evaluations and they have been tested with respect to their accuracy and consistency for least squares evaluations. Further, the library has been empirically tested for use in fission spectra determination as well as in the fluence and energy characterization of 14 MeV neutron sources.

For sensors included in the Kewaunee surveillance program, the following uncertainties in the fission spectrum averaged cross-sections are provided in the SNLRML documentation package.

Reaction	Uncertainty
$^{63}\text{Cu}(n,\alpha)^{60}\text{Co}$	4.08-4.16%
$^{54}\text{Fe}(n,p)^{54}\text{Mn}$	3.05-3.11%
$^{58}\text{Ni}(n,p)^{58}\text{Co}$	4.49-4.56%
$^{238}\text{U}(n,f)^{137}\text{Cs}$	0.54-0.64%
$^{237}\text{Np}(n,f)^{137}\text{Cs}$	10.32-10.97%
$^{59}\text{Co}(n,\gamma)^{60}\text{Co}$	0.79-3.59%

These tabulated ranges provide an indication of the dosimetry cross-section uncertainties associated with the sensor sets used in LWR irradiations.

Calculated Neutron Spectrum

The neutron spectra input to the least squares adjustment procedure were obtained directly from the results of plant specific transport calculations for each surveillance capsule irradiation period and location. The spectrum for each capsule was input in an absolute sense (rather than as simply a relative spectral shape). Therefore, within the constraints of the assigned uncertainties, the calculated data were treated equally with the measurements.

While the uncertainties associated with the reaction rates were obtained from the measurement procedures and counting benchmarks and the dosimetry cross-section uncertainties were supplied directly with the SNLRML library, the uncertainty matrix for the calculated spectrum was constructed from the following relationship:

$$M_{gg'} = R_n^2 + R_g * R_{g'} * P_{gg'}$$

where R_n specifies an overall fractional normalization uncertainty and the fractional uncertainties R_g and $R_{g'}$ specify additional random groupwise uncertainties that are correlated with a correlation matrix given by:

$$P_{gg'} = [1 - \theta]\delta_{gg'} + \theta e^{-H}$$

where

$$H = \frac{(g - g')^2}{2\gamma^2}$$

The first term in the correlation matrix equation specifies purely random uncertainties, while the second term describes the short-range correlations over a group range γ (θ specifies the strength of the latter term). The value of δ is 1.0 when $g = g'$, and is 0.0 otherwise.

The set of parameters defining the input covariance matrix for the Kewaunee calculated spectra was as follows:

Flux Normalization Uncertainty (R_n)	15%
Flux Group Uncertainties ($R_g, R_{g'}$)	
($E > 0.0055$ MeV)	15%
(0.68 eV $< E < 0.0055$ MeV)	29%
($E < 0.68$ eV)	52%
Short Range Correlation (θ)	
($E > 0.0055$ MeV)	0.9
(0.68 eV $< E < 0.0055$ MeV)	0.5
($E < 0.68$ eV)	0.5
Flux Group Correlation Range (γ)	
($E > 0.0055$ MeV)	6
(0.68 eV $< E < 0.0055$ MeV)	3
($E < 0.68$ eV)	2

A.1.3 Comparisons of Measurements and Calculations

Results of the least squares evaluations of the dosimetry from the Kewaunee surveillance capsules withdrawn to date are provided in Tables A-5 and A-6. In Table A-5, measured, calculated, and adjusted values for sensor reaction rates are given for each capsule. Also provided in this tabulation are ratios of the measured reaction rates to both the calculated and least squares adjusted reaction rates. These ratios of M/C and M/A illustrate the consistency of the fit of the calculated neutron energy spectra to the measured reaction rates both before and after adjustment. In Table A-6, comparisons of the calculated and adjusted values of neutron flux ($E > 1.0$ MeV) and iron atom displacement rate are tabulated along with the A/C ratios observed for each of the capsules.

The data comparisons provided in Tables A-5 and A-6 show that the adjustments to the calculated spectra are relatively small and well within the assigned uncertainties for the calculated spectra, measured sensor

reaction rates, and dosimetry reaction cross-sections. Further, these results indicate that the use of the least squares evaluation results in a reduction in the uncertainties associated with the exposure of the surveillance capsules. From Section 6.4 of this report, it may be noted that the uncertainty associated with the unadjusted calculation of neutron fluence ($E > 1.0$ MeV) and iron atom displacements at the surveillance capsule locations is specified as 12% at the 1σ level. From Table A-6, it is noted that the corresponding uncertainties associated with the least squares adjusted exposure parameters have been reduced to a range of from 6-7% for neutron flux ($E > 1.0$ MeV) and 7-8% for iron atom displacement rate. Again, the uncertainties from the least squares evaluation are at the 1σ level.

Further comparisons of the measurement results (from Tables A-5 and A-6) with calculations are given in Tables A-7 and A-8. These comparisons are given on two levels. In Table A-7, calculations of individual threshold sensor reaction rates are compared directly with the corresponding measurements. These threshold reaction rate comparisons provide a good evaluation of the accuracy of the fast neutron portion of the calculated energy spectra. In Table A-8, calculations of fast neutron exposure rates in terms of $\phi(E > 1.0$ MeV) and dpa/s are compared with the adjusted values obtained from the least squares evaluation of the capsule dosimetry. These two levels of comparison yield consistent and similar results with all measurement-to-calculation comparisons falling well within the 20% limits specified as the acceptance criteria in Regulatory Guide 1.190.

In the case of the direct comparison of measured and calculated sensor reaction rates, the M/C comparisons for fast neutron reactions range from 0.84 to 1.17 for the 24 samples included in the data set. The overall average M/C ratio for the entire set of Kewaunee data is 0.99 with an associated standard deviation of 7.6%.

In the comparisons of best estimate and calculated fast neutron exposure parameters, the corresponding A/C comparisons for the capsule data sets range from 0.93 to 1.03 for neutron flux ($E > 1.0$ MeV) and from 0.92 to 1.03 for iron atom displacement rate. The overall average A/C ratios for neutron flux ($E > 1.0$ MeV) and iron atom displacement rate are 0.99 with a standard deviation of 4.1% and 1.00 with a standard deviation of 4.3%, respectively.

Based on these comparisons, it is concluded that the calculated fast neutron exposures provided in Section 6.2 of this report are essentially unbiased and are validated for use in the assessment of the condition of the materials comprising the beltline region of the Kewaunee reactor pressure vessel.

Table A-1

Nuclear Parameters Used In The Evaluation Of Neutron Sensors

Monitor <u>Material</u>	Reaction of <u>Interest</u>	Target Atom <u>Fraction</u>	90% Response Range <u>(MeV)</u>	Product <u>Half-life</u>	Fission Yield <u>(%)</u>
Copper	$^{63}\text{Cu} (n,\alpha)$	0.6917	4.8 – 11.9	5.271 y	
Iron	$^{54}\text{Fe} (n,p)$	0.0585	2.1 – 8.5	312.3 d	
Nickel	$^{58}\text{Ni} (n,p)$	0.6808	1.6 – 8.4	70.82 d	
Uranium-238	$^{238}\text{U} (n,f)$	1.0000	1.3 – 7.1	30.07 y	6.02
Neptunium-237	$^{237}\text{Np} (n,f)$	1.0000	0.4 – 4.6	30.07 y	6.17
Cobalt-Aluminum	$^{59}\text{Co} (n,\gamma)$	0.0015	non-threshold	5.271 y	

Note: The 90% response range is defined such that, in the neutron spectrum characteristic of the Kewaunee surveillance capsules, approximately 90% of the sensor response is due to neutrons in the energy range specified with approximately 5% of the total response due to neutrons with energies below the lower limit and 5% of the total response due to neutrons with energies above the upper limit.

Table A-2
 Monthly Thermal Generation During The First Twenty Six Fuel Cycles
 Of The Kewaunee Reactor

<u>Year</u>	<u>Month</u>	<u>Thermal Generation (MWt-hr)</u>	<u>Year</u>	<u>Month</u>	<u>Thermal Generation (MWt-hr)</u>	<u>Year</u>	<u>Month</u>	<u>Thermal Generation (MWt-hr)</u>
1974	4	121412	1977	4	999717	1980	4	1175492
1974	5	600420	1977	5	1188560	1980	5	349621
1974	6	864909	1977	6	1156447	1980	6	137929
1974	7	776871	1977	7	1201271	1980	7	1186866
1974	8	1172100	1977	8	1049588	1980	8	1125341
1974	9	655831	1977	9	1175016	1980	9	946334
1974	10	317628	1977	10	1207031	1980	10	1181104
1974	11	752190	1977	11	1175653	1980	11	1183962
1974	12	907703	1977	12	1194097	1980	12	1188454
1975	1	781842	1978	1	1218479	1981	1	1223429
1975	2	928272	1978	2	1098398	1981	2	1077953
1975	3	1096956	1978	3	1203881	1981	3	1136912
1975	4	827400	1978	4	811877	1981	4	777154
1975	5	874521	1978	5	72462	1981	5	0
1975	6	777805	1978	6	1016869	1981	6	777459
1975	7	842326	1978	7	1129811	1981	7	1204230
1975	8	1175609	1978	8	1182936	1981	8	1222464
1975	9	604163	1978	9	1137041	1981	9	1161892
1975	10	916973	1978	10	1208085	1981	10	1170754
1975	11	823299	1978	11	1129396	1981	11	1148183
1975	12	1171599	1978	12	1200591	1981	12	1219280
1976	1	1106166	1979	1	1212033	1982	1	1203474
1976	2	501575	1979	2	1047590	1982	2	1075185
1976	3	0	1979	3	1135718	1982	3	1224649
1976	4	377039	1979	4	1151567	1982	4	326008
1976	5	685126	1979	5	979438	1982	5	208610
1976	6	1171872	1979	6	0	1982	6	1163350
1976	7	1180703	1979	7	0	1982	7	1218118
1976	8	1190960	1979	8	740156	1982	8	1222402
1976	9	1060865	1979	9	1126633	1982	9	1180708
1976	10	1198895	1979	10	1184602	1982	10	1214805
1976	11	1145875	1979	11	1167457	1982	11	1178287
1976	12	1187141	1979	12	1202648	1982	12	1077471
1977	1	606787	1980	1	713133	1983	1	1218455
1977	2	0	1980	2	1124815	1983	2	1102759
1977	3	179775	1980	3	1223050	1983	3	649484

Table A-2 cont'd
 Monthly Thermal Generation During The First Twenty Six Fuel Cycles
 Of The Kewaunee Reactor

<u>Year</u>	<u>Month</u>	<u>Thermal Generation (MWt-hr)</u>	<u>Year</u>	<u>Month</u>	<u>Thermal Generation (MWt-hr)</u>	<u>Year</u>	<u>Month</u>	<u>Thermal Generation (MWt-hr)</u>
1983	4	0	1986	4	267903	1989	4	537116
1983	5	526179	1986	5	1191848	1989	5	1221793
1983	6	1174626	1986	6	1176926	1989	6	902394
1983	7	1159011	1986	7	1218187	1989	7	1221968
1983	8	1223940	1986	8	1179835	1989	8	1221653
1983	9	1184200	1986	9	1180207	1989	9	1182431
1983	10	1224069	1986	10	1202091	1989	10	1222999
1983	11	1183857	1986	11	1179133	1989	11	1181532
1983	12	1224505	1986	12	1215853	1989	12	1182173
1984	1	1225897	1987	1	1215680	1990	1	1217978
1984	2	1139329	1987	2	924655	1990	2	1104275
1984	3	532963	1987	3	0	1990	3	69012
1984	4	0	1987	4	959357	1990	4	347514
1984	5	837414	1987	5	1185857	1990	5	1211562
1984	6	1144593	1987	6	1146829	1990	6	1172482
1984	7	1199335	1987	7	1183725	1990	7	1224388
1984	8	1222297	1987	8	1219047	1990	8	1224227
1984	9	1183431	1987	9	1168054	1990	9	1182733
1984	10	1205018	1987	10	1219759	1990	10	1224609
1984	11	1183532	1987	11	1176994	1990	11	1182652
1984	12	1222229	1987	12	1215302	1990	12	1208996
1985	1	1224279	1988	1	1217528	1991	1	1220109
1985	2	271048	1988	2	1134763	1991	2	1100105
1985	3	0	1988	3	57885	1991	3	285385
1985	4	682721	1988	4	478699	1991	4	0
1985	5	1212434	1988	5	1195654	1991	5	694766
1985	6	1179472	1988	6	1180894	1991	6	1180240
1985	7	1218713	1988	7	1196631	1991	7	1210778
1985	8	1148512	1988	8	1067560	1991	8	1211741
1985	9	1178061	1988	9	1088933	1991	9	1171047
1985	10	1222974	1988	10	1221808	1991	10	1147457
1985	11	1121094	1988	11	1169480	1991	11	1182454
1985	12	1181301	1988	12	1219313	1991	12	1211606
1986	1	1217881	1989	1	1204791	1992	1	1222525
1986	2	1067018	1989	2	755230	1992	2	1143608
1986	3	0	1989	3	0	1992	3	225433

Table A-2 cont'd
 Monthly Thermal Generation During The First Twenty Six Fuel Cycles
 Of The Kewaunee Reactor

<u>Year</u>	<u>Month</u>	<u>Thermal Generation (MWt-hr)</u>	<u>Year</u>	<u>Month</u>	<u>Thermal Generation (MWt-hr)</u>	<u>Year</u>	<u>Month</u>	<u>Thermal Generation (MWt-hr)</u>
1992	4	351235	1995	4	65	1998	4	1143027
1992	5	1226398	1995	5	388395	1998	5	1182185
1992	6	1185833	1995	6	1131317	1998	6	1125155
1992	7	1227301	1995	7	1185361	1998	7	1181037
1992	8	1228782	1995	8	1187206	1998	8	1180476
1992	9	1063233	1995	9	1107004	1998	9	1142017
1992	10	1229699	1995	10	1199601	1998	10	595143
1992	11	1113009	1995	11	1169068	1998	11	50510
1992	12	1227368	1995	12	1208346	1998	12	1075135
1993	1	1136925	1996	1	1208794	1999	1	1166738
1993	2	1085208	1996	2	1130772	1999	2	1070798
1993	3	156579	1996	3	1171857	1999	3	1194219
1993	4	381383	1996	4	1130838	1999	4	1147356
1993	5	1227217	1996	5	1205079	1999	5	1193822
1993	6	754286	1996	6	1166067	1999	6	1133072
1993	7	1226890	1996	7	1204827	1999	7	1191624
1993	8	1226800	1996	8	1174752	1999	8	1192858
1993	9	1184271	1996	9	598870	1999	9	1151703
1993	10	1227961	1996	10	0	1999	10	1193859
1993	11	1186431	1996	11	0	1999	11	1153786
1993	12	1223457	1996	12	0	1999	12	1191329
1994	1	929429	1997	1	0	2000	1	1190621
1994	2	1105268	1997	2	0	2000	2	1111904
1994	3	1200731	1997	3	0	2000	3	1190979
1994	4	22616	1997	4	0	2000	4	796780
1994	5	751549	1997	5	4975	2000	5	0
1994	6	1187510	1997	6	26	2000	6	832708
1994	7	1225867	1997	7	1164539	2000	7	1156171
1994	8	1225305	1997	8	1179559	2000	8	1163425
1994	9	1187543	1997	9	1149530	2000	9	1137281
1994	10	1228790	1997	10	1189032	2000	10	1177799
1994	11	1185472	1997	11	1148938	2000	11	1091925
1994	12	1227116	1997	12	1178977	2000	12	1176511
1995	1	1227125	1998	1	1190492	2001	1	1180239
1995	2	1108344	1998	2	720791	2001	2	1067797
1995	3	1084328	1998	3	1183303	2001	3	1179343

Table A-2 cont'd
 Monthly Thermal Generation During The First Twenty Six Fuel Cycles
 Of The Kewaunee Reactor

<u>Year</u>	<u>Month</u>	<u>Thermal Generation (MWt-hr)</u>	<u>Year</u>	<u>Month</u>	<u>Thermal Generation (MWt-hr)</u>	<u>Year</u>	<u>Month</u>	<u>Thermal Generation (MWt-hr)</u>
2001	4	1142622	2002	7	1226420	2003	10	1242270
2001	5	1161973	2002	8	1223596	2003	11	1203864
2001	6	1073786	2002	9	1187230	2003	12	1222505
2001	7	1176575	2002	10	1227937	2004	1	603941
2001	8	1176245	2002	11	1187472	2004	2	1120517
2001	9	865416	2002	12	1216854	2004	3	1199719
2001	10	0	2003	1	1226903	2004	4	1273278
2001	11	0	2003	2	1059368	2004	5	1317279
2001	12	950489	2003	3	1225395	2004	6	1271435
2002	1	1225438	2003	4	127791	2004	7	1313665
2002	2	1107933	2003	5	720780	2004	8	1306672
2002	3	1213191	2003	6	1186466	2004	9	1274881
2002	4	1185520	2003	7	1225660	2004	10	321012
2002	5	771167	2003	8	1244020			
2002	6	1186480	2003	9	1203912			

Table A-3
 Calculated C_j Factors at the Surveillance Capsule Center
 Core Midplane Elevation

Fuel Cycle	Cycle Length [EFPS]	$\phi(E > 1.0 \text{ MeV})$ [n/cm ² -s]				
		Capsule V	Capsule R	Capsule P	Capsule S	Capsule T
1	4.06E+07	1.44E+11	1.44E+11	8.10E+10	7.64E+10	8.10E+10
2	2.14E+07		1.43E+11	8.64E+10	8.43E+10	8.64E+10
3	3.24E+07		9.14E+10	7.63E+10	7.90E+10	7.63E+10
4	2.97E+07		1.10E+11	7.19E+10	6.88E+10	7.19E+10
5	2.18E+07		1.11E+11	7.25E+10	7.02E+10	7.25E+10
6	2.44E+07			7.70E+10	7.81E+10	7.70E+10
7	2.56E+07			6.91E+10	6.93E+10	6.91E+10
8	2.49E+07			7.38E+10	7.32E+10	7.38E+10
9	2.57E+07			7.33E+10	7.01E+10	7.33E+10
10	2.33E+07			7.11E+10	6.88E+10	7.11E+10
11	2.71E+07			6.93E+10	6.58E+10	6.93E+10
12	2.61E+07			6.87E+10	6.24E+10	6.87E+10
13	2.81E+07			7.48E+10	7.22E+10	7.48E+10
14	2.57E+07				6.99E+10	7.26E+10
15	2.68E+07				6.93E+10	7.30E+10
16	2.75E+07				7.06E+10	7.02E+10
17	2.53E+07				6.91E+10	7.05E+10
18	2.67E+07				7.38E+10	7.11E+10
19	2.81E+07				6.97E+10	7.15E+10
20	2.57E+07					7.33E+10
21	3.88E+07					7.09E+10
22	3.96E+07					7.21E+10
23	4.08E+07					7.33E+10
24	3.84E+07					6.87E+10
25	3.96E+07					7.12E+10
26	4.27E+07					6.36E+10
Average		1.44E+11	1.20E+11	7.44E+10	7.17E+10	7.22E+10

Table A-3 (continued)
 Calculated C_j Factors at the Surveillance Capsule Center
 Core Midplane Elevation

Fuel Cycle	Cycle Length [EFPS]	C_j				
		Capsule V	Capsule R	Capsule P	Capsule S	Capsule T
1	4.06E+07	1.000	1.200	1.089	1.066	1.122
2	2.14E+07		1.185	1.162	1.176	1.197
3	3.24E+07		0.760	1.025	1.101	1.056
4	2.97E+07		0.911	0.967	0.959	0.997
5	2.18E+07		0.924	0.975	0.979	1.005
6	2.44E+07			1.035	1.089	1.067
7	2.56E+07			0.929	0.967	0.958
8	2.49E+07			0.992	1.020	1.022
9	2.57E+07			0.985	0.978	1.015
10	2.33E+07			0.956	0.959	0.985
11	2.71E+07			0.931	0.917	0.959
12	2.61E+07			0.924	0.870	0.952
13	2.81E+07			1.006	1.007	1.036
14	2.57E+07				0.975	1.006
15	2.68E+07				0.966	1.011
16	2.75E+07				0.984	0.972
17	2.53E+07				0.964	0.976
18	2.67E+07				1.029	0.985
19	2.81E+07				0.972	0.991
20	2.57E+07					1.015
21	3.88E+07					0.982
22	3.96E+07					0.999
23	4.08E+07					1.015
24	3.84E+07					0.951
25	3.96E+07					0.987
26	4.27E+07					0.835

Table A-4

Measured Sensor Activities And Reaction Rates

Surveillance Capsule V

<u>Reaction</u>	<u>Location</u>	<u>Measured Activity (dps/g)</u>	<u>Saturated Activity (dps/g)</u>	<u>Gradient Corrected Reaction Rate (rps/atom)</u>
$^{63}\text{Cu} (n,\alpha) ^{60}\text{Co}$	Top-Middle	6.89E+04	4.85E+05	7.08E-17
	Bottom-Middle	7.83E+04	5.51E+05	8.05E-17
	Average			7.56E-17
$^{54}\text{Fe} (n,p) ^{54}\text{Mn}$	Top	1.93E+06	5.03E+06	9.24E-15
	Top-Middle	1.76E+06	4.59E+06	8.43E-15
	Middle	1.84E+06	4.80E+06	8.81E-15
	Bottom-Middle	1.82E+06	4.75E+06	8.71E-15
	Bottom	1.98E+06	5.16E+06	9.48E-15
	Average			8.93E-15
$^{58}\text{Ni} (n,p) ^{58}\text{Co}$	Middle	1.17E+07	8.26E+07	1.13E-14
	Average			1.13E-14
$^{238}\text{U} (n,f) ^{137}\text{Cs} (\text{Cd})$	Middle	2.47E+05	8.60E+06	5.65E-14
	Including ^{235}U , ^{239}Pu , and γ fission corrections:			4.62E-14
$^{237}\text{Np} (n,f) ^{137}\text{Cs} (\text{Cd})$	Middle	2.18E+06	7.59E+07	4.84E-13
	Including γ fission corrections:			4.76E-13
$^{59}\text{Co} (n,\gamma) ^{60}\text{Co}$	Top	2.27E+07	1.60E+08	1.03E-11
	Average			1.03E-11
$^{59}\text{Co} (n,\gamma) ^{60}\text{Co} (\text{Cd})$	Top	1.01E+07	7.11E+07	4.42E-12
	Bottom	1.02E+07	7.18E+07	4.46E-12
	Average			4.44E-12

Notes: 1) Measured specific activities are indexed to a counting date of August 11, 1976.

2) The average $^{238}\text{U} (n,f)$ reaction rate of 4.62E-14 includes a correction factor of 0.861 to account for plutonium build-in and an additional factor of 0.950 to account for photo-fission effects in the sensor.

3) The average $^{237}\text{Np} (n,f)$ reaction rate of 4.76E-13 includes a correction factor of 0.983 to account for photo-fission effects in the sensor.

4) Reaction rates referenced to the Cycle 1 Rated Reactor Power of 1650 Mwt.

Table A-4 cont'd

Measured Sensor Activities And Reaction Rates

Surveillance Capsule R

<u>Reaction</u>	<u>Location</u>	<u>Measured Activity (dps/g)</u>	<u>Saturated Activity (dps/g)</u>	<u>Gradient Corrected Reaction Rate (rps/atom)</u>
$^{63}\text{Cu} (n,\alpha) ^{60}\text{Co}$	Top-Middle	1.65E+05	4.20E+05	6.13E-17
	Average			6.13E-17
$^{54}\text{Fe} (n,p) ^{54}\text{Mn}$	Top	2.25E+06	4.33E+06	7.95E-15
	Top-Middle	2.09E+06	4.02E+06	7.39E-15
	Middle	2.11E+06	4.06E+06	7.46E-15
	Bottom	2.32E+06	4.47E+06	8.20E-15
	Average			7.75E-15
$^{58}\text{Ni} (n,p) ^{58}\text{Co}$	Middle	1.31E+07	7.87E+07	1.08E-14
	Average			1.08E-14
$^{238}\text{U} (n,f) ^{137}\text{Cs} (\text{Cd})$	Middle	7.99E+05	8.11E+06	5.33E-14
	Including ^{235}U , ^{239}Pu , and γ fission corrections:			4.13E-14
$^{237}\text{Np} (n,f) ^{137}\text{Cs} (\text{Cd})$	Middle			See Note 3
	Including γ fission corrections:			
$^{59}\text{Co} (n,\gamma) ^{60}\text{Co}$	Top	5.31E+07	1.35E+08	8.67E-12
	Bottom	5.57E+07	1.42E+08	9.10E-12
	Average			8.88E-12
$^{59}\text{Co} (n,\gamma) ^{60}\text{Co} (\text{Cd})$	Top	2.63E+07	6.69E+07	4.16E-12
	Bottom	2.36E+07	6.00E+07	3.73E-12
	Average			3.94E-12

Notes: 1) Measured specific activities are indexed to a counting date of October 21, 1980.

2) The average $^{238}\text{U} (n,f)$ reaction rate of 4.13E-14 includes a correction factor of 0.817 to account for plutonium build-in and an additional factor of 0.950 to account for photo-fission effects in the sensor.

3) The neptunium sensor contained in Capsule R produced erroneous results and was rejected from further consideration.

4) Reaction Rates referenced to the Cycles 1-5 Average Rated Reactor Power of 1650 MWt.

Table A-4 cont'd

Measured Sensor Activities And Reaction Rates				
Surveillance Capsule P				
<u>Reaction</u>	<u>Location</u>	<u>Measured Activity (dps/g)</u>	<u>Saturated Activity (dps/g)</u>	<u>Gradient Corrected Reaction Rate (rps/atom)</u>
^{63}Cu (n, α) ^{60}Co	Top-Middle	2.12E+05	3.19E+05	4.65E-17
	Bottom-Middle	2.44E+05	3.67E+05	5.35E-17
	Average			5.00E-17
^{54}Fe (n,p) ^{54}Mn	Top	2.74E+06	3.68E+06	6.65E-15
	Top-Middle	1.95E+06	2.62E+06	4.73E-15
	Middle	2.11E+06	2.83E+06	5.12E-15
	Bottom-Middle	2.19E+06	2.94E+06	5.31E-15
	Bottom	2.33E+06	3.13E+06	5.65E-15
	Average			5.49E-15
^{58}Ni (n,p) ^{58}Co	Middle	2.44E+07	5.03E+07	6.86E-15
	Average			6.86E-15
^{238}U (n,f) ^{137}Cs (Cd)	Middle	1.13E+06	5.16E+06	3.39E-14
	Including ^{235}U , ^{239}Pu , and γ fission corrections:			2.55E-14
^{237}Np (n,f) ^{137}Cs (Cd)	Middle	8.28E+06	3.78E+07	2.41E-13
	Including γ fission corrections:			2.37E-13
^{59}Co (n, γ) ^{60}Co	Top	4.20E+07	6.32E+07	4.08E-12
	Bottom	5.01E+07	7.54E+07	4.86E-12
	Average			4.47E-12
^{59}Co (n, γ) ^{60}Co (Cd)	Top	1.79E+07	2.70E+07	1.68E-12
	Bottom	2.04E+07	3.07E+07	1.91E-12
	Average			1.80E-12

Notes: 1) Measured specific activities are indexed to a counting date of May 12, 1988.

2) The average ^{238}U (n,f) reaction rate of 2.55E-14 includes a correction factor of 0.789 to account for plutonium build-in and an additional factor of 0.955 to account for photo-fission effects in the sensor.

3) The average ^{237}Np (n,f) reaction rate of 2.37E-13 includes a correction factor of 0.984 to account for photo-fission effects in the sensor.

4) Reaction Rates referenced to the Cycles 1-13 Average Rated Reactor Power of 1650 MWt.

Table A-4 cont'd

Measured Sensor Activities And Reaction Rates

Surveillance Capsule S

<u>Reaction</u>	<u>Location</u>	<u>Measured Activity (dps/g)</u>	<u>Saturated Activity (dps/g)</u>	<u>Gradient Corrected Reaction Rate (rps/atom)</u>
$^{63}\text{Cu} (n,\alpha) ^{60}\text{Co}$	Top-Middle	2.15E+05	3.03E+05	4.40E-17
	Bottom-Middle	2.38E+05	3.35E+05	4.87E-17
	Average			4.64E-17
$^{54}\text{Fe} (n,p) ^{54}\text{Mn}$	Top	1.53E+06	2.74E+06	4.96E-15
	Top-Middle	1.39E+06	2.49E+06	4.50E-15
	Middle	1.52E+06	2.72E+06	4.92E-15
	Bottom-Middle	1.49E+06	2.67E+06	4.83E-15
	Average			4.80E-15
$^{58}\text{Ni} (n,p) ^{58}\text{Co}$	Middle	6.92E+06	5.14E+07	6.99E-15
	Average			6.99E-15
$^{238}\text{U} (n,f) ^{137}\text{Cs} (\text{Cd})$	Middle	1.31E+06	4.42E+06	2.90E-14
	Including ^{235}U , ^{239}Pu , and γ fission corrections:			2.09E-14
$^{237}\text{Np} (n,f) ^{137}\text{Cs} (\text{Cd})$	Middle	7.90E+06	2.67E+07	1.70E-13
	Including γ fission corrections:			1.67E-13
$^{59}\text{Co} (n,\gamma) ^{60}\text{Co}$	Top	4.38E+07	6.16E+07	3.96E-12
	Bottom	4.48E+07	6.30E+07	4.05E-12
	Average			4.01E-12
$^{59}\text{Co} (n,\gamma) ^{60}\text{Co} (\text{Cd})$	Top	2.14E+07	3.01E+07	1.87E-12
	Bottom	2.10E+07	2.95E+07	1.84E-12
	Average			1.85E-12

Notes: 1) Measured specific activities are indexed to a counting date of October 13, 1994.

2) The average $^{238}\text{U} (n,f)$ reaction rate of 2.09E-14 includes a correction factor of 0.754 to account for plutonium build-in and an additional factor of 0.953 to account for photo-fission effects in the sensor.

3) The average $^{237}\text{Np} (n,f)$ reaction rate of 1.67E-13 includes a correction factor of 0.983 to account for photo-fission effects in the sensor.

4) Reaction Rates referenced to the Cycles 1-19 Average Rated Reactor Power of 1650 MWt.

Table A-4 cont'd

Measured Sensor Activities And Reaction Rates

Surveillance Capsule T

<u>Reaction</u>	<u>Location</u>	<u>Measured Activity (dps/g)</u>	<u>Saturated Activity (dps/g)</u>	<u>Gradient Corrected Reaction Rate (rps/atom)</u>
$^{63}\text{Cu} (n,\alpha) ^{60}\text{Co}$	Top-Middle	2.08E+05	3.07E+05	4.47E-17
	Bottom-Middle	2.35E+05	3.47E+05	5.05E-17
	Average			4.76E-17
$^{54}\text{Fe} (n,p) ^{54}\text{Mn}$	Top	9.21E+05	2.99E+06	5.41E-15
	Top-Middle	8.05E+05	2.62E+06	4.73E-15
	Middle	8.89E+05	2.89E+06	5.23E-15
	Bottom-Middle	8.58E+05	2.79E+06	5.04E-15
	Bottom	9.51E+05	3.09E+06	5.59E-15
	Average			5.20E-15
$^{58}\text{Ni} (n,p) ^{58}\text{Co}$	Middle	5.85E+05	5.30E+07	7.22E-15
	Average			7.22E-15
$^{238}\text{U} (n,f) ^{137}\text{Cs} (\text{Cd})$	Middle	2.16E+06	5.42E+06	3.56E-14
	Including ^{235}U , ^{239}Pu , and γ fission corrections:			2.35E-14
$^{237}\text{Np} (n,f) ^{137}\text{Cs} (\text{Cd})$	Middle	1.34E+07	3.36E+07	2.15E-13
	Including γ fission corrections:			2.11E-13
$^{59}\text{Co} (n,\gamma) ^{60}\text{Co}$	Top	4.45E+07	6.57E+07	4.22E-12
	Average			4.22E-12
$^{59}\text{Co} (n,\gamma) ^{60}\text{Co} (\text{Cd})$	Top	2.35E+07	3.47E+07	2.16E-12
	Bottom	2.16E+07	3.19E+07	1.98E-12
	Average			2.07E-12

Notes: 1) Measured specific activities are indexed to a counting date of December 28, 2005.

2) The average $^{238}\text{U} (n,f)$ reaction rate of 2.35E-14 includes a correction factor of 0.690 to account for plutonium build-in and an additional factor of 0.955 to account for photo-fission effects in the sensor.

3) The average $^{237}\text{Np} (n,f)$ reaction rate of 2.11E-13 includes a correction factor of 0.984 to account for photo-fission effects in the sensor.

4) Reaction Rates referenced to the Cycles 1-26 Average Rated Reactor Power of 1653 MWt. This lifetime average core power accounts for an uprate from 1650 MWt to 1772 MWt during Cycle 26.

Table A-5
Comparison of Measured, Calculated, and Adjusted
Reaction Rates At The Surveillance Capsule Center

Capsule V

Reaction	Reaction Rate [rps/atom]			M/C	M/A
	Measured	Calculated	Adjusted		
$^{63}\text{Cu}(n,\alpha)^{60}\text{Co}$	7.58E-17	7.37E-17	7.42E-17	1.03	1.02
$^{54}\text{Fe}(n,p)^{54}\text{Mn}$	8.93E-15	8.95E-15	8.78E-15	1.00	1.02
$^{58}\text{Ni}(n,p)^{58}\text{Co}$	1.13E-14	1.25E-14	1.19E-14	0.90	0.95
$^{238}\text{U}(n,f)^{137}\text{Cs}$ (Cd)	4.62E-14	4.79E-14	4.68E-14	0.96	0.99
$^{237}\text{Np}(n,f)^{137}\text{Cs}$ (Cd)	4.76E-13	4.17E-13	4.44E-13	1.14	1.07
$^{59}\text{Co}(n,\gamma)^{60}\text{Co}$	1.03E-11	1.05E-11	1.03E-11	0.98	1.00
$^{59}\text{Co}(n,\gamma)^{60}\text{Co}$ (Cd)	4.44E-12	4.17E-12	4.43E-12	1.06	1.00

Note: See Section A.1.2 for details describing the Adjusted (A) reaction rates.

Capsule R

Reaction	Reaction Rate [rps/atom]			M/C	M/A
	Measured	Calculated	Adjusted		
$^{63}\text{Cu}(n,\alpha)^{60}\text{Co}$	6.13E-17	6.40E-17	6.24E-17	0.96	0.98
$^{54}\text{Fe}(n,p)^{54}\text{Mn}$	7.75E-15	7.60E-15	7.68E-15	1.02	1.01
$^{58}\text{Ni}(n,p)^{58}\text{Co}$	1.08E-14	1.06E-14	1.07E-14	1.02	1.01
$^{238}\text{U}(n,f)^{137}\text{Cs}$ (Cd)	4.13E-14	4.02E-14	4.12E-14	1.03	1.00
$^{59}\text{Co}(n,\gamma)^{60}\text{Co}$	8.88E-12	8.67E-12	8.90E-12	1.02	1.00
$^{59}\text{Co}(n,\gamma)^{60}\text{Co}$ (Cd)	3.94E-12	3.43E-12	3.92E-12	1.15	1.01

Note: See Section A.1.2 for details describing the Adjusted (A) reaction rates.

Capsule P

Reaction	Reaction Rate [rps/atom]			M/C	M/A
	Measured	Calculated	Adjusted		
$^{63}\text{Cu}(n,\alpha)^{60}\text{Co}$	5.00E-17	5.04E-17	4.98E-17	0.99	1.00
$^{54}\text{Fe}(n,p)^{54}\text{Mn}$	5.49E-15	5.36E-15	5.35E-15	1.02	1.03
$^{58}\text{Ni}(n,p)^{58}\text{Co}$	6.86E-15	7.36E-15	7.16E-15	0.93	0.96
$^{238}\text{U}(n,f)^{137}\text{Cs}$ (Cd)	2.55E-14	2.60E-14	2.60E-14	0.98	0.98
$^{237}\text{Np}(n,f)^{137}\text{Cs}$ (Cd)	2.37E-13	2.03E-13	2.21E-13	1.17	1.07
$^{59}\text{Co}(n,\gamma)^{60}\text{Co}$	4.47E-12	4.69E-12	4.48E-12	0.95	1.00
$^{59}\text{Co}(n,\gamma)^{60}\text{Co}$ (Cd)	1.80E-12	1.77E-12	1.80E-12	1.02	1.00

Note: See Section A.1.2 for details describing the Adjusted (A) reaction rates.

Table A-5 (continued)
 Comparison of Measured, Calculated, and Adjusted
 Reaction Rates At The Surveillance Capsule Center

Capsule S

Reaction	Reaction Rate [rps/atom]			M/C	M/A
	Measured	Calculated	Adjusted		
$^{63}\text{Cu}(n,\alpha)^{60}\text{Co}$	4.64E-17	4.47E-17	4.60E-17	1.04	1.01
$^{54}\text{Fe}(n,p)^{54}\text{Mn}$	4.80E-15	4.93E-15	4.84E-15	0.97	0.99
$^{58}\text{Ni}(n,p)^{58}\text{Co}$	6.99E-15	6.80E-15	6.75E-15	1.03	1.04
$^{238}\text{U}(n,f)^{137}\text{Cs}$ (Cd)	2.09E-14	2.47E-14	2.33E-14	0.85	0.90
$^{237}\text{Np}(n,f)^{137}\text{Cs}$ (Cd)	1.67E-13	1.99E-13	1.75E-13	0.84	0.95
$^{59}\text{Co}(n,\gamma)^{60}\text{Co}$	4.01E-12	4.61E-12	4.03E-12	0.87	1.00
$^{59}\text{Co}(n,\gamma)^{60}\text{Co}$ (Cd)	1.85E-12	1.79E-12	1.84E-12	1.03	1.01

Note: See Section A.1.2 for details describing the Adjusted (A) reaction rates.

Capsule T

Reaction	Reaction Rate [rps/atom]			M/C	M/A
	Measured	Calculated	Adjusted		
$^{63}\text{Cu}(n,\alpha)^{60}\text{Co}$	4.76E-17	4.92E-17	4.80E-17	0.97	0.99
$^{54}\text{Fe}(n,p)^{54}\text{Mn}$	5.20E-15	5.25E-15	5.19E-15	0.99	1.00
$^{58}\text{Ni}(n,p)^{58}\text{Co}$	7.22E-15	7.20E-15	7.15E-15	1.00	1.01
$^{238}\text{U}(n,f)^{137}\text{Cs}$ (Cd)	2.35E-14	2.52E-14	2.51E-14	0.93	0.94
$^{237}\text{Np}(n,f)^{137}\text{Cs}$ (Cd)	2.11E-13	1.97E-13	2.04E-13	1.07	1.03
$^{59}\text{Co}(n,\gamma)^{60}\text{Co}$	4.22E-12	4.52E-12	4.25E-12	0.93	0.99
$^{59}\text{Co}(n,\gamma)^{60}\text{Co}$ (Cd)	2.07E-12	2.05E-12	2.05E-12	1.21	1.01

Note: See Section A.1.2 for details describing the Adjusted (A) reaction rates.

Table A-6
Comparison of Calculated and Adjusted Exposure Rates
At The Surveillance Capsule Center

Capsule ID	$\phi(E > 1.0 \text{ MeV}) [\text{n/cm}^2\text{-s}]$			
	Calculated	Adjusted	Uncertainty (1σ)	A/C
V	1.45E+11	1.42E+11	6%	0.98
R	1.21E+11	1.25E+11	7%	1.03
P	7.46E+10	7.55E+10	6%	1.01
S	7.20E+10	6.67E+10	6%	0.93
T	7.24E+10	7.24E+10	6%	1.00

Note: Calculated results are based on the synthesized transport calculations taken at the core midplane following the completion of each respective capsules irradiation period and are the average neutron exposure rates over the irradiation period for each capsule. See Section A.1.2 for details describing the adjusted exposure rates.

Capsule ID	Iron Atom Displacement Rate [dpa/s]			
	Calculated	Adjusted	Uncertainty (1σ)	BE/C
V	2.58E-10	2.58E-10	7%	1.00
R	2.14E-10	2.21E-10	8%	1.03
P	1.27E-10	1.29E-10	7%	1.02
S	1.23E-10	1.14E-10	7%	0.92
T	1.23E-10	1.24E-10	7%	1.00

Note: Calculated results are based on the synthesized transport calculations taken at the core midplane following the completion of each respective capsules irradiation period and are the average neutron exposure rate over the irradiation period for each capsule. See Section A.1.2 for details describing the adjusted exposure rates.

Table A-7
Comparison of Measured/Calculated (M/C) Sensor Reaction Rate
Ratios Including all Fast Neutron Threshold Reactions

Reaction	M/C Ratio				
	Capsule V	Capsule R	Capsule P	Capsule S	Capsule T
$^{63}\text{Cu}(n,\alpha)^{60}\text{Co}$	1.03	0.96	0.99	1.04	0.97
$^{54}\text{Fe}(n,p)^{54}\text{Mn}$	1.00	1.02	1.02	0.97	0.99
$^{58}\text{Ni}(n,p)^{58}\text{Co}$	0.90	1.02	0.93	1.03	1.00
$^{238}\text{U}(n,p)^{137}\text{Cs}$ (Cd)	0.96	1.03	0.98	0.85	0.93
$^{237}\text{Np}(n,f)^{137}\text{Cs}$ (Cd)	1.14		1.17	0.84	1.07
Average	1.01	1.01	1.02	0.94	0.99
% Standard Deviation	8.7	3.2	8.8	10.2	5.2

Note: The overall average M/C ratio for the set of 24 sensor measurements is 0.99 with an associated standard deviation of 7.6%.

Table A-8
Comparison of Adjusted/Calculated (A/C) Exposure Rate Ratios

Capsule ID	BE/C Ratio	
	$\phi(E > 1.0 \text{ MeV})$	dpa/s
V	0.98	1.00
R	1.03	1.03
P	1.01	1.02
S	0.93	0.92
T	1.00	1.00
Average	0.99	1.00
% Standard Deviation	4.1	4.3

Appendix A References

- A-1. Regulatory Guide RG-1.190, "Calculational and Dosimetry Methods for Determining Pressure Vessel Neutron Fluence," U. S. Nuclear Regulatory Commission, Office of Nuclear Regulatory Research, March 2001.
- A-2. WCAP-16083-NP-A, Revision 0, "Benchmark Testing of the FERRET Code for Least Squares Evaluation of Light Water Reactor Dosimetry," May 2006.
- A-3. WCAP-8107, Revision 0, "Wisconsin Public Service Corp. Kewaunee Nuclear Power Plant Reactor Vessel Radiation Surveillance Program," April 1973.
- A-4. RSIC Data Library Collection DLC-178, "SNLRML Recommended Dosimetry Cross-Section Compendium", July 1994

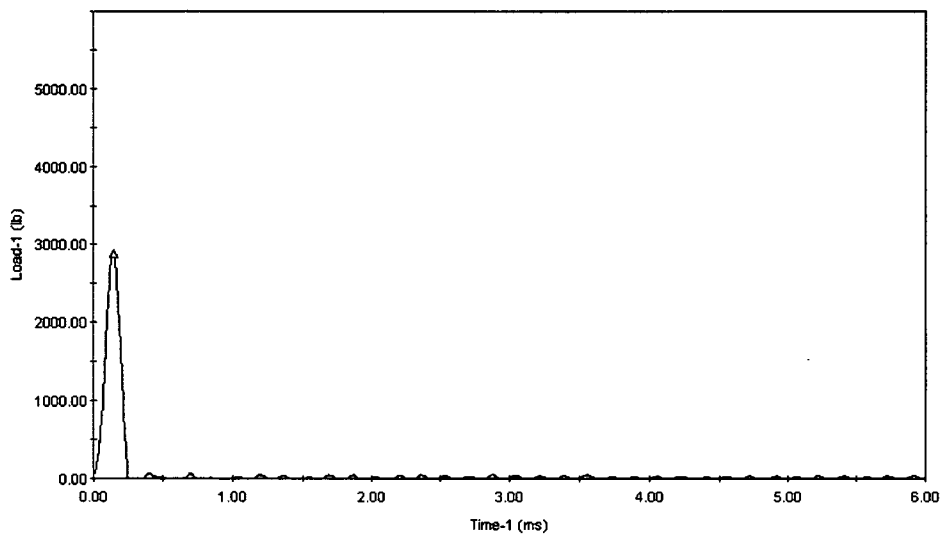
APPENDIX B

LOAD-TIME RECORDS FOR CHARPY SPECIMEN TESTS

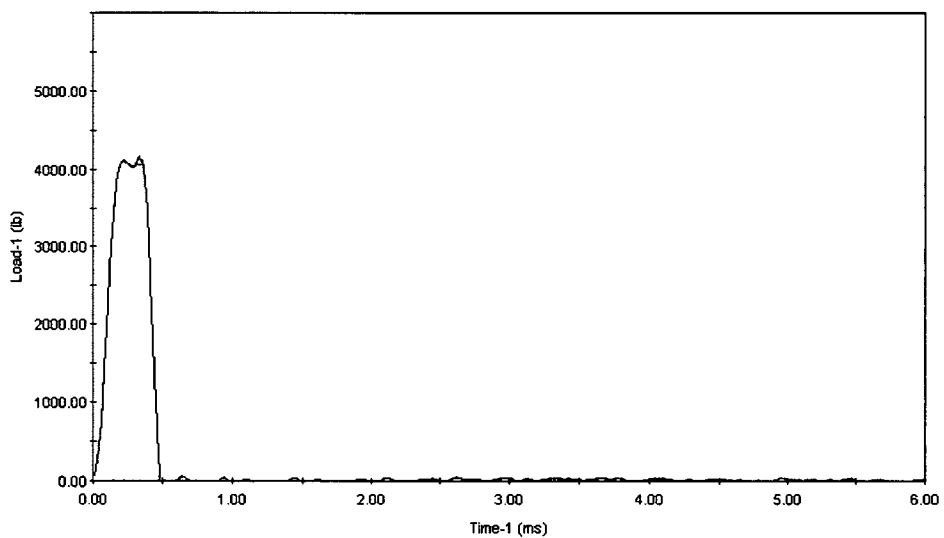
INSTRUMENTED CHARPY IMPACT TEST CURVES

- Specimen prefix “P” denotes intermediate shell forging 122X208VA1, Tangential Orientation
- Specimen prefix “S” denotes lower shell forging 123X167VA1, Tangential Orientation
- Specimen prefix “R” denotes A533 Grade B Class 1 Standard Reference Material
- Specimen prefix “H” denotes reconstituted Weld Material

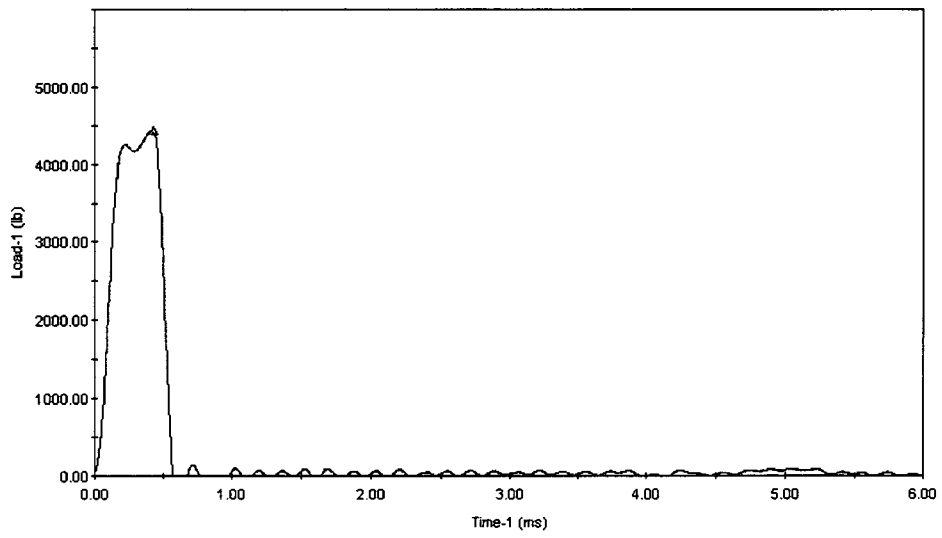
This page intentionally blank



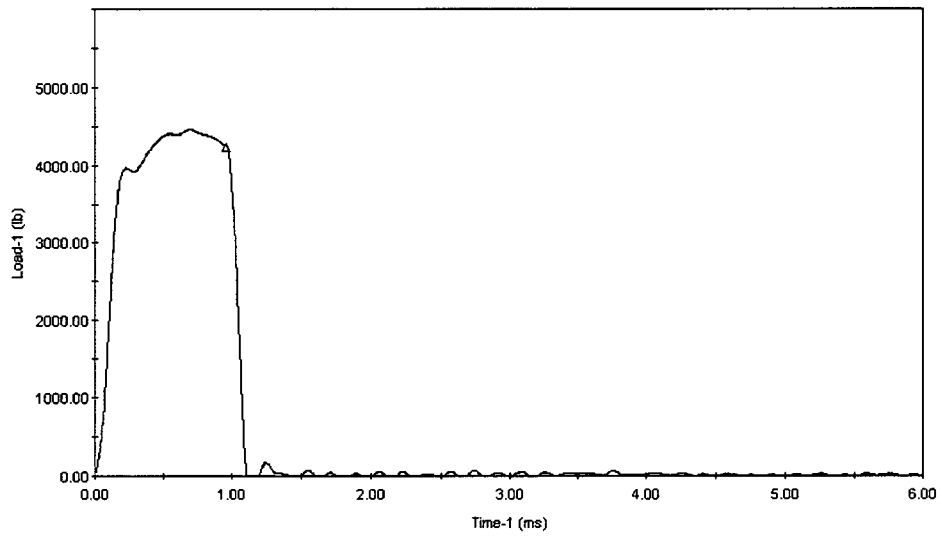
P47, -50°F



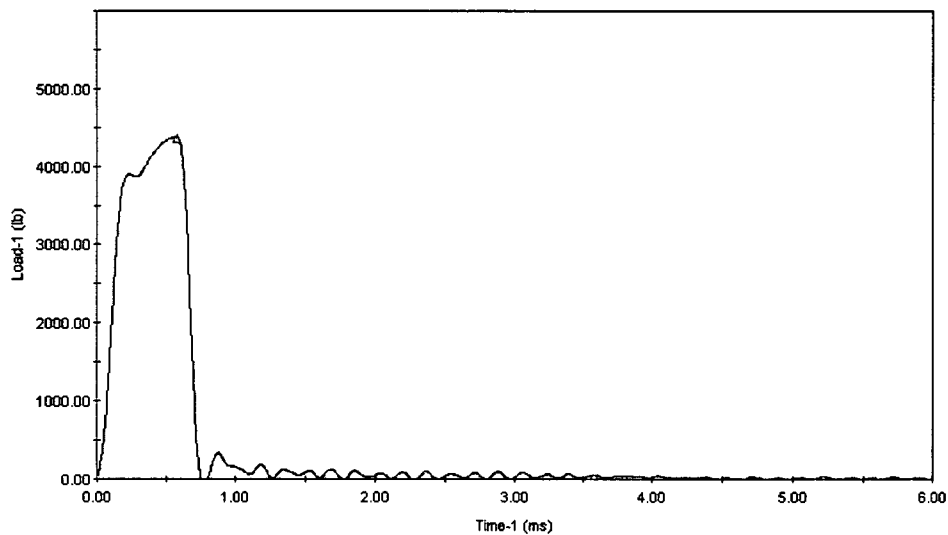
P46, 50°F



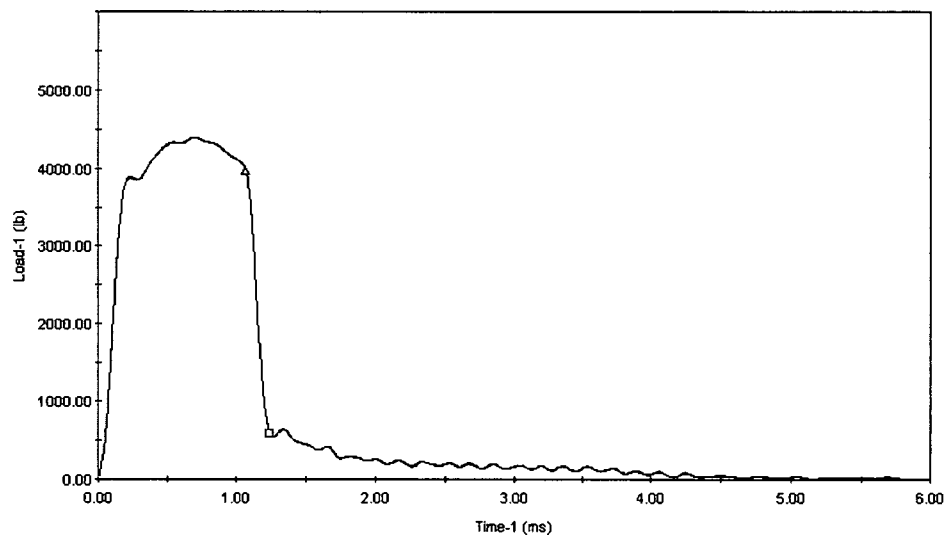
P45, 75°F



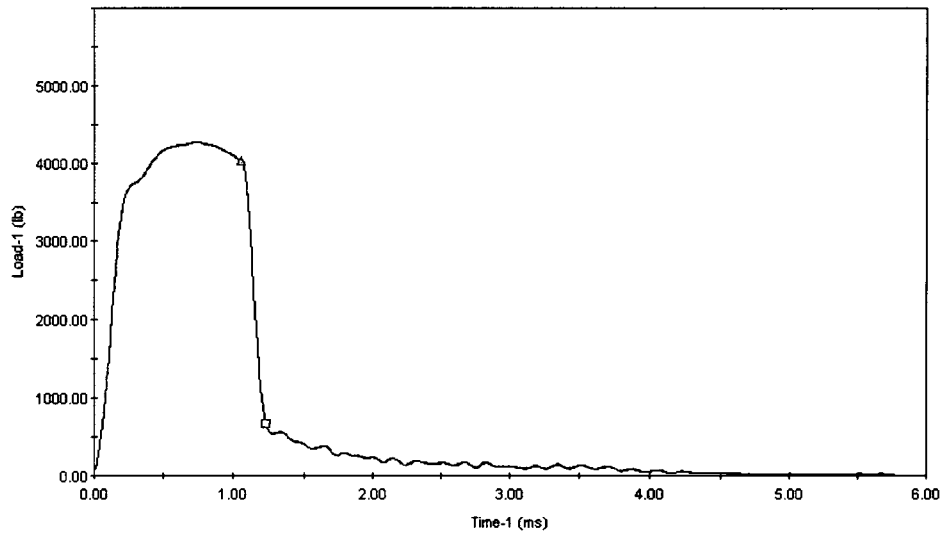
P43, 100°F



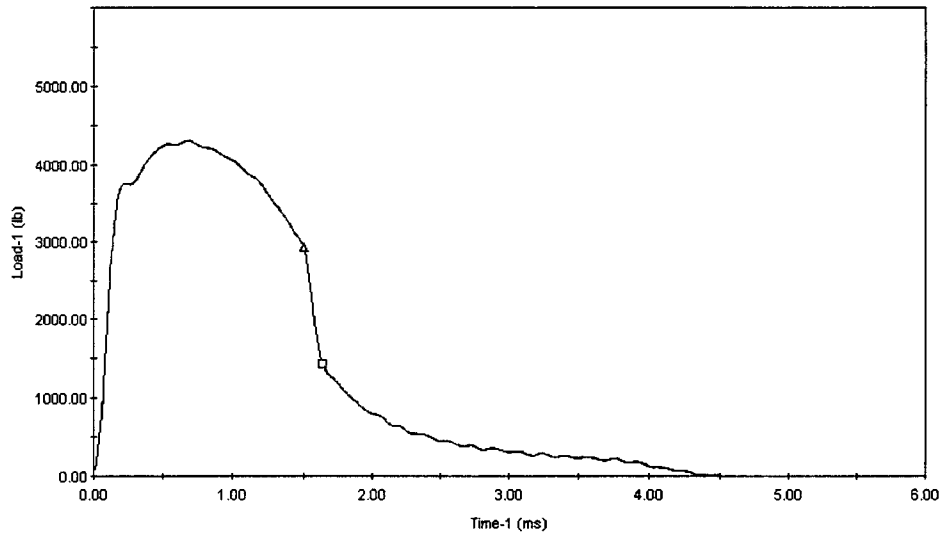
P40, 125°F



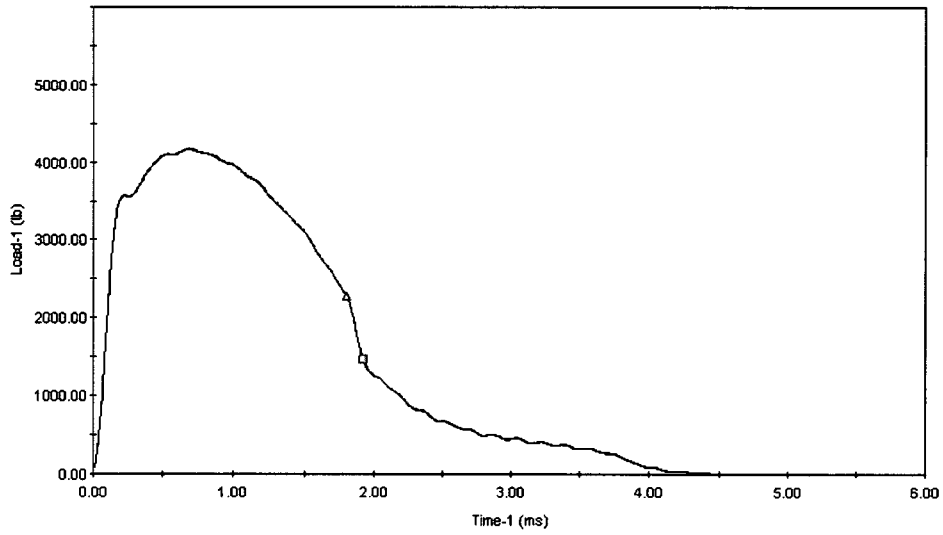
P37, 150°F



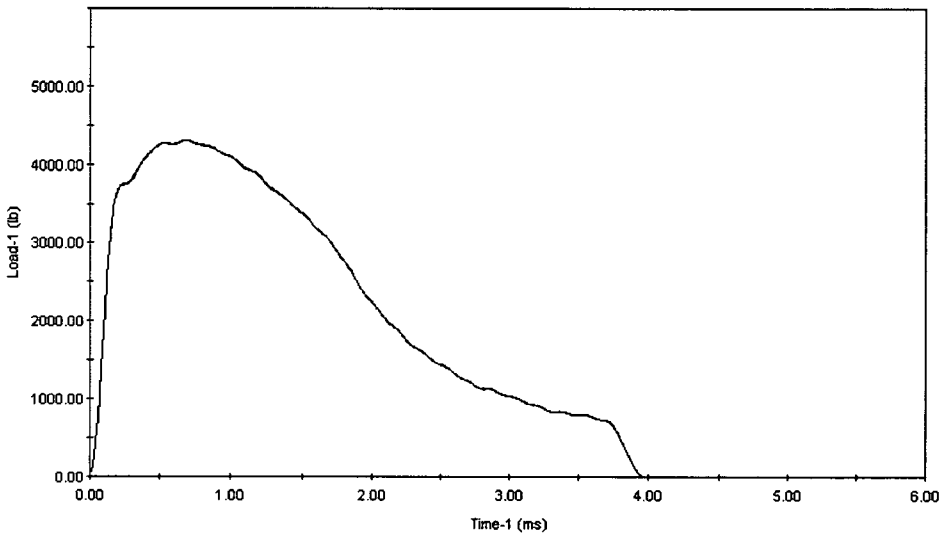
P44, 175°F



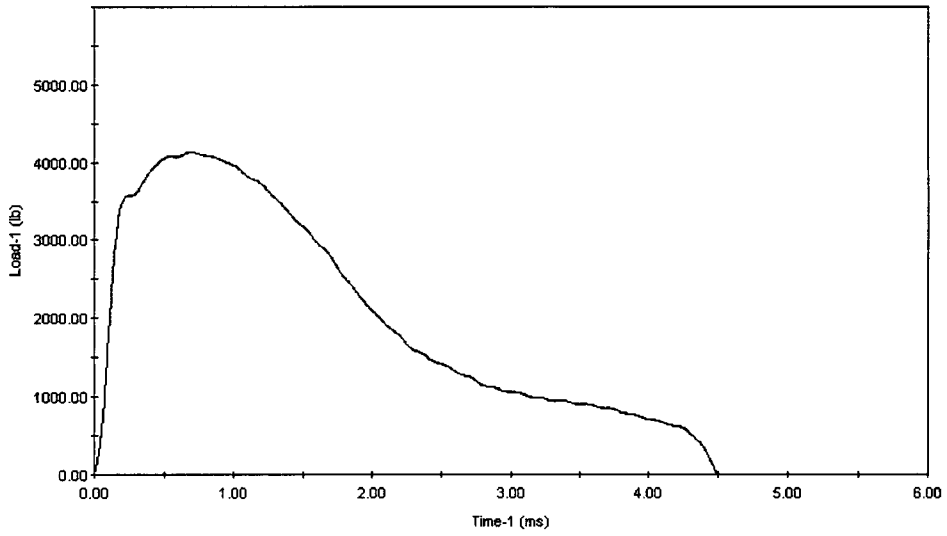
P41, 200°F



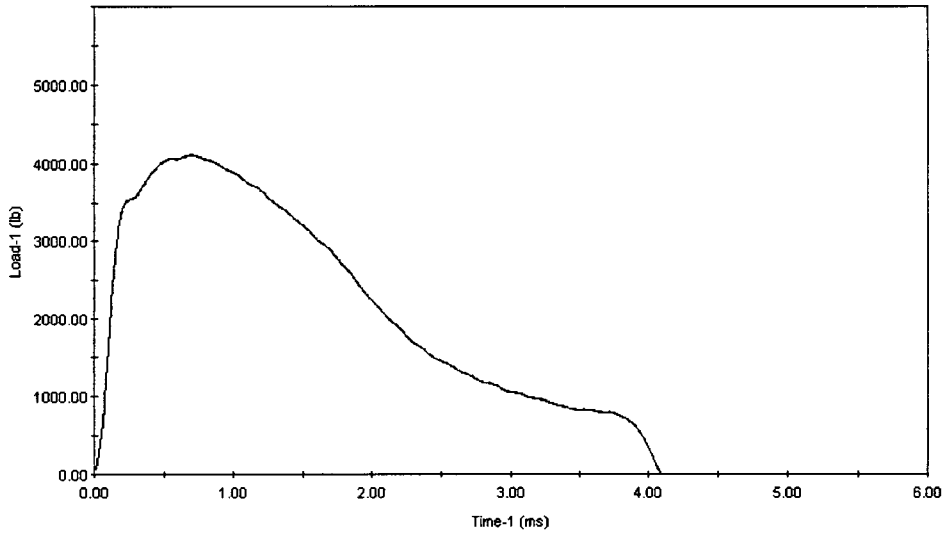
P48, 250°F



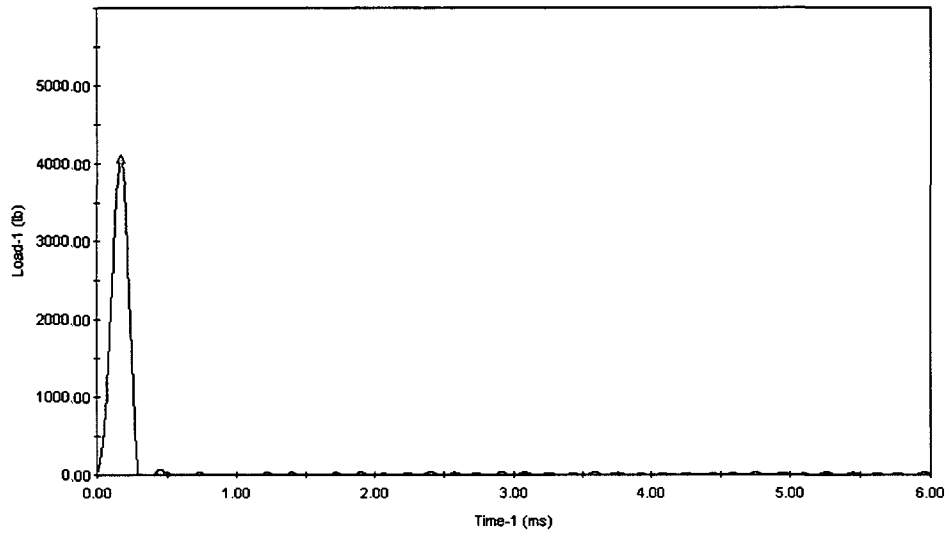
P38, 325°F



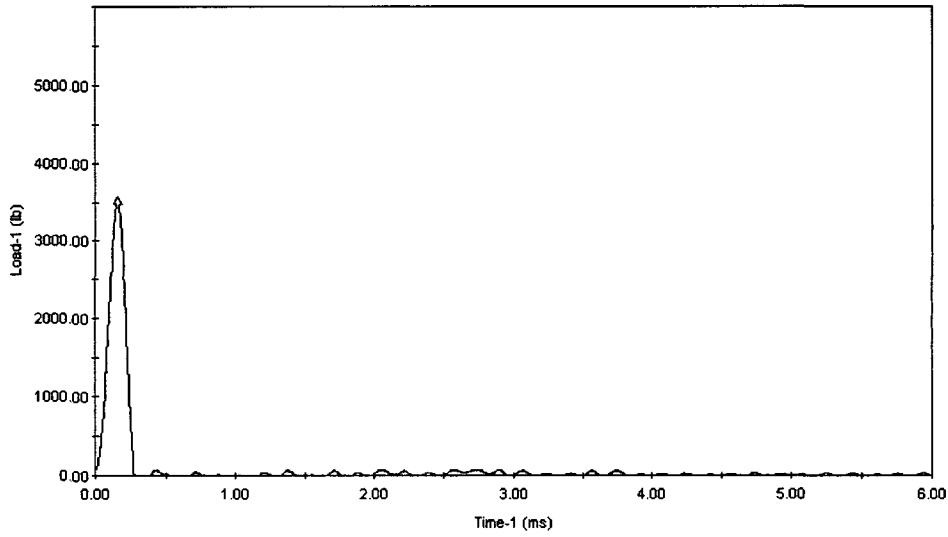
P39, 350°F



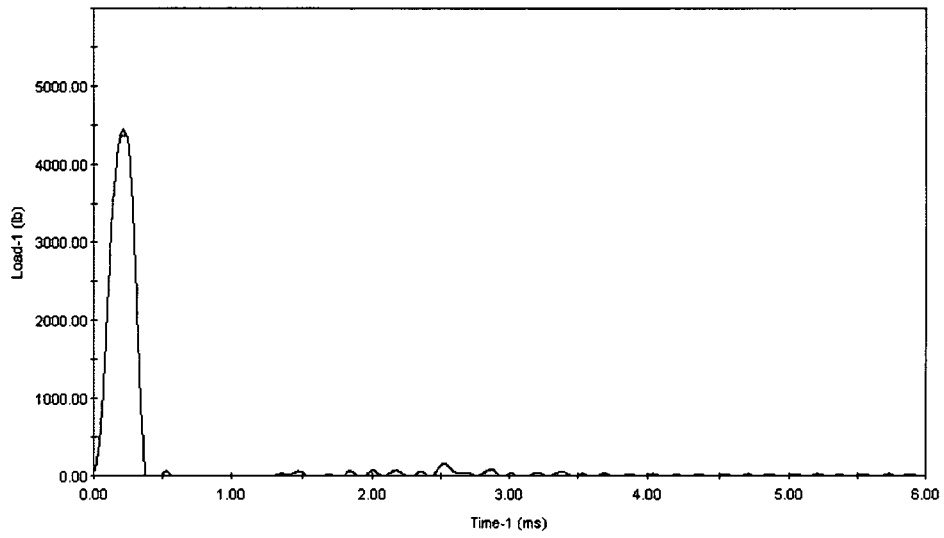
P42, 400°F



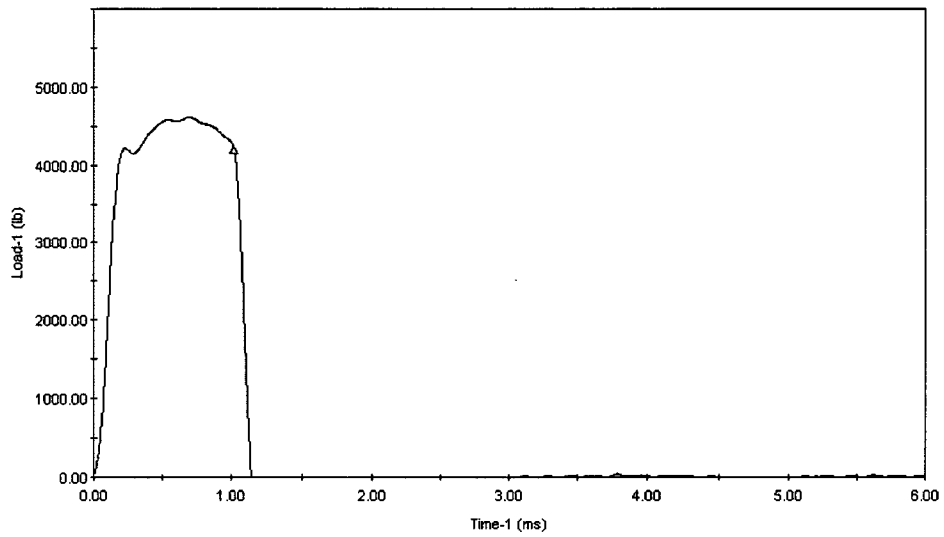
S45, -50°F



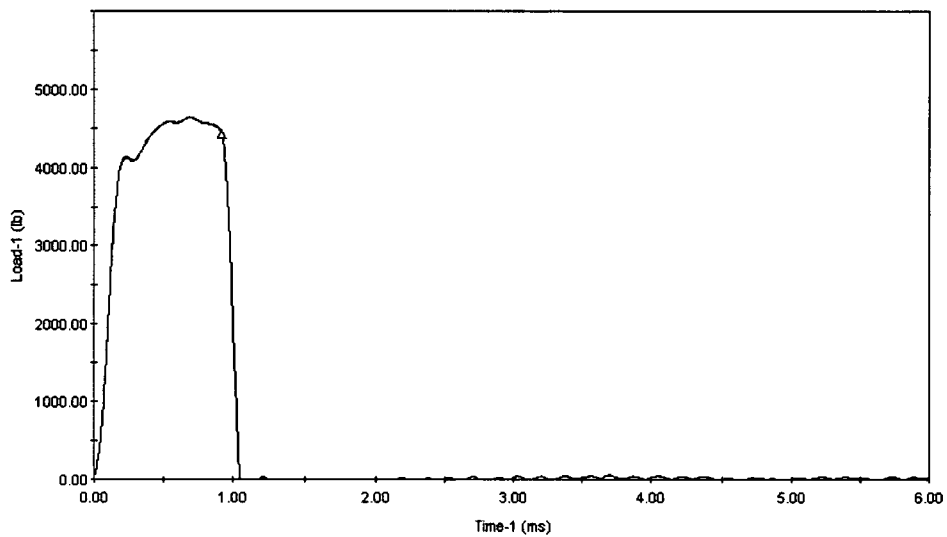
S47, 0°F



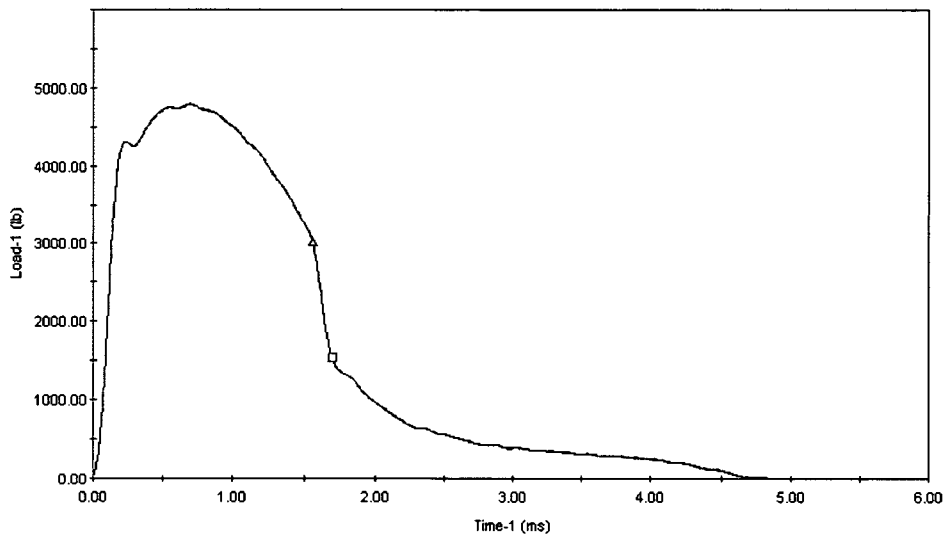
S40, 25°F



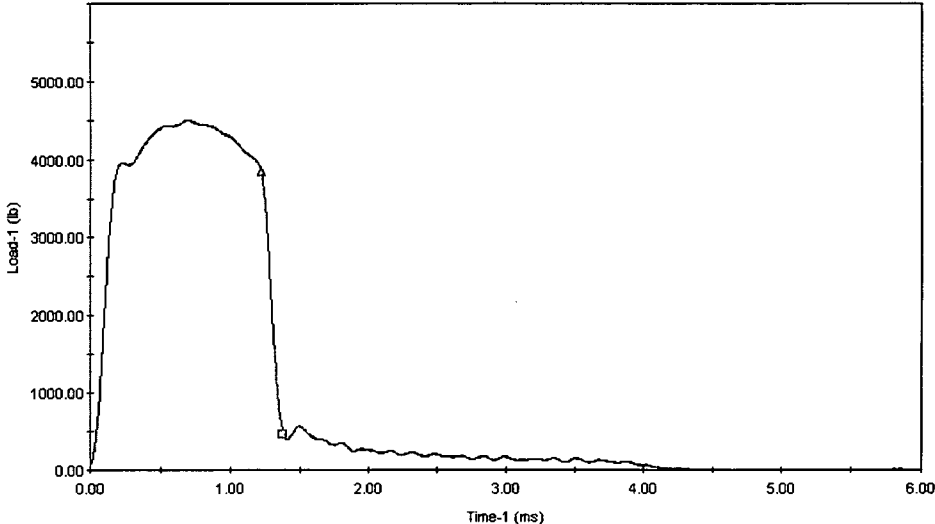
S38, 50°F



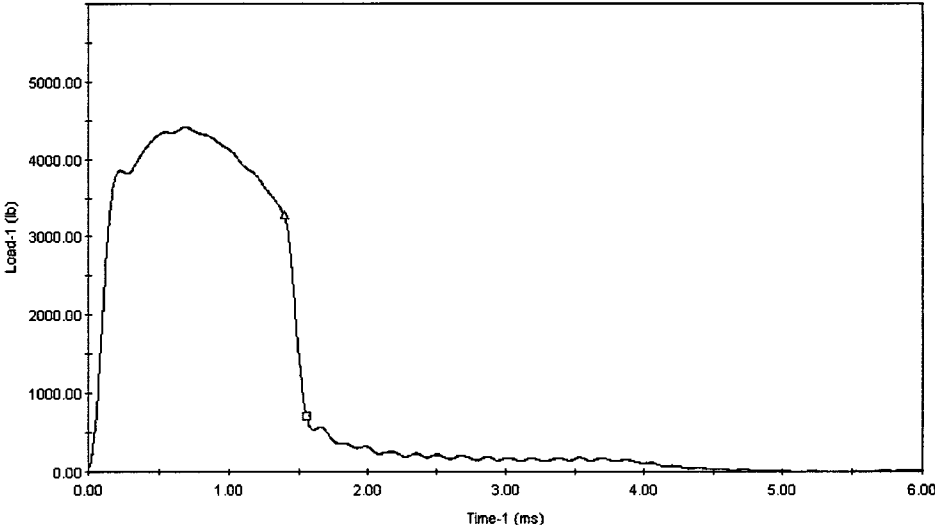
S37, 75°F



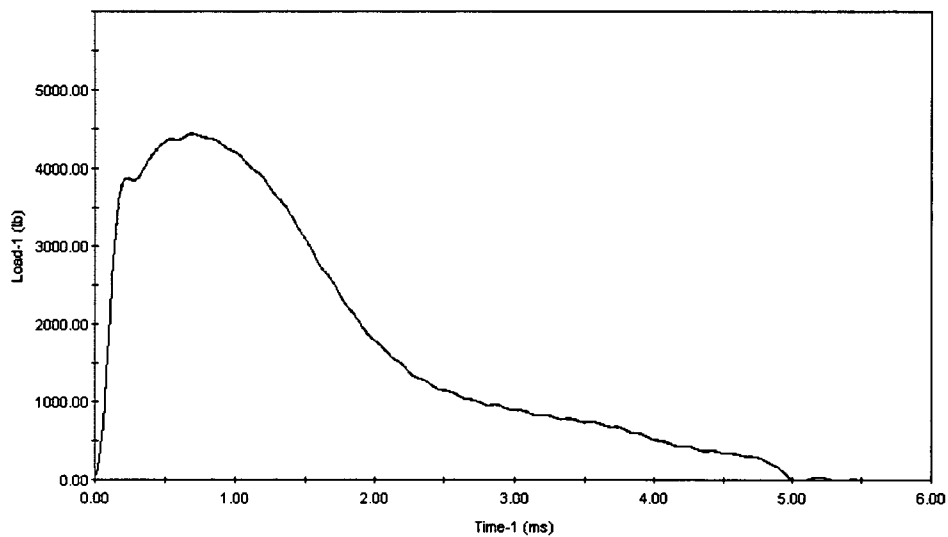
S48, 100°F



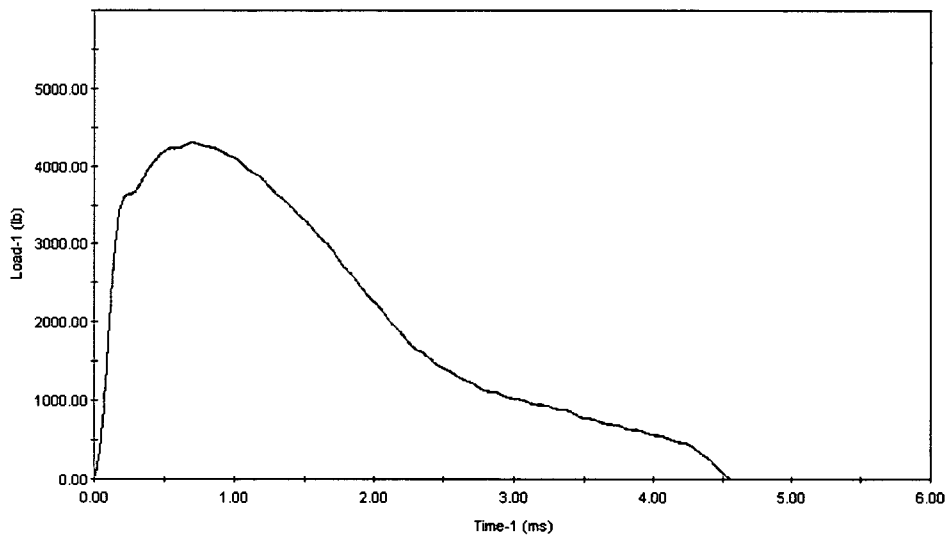
S43, 125°F



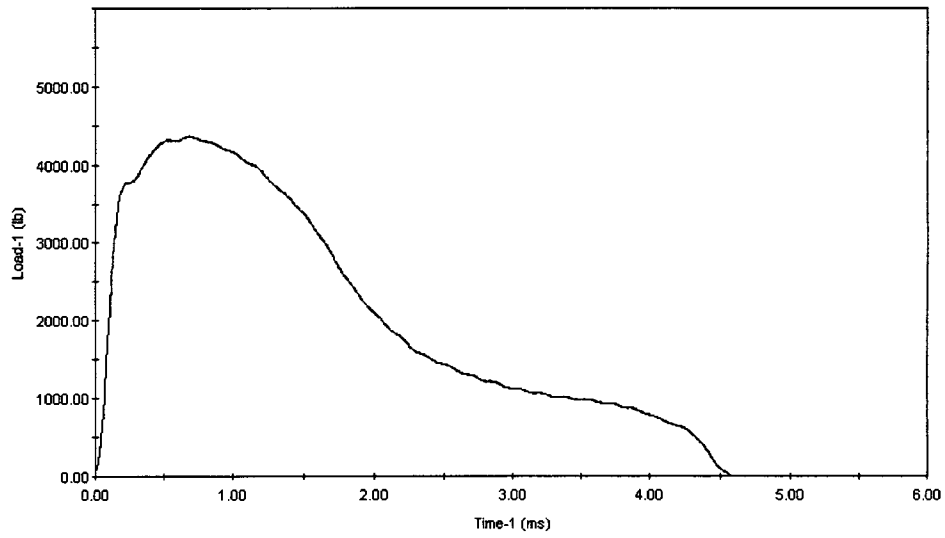
S44, 150°F



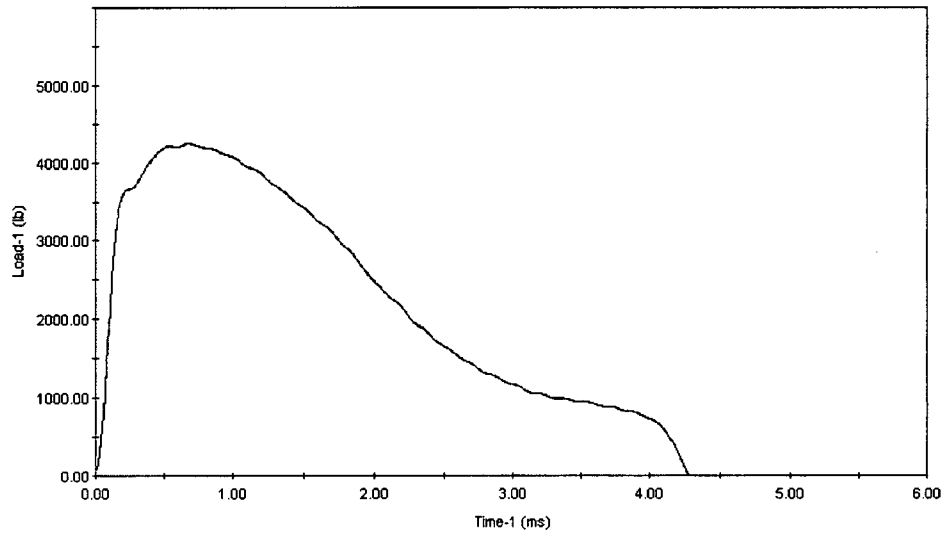
S46, 175°F



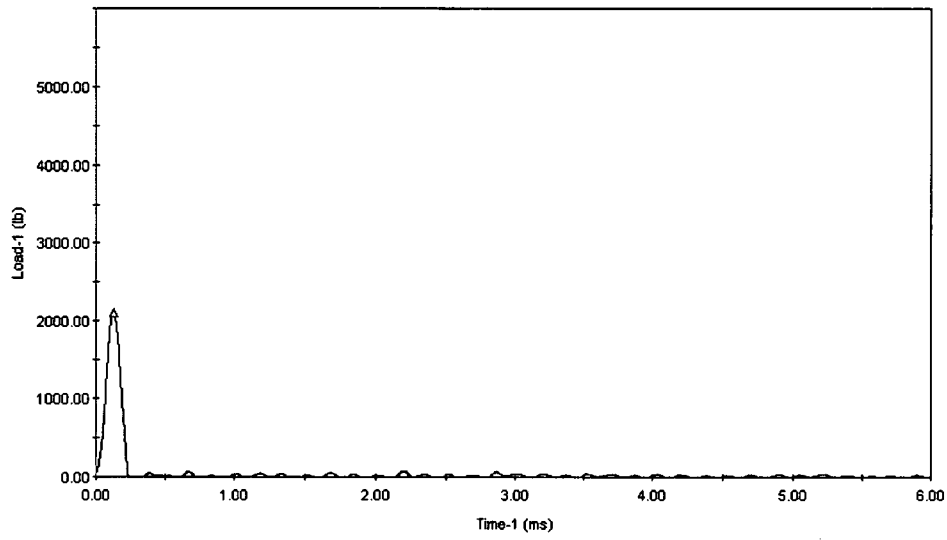
S41, 250°F



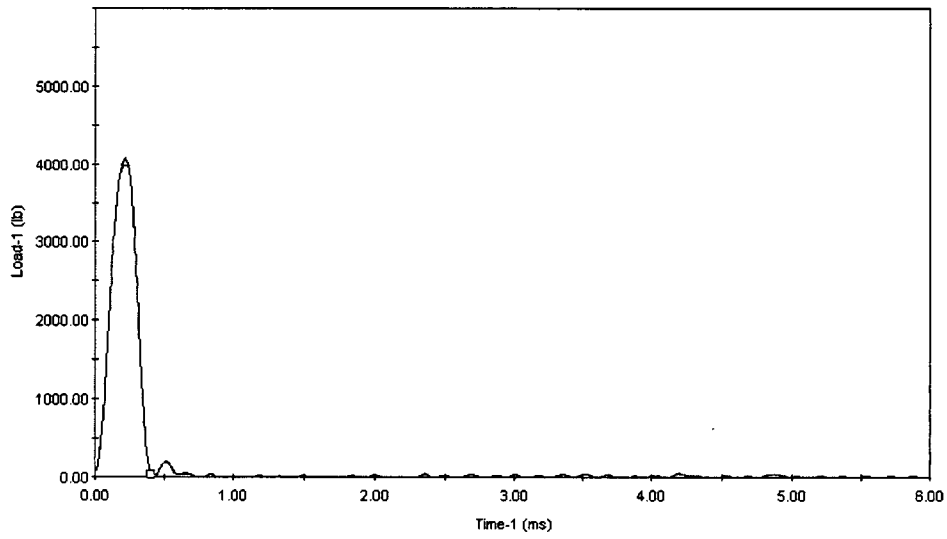
S39, 300°F



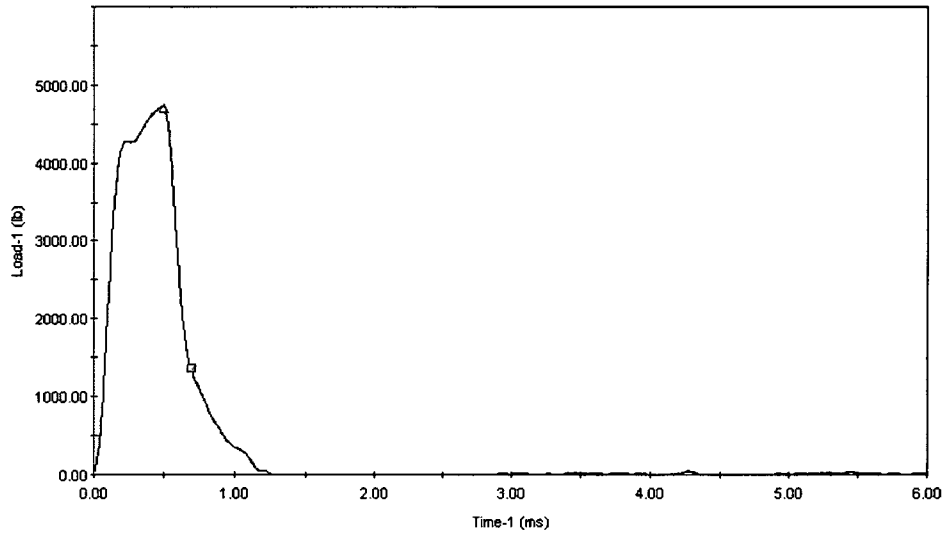
S42, 350°F



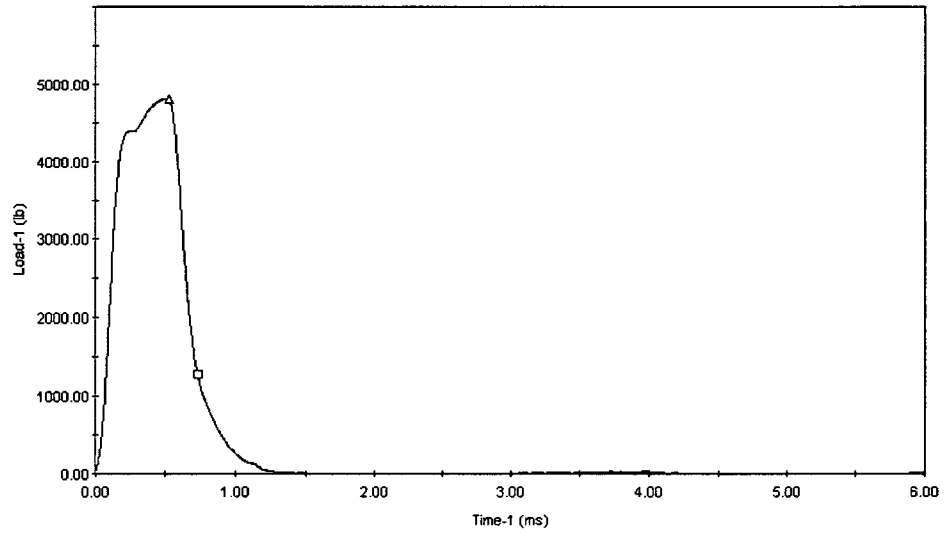
R31, 100°F



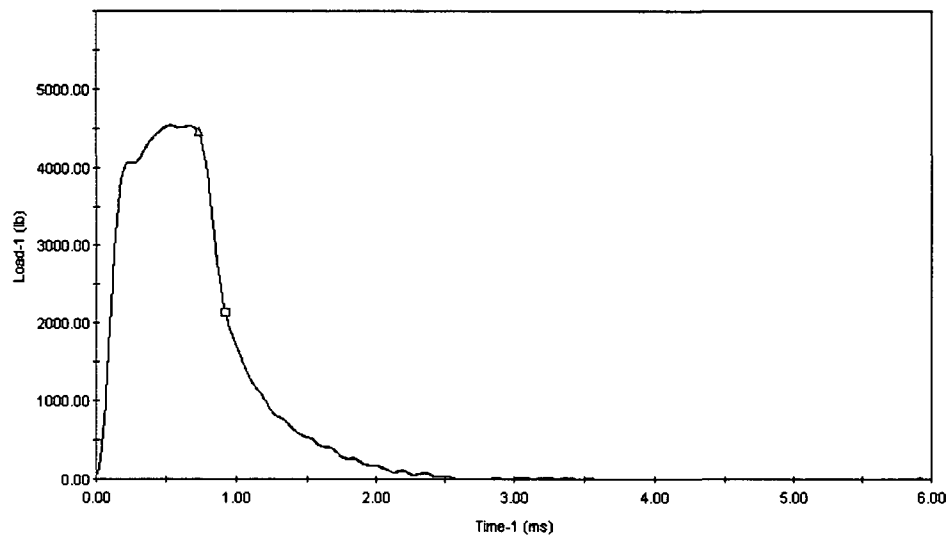
R30, 200°F



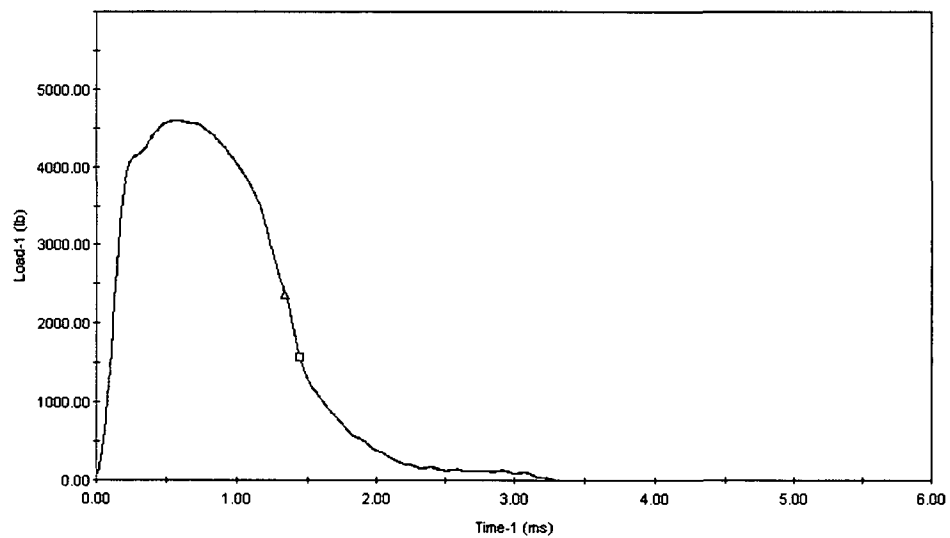
R28, 225°F



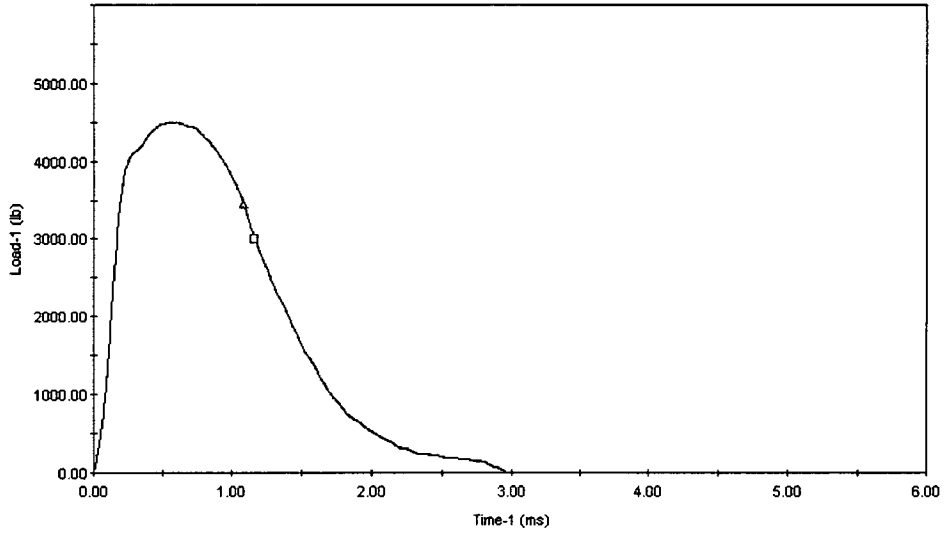
R26, 250°F



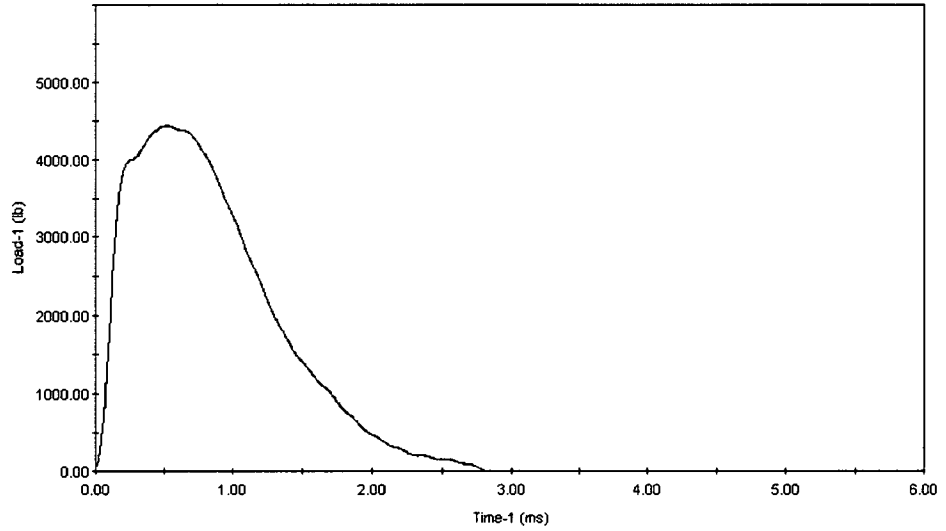
R275, 275°F



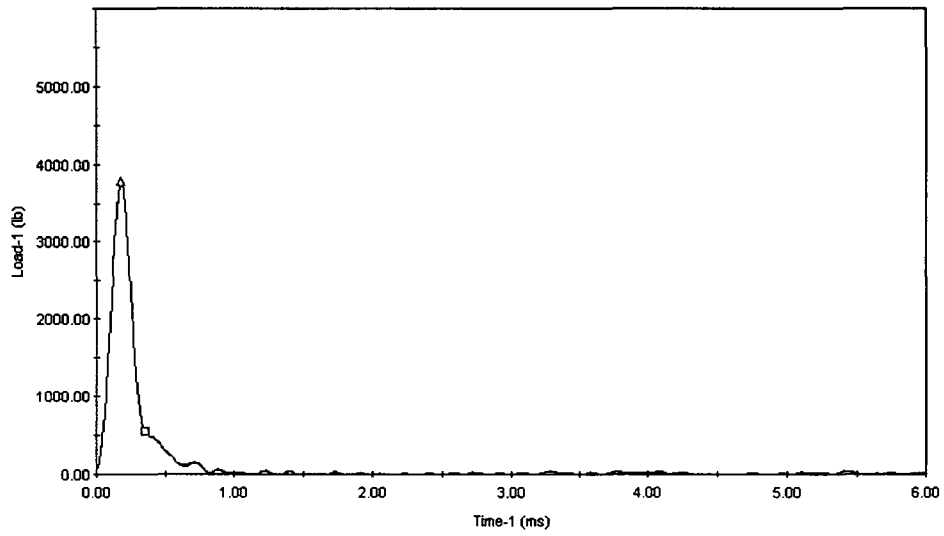
R29, 300°F



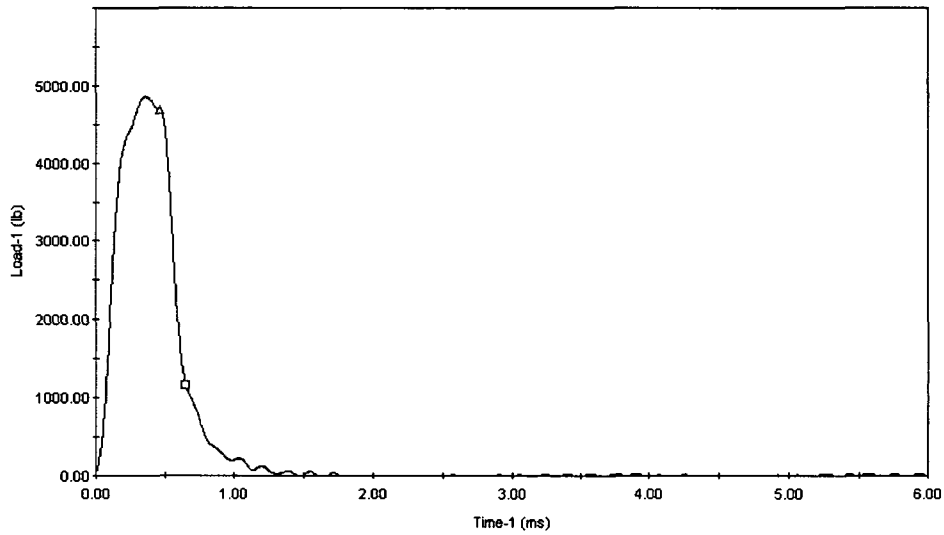
R32, 400°F



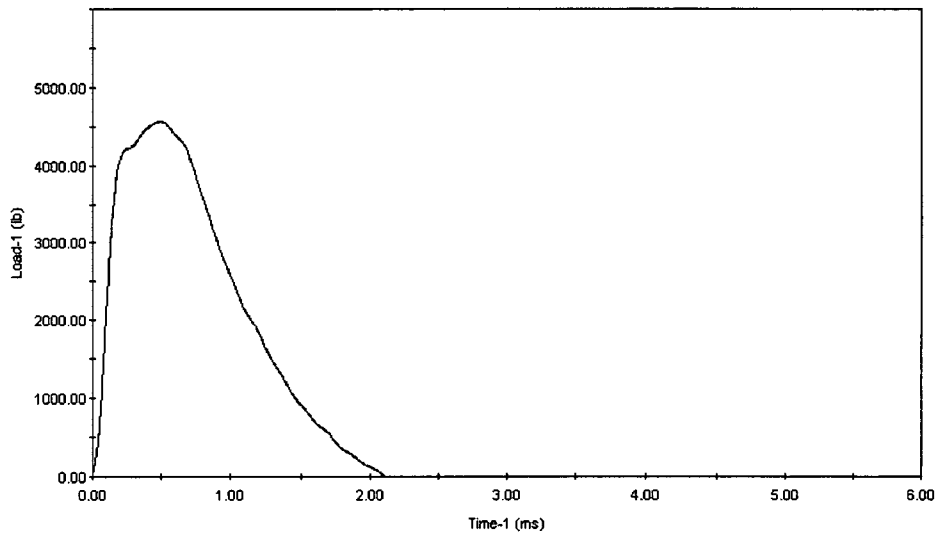
R25, 450°F



H26, 190°F



H27, 215°F



H32, 400°F

APPENDIX C

MASTER CURVE RESULTS FROM CAPSULE T AND PREVIOUS FRACTURE TOUGHNESS TESTS

This page intentionally blank

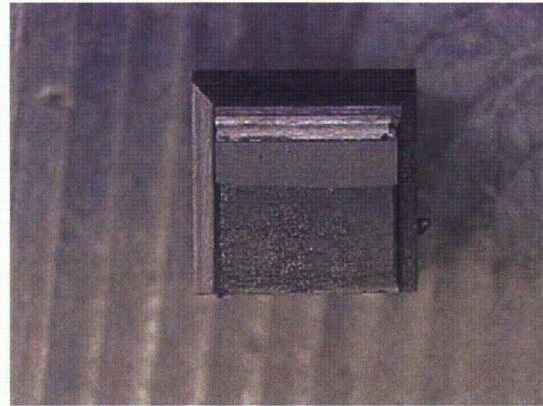
Table C-1 KPS Capsule T Fracture Toughness Test Results

SPECIMEN ID	<i>W25</i>	<i>W26</i>	<i>W27</i>	<i>W28</i>	<i>W29</i>	<i>W30</i>	<i>W31</i>	<i>W32</i>	<i>H25</i>	<i>H29</i>	<i>H30</i>	<i>H31</i>
<i>P_{max} (lbs) - determined from test</i>	934	918	1120	1158	1014	1214	816	913	1008	723	588	819
<i>LL Compliance (mils/lb)</i>	0.0055	0.0045	0.0045	0.0048	0.0055	0.0044	0.0050	0.0060	0.0057	0.0080	0.0090	0.0053
<i>Total Area (in-lbs)</i>	2.95	3.56	7.35	22.15	6.19	6.51	1.86	3.40	13.20	4.80	2.18	2.94
<i>Plastic Area (in-lbs), calculated</i>	0.58	1.65	4.53	18.93	3.38	3.29	0.21	0.92	10.28	2.72	0.62	1.16
<i>A_o, Initial Crack length, (in.)</i>	0.2068	0.2110	0.2040	0.2020	0.2076	0.1907	0.2094	0.2138	0.2140	0.2356	0.2470	0.2010
<i>b_o, Remaining Ligament (in.)</i>	0.1872	0.1829	0.1900	0.1920	0.1864	0.2033	0.1846	0.1802	0.1800	0.1584	0.1470	0.1930
<i>A_o/W, Crack/width Ratio</i>	0.5249	0.5357	0.5178	0.5127	0.5268	0.4840	0.5314	0.5427	0.5431	0.5980	0.6269	0.5102
<i>f(A_o/W)</i>	2.8863	2.9923	2.8193	2.7731	2.9046	2.5322	2.9495	3.0641	3.0691	3.7423	4.1973	2.7504
<i>K_e (ksi-in^{0.5})</i>	48.85	49.79	57.19	58.18	53.33	55.67	43.58	50.69	56.04	48.99	44.68	40.81
<i>J_e (in-lbs/in²)/1000</i>	0.0749	0.0778	0.1026	0.1062	0.0893	0.0973	0.0596	0.0806	0.0985	0.0753	0.0626	0.0523
<i>J_p (in-lbs/in²)/1000</i>	0.0186	0.0547	0.1518	0.5966	0.1096	0.0980	0.0068	0.0308	0.3456	0.1039	0.0257	0.0364
<i>J_t (in-lbs/in²)/1000</i>	0.0935	0.1325	0.2545	0.7029	0.1988	0.1952	0.0664	0.1114	0.4442	0.1792	0.0883	0.0887
<i>K_{JC} (ksi-in^{0.5})</i>	54.6	65.0	90.1	149.7	79.6	78.9	46.0	59.6	119.0	75.6	53.1	53.2
<i>K_{JC}(IT Adjusted) - (ksi-in^{0.5})</i>	47.0	55.3	75.1	122.4	66.8	66.3	40.2	51.0	98.0	63.6	45.8	45.9

This page intentionally blank

Specimen W-25 Test Temperature 136°F

SPECIMEN ID	W25
<i>P</i> max (lbs) - determined from test	934
LL Compliance (mils/lb)	0.0055
Total Area (in-lbs)	2.95
Plastic Area (in-lbs), calculated	0.58
<i>A</i> _o , Initial Crack length, (in.)	0.2068
<i>b</i> _o , Remaining Ligament (in.)	0.1872
<i>A</i> _o / <i>W</i> , Crack/width Ratio	0.5249
<i>f</i> (<i>A</i> _o / <i>W</i>)	2.8863
<i>K</i> _e (ksi-in ^{0.5})	48.85
<i>J</i> _e (in-lbs/in ²)/1000	0.0749
<i>J</i> _p (in-lbs/in ²)/1000	0.0186
<i>J</i> _t (in-lbs/in ²)/1000	0.0935
<i>K</i> <i>J</i> <i>C</i> (ksi-in ^{0.5})	54.6
<i>K</i> <i>J</i> <i>C</i> (1 <i>T</i> Adjusted) - (ksi-in ^{0.5})	47.0

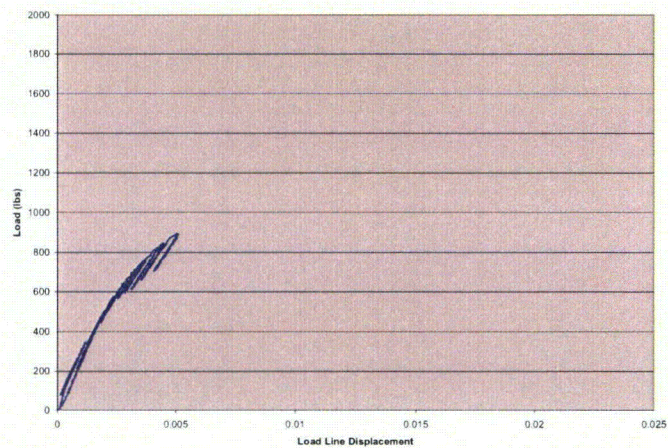


B	B _{net}	W	Span	Y.S.	T.S.
(in.)	(in.)	(in.)	(in.)	(ksi)	(ksi)
0.394	0.314	0.394	1.576	107	111

Precracking/Straightness

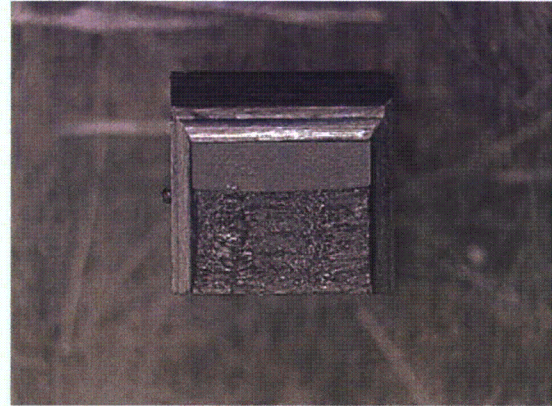
<i>K</i> _{max}	% of <i>a</i> _o	% of <i>B</i>
16.8	4.11%	2.16%

Load Rate: 0.71 ksi-in^{1/2}/sec



SPECIMEN ID	W26
<i>P_{max} (lbs) - determined from test</i>	918
<i>LL Compliance (mils/lb)</i>	0.0045
<i>Total Area (in-lbs)</i>	3.56
<i>Plastic Area (in-lbs), calculated</i>	1.65
<i>A_o, Initial Crack length, (in.)</i>	0.211063
<i>b_o, Remaining Ligament (in.)</i>	0.1829
<i>A_o/W, Crack/width Ratio</i>	0.5357
<i>f(A_o/W)</i>	2.9923
<i>K_e (ksi-in^{0.5})</i>	49.79
<i>J_e (in-lbs/in²)/1000</i>	0.0778
<i>J_p (in-lbs/in²)/1000</i>	0.0547
<i>J_t (in-lbs/in²)/1000</i>	0.1325
<i>K_{JC} (ksi-in^{0.5})</i>	65.0
<i>K_{JC}(1T Adjusted) - (ksi-in^{0.5})</i>	55.3

Specimen W-26
Test Temperature 136°F

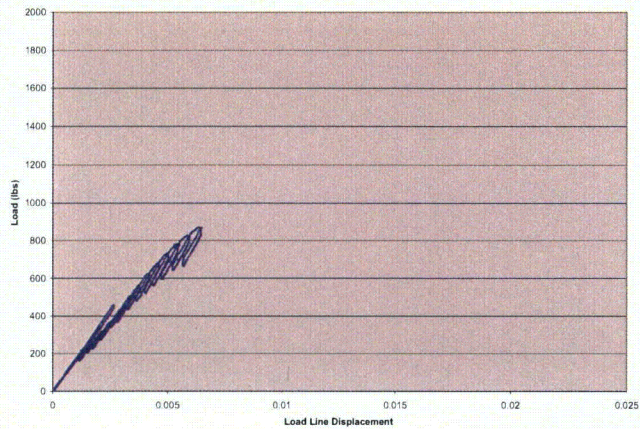


B	Bnet	W	Span	Y.S.	T.S.
(in.)	(in.)	(in.)	(in.)	(ksi)	(ksi)
0.394	0.314	0.394	1.576	107	111

Precracking/Straightness

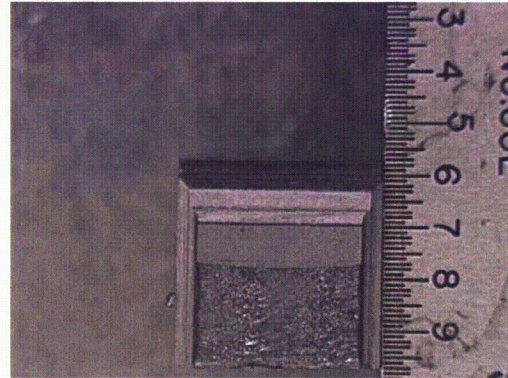
Kmax	%of a _o	%of B
23.7	5.45%	2.92%

Load Rate: 0.73 ksi-in^{1/2}/sec



SPECIMEN ID	W27
<i>Pmax (lbs) - determined from test</i>	1120
<i>LL Compliance (mils/lb)</i>	0.0045
<i>Total Area (in-lbs)</i>	7.35
<i>Plastic Area (in-lbs), calculated</i>	4.53
<i>Ao, Initial Crack length, (in.)</i>	0.2040
<i>bo, Remaining Ligament (in.)</i>	0.1900
<i>Ao/W, Crack/width Ratio</i>	0.5178
<i>f(Ao/W)</i>	2.8193
<i>Ke (ksi-in^{0.5})</i>	57.19
<i>Je (in-lbs/in²)/1000</i>	0.1026
<i>Jp (in-lbs/in²)/1000</i>	0.1518
<i>Jt (in-lbs/in²)/1000</i>	0.2545
<i>KJC (ksi-in^{0.5})</i>	90.1
<i>KJC(1T Adjusted) - (ksi-in^{0.5})</i>	75.1

Specimen W-27
Test Temperature 136°F

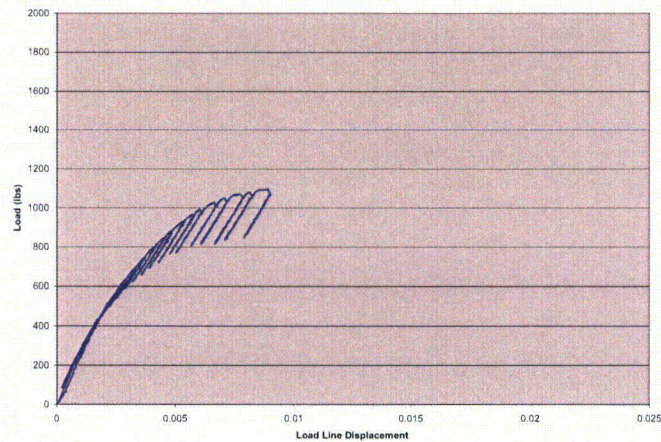


B	Bnet	W	Span	Y.S.	T.S.
(in.)	(in.)	(in.)	(in.)	(ksi)	(ksi)
0.394	0.314	0.394	1.576	107	111

Precracking/Straightness

Kmax	%of a _o	%of B
22.2	3.67%	1.90%

Load Rate: 0.74 ksi-in^{1/2}/sec



Specimen W-28 Test Temperature 136°F

SPECIMEN ID	W28
<i>P_{max} (lbs) - determined from test</i>	1158
<i>LL Compliance (mils/lb)</i>	0.0048
<i>Total Area (in-lbs)</i>	22.15
<i>Plastic Area (in-lbs), calculated</i>	18.93
<i>A_o, Initial Crack length, (in.)</i>	0.2020
<i>b_o, Remaining Ligament (in.)</i>	0.1920
<i>A_o/W, Crack/width Ratio</i>	0.5127
<i>f(A_o/W)</i>	2.7731
<i>K_e (ksi-in^{0.5})</i>	58.18
<i>J_e (in-lbs/in²)/1000</i>	0.1062
<i>J_p (in-lbs/in²)/1000</i>	0.5966
<i>J_t (in-lbs/in²)/1000</i>	0.7029
<i>K_{JC} (ksi-in^{0.5})</i>	149.7
<i>K_{JC}(IT Adjusted) - (ksi-in^{0.5})</i>	122.4

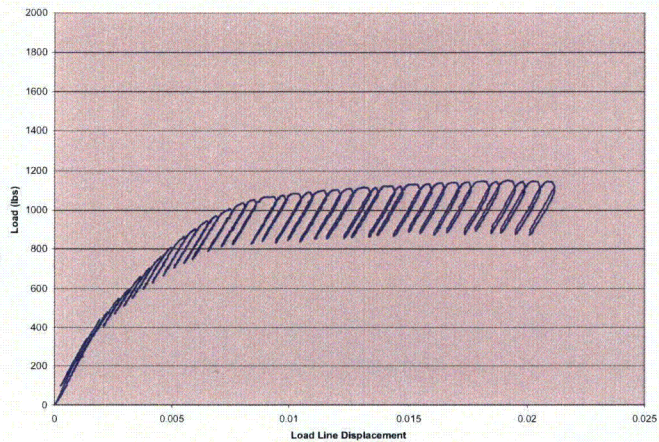


B	B _{net}	W	Span	Y.S.	T.S.
(in.)	(in.)	(in.)	(in.)	(ksi)	(ksi)
0.394	0.314	0.394	1.576	107	111

Precracking/Straightness

K _{max}	Straight
22.1	3.96%

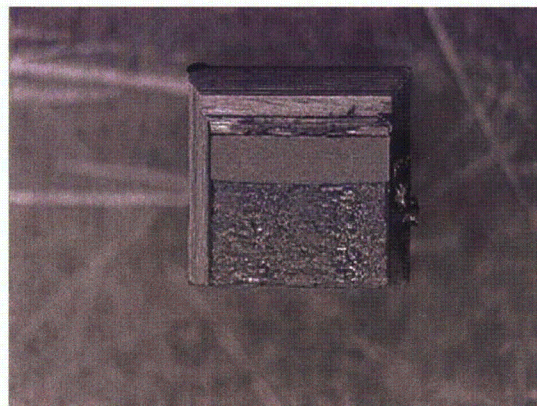
Load Rate: 0.74 ksi-in^{1/2}/sec



Specimen W-29

Test Temperature 136°F

SPECIMEN ID	W29
<i>Pmax (lbs) - determined from test</i>	1014
<i>LL Compliance (mils/lb)</i>	0.0055
<i>Total Area (in-lbs)</i>	6.19
<i>Plastic Area (in-lbs), calculated</i>	3.38
<i>Ao, Initial Crack length, (in.)</i>	0.2076
<i>bo, Remaining Ligament (in.)</i>	0.1864
<i>Ao/W, Crack/width Ratio</i>	0.5268
<i>f(Ao/W)</i>	2.9046
<i>Ke (ksi-in^{0.5})</i>	53.33
<i>Je (in-lbs/in²)/1000</i>	0.0893
<i>Jp (in-lbs/in²)/1000</i>	0.1096
<i>Jt (in-lbs/in²)/1000</i>	0.1988
<i>KJC (ksi-in^{0.5})</i>	79.6
<i>KJC(1T Adjusted) - (ksi-in^{0.5})</i>	66.8

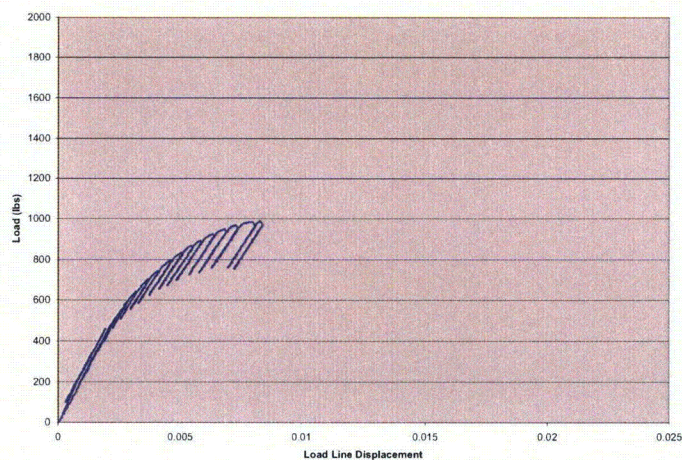


B	Bnet	W	Span	Y.S.	T.S.
(in.)	(in.)	(in.)	(in.)	(ksi)	(ksi)
0.394	0.314	0.394	1.576	107	111

Precracking/Straightness

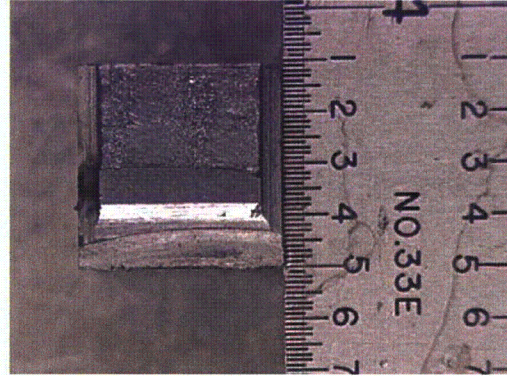
Kmax	% of a_0	% of B
22.9	4.10%	2.16%

Load Rate: 0.73 ksi-in^{1/2}/sec



Specimen W-30 Test Temperature 136 °F

SPECIMEN ID	W30
<i>P_{max} (lbs) - determined from test</i>	1214
<i>LL Compliance (mils/lb)</i>	0.0044
<i>Total Area (in-lbs)</i>	6.51
<i>Plastic Area (in-lbs), calculated</i>	3.29
<i>A_o, Initial Crack length, (in.)</i>	0.1907
<i>b_o, Remaining Ligament (in.)</i>	0.2033
<i>A_o/W, Crack/width Ratio</i>	0.4840
<i>f(A_o/W)</i>	2.5322
<i>K_e (ksi-in^{0.5})</i>	55.67
<i>J_e (in-lbs/in²)/1000</i>	0.0973
<i>J_p (in-lbs/in²)/1000</i>	0.0980
<i>J_t (in-lbs/in²)/1000</i>	0.1952
<i>K_{JC} (ksi-in^{0.5})</i>	78.9
<i>K_{JC}(1T Adjusted) - (ksi-in^{0.5})</i>	66.3

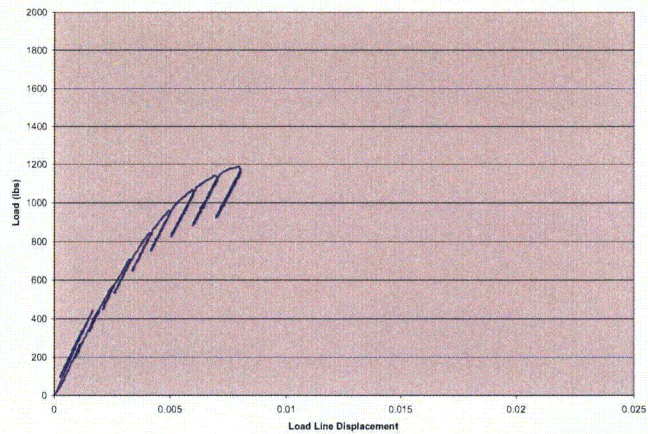


B	Bnet	W	Span	Y.S.	T.S.
(in.)	(in.)	(in.)	(in.)	(ksi)	(ksi)
0.394	0.314	0.394	1.576	107	111

Precracking/Straightness

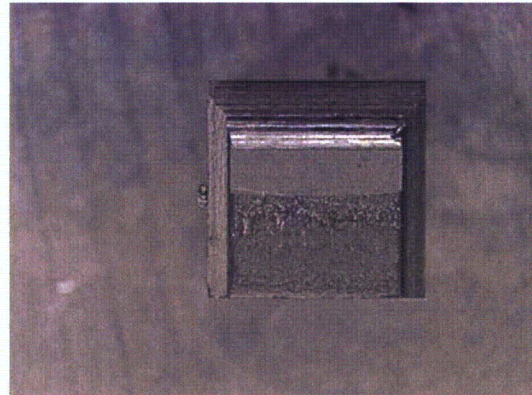
Kmax	% of a _o	% of B
19.9	7.08%	3.43%

Load Rate: 0.69 ksi-in^{1/2}/sec



Specimen W-31 Test Temperature 136°F

SPECIMEN ID	W31
<i>Pmax (lbs) - determined from test</i>	816
<i>LL Compliance (mils/lb)</i>	0.0050
<i>Total Area (in-lbs)</i>	1.86
<i>Plastic Area (in-lbs), calculated</i>	0.21
<i>Ao, Initial Crack length, (in.)</i>	0.2094
<i>bo, Remaining Ligament (in.)</i>	0.1846
<i>Ao/W, Crack/width Ratio</i>	0.5314
<i>f(Ao/W)</i>	2.9495
<i>Ke (ksi-in^{0.5})</i>	43.58
<i>Je (in-lbs/in²)/1000</i>	0.0596
<i>Jp (in-lbs/in²)/1000</i>	0.0068
<i>Jt (in-lbs/in²)/1000</i>	0.0664
<i>KJC (ksi-in^{0.5})</i>	46.0
<i>KJC(IT Adjusted) - (ksi-in^{0.5})</i>	40.2



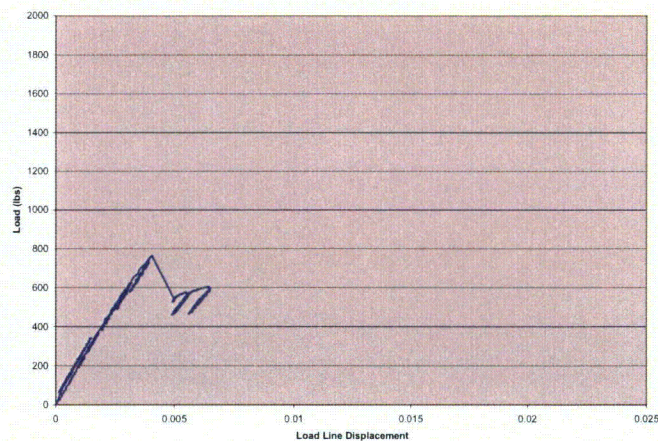
B	Bnet	W	Span	Y.S.	T.S.
(in.)	(in.)	(in.)	(in.)	(ksi)	(ksi)
0.394	0.314	0.394	1.576	107	111

Precracking/Straightness

Kmax	%of a _o	%of B
19.6	2.87%	1.52%

Load Rate: 0.7391 ksi-in^{1/2}/sec

Pop-in:
Ci/Co = 1.32 > 1.029
Pop-in terminated test record.



Specimen W-32 Test Temperature 136°F

SPECIMEN ID	W32
<i>P_{max} (lbs) - determined from test</i>	913
<i>LL Compliance (mils/lb)</i>	0.0060
<i>Total Area (in-lbs)</i>	3.40
<i>Plastic Area (in-lbs), calculated</i>	0.92
<i>A_o, Initial Crack length, (in.)</i>	0.2138
<i>b_o, Remaining Ligament (in.)</i>	0.1802
<i>A_o/W, Crack/width Ratio</i>	0.5427
<i>f(A_o/W)</i>	3.0641
<i>K_e (ksi-in^{0.5})</i>	50.69
<i>J_e (in-lbs/in²)/1000</i>	0.0806
<i>J_p (in-lbs/in²)/1000</i>	0.0308
<i>J_t (in-lbs/in²)/1000</i>	0.1114
<i>K_{JC} (ksi-in^{0.5})</i>	59.6
<i>K_{JC}(1T Adjusted) - (ksi-in^{0.5})</i>	51.0

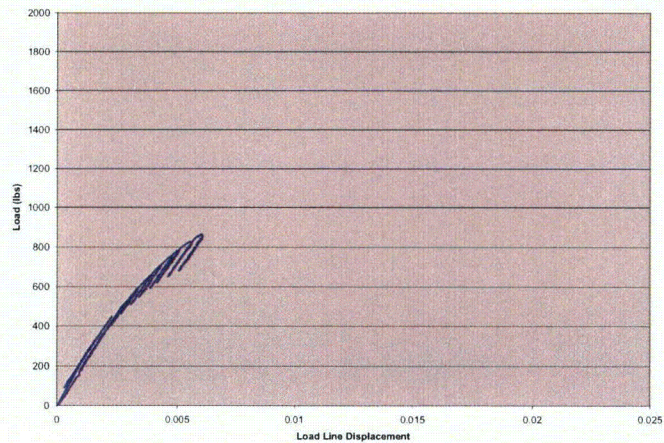


B	B _{net}	W	Span	Y.S.	T.S.
(in.)	(in.)	(in.)	(in.)	(ksi)	(ksi)
0.394	0.314	0.394	1.576	107	111

Precracking/Straightness

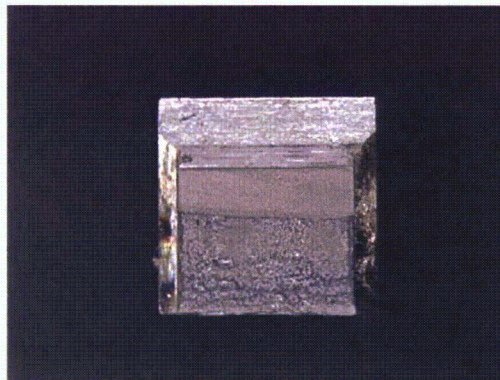
K _{max}	% of a _o	% of B
23.9	3.51%	1.90%

Load Rate: 0.73 ksi-in^{1/2}/sec



Specimen H-25
Test Temperature
136°F

SPECIMEN ID	H25
<i>Pmax (lbs) - determined from test</i>	1008
<i>LL Compliance (mils/lb)</i>	0.0057
<i>Total Area (in-lbs)</i>	13.20
<i>Plastic Area (in-lbs), calculated</i>	10.28
<i>Ao, Initial Crack length, (in.)</i>	0.2140
<i>bo, Remaining Ligament (in.)</i>	0.1800
<i>Ao/W, Crack/width Ratio</i>	0.5431
<i>f(Ao/W)</i>	3.0691
<i>Ke (ksi-in^{0.5})</i>	56.04
<i>Je (in-lbs/in²)/1000</i>	0.0985
<i>Jp (in-lbs/in²)/1000</i>	0.3456
<i>Jt (in-lbs/in²)/1000</i>	0.4442
<i>KJC (ksi-in^{0.5})</i>	119.0
<i>KJC(IT Adjusted) - (ksi-in^{0.5})</i>	98.0

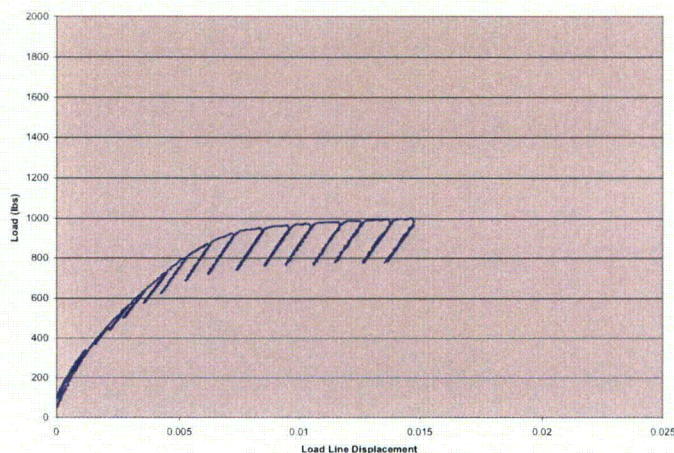


B	Bnet	W	Span	Y.S.	T.S.
(in.)	(in.)	(in.)	(in.)	(ksi)	(ksi)
0.394	0.314	0.394	1.576	107	111

Precracking/Straightness

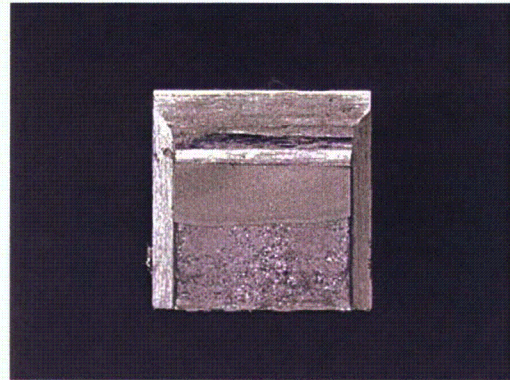
Kmax	%of a _o	%of B
18.7	5.15%	2.79%

Load Rate: 0.36 ksi-in^{1/2}/sec



Specimen H-29 Test Temperature 136°F

SPECIMEN ID	H29
<i>P_{max} (lbs) - determined from test</i>	723
<i>LL Compliance (mils/lb)</i>	0.0080
<i>Total Area (in-lbs)</i>	4.80
<i>Plastic Area (in-lbs), calculated</i>	2.72
<i>A_o, Initial Crack length, (in.)</i>	0.2356
<i>b_o, Remaining Ligament (in.)</i>	0.1584
<i>A_o/W, Crack/width Ratio</i>	0.5980
<i>f(A_o/W)</i>	3.7423
<i>K_e (ksi-in^{0.5})</i>	48.99
<i>J_e (in-lbs/in²)/1000</i>	0.0753
<i>J_p (in-lbs/in²)/1000</i>	0.1039
<i>J_t (in-lbs/in²)/1000</i>	0.1792
<i>K_{JC} (ksi-in^{0.5})</i>	75.6
<i>K_{JC}(1T Adjusted) - (ksi-in^{0.5})</i>	63.6

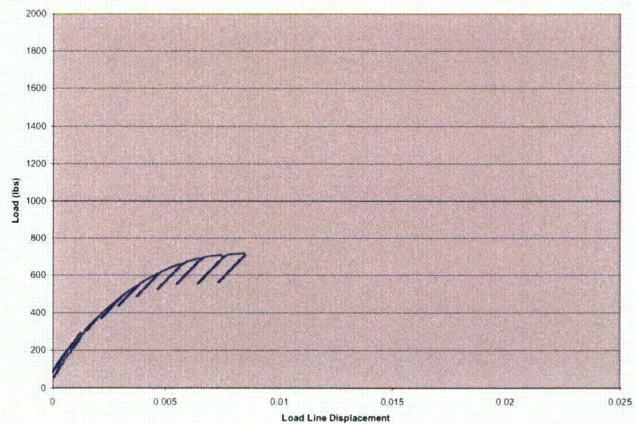


B	Bnet	W	Span	Y.S.	T.S.
(in.)	(in.)	(in.)	(in.)	(ksi)	(ksi)
0.394	0.314	0.394	1.576	107	111

Precracking/Straightness

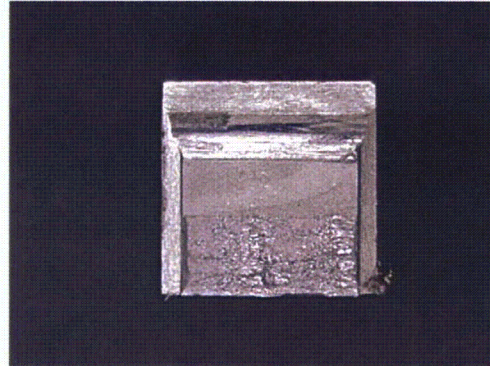
Kmax	% of a _o	% of B
19.1	7.22%	4.31%

Load Rate: 0.38 ksi-in^{1/2}/sec



Specimen H-30 Test Temperature 136°F

SPECIMEN ID	<i>H30</i>
<i>P_{max} (lbs) - determined from test</i>	588
<i>LL Compliance (mils/lb)</i>	0.0090
<i>Total Area (in-lbs)</i>	2.18
<i>Plastic Area (in-lbs), calculated</i>	0.62
<i>A_o, Initial Crack length, (in.)</i>	0.2470
<i>b_o, Remaining Ligament (in.)</i>	0.1470
<i>A_o/W, Crack/width Ratio</i>	0.6269
<i>f(A_o/W)</i>	4.1973
<i>K_e (ksi-in^{0.5})</i>	44.68
<i>J_e (in-lbs/in²)/1000</i>	0.0626
<i>J_p (in-lbs/in²)/1000</i>	0.0257
<i>J_t (in-lbs/in²)/1000</i>	0.0883
<i>K_{JC} (ksi-in^{0.5})</i>	53.1
<i>K_{JC} (1T Adjusted) - (ksi-in^{0.5})</i>	45.8

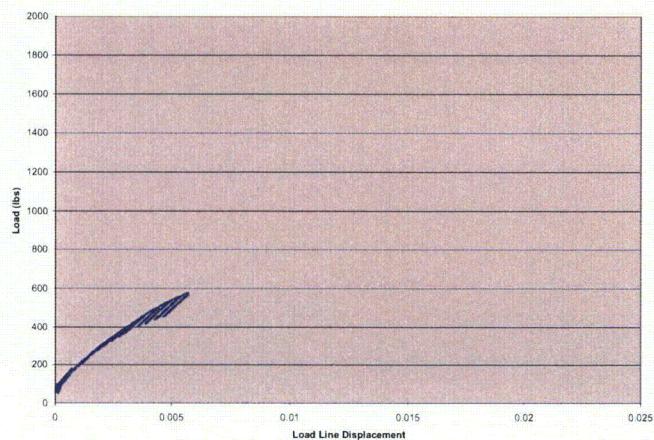


B	B _{net}	W	Span	Y.S.	T.S.
(in.)	(in.)	(in.)	(in.)	(ksi)	(ksi)
0.394	0.314	0.394	1.576	107	111

Precracking/Straightness

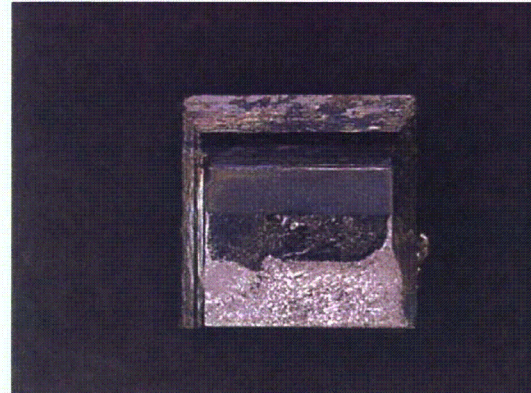
K _{max}	% of a _o	% of B
13.2	3.44%	2.16%

Load Rate: 0.37 ksi-in^{1/2}/sec



Specimen H-31
Test Temperature 136°F

SPECIMEN ID	H31
<i>P_{max} (lbs) - determined from test</i>	819
<i>LL Compliance (mils/lb)</i>	0.0053
<i>Total Area (in-lbs)</i>	2.94
<i>Plastic Area (in-lbs), calculated</i>	1.16
<i>A_o, Initial Crack length, (in.)</i>	0.2010
<i>b_o, Remaining Ligament (in.)</i>	0.1930
<i>A_o/W, Crack/width Ratio</i>	0.5102
<i>f(A_o/W)</i>	2.7504
<i>K_e (ksi-in^{0.5})</i>	40.81
<i>J_e (in-lbs/in²)/1000</i>	0.0523
<i>J_p (in-lbs/in²)/1000</i>	0.0364
<i>J_t (in-lbs/in²)/1000</i>	0.0887
<i>K_{JC} (ksi-in^{0.5})</i>	53.2
<i>K_{JC}(1T Adjusted) - (ksi-in^{0.5})</i>	45.9



B	Bnet	W	Span	Y.S.	T.S.
(in.)	(in.)	(in.)	(in.)	(ksi)	(ksi)
0.394	0.314	0.394	1.576	107	111

Precracking/Straightness

Kmax	%of a _o	%of B
16.4	1.99%	1.02%

Load Rate: 0.34 ksi-in^{1/2}/sec

Pop-in:
C_i/C_o = 1.032 > 1.029
Pop-in terminated test record.

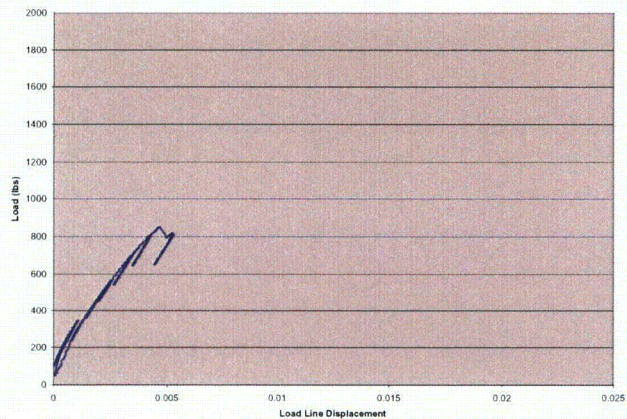


Table C-2 Unirradiated Pre-cracked Charpy Specimens Tested at -200°F

SPECIMEN ID	<i>wps201</i>	<i>wps202</i>	<i>wps203*</i>	<i>wps204*</i>	<i>wps205</i>	<i>wps206</i>	<i>wps207</i>	<i>wps208</i>	<i>wps209</i>	<i>wps210</i>
<i>Pmax (lbs) - determined from test</i>	1341	1253	1550	1261	1250	1274	1253	1364	1374	1468
<i>LL Compliance (mils/lb)</i>	0.0062	0.0081	0.0071	0.0115	0.0081	0.0068	0.0087	0.0059	0.0079	0.0059
<i>Total Area (in-lbs)</i>	15.40	6.92	9.49	16.60	7.52	6.12	7.76	8.56	10.65	9.66
<i>Plastic Area (in-lbs), calculated</i>	9.87	0.58	0.97	7.43	1.21	0.57	0.95	3.12	3.17	3.33
<i>Ao, Initial Crack length, (in.)</i>	0.2080	0.2060	0.1988	0.1988	0.2100	0.2030	0.2100	0.2050	0.2030	0.1988
<i>bo, Remaining Ligament (in.)</i>	0.1860	0.1880	0.1953	0.1953	0.1840	0.1910	0.1840	0.1890	0.1910	0.1953
<i>Ao/W, Crack/width Ratio</i>	0.528	0.523	0.504	0.504	0.533	0.515	0.533	0.520	0.515	0.504
<i>f(Ao/W)</i>	2.915	2.867	2.700	2.700	2.965	2.796	2.965	2.843	2.796	2.700
<i>Ke (ksi-in^{0.5})</i>	63.24	58.09	67.70	55.08	59.95	57.61	60.10	62.71	62.14	64.12
<i>Je (in-lbs/in²)</i>	0.1333	0.1125	0.1528	0.1011	0.1198	0.1106	0.1204	0.1311	0.1287	0.1371
<i>Jp (in-lbs/in²)</i>	0.2558	0.0149	0.0240	0.1834	0.0317	0.0145	0.0250	0.0795	0.0800	0.0822
<i>Jt (in-lbs/in²)</i>	0.3891	0.1274	0.1768	0.2845	0.1515	0.1251	0.1454	0.2106	0.2087	0.2193
<i>KJC (ksi-in^{0.5})</i>	108.0	61.8	72.8	92.4	67.4	61.3	66.1	79.5	79.1	81.1
<i>KJC(IT Adjusted) - (ksi-in^{0.5})</i>	89.4	52.8	61.5	77.0	57.2	52.3	56.1	66.8	66.5	68.0

* Invalid precracks

Table C-3 Unirradiated Reconstituted Pre-cracked Charpy Specimens Tested at -200°F

SPECIMEN ID	<i>rkw1</i>	<i>rkw3</i>	<i>rkw6</i>	<i>rkw7</i>	<i>rkw8</i>	<i>rkw10</i>	<i>rkw11</i>	<i>rkw2</i>
<i>Pmax (lbs) - determined from test</i>	1255	1378	1472	1421	1582	1468	1422	1556
<i>LL Compliance (mils/lb)</i>	0.0045	0.0049	0.0065	0.0059	0.0043	0.0043	0.0057	0.0040
<i>Total Area (in-lbs)</i>	10.12	8.02	6.01	8.54	11.56	14.12	6.32	19.90
<i>Plastic Area (in-lbs), calculated</i>	6.58	3.37	0.00	2.59	6.18	9.49	0.56	15.01
<i>Ao, Initial Crack length, (in.)</i>	0.2040	0.1970	0.1880	0.1940	0.1870	0.1920	0.1910	0.1920
<i>bo, Remaining Ligament (in.)</i>	0.1900	0.1970	0.2060	0.2000	0.2070	0.2020	0.2030	0.2020
<i>Ao/W, Crack/width Ratio</i>	0.5178	0.5000	0.4772	0.4924	0.4746	0.4873	0.4848	0.4873
<i>f(Ao/W)</i>	2.819	2.663	2.480	2.599	2.460	2.558	2.538	2.558
<i>Ke (ksi-in^{0.5})</i>	57.22	59.32	59.02	59.72	62.97	60.73	58.37	64.38
<i>Je (in-lbs/in²)</i>	0.1091	0.1173	0.1161	0.1189	0.1322	0.1229	0.1136	0.1382
<i>Jp (in-lbs/in²)</i>	0.1669	0.0825	0.0000	0.0624	0.1439	0.2266	0.0133	0.3584
<i>Jt (in-lbs/in²)</i>	0.2761	0.1998	0.1161	0.1813	0.2761	0.3495	0.1269	0.4966
<i>KJC (ksi-in^{0.5})</i>	91.0	77.4	59.0	73.7	91.0	102.4	61.7	122.1
<i>KJC(1T Adjusted) - (ksi-in^{0.5})</i>	75.9	65.1	50.5	62.2	75.9	84.9	52.7	100.5

Table C-4 Unirradiated ½ T Compact Tension Specimens Tested at -187°F

SPECIMEN ID	<i>wps101</i>	<i>wps102</i>	<i>wps103</i>	<i>wps104</i>	<i>wps105</i>	<i>wps106</i>
<i>Pmax (lbs) - determined from test</i>	3869	2867	3750	3445	3433	2416
<i>LL Compliance (mils/lb)</i>	0.0026	0.0029	0.0025	0.0029	0.0027	0.0024
<i>Total Area (in-lbs)</i>	24.02	13.69	22.25	17.49	17.13	7.13
<i>Plastic Area (in-lbs), calculated</i>	4.56	1.77	5.00	0.41	1.14	0.04
<i>Ao, Initial Crack length, (in.)</i>	0.5200	0.5280	0.5230	0.5250	0.5220	0.5170
<i>bo, Remaining Ligament (in.)</i>	0.4800	0.4720	0.4770	0.4750	0.4780	0.4830
<i>Ao/W, Crack/width Ratio</i>	0.5200	0.5280	0.5230	0.5250	0.5220	0.5170
<i>f(Ao/W)</i>	10.134	10.400	10.233	10.299	10.200	10.038
<i>Ke (ksi-in^{0.5})</i>	78.42	59.63	76.74	70.96	70.03	48.50
<i>Je (in-lbs/in²)</i>	0.2050	0.1185	0.1963	0.1678	0.1635	0.0784
<i>Jp (in-lbs/in²)</i>	0.0427	0.0169	0.0471	0.0039	0.0108	0.0004
<i>Jt (in-lbs/in²)</i>	0.2477	0.1354	0.2434	0.1717	0.1742	0.0788
<i>KJC (ksi-in^{0.5})</i>	86.2	63.7	85.5	71.8	72.3	48.6
<i>KJC(1T Adjusted) - (ksi-in^{0.5})</i>	75.4	56.5	74.8	63.3	63.7	43.8

Table C-5 Irradiated Pre-cracked Capsule S Charpy Specimens Tested at 136°F

SPECIMEN ID	<i>w24</i>	<i>W19</i>	<i>h17</i>	<i>h18</i>	<i>w23</i>	<i>h 20*</i>	<i>h19</i>	<i>w17</i>	<i>h21</i>
<i>Pmax (lbs) - determined from test</i>	1514	1349	1433	1285	1490	1319	1273	1323	1076
<i>LL Compliance (mils/lb)</i>	0.0069	0.0070	0.0071	0.0073	0.0071	0.0071	0.0071	0.0071	0.0082
<i>Total Area (in-lbs)</i>	15.80	8.49	25.90	20.36	23.03	29.60	9.97	15.57	15.09
<i>Plastic Area (in-lbs), calculated</i>	7.90	2.12	18.61	14.34	15.13	23.42	4.19	9.35	10.33
<i>Ao, Initial Crack length, (in.)</i>	0.1920	0.1920	0.1960	0.2030	0.1990	0.2000	0.1970	0.1970	0.2100
<i>bo, Remaining Ligament (in.)</i>	0.2020	0.2020	0.1980	0.1910	0.1950	0.1940	0.1970	0.1970	0.1840
<i>Ao/W, Crack/width Ratio</i>	0.4873	0.4873	0.4975	0.5152	0.5051	0.5076	0.5000	0.5000	0.5330
<i>f(Ao/W)</i>	2.5585	2.5585	2.6412	2.7960	2.7059	2.7280	2.6625	2.6625	2.9652
<i>Ke (ksi-in^{0.5})</i>	62.65	55.84	61.20	58.10	65.20	58.20	54.81	56.97	51.60
<i>Je (in-lbs/in²)</i>	0.1308	0.1039	0.1248	0.1125	0.1417	0.1129	0.1001	0.1082	0.0888
<i>Jp (in-lbs/in²)</i>	0.1887	0.0505	0.4534	0.3620	0.3742	0.5821	0.1025	0.2289	0.2707
<i>Jt (in-lbs/in²)</i>	0.3195	0.1545	0.5782	0.4745	0.5159	0.6950	0.2026	0.3371	0.3594
<i>KJC (ksi-in^{0.5})</i>	97.9	68.1	131.7	119.3	124.4	144.4	78.0	100.6	103.8
<i>KJC(1T Adjusted) - (ksi-in^{0.5})</i>	81.3	57.7	108.1	98.3	102.3	118.2	65.6	83.5	86.1

Table C-6 Irradiated Pre-cracked Capsule S Charpy Specimens Tested at 59°F

SPECIMEN ID	<i>W21</i>	<i>W20</i>	<i>W22</i>
<i>P_{max} (lbs) - determined from test</i>	1100	1220	1330
<i>CLL (mils/lb) - determined from initial unloadings of test</i>	0.0071	0.0071	0.0071
<i>Total Area beneath Load-Disp Curve</i>	3.77	3.77	3.85
<i>Plastic Area (in-lbs), calculated</i>	0.00	0.00	-2.43
<i>A_o, Initial Crack length, (in.)</i>	0.2	0.2	0.2
<i>b_o, Remaining Ligament (in.)</i>	0.194	0.194	0.194
<i>A_o/W, Crack/width Ratio</i>	0.508	0.508	0.508
<i>f(A_o/W)</i>	2.728	2.728	2.728
<i>K_e</i>	48.54	53.83	58.68
<i>J_e</i>	0.0785	0.0966	0.1148
<i>J_p</i>	0.0000	0.0000	-0.0604
<i>J_t</i>	0.0785	0.0966	0.0544
<i>K_{JC} (ksi-in^{0.5})</i>	48.5	53.8	40.4
<i>K_{JC}(IT Adjusted) - (ksi-in^{0.5})</i>	42.2	46.4	35.8

Table C-7 Irradiated Precracked Maine Yankee Specimens Tested at 210°F

SPECIMEN ID	<i>322</i>	<i>36a</i>	<i>313</i>	<i>371a</i>	<i>33u</i>	<i>375</i>	<i>371b</i>	<i>37ua</i>
<i>Pmax (lbs) - determined from test</i>	1482	1220	1373	1570	1259	1436	1457	1722
<i>LL Compliance (mils/lb)</i>	0.0065	0.0071	0.0071	0.0059	0.0073	0.0071	0.0060	0.0064
<i>Total Area (in-lbs)</i>	9.96	5.28	14.77	35.00	7.26	10.57	9.52	15.82
<i>Plastic Area (in-lbs), calculated</i>	2.82	0.00	8.07	27.70	1.48	3.26	3.18	6.35
<i>Ao, Initial Crack length, (in.)</i>	0.1840	0.2020	0.1930	0.1860	0.2020	0.1960	0.1900	0.1970
<i>bo, Remaining Ligament (in.)</i>	0.2100	0.1920	0.2010	0.2080	0.1920	0.1980	0.2040	0.1970
<i>Ao/W, Crack/width Ratio</i>	0.4670	0.5127	0.4898	0.4721	0.5127	0.4975	0.4822	0.5000
<i>f(Ao/W)</i>	2.4042	2.7731	2.5788	2.4415	2.7731	2.6412	2.5185	2.6625
<i>Ke (ksi-in^{0.5})</i>	57.63	54.72	57.27	62.00	56.47	61.34	59.35	74.15
<i>Je (in-lbs/in²)</i>	0.1107	0.0998	0.1093	0.1281	0.1063	0.1254	0.1174	0.1833
<i>Jp (in-lbs/in²)</i>	0.0648	-0.0001	0.1936	0.6423	0.0372	0.0794	0.0752	0.1553
<i>Jt (in-lbs/in²)</i>	0.1755	0.0997	0.3029	0.7704	0.1435	0.2048	0.1927	0.3386
<i>KJC (ksi-in^{0.5})</i>	72.6	54.7	95.3	152.0	65.6	78.4	76.0	100.8
<i>KJC(IT Adjusted) - (ksi-in^{0.5})</i>	61.3	47.1	79.3	124.2	55.8	65.9	64.0	83.6

Table C-8 Unirradiated Maine Yankee Weld Specimen Data

SPECIMEN ID	<i>CO4-4</i>	<i>CO4-5</i>	<i>CO4-2</i>	<i>CO4-7</i>	<i>CO4-8</i>	<i>CO4-3</i>	<i>CO4-6</i>
<i>Pmax (lbs) - determined from test</i>	1070	1110	1230	1150	1170	1180	1180
<i>LL Compliance (mils/lb)</i>	0.0090	0.0090	0.0089	0.0095	0.0096	0.0088	0.0089
<i>Total Area (in-lbs)</i>	7.01	7.98	12.93	12.29	13.42	13.61	14.09
<i>Plastic Area (in-lbs), calculated</i>	1.86	2.44	6.20	6.00	6.84	7.49	7.89
<i>Ao, Initial Crack length, (in.)</i>	0.2031	0.2040	0.2003	0.2084	0.2032	0.2060	0.2045
<i>bo, Remaining Ligament (in.)</i>	0.1909	0.1900	0.1937	0.1856	0.1908	0.1880	0.1895
<i>Ao/W, Crack/width Ratio</i>	0.5155	0.5178	0.5084	0.5289	0.5157	0.5228	0.5190
<i>f(Ao/W)</i>	2.7984	2.8193	2.7347	2.9252	2.8007	2.8667	2.8310
<i>Ke (ksi-in^{0.5})</i>	49.14	51.35	55.20	55.20	53.77	55.51	54.82
<i>Je (in-lbs/in²)/1000</i>	0.0792	0.0865	0.0999	0.0999	0.0948	0.1011	0.0986
<i>Jp (in-lbs/in²)/1000</i>	0.0469	0.0618	0.1543	0.1560	0.1730	0.1920	0.2008
<i>Jt (in-lbs/in²)/1000</i>	0.126	0.148	0.254	0.256	0.268	0.293	0.299
<i>KJC (ksi-in^{0.5})</i>	62.0	67.2	88.0	88.3	90.4	94.5	95.5
<i>KJC(IT Adjusted) - (ksi-in^{0.5})</i>	52.9	57.1	73.5	73.8	75.4	78.7	79.5

This page intentionally blank

APPENDIX D

CHARPY V-NOTCH PLOTS FOR THE KPS CAPSULE T SURVEILLANCE MATERIALS

This page intentionally blank

A summary of the Upper Shelf Energy values for all of the capsule materials for the Kewaunee Power Station are shown in Table D-1. The definition for Upper Shelf Energy (USE) is given in ASTM E185-82, Section 4.18, and reads as follows:

“upper shelf energy level – the average energy value for all Charpy specimens (normally three) whose test temperature is above the upper end of the transition region. For specimens tested in sets of three at each test temperature, the set having the highest average may be regarded as defining the upper shelf energy.”

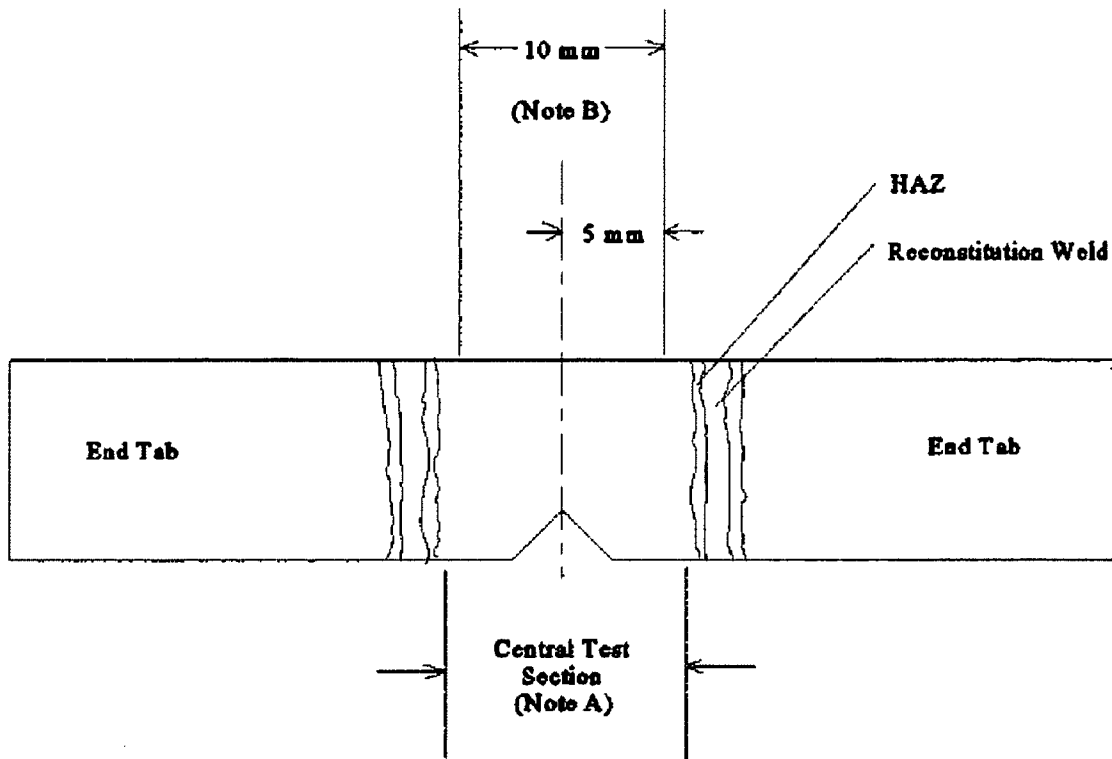
Westinghouse typically reports the average of all Charpy data $\geq 95\%$ shear as the USE. In some instances, there may be data deemed ‘out of family’ and are removed from the determination of the USE based on engineering judgement. For the weld material, only one data point exists from Capsule T, so the upper shelf will be set to that value of 72 ft-lbs.

Material	Unirradiated	Capsule V	Capsule R	Capsule P	Capsule S	Capsule T
Intermediate Shell Forging 122X208VA1 (Tangential)	160 ft-lbs	180 ft-lbs	160 ft-lbs	157 ft-lbs	148 ft-lbs	139 ft-lbs
Lower Shell Forging 123X167VA1 (Tangential)	157 ft-lbs	178 ft-lbs	153 ft-lbs	159 ft-lbs	152 ft-lbs	144 ft-lbs
Weld Metal (Heat # 1P3571)	126 ft-lbs	82 ft-lbs	78 ft-lbs	76 ft-lbs	64 ft-lbs	72 ft-lbs
Heat Affected Zone Material	180 ft-lbs	145 ft-lbs	141 ft-lbs	136 ft-lbs	139 ft-lbs	---
Correlation Monitor Material	123 ft-lbs	109 ft-lbs	95 ft-lbs	101 ft-lbs	98 ft-lbs	91 ft-lbs

Westinghouse typically reports the average of all Charpy data $\geq 95\%$ shear as the USE. In some instances, there may be data deemed ‘out of family’ and are removed from the determination of the USE based on engineering

Weld Metal

There were three data points generated for the surveillance weld based on the reconstitution of the HAZ charpy specimens. The specimens were reconstituted in accordance with ASTM E 1253 [Reference D-1] with the weld portion of the HAZ specimen used to represent the weld metal (see Figure 1 from ASTM E 1253-99 shown below).



NOTE A—No plastic deformation from previous testing is permitted in the region between the HAZs caused by the reconstitution welds (the central test section).

NOTE B—Temperature during welding shall not exceed the irradiation temperature.

FIG. 1 Schematic of a Reconstituted Charpy Specimen

The actual values obtained from the Charpy testing of the HAZ reconstituted specimens are shown below [Reference D-2]:

Specimen ID	Test Temperature (°F)	Charpy Energy (ft-lbs)	Lateral Expansion (mils)	% Shear
H26	190	13	13	25
H27	215	36	28	45
H32	400	72	59	100

With only three data points available, using a tanh fit to the data is not an option. In order to best estimate the T_{30} and T_{50} energy values through the transition regions, a review of the data from Capsule S will be done to see how the material behaved. Typically, through engineering experience, the slope through the transition region will decrease with increased fluence. If the slope through transition region of Capsule S data is a known quantity, we can then approximate the anticipated slope through the Capsule T data. This will allow estimated T_{30} and T_{50} values to be determined.

The approach taken to determine the T_{30} and T_{50} values for Capsule T is described below:

1. Determine the slope of the transition region for Capsule S weld Charpy data (this is the latest data set available from Kewaunee) based on the T_{30} and T_{50} values previously determined.
2. Based on engineering experience, the slope decrease with increases in fluence. Therefore, based on engineering judgement, the slope determined for the Capsule S transition region will be decreased by 10%.
3. Apply the slope from the Capsule S data (minus 10%) to the Charpy data obtained from the Capsule T testing and establish a best fit through the transition region.
4. Determine the value of T_{30} and T_{50} based on the best fit through the transition region.

Using this approach, the slope through the transition region for Capsule S data was determined by calculating the slope going from the T_{30} value to the T_{50} value. Shown below:

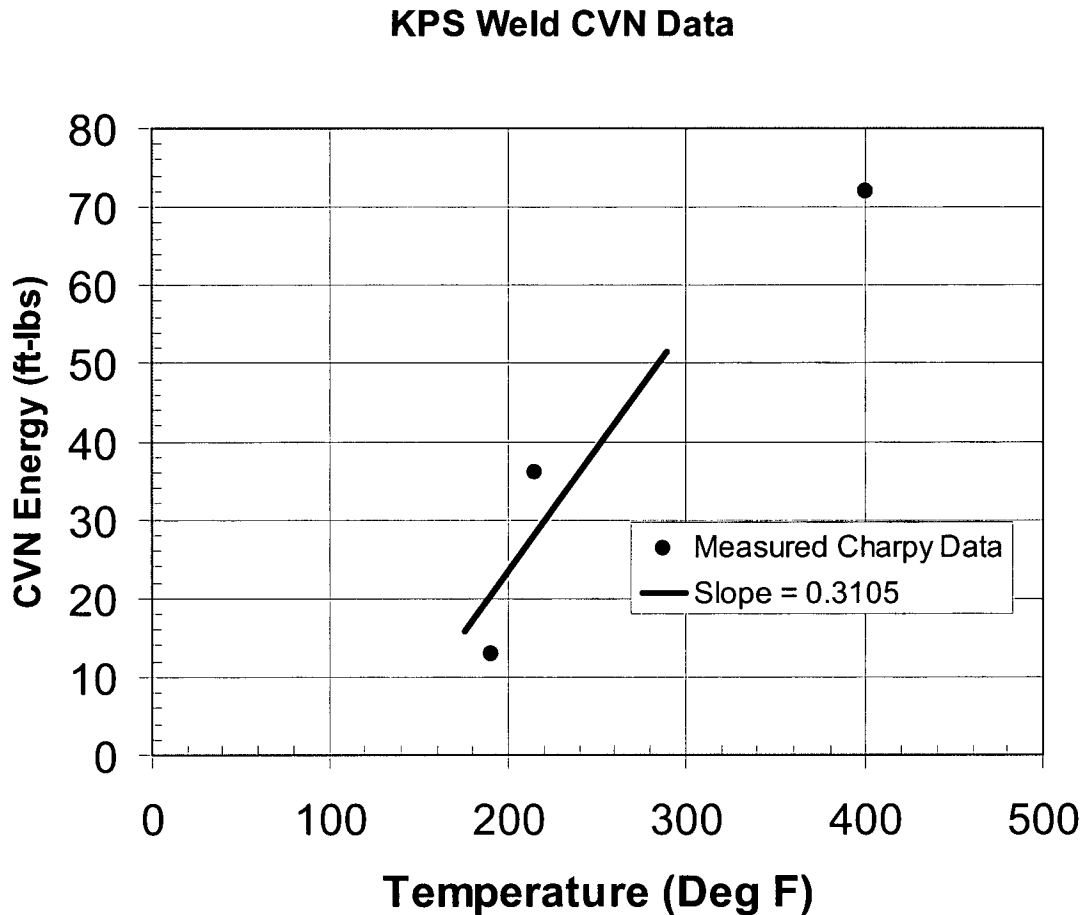
$$\text{Measured } T_{30} = 200\text{F}$$

$$\text{Measured } T_{50} = 258\text{F}$$

$$\text{Slope} = (50-30)/(258/200) = 0.345$$

A decrease of 10% would result in a slope of 0.3108 through the transition region of the Capsule T data.

Taking this ratio and applying this slope through the transition region of the Capsule T weld data results in the fit shown in Figure D-1. Note the sloped line was shifted left and right until the line represented what was considered to be the best fit through the data.



Based on the results of the best fit line through the transition region, the T_{30} value for the weld material will be approximated to **221°F**. The T_{50} value for the weld material will be approximated to be **285°F**.

A similar approach was taken for the lateral expansion data where the data from Capsule S was used to determine the slope through the Capsule T data (minus 10%).

Based on the results from the Capsule S report, there is a measured value of T_{35} and from the chart in Reference D-2, a second value can be determined. This data is shown below.

From Table 5-13 [Reference D-3]

$$T_{35} = 238^{\circ}\text{F}$$

From Figure 5-4 [Reference D-3], an approximated value was:

@ 200°F, LE = 22 mils

$$\text{Slope} = (35-22)/(238-200) = 0.342$$

A 10% decrease results in a lateral expansion transition region slope value of 0.308 for Capsule T. This value was then used to approximate a best fit line with the results plotted in Figure D-2.

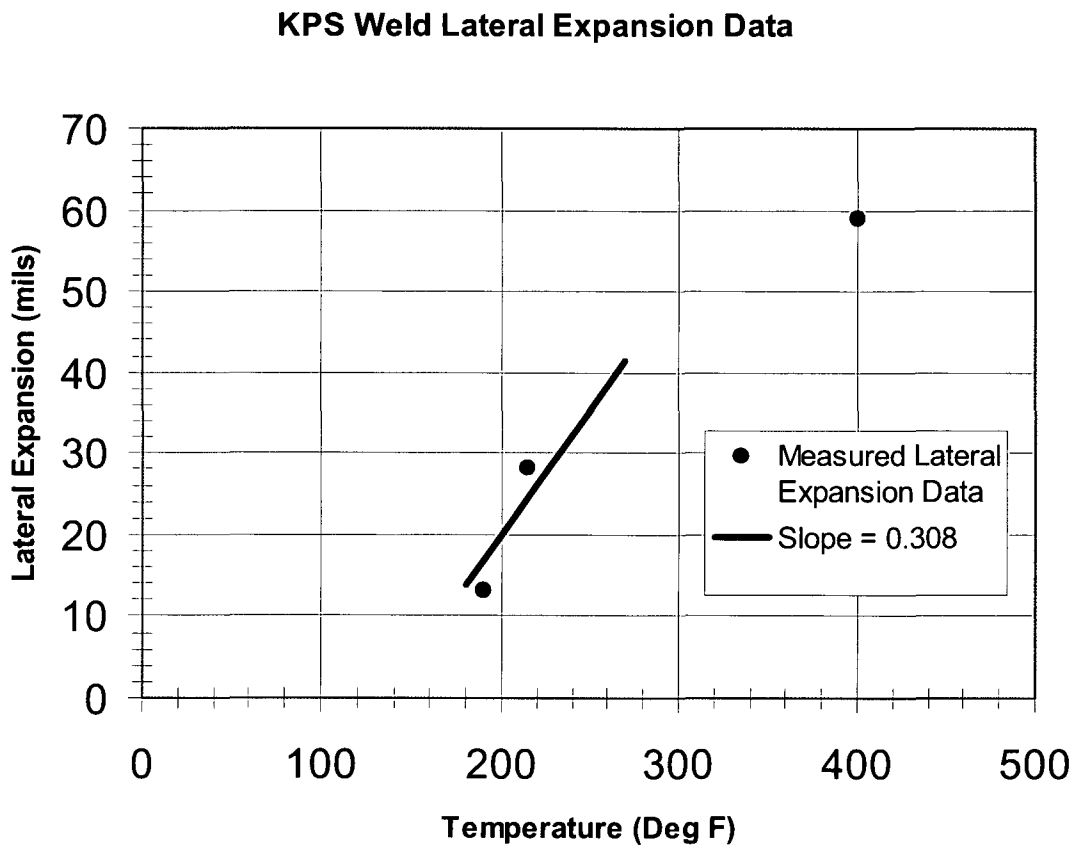


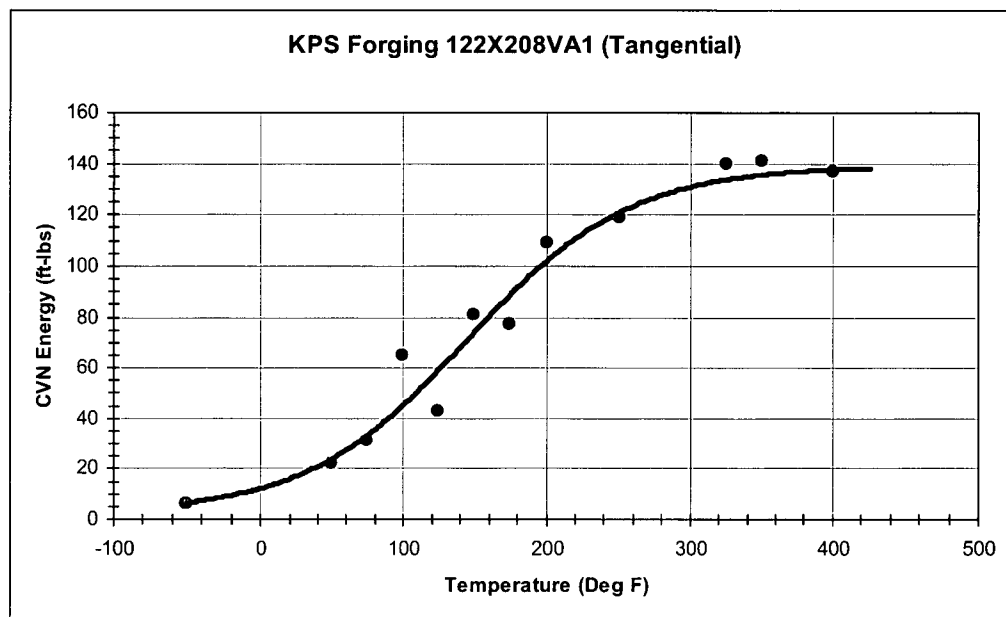
Figure D-2

Based on the results of the best fit line through the transition region, the T_{35} mils value for the weld material will be approximated to **249°F**.

Forging and Correlation Monitor Materials

For the remaining materials within the capsule, a generic fit to the data, as was done in previous WCAPs, was performed to determine the material properties.

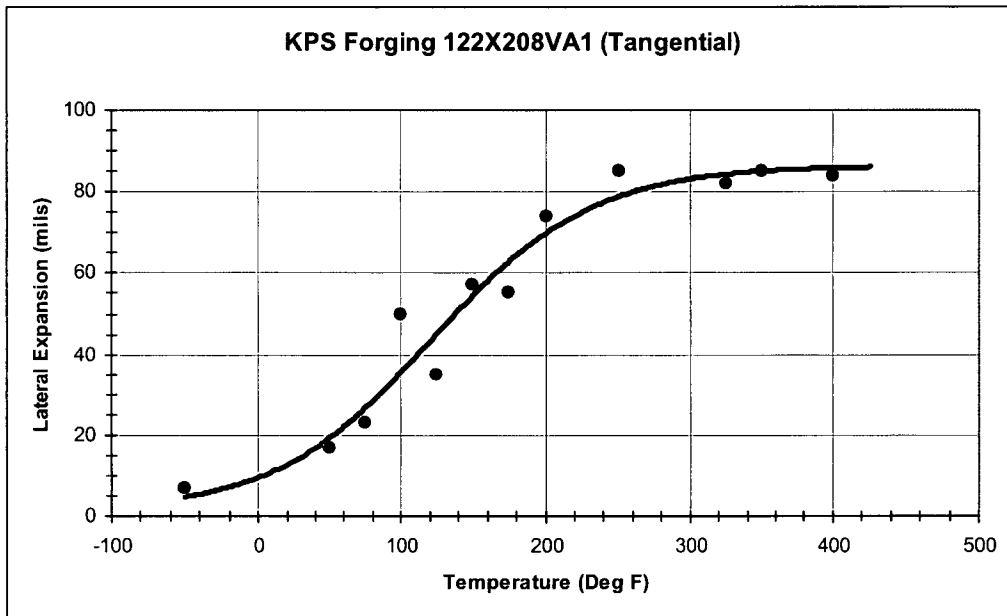
For the KPS Forging 122X208VA1 material, the data was plotted onto a chart with a fitted curve drawn through the data to represent a best-fit for the Charpy Energy, Lateral Expansion and Shear Data. Shown in the following Figures are the results for this fit.



From the fitted curve, the resulting T_{30} and T_{50} values for Charpy Energy are:

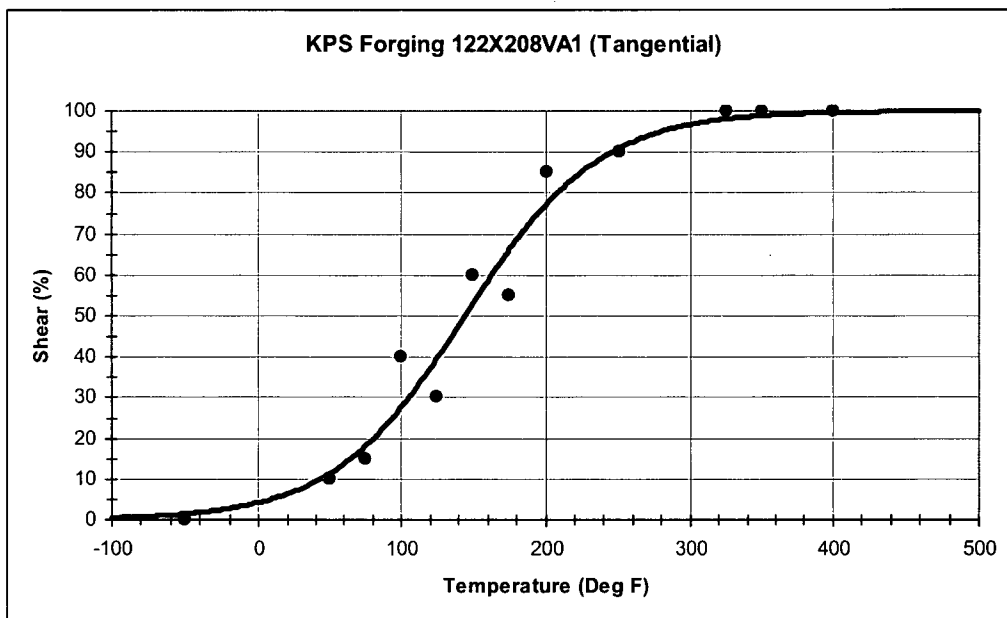
$$T_{30} = 65^{\circ}\text{F}$$

$$T_{50} = 110^{\circ}\text{F}$$

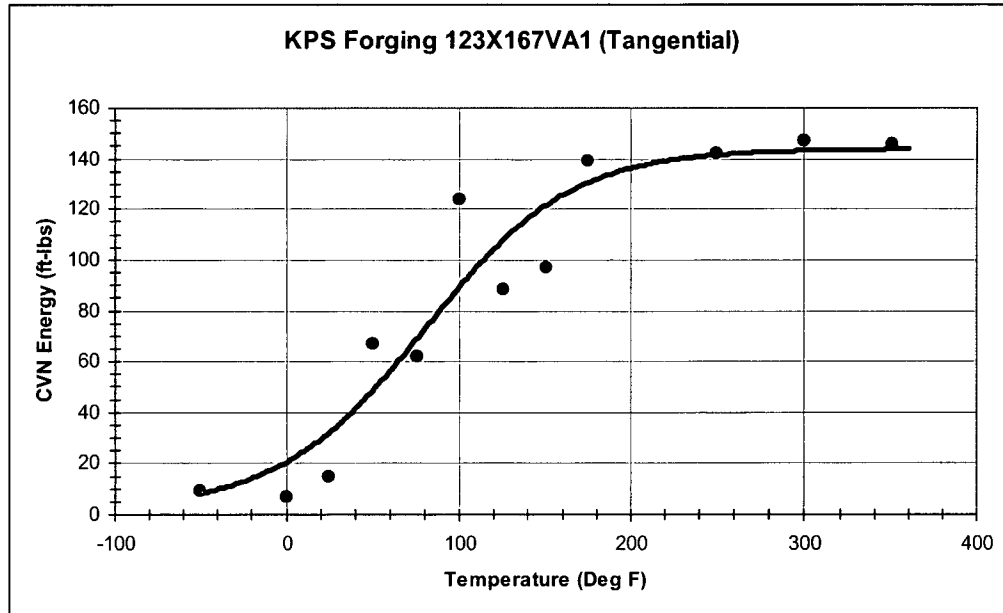


From the fitted curve, the resulting T_{35} value for lateral Expansion is:

$$T_{35\text{mils}} = 100^{\circ}\text{F}$$



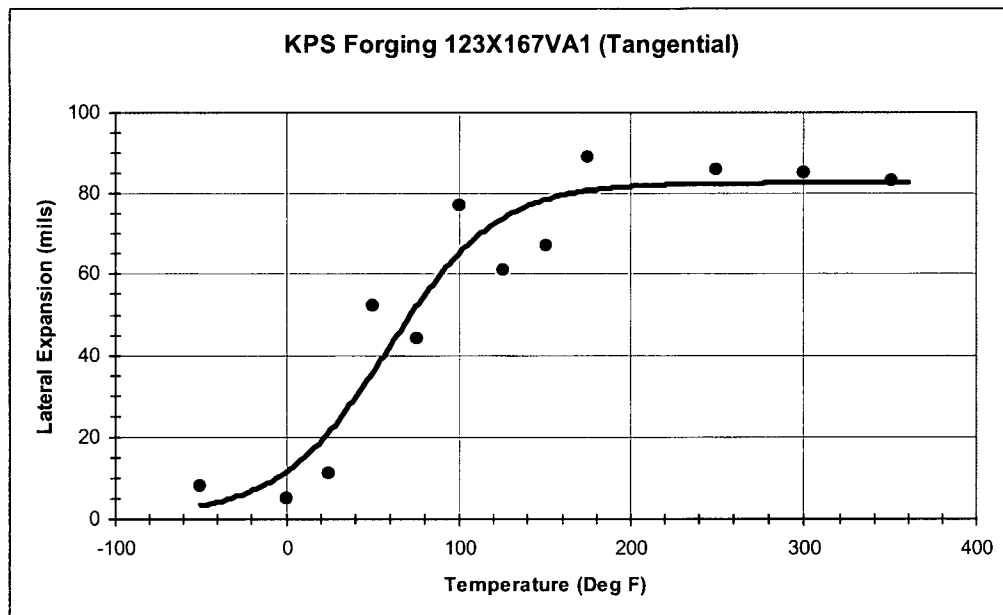
For the KPS Forging 123X167VA1 material, the data was plotted onto a chart with a fitted curve drawn through the data to represent a best-fit for the Charpy Energy, Lateral Expansion and Shear Data. Shown in the following Figures are the results for this fit.



From the fitted curve, the resulting T_{30} and T_{50} values for Charpy Energy are:

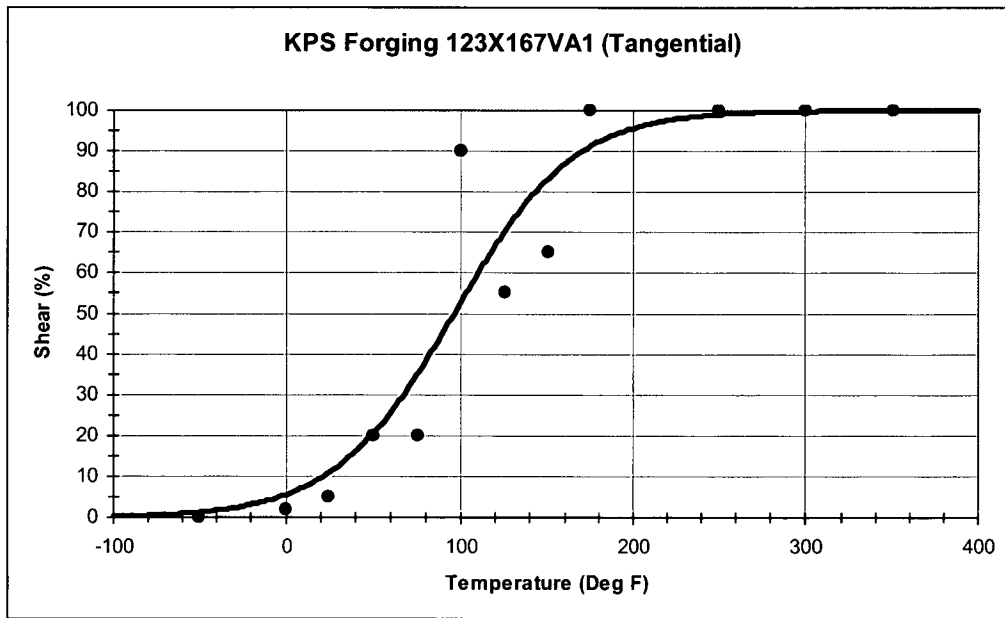
$$T_{30} = 20^{\circ}\text{F}$$

$$T_{50} = 50^{\circ}\text{F}$$

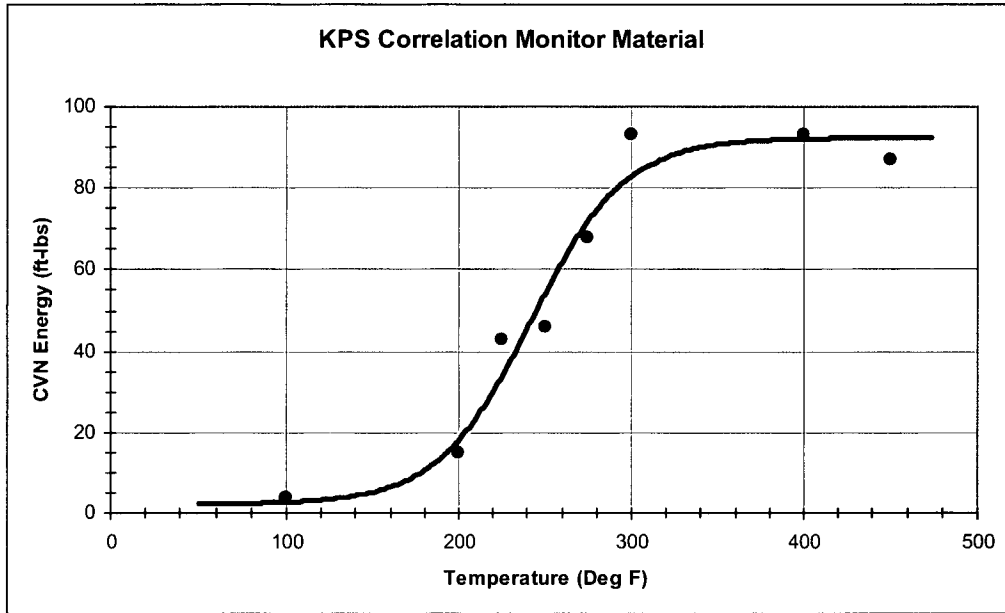


From the fitted curve, the resulting T_{35} value for lateral Expansion is:

$$T_{35\text{mils}} = 50^{\circ}\text{F}$$



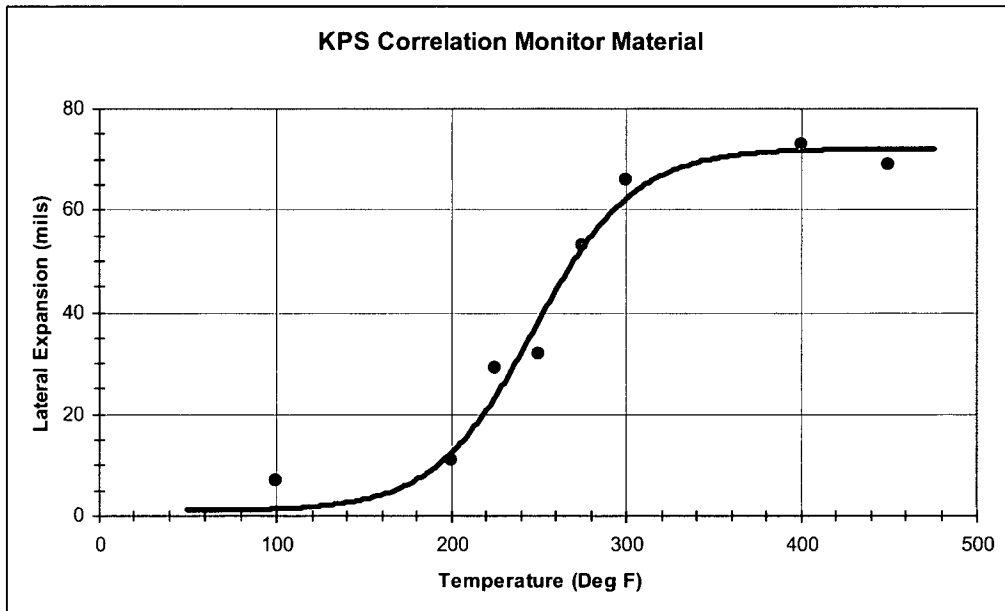
For the KPS Forging Correlation Monitor material, the data was plotted onto a chart with a fitted curve drawn through the data to represent a best-fit for the Charpy Energy, Lateral Expansion and Shear Data. Shown in the following Figures are the results for this fit.



From the fitted curve, the resulting T_{30} and T_{50} values for Charpy Energy are:

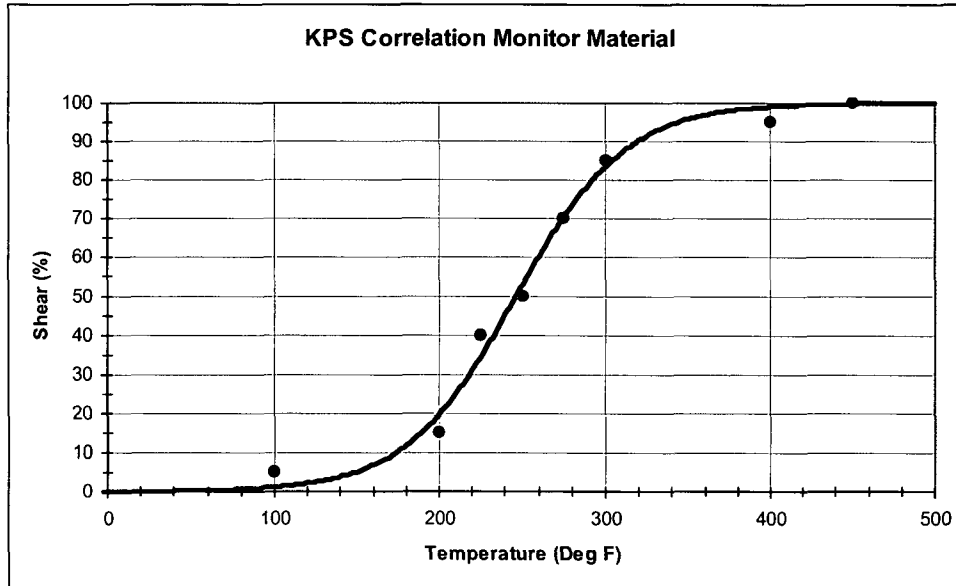
$$T_{30} = 220^{\circ}\text{F}$$

$$T_{50} = 245^{\circ}\text{F}$$



From the fitted curve, the resulting T_{35} value for Lateral Expansion is:

$$T_{35\text{mils}} = 245^{\circ}\text{F}$$



Appendix D References

- D-1 ASTM E 1253-99, Annual Book of Standards, *Standard Guide for Reconstitution of Irradiated Charpy-Sized Specimen*.
- D-2 STC Report STD-MCE-06-43, Charpy V-notch and Tensile Test Results of the Dominion Nuclear Operating Company Kewaunee Nuclear Plant Unit No. 1 Reactor Vessel Radiation Surveillance Program, Capsule T, R.G. Lott, et al, October 2006.
- D-3 WCAP-14279, Revision 1, *Evaluation of Capsules from the Kewaunee and Capsule A-35 from the Maine Yankee Nuclear Plant Reactor Vessel Radiation Surveillance Programs*, C.C. Kim, et al, September 1998.

This page intentionally blank

APPENDIX E

**KEWAUNEE POWER STATION SURVEILLANCE
PROGRAM CREDIBILITY EVALUATION**

This page intentionally blank

INTRODUCTION:

Regulatory Guide 1.99, Revision 2, describes general procedures acceptable to the NRC staff for calculating the effects of neutron radiation embrittlement of the low-alloy steels currently used for light-water-cooled reactor vessels. Position C.2 of Regulatory Guide 1.99, Revision 2, describes the method for calculating the adjusted reference temperature and Charpy upper-shelf energy of reactor vessel beltline materials using surveillance capsule data. The methods of Position C.2 can only be applied when two or more credible surveillance data sets become available from the reactor in question.

To date there have been five surveillance capsules removed from the KPS reactor vessel. To use these surveillance data sets, they must be shown to be credible. In accordance with the discussion of Regulatory Guide 1.99, Revision 2, there are five requirements that must be met for the surveillance data to be judged credible.

The purpose of this evaluation is to apply the credibility requirements of Regulatory Guide 1.99, Revision 2, to the KPS reactor vessel surveillance data and determine if the KPS surveillance data is credible.

EVALUATION:

Criterion 1: Materials in the capsules should be those judged most likely to be controlling with regard to radiation embrittlement.

The beltline region of the reactor vessel is defined in Appendix G to 10 CFR Part 50, "Fracture Toughness Requirements," as follows:

...the reactor vessel (shell material including welds, heat affected zones, and plates or forgings) that directly surrounds the effective height of the active core and adjacent regions of the reactor vessel that are predicted to experience sufficient neutron radiation damage to be considered in the selection of the most limiting material with regard to radiation damage.

The KPS reactor vessel consists of the following beltline region materials:

Intermediate shell forging 122X208VA1

Lower Shell forging 123X167VA1

Circumferential Weld 1P3571

All of these beltline materials were contained in the surveillance program. Based on this discussion, Criterion 1 is met for the KPS reactor vessel.

Criterion 2: Scatter in the plots of Charpy energy versus temperature for the irradiated and unirradiated conditions should be small enough to permit the determination of the 30 ft-lb temperature and upper shelf energy unambiguously.

Based on engineering judgment, the scatter in the data presented in these plots is small enough to permit the determination of the 30 ft-lb temperature and USE of the KPS surveillance materials. Hence, the KPS surveillance program meets this criterion. This holds true for the weld in that a 30 ft-lb temperature could be determined and an USE established even with only three data points.

Criterion 3: When there are two or more sets of surveillance data from one reactor, the scatter of ΔRT_{NDT} values about a best-fit line drawn as described in Regulatory Position 2.1 normally should be less than 28°F for welds and 17°F for base metal. Even if the fluence range is large (two or more orders of magnitude), the scatter should not exceed twice those values. Even if the data fail this criterion for use in shift calculations, they may be credible for determining decrease in upper shelf energy if the upper shelf can be clearly determined, following the definition given in ASTM E185-82.

The functional form of the least squares method as described in Regulatory Position 2.1 will be utilized to determine a best-fit line for these data and to determine if the scatter of ΔRT_{NDT} values about this line is less than 28°F for welds and less than 17°F for the plate.

The KPS intermediate and lower shell forgings and surveillance weld will be evaluated for credibility.

Table E-1 contains the calculation of chemistry factors for the KPS reactor vessel beltline materials contained in the surveillance program. These chemistry factors are calculated per Regulatory Guide 1.99, Revision 2, Position 2.1. *[Note that when applying surveillance weld data to determine the vessel CF per position 2.1, an adjustment called the "Ratio Procedure" is applied. This "Ratio" is not required when evaluating the credibility of the surveillance weld data since we want to determine the CF for the surveillance weld so that predicted surveillance weld shifts can be measured against measured shifts.]*

Table E-1

Chemistry Factor Determination for the Kewaunee Power Station Surveillance Materials

Material	Capsule	Capsule $f^{(a)}$	FF ^(b)	$\Delta RT_{NDT}^{(c)}$	FF* ΔRT_{NDT}	FF ²	
Intermediate Shell Forging 122X208VA1	V	0.586	0.850	0	0	0.723	
	R	1.76	1.155	15	17.33	1.334	
	P	2.61	1.257	25	31.43	1.580	
	S	3.67	1.337	60	80.22	1.788	
	T	5.62	1.425	90	128.25	2.031	
	SUM					257.23	7.456
	$CF = \Sigma(FF * \Delta RT_{NDT}) \div \Sigma(FF^2) = (257.23) \div (7.456) = 34.50$						
Lower Shell Forging 123X167VA1	V	0.586	0.850	0	0	0.723	
	R	1.76	1.155	20	23.1	1.334	
	P	2.61	1.257	20	25.14	1.580	
	S	3.67	1.337	50	66.85	1.788	
	T	5.62	1.425	70	99.75	2.031	
	SUM:					214.84	7.456
	$CF = \Sigma(FF * \Delta RT_{NDT}) \div \Sigma(FF^2) = (214.84) \div (7.456) = 28.81$						
Circumferential Weld 1P3571	V	0.586	0.850	175	148.75	0.723	
	R	1.76	1.155	235	271.43	1.334	
	P	2.61	1.257	230	289.11	1.580	
	S	3.67	1.337	250	334.25	1.788	
	T	5.62	1.425	271	386.18	2.031	
	SUM:					1430.04	7.456
	$CF = \Sigma(FF * \Delta RT_{NDT}) \div \Sigma(FF^2) = (1430.04) \div (7.456) = 191.8$						

The scatter of ΔRT_{NDT} values about the functional form of a best-fit line drawn as described in Regulatory Position 2.1 is presented in Table D-2

Table E-2.

Calculation and Comparison of ΔRT_{NDT} Values for Kewaunee Power Station Surveillance Materials

Material	CF (°F)	Capsule	Capsule Fluence	FF	Predicted ΔRT_{NDT} (°F)	Measured ΔRT_{NDT} (°F)	Scatter ΔRT_{NDT} (°F)	<17°F (Base Metals) <28°F (Weld)
Intermediate Shell Forging 122X208VA1	34.5	V	0.586	0.850	29.3	0	29.3	N
	34.5	R	1.76	1.155	39.9	15	24.9	N
	34.5	P	2.61	1.257	43.4	25	18.4	N
	34.5	S	3.67	1.337	46.1	60	-13.9	Y
	34.5	T	5.62	1.425	49.2	90	-40.8	N
Lower Shell Forging 123X167VA1	28.81	V	0.586	0.850	24.5	0	24.5	N
	28.81	R	1.76	1.155	33.3	20	13.3	N
	28.81	P	2.61	1.257	36.2	20	16.2	N
	28.81	S	3.67	1.337	38.5	50	-11.5	Y
	28.81	T	5.62	1.425	41.0	70	-29.0	Y
Surveillance Weld 1P3571	191.8	V	0.586	0.850	163.03	175	-12	Y
	191.8	R	1.76	1.155	221.53	235	-13	Y
	191.8	P	2.61	1.257	241.09	230	11	Y
	191.8	S	3.67	1.337	256.44	250	6	Y
	191.8	T	5.62	1.425	273.32	271	2	Y

These results in Table E-2 indicate that data points fall outside the $\pm 1\sigma$ of 17°F scatter band for both forgings. Therefore, the forging surveillance data are deemed not-credible per the third criterion. No weld data points fall outside the $\pm 1\sigma$ of 28°F scatter band for the surveillance weld data; therefore, the weld data are deemed credible per the third criterion.

Criterion 4: The irradiation temperature of the Charpy specimens in the capsule should match the vessel wall temperature at the cladding/base metal interface within +/- 25°F.

The capsule specimens are located in the reactor between the fuel and the vessel wall opposite the center of the core. The test capsules are in baskets attached to the thermal shield. The location of the specimens with respect to the reactor vessel beltline provides assurance that the reactor vessel wall and the specimens are subjected to equivalent operating conditions such that the temperatures will not differ by more than 25°F. Hence, this criterion is met.

Criterion 5: The surveillance data for the correlation monitor material in the capsule should fall within the scatter band of the database for that material.

The KPS surveillance program does contain correlation monitor material. NUREG/CR-6413, ORNL/TM-13133 contains a plot of residual versus fast fluence for the correlation monitor material (Figure 11 in the report). The measured versus predicted reference temperature shifts are presented in Table E-3 for the Kewaunee Correlation Monitor Material.

Table E-3
 Predicted versus Measured ΔRT_{NDT} Values for the Kewaunee Correlation Monitor Material

Material	CF (°F)	Capsule	Capsule Fluence	FF	Predicted ΔRT_{NDT} (°F)	Measured ΔRT_{NDT} (°F)
Correlation Monitor	102	V	0.586	0.850	86.7	95
	102	R	1.76	1.155	117.81	140
	102	P	2.61	1.257	128.21	155
	102	S	3.67	1.337	136.37	158
	102	T	5.62	1.425	145.35	175

Table E-3 shows a 2σ uncertainty of less than 50°F, which is the allowable scatter in NUREG/CR-6413, ORNL/TM-13133. Hence, this criterion is met.

Conclusion

Based on the preceding responses to all five criteria of Regulatory Guide 1.99, Revision 2, the plant forging surveillance data is deemed “non-credible,” the weld surveillance data is deemed “credible.”

This page intentionally blank